ARMY RESEARCH LABORATORY

Dark Zones of Solid Propellant Flames: Critical Assessment and Quantitative Modeling of Experimental Datasets With Analysis of Chemical Pathways and Sensitivities

by William R. Anderson, Nancy E. Meagher, and John A. Vanderhoff

ARL-TR-5424 **January 2011**

NOTICES

Disclaimers

The findings in this report are not to be construed as an official Department of the Army position unless so designated by other authorized documents.

Citation of manufacturer's or trade names does not constitute an official endorsement or approval of the use thereof.

Destroy this report when it is no longer needed. Do not return it to the originator.

Army Research Laboratory
Aberdeen Proving Ground, MD 21005-5069

ARL-TR-5424 **January 2011**

Dark Zones of Solid Propellant Flames: Critical Assessment and Quantitative Modeling of Experimental Datasets With Analysis of Chemical Pathways and Sensitivities

William R. Anderson, Nancy E. Meagher, and John A. Vanderhoff
Weapons and Materials Research Directorate, ARL

REPORT DOCUMENTATION PAGE	Form Approved OMB No. 0704-0188

1. REPORT DATE *(DD-MM-YYYY)*	2. REPORT TYPE	3. DATES COVERED (From - To)
January 2011	Final	March 2007–November 2009

4. TITLE AND SUBTITLE

Dark Zones of Solid Propellant Flames: Critical Assessment and Quantitative Modeling of Experimental Datasets With Analysis of Chemical Pathways and Sensitivities

5a. CONTRACT NUMBER

5b. GRANT NUMBER

5c. PROGRAM ELEMENT NUMBER

6. AUTHOR(S)

William R. Anderson, Nancy E. Meagher,[*] and John A. Vanderhoff[†]

5d. PROJECT NUMBER

H43

5e. TASK NUMBER

5f. WORK UNIT NUMBER

7. PERFORMING ORGANIZATION NAME(S) AND ADDRESS(ES)

U.S. Army Research Laboratory
ATTN: RDRL-WML-D
Aberdeen Proving Ground, MD 21005-5069

8. PERFORMING ORGANIZATION REPORT NUMBER

ARL-TR-5424

9. SPONSORING/MONITORING AGENCY NAME(S) AND ADDRESS(ES)

10. SPONSOR/MONITOR'S ACRONYM(S)

11. SPONSOR/MONITOR'S REPORT NUMBER(S)

12. DISTRIBUTION/AVAILABILITY STATEMENT

Approved for public release; distribution is unlimited.

13. SUPPLEMENTARY NOTES

[*]Contribution initiated while an ASEEE Postdoctoral Research Associate at ARL with WRA, and largely completed more recently while at Dept. of Chem., SUNY, Cortland, NY. Currently unaffiliated.

[†]Former ARL employee, retired in 2001.

14. ABSTRACT

The formation of propellant dark zone (DZ) structures in the gaseous flames above many solid propellants has been a subject of recurrent interest at ARL for about 20 years. The DZ structure is controlled by small molecule chemistry. The DZ chemistry is very important in controlling both the flame structure at low pressure (10–100 atm) and burning rates at high pressure (above ~500 atm), even though DZs collapse at higher pressures. We have developed a detailed mechanism to model it, which has been updated many times. For many years, we have promised to provide an extensive review on the subject. This report fulfills that promise, reviews prior work as well as introduces our most recent modeling results, and documents the first quantitative tests of several key assumptions. All relevant experimental literature is critically assessed to identify datasets for testing our model. Comparison of predictions and experimental results shows reasonable agreement; thus, we advocate use of our mechanism. However, the precision of both experiments and predictions is not tight, nor are there many test datasets. Thus, further experimentation is needed, and possibilities that would be of greatest help are briefly discussed. A detailed discussion of the chemistry that controls the DZ structure is presented.

15. SUBJECT TERMS

solid propellants, dark zones, combustion

16. SECURITY CLASSIFICATION OF:			17. LIMITATION OF ABSTRACT	18. NUMBER OF PAGES	19a. NAME OF RESPONSIBLE PERSON
a. REPORT	b. ABSTRACT	c. THIS PAGE			William R. Anderson
Unclassified	Unclassified	Unclassified	UU	202	19b. TELEPHONE NUMBER (*Include area code*) 410-278-2916

Contents

List of Figures

List of Tables

Foreword

The formation of dark zone (DZ) structures in the gaseous flames above many solid propellants has been a subject of recurrent interest at the U.S. Army Research Laboratory for about 20 years. Propellant DZs are nonluminous regions that may form between the solid propellant surface and the luminous flame. This phenomenon involves small-molecule chemistry. Beginning in the early 1990s, we developed a detailed mechanism to model it, which has been updated many times. The DZ chemistry is extremely important in controlling the flame structure at lower pressures of interest in rocket propulsion (~10–100 atm), where the DZ phenomenon may affect a physically complex flow. Reactions of central importance to DZ structure at low pressures have little effect on propellant burning rates at those pressures. However, those same reactions that control DZ structure at low pressures do strongly affect the burning rates at higher pressures in guns (above ~500 atm), even though (or, perhaps more properly, *because*) the DZ structure collapses at the higher pressures. In addition, versions of our small-molecule DZ reaction mechanism have formed a crucial core subset used in all of our larger mechanisms for modeling combustion of many energetic ingredients and mixtures. This subject is therefore of interest both for modeling propellant combustion and for understanding how propellants function in applications.

We have focused our interest on providing a quantitative description of the structure, especially the length of the DZ in a given flame, and on detailing how the gaseous chemistry affects that structure. Our work concerns nitrate ester and nitramine propellants. For many years, we have promised to provide an extensive, definitive review critically assessing our current understanding of DZ structure and chemistry, and providing a documented DZ mechanism. This report fulfills that promise. In it, much of our own and others' prior work is reviewed. All relevant available experimental literature is critically evaluated to identify reliable datasets for testing our model. It should be noted that our conclusions regarding which experimental studies can be retained for that purpose has changed from our prior works, and that small but important corrections were made to measured parameters from some of the retained datasets; reasons for the changes will be evident. We also detail reasons why many promising datasets had to be discarded for the present purpose of modeling the DZs of propellant flames in isolation from the rest of the flame structure. The criterion for the critical selection of experiments, the simplifying assumptions used in analysis of the retained experiments, and the simplifying assumptions used in the model are all presented in detail. Accuracy of the key simplifying assumptions is also herein quantitatively examined for the first time. We compare our predicted DZ ignition delay times, τ_{DZ}, which is the most important parameter, to experimental values extracted from DZ length data. We also compare evolution of species in those few cases where experimental data permit. Sensitivity of the predicted results to various input parameters, such as rate constants of elementary reactions and initial conditions obtained from the experiments, is assessed; besides

highlighting the most sensitive input parameters whose further study might yield the highest benefits, the results can be used to obtain estimates of precision for the predicted τ_{DZ} values as implied by the precisions of the many input parameters. Finally, details of the chemistry controlling the resulting solutions for several representative cases are presented; this yields deep insight into the key DZ reactions that has not appeared anywhere previously. Experimental and predicted τ_{DZ} values generally agree within their combined precision limits. Thus, the results encourage one to conclude that our DZ chemical mechanism captures all key reactions reasonably well, and we recommend using this core reaction set in modeling studies. But, both the predicted and experimental precision limits are fairly large. Also, the number of experimental studies that could be retained is quite small, and the available ranges of conditions (e.g., initial DZ temperature, pressure, and composition) at which they were performed are short. Because of these limitations, further experimental studies to provide more stringent tests are needed. Suggestions for future study that could yield improved test data are discussed.

Acknowledgments

Many people have had significant inputs to this work over the nearly 20 years since we first began studying dark zone (DZ) behavior, and we have undoubtedly forgotten some, for which we herewith apologize. We express gratitude to some of those most influential:

- Dr. R. A. Fifer (U.S. Army Research Laboratory [ARL], deceased in 2001). Fifer's efforts were seminal at ARL, directing our attention to the dark zone subject (see the Introduction).
- Dr. R. C. Sausa (ARL) for discussions about thermocouple measurements, especially quantitative radiative corrections, and for DZ-related chemistry discussions.
- Profs. V. Yang (Georgia Institute of Technology) and M. W. Beckstead (Brigham Young University) for encouragement to continue this effort, and Yang for providing the opportunity and experience gained from his request to critically evaluate a draft of his group's more qualitative review of DZ behavior.
- Dr. C. C. Chen (ARL) and Prof. A. Fontijn (Rensselaer Polytechnic Institute) for critical review of the present manuscript and several helpful discussions.
- Prof. J. W. Bozzelli (New Jersey Institute of Technology) for many discussions about the chemical mechanism.
- Dr. D. Davidson (Stanford University) and Prof. M. C. Lin (Emory University) for discussions about the controversy regarding HCN decomposition paths.
- Dr. A. J. Kotlar (ARL) for discussions regarding DZ relevant thermodynamics.
- Dr. B. E. Homan (ARL) for discussions regarding strand burner experiments, especially on nitramine-propellant combustion behavior.
- Drs. T. Parr and D. Hanson-Parr (both formerly with Naval Air Warfare Center, China Lake, CA, retired) kindly sent unpublished data, answered questions about their techniques and attempted a re-evaluation of one of their datasets with us, and critically reviewed the sections wherein the evaluations of their datasets are documented.

1. Introduction

Solid propellants commonly used in gun or rocket/missile applications can burn across a wide range of pressures. Depending on formulation, the lower limit is typically in the range of slightly sub-atmospheric to a few atm, while the upper limit in applications is roughly a few thousand atm, as seen in guns. Single, cylindrical strands of solid propellant are frequently made to burn at one end, that is, in "cigarette" fashion, for laboratory study in so-called strand burners. Strand burners with windows are typically used at constant pressure and can usually cover a range of about 0.5 to 100 atm—this entire range being viewed as "low pressure" by developers in the propellant community. Within this range of relatively low pressures, if the researcher works diligently—and is perhaps somewhat fortunate—the burn can exhibit a laminar, relatively steady, one-dimensional, gas-phase flame, with condensed surface regression at right angles to the end of the propellant strand. Then, under the proper conditions (e.g., ~5–50 atm), and with proper propellant compositions, the flame exhibits a very interesting structure. For an exemplary photo, see figure 1, which shows a solid, cylindrical strand of the propellant M43, a composite type based on the nitramine ingredient RDX (1, 3, 5-trinitro-1, 3, 5-triazine), burning at 15.5 atm (Vanderhoff and coworkers [*1*]). A few other excellent photos displaying similar flame structure are presented by Kubota (*2*, plate 1, figures a1–a3 for three nitrate ester-based propellants and figures d, e for two nitramine-based propellants). Gases leaving the surface are nonluminous while they move convectively upwards through a fairly long distance above the surface. At some sharply defined boundary above the surface a luminous flame suddenly forms.* Experimental evidence (vide infra) clearly establishes that usually, though not always, a near-equilibrium mixture of products is formed in the luminous region, and a temperature close to the adiabatic limit is reached. The nonluminous gas-phase region in the flame structure is commonly referred to as the burning propellant's "dark zone" (DZ). The DZ region and its structure, especially its length and gaseous phase transit time to which the length correlates, are the foci of the present work. We have recently determined that the chemistry controlling the DZ length is much more important for combustion of most solid propellants than anyone has previously appreciated; the reasons are delineated a few paragraphs hence. This finding inspired the present, renewed effort to test our current best models of the dark zone structure and chemistry vs. available experimental data and provide detailed documentation of the results.

*Note that if the pressure is too low, the luminous flame may not form before the gases exit the apparatus and/or mixing with surrounding gases cools the mixture.

A review of the main qualitative features of the gas-phase kinetics pertaining to the entire flame structure of typical nitrate ester- and nitramine-based propellants is given in Anderson and Fontijn (*3*). In addition to other points, this reference includes considerable discussion of the chemistry of the flames, especially of the interesting DZ portion and the typical species forming in all the various regions and sensitive reactions within them, discussion of reactions whose kinetics and products are in most need of study, and a section on methods that have been and might be used for said studies.* An idealized schematic of the flame structure is also given, see figure 2, to introduce some of the main observations and understanding concerning DZ formation; some of the present introduction is also adapted from that source. In typical strand burner experiments, the propellant burns at a chosen, constant pressure. The solid surface regresses as the combustion wave moves through the strand. The "burning rate," a characteristic of the propellant at the given pressure, is the steady rate of regression of the wave through the solid strand. At the propellant surface, heat transfer from the gas phase causes condensed phase gasification, typically through very complex processes not represented in the diagram, yielding the initial gas-phase intermediates. In a very narrow region just above the surface, these intermediates undergo a rapid, exothermic, global reaction, converting them to the DZ intermediate species. Coupled with this reaction is a strong upward gradient in the temperature profile. This narrow, near-surface, gas-phase region is also often called the "first-stage flame." At the end of the first-stage flame, the comparatively low reactivity of the major DZ intermediates causes their concentrations and the temperature to linger at near-plateau levels—perhaps not with such near-zero gradient as caricatured in the schematic, especially at higher pressures—for a short time, referred to as the "dark zone ignition delay," τ_{DZ}. This chemical delay time, coupled with gas convection, causes formation of the DZ. The global reaction slows as the concentrations of trace radicals slowly build within the DZ. At some point, the chemical rates rapidly increase, the conversion of DZ intermediates to nearly equilibrium products quickly occurs, and heat is released, driving the temperature upwards to approximately the adiabatic limit. (Note that slightly nonequilibrium conditions typically prevail in the burnt gases until trace species concentrations more slowly relax to their equilibrium values.) The thin region at the end of the DZ where this occurs is called the "second-stage flame." At the end of the second-stage flame, the temperature is high enough that the gases typically become luminous; the entire luminous region is often referred to as the "luminous flame."

It appears likely that the primary reason for DZ formation is simply the chemical ignition delay time within the DZ region, coupled with gas-phase convection (see Vanderhoff et al. [*4*]) and the further discussion herein). It should be mentioned that whereas the DZ feature is interesting and often puzzling to the uninitiated, the observation of a delay time prior to global reaction of rapidly heated fuel-oxidizer mixtures is quite common; it has often been used, e.g., in shock tube experiments, as an observable to investigate ignition chemistry. The key to quantitative

*The DZ feature and its chemistry have been a focal point of our group at various times over the last ~20 years (see, e.g., refs *4–10*).

understanding of the DZ structure is knowledge of the initial conditions therein and a relevant chemical mechanism and model. These points are the central issues of the present work. The scope is confined to nitrate ester and nitramine propellants. Other energetic materials, such as ammonium dinitramide (ADN), are known to form even more complex, staged flame structures (*11*, *12*). These materials were ignored due to a lack of sustained interest within our organization.

A brief introduction of typical DZ conditions seen in experiments is given here. The adiabatic flame temperature of nitrate ester and nitramine propellants is typically about 3000 and 2100 K, respectively. Within the DZ region, the temperature is much lower, typically about 1600 K in nitrate ester and 1200 K in nitramine propellants. In nitrate ester propellants, the first-stage flame involves species produced near the surface, e.g., aldehydes, such as CH_2O, and NO_x oxidizers, such as NO_2 and/or HONO, which rapidly undergo global reaction to the intermediate DZ mixture, providing the first-stage exothermicity. The aldehydes are converted to CO and CO_2, while HONO and NO_2 are converted to intermediate species NO, some H_2 and H_2O, and traces of other species. The DZ mixture in nitrate ester propellants consists primarily of CO, CO_2, H_2, H_2O, NO, and perhaps appreciable traces of N_2. Nitramine propellants at or near the condensed phase surface also produce considerable CH_2O, NO_2, and/or HONO. In addition to these species, gaseous nitramines can, by competing pathways, produce HCN and N_2O (*13*, *14*). Most of the CH_2O, NO_2 and/or HONO, and N_2O typically are consumed in the first-stage flame, but HCN is much less reactive and typically survives into the DZ region. In the case of nitramines, its low reactivity, as well as that of NO, contributes to the DZ formation.* Thus, in addition to the CO, CO_2, H_2, H_2O, NO, and traces of N_2 seen in nitrate ester DZs, nitramine DZs also typically contain HCN, perhaps more N_2 (from conversion of much of the N_2O in the first-stage flame), and often kinetically important traces of leftover N_2O, CH_2O, and NO_2 from the first-stage flame. Traces of the other, less kinetically important species may also be observed at the leading edge of the DZ. The HCN and NO are intermediates whose slow reactions delay the final heat release, the final products at the end of the second-stage flame for the typical fuel-rich propellant being instead a mixture of N_2, H_2O, H_2, CO, CO_2 and trace components. The major species typically exhibit strong gradients at the first- and second-stage flame regions indicative of their interconversion, and plateau regions coincident with that in the temperature profile. Each type of propellant can also, of course, produce other trace DZ components. It is important to note that some propellants only exhibit a single-stage flame structure even at low pressures—that is, no DZ region or plateaus in the profiles form, and the mixture converts to equilibrium products at the adiabatic flame temperature close to the surface. For many of these, this may result from the formation of large amounts of intermediate NH_x species (x = 1–3) from certain

*We believe we were the first to note this important point (*3*, *7*, *10*). Most reactions of HCN are rather slow because of its unusual, extremely strong bonding. Its weaker bond, of course, is the H-C single bond. That bond energy is about 124 kcal/mol (298K), which is comparable to that of HF. These are two of the strongest covalent single bonds known in any molecules. Compare this to the 104 kcal/mol bond of H_2, and ~85–100 kcal/mol H-C bonds in typical hydrocarbons, aldehydes, and other organic species.

ingredients (e.g., in the case of M30 propellant, the nitroguanidine ingredient, NQ); NH and NH_2 react rapidly with NO, even at room temperature, leading to final product N_2 formation and faster radical growth and heat release, which likely explains the lack of a DZ (*3*).

Some researchers (unpublished) have suggested that aerosol or dust formation from the first-stage flame might contribute to DZ formation via extraction of heat from the gaseous mixture retarding reactions as the particles gasify. We believe this is not a major contributing factor in most cases. There is little experimental photographic or other evidence to support it. This suggestion was made in workshops on propellant combustion many years ago, at a time when modelers of pure RDX combustion, who were calculating the entire combustion wave from unreacted solid to equilibrium products, were having trouble predicting formation of a DZ as observed in CO_2 laser heated combustion; that is, the predicted DZ lengths were far too small (*15*). More recent efforts yield DZ structures in better agreement with experiment without invoking an aerosol or dust (*16*, *17*). See also the recent, very comprehensive review of modeling results for RDX and many other materials by Beckstead and coworkers (*18*). The initial problems were corrected by introducing a two-dimensional area expansion of the gas-phase flow, taken from experiments, into the models. On the contrary, in our earlier works where we focused instead on singling out and modeling just the observed DZ feature (*4–10*), we experienced difficulties making the ignition delays short enough; that is, the predicted global chemistry was too slow, and the DZ lengths were too large—unless some uncomfortable assumptions about the input DZ conditions were made. The current status will be discussed. Although an aerosol or dust is not necessary to obtain prediction of a DZ, and we believe it typically does not play a major role, from analysis of the experimental species profiles of one unusual nitramine case that is retained, it appears the effects of particulates in the gas flow might explain some of the observations. These issues, and suggestions for future work, are discussed.

We discuss here why we have come to believe that achieving an accurate understanding of the DZ feature is very practically important, not just an academic exercise. Years ago like most researchers, we noted that if a DZ were present in the gas-phase flame, e.g., at lower pressures, the second-stage flame would be so far from the surface its heat could not reach there and affect the pyrolysis, hence burning rate, due to the near zero temperature gradient in the DZ region. For higher pressures where the DZ collapses and the structure appears single-staged, one naturally assumes if a DZ is not present, the phenomenon is immaterial to the major combustion features. A colleague at the U.S. Army Research Laboratory (ARL), D. E. Kooker, suggested that in spite of these observations the DZ feature could be very important to the interior ballistics cycle of guns: formation of the DZ gases at early times during the flamespread in a propellant bed, when the pressure is still relatively low, may be intimately connected with undesirably long, erratic gun ignition delay times,[*] especially for nitramine propellants (*19–22*). We spent

[*] A gun's ignition delay is the time between initial application of propellant ignition stimulus and strong pressure rise and may be connected with, but is not to be confused with, the DZ ignition delay time.

considerable effort deriving reduced mechanisms for use by Kooker et al. in interior ballistics modeling (*6–9*), but those mechanisms only received limited usage due to Kooker later becoming involved in other pressing endeavors (*19*); thus, whether the DZ mixture formation and its slow kinetics might be involved in the gun ignition delay issue was never explored definitively. Therefore, our interest in the DZ modeling waned for a considerable time. More recently, another ARL colleague, M. J. Nusca, has informed us of a growing interest to include realistic finite-rate chemistry in computational fluid dynamics simulations of solid rocket engine function (*23*). DZ structures are likely very significant in the complex, possibly turbulent, flow fields at the typical rocket pressures of 10–100 atm. In addition, DZ chemistry has been determined to be important at gun pressures (above ~1500 atm), even though the DZ structure collapses. Miller and Anderson have modeled the combustion of several fielded nitrate ester propellants, including the entire gas-phase flame structure (*24*). In that work, it was clearly established from analysis of the major gas-phase reaction pathways, characteristic distances for heat transfer, and, especially, sensitivities of the solutions' temperatures near the propellant surface to the various reactions' rate coefficients* that *the same reactions that control the lengths of the dark zones at low pressures (below about 300 atm) are extremely important to the burning rates of these propellants at high pressures*, even though the high-pressure temperature profiles indicate the flames are single staged. Predicted low-pressure burning rates are not very sensitive to the main DZ reactions' rate coefficients because, as everyone expected, the second-stage flame is indeed too far from the surface for its heat release to reach there. The chemistry in the DZ is so slow compared to that in the first-stage zone that there is relatively much less heat released there (note the near plateau in DZ temperature profiles). However, above ~300 atm, there is no dark zone and the temperature profile becomes indicative of a single-staged flame—there is, of course, actual staging of the chemical processes within heavily blended layers. But the main point is that the second-stage flame zone is close enough to the surface, within the characteristic distance for heat transfer, that its exothermicity strongly affects the near-surface region. The reactions taking place towards the upper layers of the blended flame zones are the same ones that control the length of the DZ at low pressures. In fact, it was found at the highest pressures that the reactions whose temperature sensitivities are highest near the surface are the same ones to which the DZ lengths are most sensitive at low pressures. Therefore, the temperature gradient near the surface is most sensitive to these same reactions; thus, the burning rates, which are primarily controlled by the heat feedback from the gas-phase flame to the surface, will also exhibit the same sensitivities. Even more recently, we have run across another possible example related to this issue in modeling pure RDX. We have just begun an effort to upgrade the model for RDX combustion, beginning with upgrades to the gas-phase chemical mechanism for RDX combustion (*25–29*). The first upgrade is from a gas-phase mechanism developed ~10 years ago

*The sensitivities of the computed solutions' near surface temperatures to the input rate coefficients are not to be confused with the so-called propellant "burning rate temperature sensitivity," which is instead the response of the propellant burning rate to changes in the solid's initial, ambient temperature.

by Yetter (Y2, Yetter's second, final version [*30*]) to a more recent one developed by a California Institute of Technology (CTM) group (*31–33*) based upon better quantum chemical methods. We investigated the main RDX decomposition steps of each mechanism for detailed comparison (*25*). To our knowledge, the latter mechanism has not previously been tested in a combustion model. We find, to our surprise, the initial gas-phase RDX decomposition reaction is very different for the two mechanisms—NO_2 scission for Y2 and HONO elimination for CTM. In spite of this, the computed burning rates are very similar, both comparing well with experiment. An examination of the temperature sensitivities near the surface, even at low pressure, reveals the decomposition steps of RDX and its large daughter fragments are far down the list of the most important reactions. The largest sensitivities are for reactions that control the rate of conversion of HCN and NO to final products, i.e., those that would control the length of a DZ were one present.* Thus, this example is also suggestive that typical nitramine DZ chemistry is extremely important when pressure is high enough that the DZ collapses. For these several reasons, we have deemed it very important to take a renewed interest in the dark zone chemistry and to complete and provide detailed documentation on an effort we commenced nearly 20 years ago.

To single out and model the DZ feature in absence of the rest of the propellant combustion wave with its many associated unknowns, a number of simplifying assumptions are made (presented in section 2.1). These have the effect of reducing the problem to what is termed "plug flow," wherein heat and mass transport between neighboring spatial gaseous slabs are negligible. In this case, a simple, time-dependent, homogeneous reactor model can be properly used. It appears that the first person to use this approach, albeit couched in a different formalism stressing DZ length rather than τ_{DZ}, was probably Sotter (*34*). He was also likely the first to use computer methods to evaluate a detailed kinetics network for propellant combustion. Sotter performed his work in a period when computers were in their infancy, and relevant gas-phase reaction kinetics were not at all well established. And so, the size and quality of his mechanism were both very limited. But his innovation showed this type of modeling is feasible. The present formalism has been used many times to extract τ_{DZ} from experimental data, perhaps first by Aoki and Kubota (*35*), later by Fifer et al. (*36*), and Anderson and coworkers (*4*, *6–10*). The study by Fifer et al. raised awareness at ARL of the possibility of modeling strand burner data from our early experiments using this simple approach, which we first did in Vanderhoff et al. (*4*) and has ultimately led to the present contribution.† Not only does this approach allow testing

*Recall, as we mentioned previously, pure RDX flames—with no outside heating as, for example, by CO_2 laser beam impingement—exhibit no DZ even at the lowest pressure we modeled, 0.5 atm. Incidentally, the fact that the similar DZ reactions are present in these sensitivities lists for both mechanisms suggests a reason why models of RDX burning rates are typically insensitive to many assumptions. The small molecule DZ chemistry controls the burning rate and is very similar in the mechanisms from most sources. The situation is apparently very forgiving of major errors in the large-molecule decomposition chemistry. This point may be true for many other propellants as well, even when a DZ is present if small-molecule chemistry is the controlling factor in the first-stage flame.

†Though Fifer's model contained some significant errors (e.g., discussed briefly regarding one key erroneous reaction in section 2.2.2), he deserves considerable credit for his seminal contributions at ARL in this and many areas.

of the DZ model vs. experimental data, but it also allows investigation of the details of the DZ chemistry without the confusing, uncertain effects of the first-stage flame chemistry. The latter is typically much more complex and dependent on very uncertain assumptions, especially about what the initial gas-phase species from the propellant surface are. After we obtain solutions, we use sophisticated postprocessing codes to dissect the chemistry that gives rise to them. This information should prove invaluable in providing direction regarding which reactions and issues need further study to increase fidelity of the related chemistry.

Some aspects of solid propellant dark zones have been recently discussed in the extensive review by V. Yang and coworkers (YTLY06) (*37*).[*] While this contribution is extremely informative to the uninitiated, it primarily focuses on qualitative aspects of the DZ phenomena. The present effort involves a critical assessment of datasets and quantitative modeling thereof. Also, note most of the previous quantitative modeling of propellant combustion cited in Yang et al. (*37*) incorporated the entire flame structure; that is, it accounts for many physico-chemical effects within the entire solid region, liquid—or foam—layer, and gaseous region. While this is clearly a worthy goal, any modeling approach which takes both condensed and gaseous details—both physics and, especially, the likely very complicated chemistry—into account necessarily introduces a great deal of uncertainty to the DZ structure predictions. This follows because the condensed phase chemical mechanisms—not just the kinetic rates, but also the very identities of the elementary reactions themselves and products thereof—cannot currently be both precisely and accurately measured or predicted for any practical solid energetic material (*18*, *58*). This is the case for experiments because in decomposition studies the reactions cannot be completely quenched during sampling, and there are a host of other difficulties (*3*, *58*). A priori theories cannot currently be trusted to provide the necessary accuracy due to the complexity of the problems, e.g., forbiddingly huge numbers of atoms and/or time steps needed for atomistic approaches and inaccuracies of current force field-based calculations. Logically, one is compelled, therefore, to conclude the prediction of exact conditions—e.g., initial gas-phase mixture composition, rate of formation, and even the temperature—in these models at the leading edge of the DZ region is unfortunately fraught with uncertainty. Differences in predicted conditions at the leading edge of the DZ vs. experiments are almost inevitable; furthermore, the present results show the DZ structure can be extremely sensitive to these conditions (vide infra). Thus, for quantitative investigation of just the DZ chemistry, it is better to model measured DZ

[*]It is important to mention there are several DZ relevant studies YTLY06 missed: for nitrate ester propellants (*35*, *38–42*), for nitramine propellants (*43–51*), and for both types (*52–57*). Also, in YTLY06's table 10, the following citation corrections are noted: the JA2 (1 atm) entry was ascribed to Vanderhoff et al. (*4*), it is more properly ascribed to the original source (*41*); the M9 (16 atm) and M9 (1 atm) entries were ascribed to M. W. Teague, G. Singh, and J. A. Vanderhoff (30th JANNAF Combustion Subcommittee Meeting, CPIA Publications No. 606, Vol. II, 1993, pp 217–226), they are more properly ascribed to the original sources, Vanderhoff et al. (*53*) and Liiva et al. (*41*), respectively.

data in isolation where possible.* We will discuss the sensitivity of DZ length to some of these and other uncertainties (vide infra). There have been few modeling studies focused only on the DZ structure itself and, to our knowledge, no comprehensive testing vs. critically selected experimental data. We include a detailed critical review of the most reliable DZ data sets and input parameters, comparison of modeling results to the selected data sets, discussion of the detailed chemical pathways and sensitivity analysis— which shows exactly what a state-of-the-art mechanism indicates is the controlling chemistry for DZs of the two major propellant types— and discuss what future efforts might be most helpful to improve the model. The earlier (*37*) and present contributions, thus, are quite complimentary and together provide an excellent introduction to the observations and current status of DZ understanding. It should be mentioned that preliminary results of the present effort appear in Anderson et al. (*59*, *60*). The present report is much more detailed, and the analysis of controlling chemistry has been considerably extended. Also, results have undergone some changes since those preliminary reports. This is primarily due to reanalysis of some of the initial mixture conditions from the experiments. For the nitramines, some of the stable trace components that were previously ignored due to not being in earlier, simpler versions of the chemical mechanism are now included and found to have important influences on the modeling—especially traces of CH_2O and NO_2 remaining from the first stage. Sensitivity of the results to some trace species concentrations was explored and is discussed in section 4.

In the current work, we present our modeling results for the DZs in cases where the experimental datasets are complete enough to permit the ignition delays to be calculated in isolation from the rest of the flame structure (subsurface and first-stage flame regions). In section 2, we present the method for analysis of experiments, the modeling approach, and discuss some key issues regarding the mechanism. In section 3, we present results of the critical selection of experimental datasets, including both those that were retained and details on why some promising datasets had to be discarded. In section 4, the modeling results and comparisons to the retained datasets are given. Two important issues are examined in the first part of section 4: (1) important simplifications are made to enable analysis of available experimental data, and the accuracy of the results via this approach is considered for the first time, and (2) a consideration of steady-state behavior of radicals at early times has led us to a conclusion that it is highly unlikely that significant concentrations of radicals in the initial mixture are missing; that issue has been a concern in the community for many years. In section 5, a detailed analysis is presented indicating which of the several hundred reactions in the mechanism are most important to DZ chemistry and why. Finally, in section 6, Conclusions, we discuss some of the most important implications of this work, and what future efforts might be of highest value to improve our understanding and quantitative modeling of DZ structure.

*Of course, one can conversely point out a concern that important trace species, especially radicals, might be present in the DZ and missed in the experiments, and draw an argument that modeling of the full combustion wave might properly predict them and thus be preferable to modeling the DZ in isolation. Present results, however, yield a strong indication that, due to steady-state considerations, the radical concentrations are negligible. Missing an important stable trace species seems unlikely, but could be more problematic. These points will be discussed in detail (vide infra).

2. Modeling Approach

2.1 Analysis of Experiments; Modeling Physics and Codes

As mentioned in the introduction, when enough experimental data regarding initial DZ conditions are available, assumptions can be made leading to a simple model allowing for the testing of dark zone kinetics in isolation from processes taking place in the condensed phases and first-stage flames. We discuss a test of how well results using these assumptions compare to a more accurate premixed flame simulation resulting from a more complicated nitrate ester propellant model in a later section. The focus of the present section will be to explain the theory and point out the data that are needed from experiment to use this approach. As noted previously, the temperature and majority species profiles plateau in the region of the dark zone (see the idealization in figure 2). Since this is the case, heat and mass transfer by diffusion and conduction through the DZ region are small. The assumption that these processes can be ignored is made, leading to "plug flow" conditions. Each infinitesimally thin slab of gas perpendicular to the flow direction is assumed to be homogeneous, and a simple time-dependent chemistry model is then appropriate to compute the evolution of species as function of time, which can be correlated with distance along the flow. The initial temperature and mixture at the beginning of the DZ are obtained from experiment. These initial conditions are used along with an assumed detailed chemical mechanism in a homogeneous reactor model. The model predicts a time to chemical runaway, which we define as the time to maximum heat release. Since the temperature rise is typically gradual up to this time (distance) and then rises sharply, this ignition delay time, τ_{DZ}, is recognized as the time for convection along the gas-phase flow through the DZ region of length L_{DZ}:

$$\tau_{DZ} = L_{DZ}/v \,, \tag{1}$$

where v is the convective flow velocity. The flow velocity may be obtained from the continuity equation across the combustion boundary as follows:

$$v = r_b \rho_s / \rho_g \,, \tag{2}$$

where r_b is the solid propellant burning rate, and ρ_s and ρ_g are the solid and gas-phase mixture densities, respectively. Combining equations 1 and 2 and using the ideal gas law, one obtains the following:

$$\tau_{DZ} = L_{DZ} M P / R T_{DZ} r_b \rho_s \,, \tag{3}$$

where R is the ideal gas constant, M is the average molecular weight of the DZ gas mixture, P is the pressure, and T_{DZ} is the measured DZ temperature. We determined for measured DZ gas mixtures (see section 3), that M is generally about 26 g/mol. Equation 3 is used to analyze experimental data and obtain measured DZ ignition delay times to compare with computed times

to maximum heat release from the model. The main contribution to error limits in measured τ_{DZ} was primarily from that in L_{DZ}, with smaller contributions from those in T_{DZ} and/or r_b. Note that for the analysis, the measured T_{DZ} in the DZ plateau region is assumed to be constant. This assumption is typically best at lower pressures and may contribute a separate, systematic error, which is discussed in section 4.1.

To model the DZ using this approach, one needs an appropriate chemical mechanism and the initial DZ temperature and mixture ratio. The information is used to predict τ_{DZ}. Note that it is an equivalent test to compare either predicted and experimental τ_{DZ} or L_{DZ}; it is simplest to compare τ_{DZ}. Discussion of codes and methods used is given in the next paragraph. An illustrative example given at the beginning of section 4.1 will help to clarify. Per equation 3, to extract τ_{DZ} from experiment for comparison to the model, one needs the DZ temperature, DZ length, the solid propellant's density and its burning rate at the pressure of interest.

We use the SENKIN II (version 3.0) computer code (*61*) to model the homogeneous DZ kinetics. This model is based on the CHEMKIN II (version 3.6) package of gas-phase chemical kinetics code libraries and mechanism interpreter (*62*). It is important to note that we normally instruct the codes to include reverse reactions via computation of the reverse rate constants using the forward reaction rate constants and the thermodynamics (as does nearly everyone since about the mid 1980s). SENKIN allows several options in regards to temperature and pressure variation during a reaction. The appropriate choice for the current application is the constant pressure and adiabatic system assumption, so that heat evolving during the reaction is properly accounted for and causes the temperature to rise until equilibrium is reached. SENKIN also allows for computation of a given solution's temperature and species sensitivities to the rate coefficients of the various reactions. After a solution is obtained, we can use postprocessing codes developed over the last 20 years at ARL to investigate the results, in particular, to find the maximum heat release point for comparison with experimental τ_{DZ}. Note that an assumption is being made that the chemistry is very rapid once the delay time has elapsed so that gradients in the profiles are sharp, and this comparison is thus valid. Also note that some care must be taken to look at plotted results and insure that if multiple maxima occur, the one corresponding to the conversion of initial mixture to equilibrium products is being obtained. Our postprocessors also allow for dissection of the detailed chemistry that gives rise to the solution. That is, we can investigate the pathways—also known as performing "rate flux" analysis—and sensitivities related to the predicted results. We generally use sensitivities that are logarithmically normalized using the maximum dependent solution variables—that is, computed temperature and species mole fractions—obtained on the entire domain (time interval of the calculation), namely:

$$S_k = \frac{A_k}{F_m}\left(\frac{\partial F}{\partial A_k}\right), \tag{4}$$

where S_k represents a sensitivity to reaction k, A_k is the Arrhenius A-factor for reaction k, F is the computed solution variable, and F_m is its predicted maximum value. Normalization in this way allows for ready comparison of relative sensitivities, both between reactions and at different times. Note that the predominant direction of a reaction can be its reverse, which can sometimes explain a sensitivity result with an unexpected sign; and in unusual cases, the predominant direction of a reaction can even change vs. time (distance along the flow) which can yield puzzling sensitivity results. The net direction of the reactions is not indicated in the sensitivities tables, though for the most important ones it can usually be determined in the pathway diagrams and may be mentioned in the text. As presented in section 5, the ability to analyze the detailed chemistry yields great insight into the reactions responsible for the predicted results, gives clues as to which reactions to study to improve the mechanism and was used extensively.

2.2 Chemical Mechanism

The mechanism for the present work was obtained by starting with the mechanism used by Miller and Anderson to model nitrate ester solid propellant combustion (*24*). We have recently updated this mechanism by incorporating revisions of our choosing to 5 species heats of formation and to 34 reactions. Most of the revisions have to do with nitrogen chemistry, especially N_xH_y reactions, because of a new interest we have developed in modeling propellants whose reactions may involve N_xH_y intermediates. The updates have produced only very modest or negligible changes for DZ results vs. the earlier mechanism, but we of course present results using our current best mechanism.* Because thermodynamics of the species, especially the heats of formation, can strongly influence calculations such as this, a listing of the values used is given in appendix A. The full mechanism is given in appendix B.

We have worked for many years developing mechanisms related to propellant combustion, with much of our effort focused on the DZ chemistry (see e.g., Anderson and coworkers [*3–10*]). DZ chemistry involves reactions of small molecules composed of H/N/C/O elements that underlie virtually all propellant mechanisms. The current mechanism is the result of continuing critical review of the literature beginning in about 1990; we have had many versions with a variety of updates. The primary source of reactions for the original version was the mechanism developed by Miller and Bowman and used in their milestone 1989 review of the chemistry of nitrogen in combustion, especially that relating to NO_x emissions (*63*); over the years, many, perhaps most, of their reactions and rate coefficient expressions have been retained. A second major source of reactions, especially those related to small hydrocarbon (HC) species combustion in air, was the mechanism of Smith et al., commonly referred to as the Gas Research Institute (GRI)-funded group and mechanism (*64*). However, after critical evaluation, we have included updates and additional reactions from many other sources, including some of our own works, and a few

*Note that electronic files containing both mechanisms may be obtained by contacting us. For the Miller and Anderson (*24*) mechanism, mention version 072398.062701, and for the current one, version 040610.

estimates by analogy by ourselves or others, though we have attempted to avoid the latter insofar as possible. Our revisions and amount of effort have, naturally, primarily focused either on reactions that were originally included that were found to be extremely important as a result of postprocessing study (pathway and sensitivity analysis) or a few new reactions we conjectured might be important and so included an estimated rate coefficient. In the remainder of this section, we give detailed discussions of a few reactions that are especially important for modeling DZ chemistry and structure. Detailed discussion for a few more reactions may be found in Anderson and Fontijn (*3*) and Anderson et al. (*7*). Brief discussions of our estimation or reanalysis of experiments used to obtain expressions for several of the other reactions in our mechanism are given in the notes to table B-1, appendix B.

2.2.1 HNO + NO = N_2O + OH

Typically,

$$HNO + NO = N_2O + OH \qquad (R19)^*$$

is one of the most sensitive reactions for nitrate ester DZ conditions (see section 5). Originally (*4*), we used k_{19} from Wilde (*65*).* Wilde's result was based on complex modeling of earlier static reactor experiments on H_2/NO mixtures, with an assumption that R19 is the primary radical source. His work of 1969 was performed when computer simulation was in its infancy, and ancillary kinetics data in his brief mechanism were not well developed. At our behest, Bunte et al. (*66*) performed QCISD (quadratic configuration interaction with single and double excitations) quantum calculations of the potential energy surface which showed that Wilde's activation energy was reasonable. These calculations also showed that an A factor considerably smaller than collisional, as Wilde reported, is plausible because the reaction proceeds through a 4-center, cyclic transition state, which would imply a loss of entropy at the transition state. These results confirmed Wilde's assumption that the reaction is reasonable. As discussed in more detail in Miller and Anderson (*24*), we (Anderson, unpublished, 1994) were in the process of reanalyzing the older, intermediate temperature H_2/NO mixture data (~900–1300 K) to obtain k_{19} with a more modern ancillary mechanism when we learned Lin and coworkers (Diau et al. [*67*]) had already reanalyzed that older data, as well as their new, similar data on H_2/NO and H_2/NO/CO mixtures. They obtained results very similar to our own and somewhat similar to Wilde's original result. However, in their analysis, they used an ancillary datum, $\Delta H^{\circ}_{f,298}$(HNO) = 23.4 kcal/mol, which resulted from BAC-MP4 quantum calculations (*68*). Although this value agrees well with the older JANAF (Joint Army, Navy, Air Force) recommendation, 23.8 kcal/mol (*69*), it is now known (*5*, *70*) to be in considerable error. The value 25.6 kcal/mol is currently recommended (*70*) and has been widely accepted (see, e.g., refs *71–73*). Differences of the BAC-MP4 method vs. experiment of 1–2 kcal/mol are common. Usage of the older datum

*"R19" means reaction 19 in our mechanism (see appendix A) and "k_{19}" refers to its rate coefficient expression. Also, –R19 and k_{-19} refer to the reverse direction. Where other, or no, nomenclature is used where a number after R or *k* would be expected, the reaction is not included in the current mechanism.

induces an error by about a factor of 2 in the computed concentrations of HNO in the various mixtures; the sensitivity of HNO concentration, in turn, is the result of a strong influence of the reactions that primarily control it:

$$H + HNO = H_2 + NO \,, \qquad \text{(R161)}$$

and

$$H + NO\ (+ M) = HNO\ (+ M) \,. \qquad \text{(R3)}$$

Both these reactions are, in some cases rather approximately, in partial equilibrium (forward and backward rates of nearly equal magnitude for both H_2/NO mixtures in the kinetics studies and also in nitrate ester DZ mixtures), which is controlled by the species' thermodynamics. For this reason, the assumed heat of formation of HNO changes the computed HNO concentration between the two enthalpy values for temperatures of interest. The consequence is that Lin and coworkers' fitted experimental rate coefficient expression is low by a factor of ~2 across the entire range of temperature in the experiments (900–1430 K). It should be noted that this revision makes agreement with quantum based calculations of Lin and coworkers somewhat tenuous at the high-temperature end of the range; our recommendation is larger than their quantum rate constant prediction by about a factor of 5 there. Lin (*74*) suggested this might mean there is instead some moderately important radical source reaction missing from the mechanism (note such a reaction could influence DZ mixtures as well as interpretation of the H_2/NO kinetics experiments). We agree this might be correct, but it is also possible this example is merely at the edge of typical agreement between experiment and theory. It would only take an error of ~3 kcal/mol in the reaction's barrier to produce an error of ~5 in the calculated rate coefficient; thus this is possible. In any case, the evidence for the revision of $\Delta H^{\circ}_{f,298}$(HNO) is quite strong (*70*). Since many other HNO reactions in the mechanism could be influenced by this datum, it must be used. This necessitates our current recommendation to increase Lin and coworkers' rate constant expression by a factor of 2, or else a serious error in the rate of R19 will be introduced. This rate coefficient very strongly influences τ_{DZ} and L_{DZ} for nitrate ester propellants (see section 5). The underlying chemistry and these effects will be further discussed in a later section. Obviously, further effort on these issues could be fruitful.

2.2.2 N + CO_2 = NO + CO

Many early mechanisms for combustion of propellants, especially those used for DZ modeling, have included the spin-forbidden reaction:

$$N + CO_2 = NO + CO \qquad \text{(HR1)}^*$$

*HR1 means "Hypothetical Reaction 1." It is not included in the reaction mechanism. –HR1, used subsequently, means the reverse of HR1.

(see, e.g., Fifer et al. [*36*]). This reaction is probably too slow in either direction to be significant to combustion (see below). Because there are initially high concentrations of NO and CO in DZ mixtures, and little N or other radicals, if HR1 is included in mechanisms, the reverse reaction, –HR1, is predicted to occur under DZ conditions and is typically an important radical source *in the model*. We became aware of this issue shortly after we began modeling DZ chemistry and examining DZ reaction sensitivities in the early 1990s. A literature review, presented in Vanderhoff et al. (*4*), immediately suggested that there was a serious error in the commonly used rate coefficient expression, k_{HR1}(291–523 K) = 1.9×10^{11} exp(–3.4 kcal/mol/RT) cm^3/mol/s, reported in Avramen'kov and Krasnen'kov (AK67) (*75*). The fairly large rates implied by this expression are surprising because of the required quartet to doublet electron spin change. Subsequent experiments of Herron and Huie (*76*) and Rawlins and Kaufman (*77*) showed a reaction in fact does not occur at low N-atom concentrations, at least for lower temperatures; reported upper limits to the rate coefficients were 1×10^8 cm^3/mol/s (550 K) and 6×10^4 cm^3/mol/s (300 K), respectively. These are factors of 80 and 10,000, respectively, lower than the expression of AK67. Furthermore, N-atom reaction order studies (*77*) revealed a second-order dependence, an indication that the reaction that actually occurred in the AK67 study was probably $N + N + CO_2 = N_2 + CO + O$; some of these products may be produced in excited electronic states since the reaction connecting the ground state species is 98.7 kcal/mol exothermic. The propellant modeling community has had considerable reluctance to remove HR1 from propellant models, probably because there was originally much difficulty predicting short enough DZ ignition delay times (lengths) without the radical source provided *in the models* by the reverse of HR1. Thus, at least until recently, there has been a strong temptation in the community to retain the reaction with the AK67 expression. However, we (Anderson, unpublished, 1995) had modeled the Lin and coworker isothermal reactor experiments (Diau et al. [*67*]) on H_2/CO/NO mixtures at ~1000 K shortly after they appeared and more recently presented a comparison (see figure 2a and 2b of Anderson and Fontijn [*3*]). A precursor of our current mechanism was used; the main difference from the current one was that hydrocarbon chemistry, which is unimportant for such mixtures, was left out. This model predicts overall reaction rates, e.g., from the CO_2 appearance profiles, in good agreement with the experiments; however, if HR1 is included with the AK67 expression, the computed CO_2 appearance rate is 100× too fast, which is a clear suggestion the reaction might need to be completely excluded. We have excluded it since about 1995 (cf. discussion in Anderson et al. [*7*]). But in the early 1990s, we were not sure the reaction does not occur significantly, especially at high temperatures, albeit with rates far less than suggested by the AK67 expression. At our behest, two further studies on HR1 were then performed. The first was a quantum study by Manaa and Chabalowski (*78*) that indicates the barrier to reaction—lowest point of the quartet-doublet curve-crossing—is ~37 kcal/mol above the reactants. This is far larger than E_a ~3.4 kcal/mol from AK67. The second was an attempt by Fernandez et al. (*79*) to measure the isolated reaction rate via the high-temperature photochemistry (HTP) method. However, once again, no reaction

was observed. A measured upper limit of 3×10^8 cm^3/mol/s was obtained for the 285–1142 K range, extending to temperatures much higher than the Herron and Huie and Rawlins and Kaufman experiments and nearly to those of DZ conditions. These several studies provide strong evidence that the AK67 result is incorrect, as our modeling of the Diau et al. experiments indicated, and that HR1 is negligible towards low combustion temperatures, e.g., as apply to the DZ ignition delay conditions.

We consider further whether HR1 might matter at higher temperatures. Lindackers et al. (*80*) performed high-temperature reflected shock measurements on C_2N_2/CO_2/Ar mixtures, following the N- and O-atom concentrations via atomic resonance absorption spectroscopy (ARAS). They obtained k_{HR1} (2510–3510 K) = 8.6×10^{11} exp(–2 kcal/mol/RT) cm^3/mol/s, which is ~5× larger than extrapolation of the AK67 expression would suggest. Using an estimated E_a ~37 kcal/mol from the crossing point computed by Manaa and Chabalowski (*78*), with a generous A factor of 2×10^{13} cm^3/mol/s (this is probably much too large, given that a quartet-doublet transition must occur), we estimate an upper limit, at 2510 K, for k_{HR1} of ~1×10^{10} cm^3/mol/s, which is a factor of ~50 smaller than Lindackers et al.'s expression. Lindackers et al.'s primary objective was to obtain rate constants for CN + CO_2 → NCO + CO. Our modeling of their experiments (not shown) agrees with them that only that reaction and C_2N_2 + M = CN + CN + M matter initially after the shock. Their results for CN + CO_2 were determined primarily by the early time data via analysis with those assumed reactions; thus those results appear to be valid. They fitted results at much later times to obtain rate coefficients for HR1 and two other N-atom reactions. However, results at later times involve species evolving secondarily via a more complex, less certain mechanism; several source and consumption terms for reactions of quite similar rates arise in the analysis, competing for N-atom fate. Also, we note the reactions N + NO = N_2 + O (R163) and N + NCO = N_2 + CO (R98), both of which have very large rate coefficients (see appendix B), were not considered in Lindackers et al.'s analysis. Their resulting rate constants of N atom reactions might therefore be subject to considerable systematic error. Additionally, Lindackers et al. mention the Arrhenius plots (log k vs. 1/T, not shown in their paper) for the secondary reactions, including HR1, exhibited considerable random scatter, which also suggests the possibility of problems. Furthermore, if we combine Fernandez et al.'s measured upper limit at 1142 K with Lindackers' result at 2510 K, we obtain k_{HR1} ~3.2×10^{14} exp(–31.5 kcal/mol/RT) cm^3/mol/s; since the Fernandez point is an upper limit, the A factor and E_a values of this expression are lower limits. Tests indicate that if the reaction is inserted in the mechanism using this expression, it would have important effects. However, it seems unlikely the actual rate constant expression is nearly so large. The A factor seems too large by at least a factor of 10 (compare to other reactions involving abstraction by N atoms, cf. Dean and Bozzelli [*81*], section 2.7.1). Furthermore, the A factor is likely even smaller than that since the reaction does not conserve electronic spin.

Finally, Sulzmann et al. (*82*) have studied NO/CO/Ar mixtures in a shock tube over the 3200–4500 K range, the upper temperature limit being much higher than typical combustion conditions. Upon shock heating, this mixture would *immediately* lead to occurrence of reaction –HR1 were it to have an appreciable rate. From the –HR1 endothermicity and the quartet-doublet crossing point estimated by Manaa and Chabalowski, the barrier to the reverse reaction is estimated as ~60 kcal/mol. Especially at the highest temperatures reached in the Sulzmann study, if the barrier were this low and the A factor appreciable, it seems –HR1 would have been observable. To the contrary, Sulzmann et al. found the CO_2 emission signal to initially be negligible, and further, to have zero initial slope. This result indicates CO_2 is produced only at later times via secondary reactions, not via –HR1. Unfortunately, no quantitation of the rate coefficient upper limit was given. These observations nonetheless suggest the reaction is negligible in either direction for combustion conditions.

Our current recommendation is to leave HR1 out for all conditions. The previous observations, especially the Sulzmann et al. study, suggest it is likely unimportant even for higher temperature combustion.

Our modeling tests indicate if HR1 with the AK67 (*75*) k(T), which is decidedly incorrect, is improperly included, then for typical nitrate ester DZ conditions (see, e.g., section 3.1), the predicted reaction orders, especially for CO, are far different from those predicted if HR1 is excluded, which is not at all surprising (not shown). Thus, if the reaction is included, not only will there be quantitative errors, but even the qualitative behavior as DZ mixture ratio is varied, e.g., as might occur due to propellant formulation changes, may be misleading. That is very significant, because one of the most important applications of propellant combustion modeling is formulation guidance. Fifer et al. (*36*) did include HR1 with the AK67 expression. Our tests also indicate when this is done, using either the Fifer et al. or the present mechanism, the effects on predicted ignition delays are very strong. The delays decrease (not shown) by factors of 2 to 4 vs. without the reaction for (1) nitrate ester DZs at all conditions of interest and for (2) nitramine DZs when it is assumed the initial N_2O concentrations are zero, a possibility explored by Fifer et al. (for an experimental study discarded in the present critical review). Effects on the two nitramine cases that survived our critical review (see sections 3.2.1 and 3.2.2) were negligible because the initial mixtures contained significant traces of N_2O; for these, the N_2O (+ M) → N_2 + O (+ M) reaction, R2, is by far the predicted major source of radicals, overshadowing HR1, even if it is incorrectly included.

We consider briefly whether modeling from a few studies in the literature may have been affected by inclusion of HR1. HR1 was first included in DZ modeling by Fifer et al. (*36*) and then by us (*4*), due to each starting with Miller and Bowman's 1989 mechanism (*63*), which included the reaction with the AK67 expression (*75*). Concern about the reaction is expressed in Vanderhoff et al. (*4*), where, as mentioned previously, our attention was initially drawn to it, and we first tested results vs. its inclusion. All portions of the Fifer et al. results based on predictions using their detailed mechanism are suspect. It appears inclusion of HR1 does not affect the

Miller and Bowman results because considerably detailed discussion of the reactions affecting the modeled mixtures is given therein and apparently the reaction played no significant role. To our knowledge, Miller and Glarborg, renowned NO_x chemistry experts and, more recently, frequent collaborators, have excluded the reaction from their many more recent mechanisms (see, e.g., Miller and Bowman [*83*] and Glarborg et al. [*84*]). Liau et al. (*17*) modeled RDX ignition and combustion. The mechanism from Yetter et al. (*30*), which has frequently been used in the development of RDX and HMX (1, 3, 5, 7-tetranitro-1, 3, 5, 7-tetrazocane) models (see the review, Anderson et al. [*7*]), contains HR1 with AK67 (*75*) *k*(T). Liau et al. used a modified version of that mechanism but retained HR1. Their results indicate a DZ forms in the RDX flames at 1 atm when the flame is augmented by CO_2 laser heating but not without the heating, in agreement with experiments. We have modeled, via the approach described herein, the evolution of Liau et al.'s computed initial DZ mixtures from their figures 4 and 13, using both our own and the Yetter et al.'s (*30*) mechanism, with and without HR1. The results are, fortunately, not strongly affected by HR1. We determined the reason is that there is initially ~0.05 mole fraction N_2O in the mixtures, a relatively large trace component. As mentioned previously, the N_2O has an overshadowing effect via the initiation reaction N_2O (+ M) → N_2 + O (+ M), R2.

2.2.3 NH + CO_2 = HNO + CO and NH + H_2O = HNO + H_2

Rorhig and Wagner (*85*) studied the reactions of NH with CO_2 and NH with H_2O in shocked mixtures in the range ~1250–1910 K. NH was produced in its electronic ground state by their newly developed method, thermal dissociation of HN_3, and monitored via ultraviolet (UV) absorption in its A-X system. With either reactant CO_2 or H_2O added to the mixtures, the NH concentration initially rises as HN_3 decomposes; then, after HN_3 is consumed, NH decays due to reaction, presumably with the added compound, thus exhibiting a single peak. Fits yielded NH disappearance rate coefficients, which they attributed to the following reactions:

$$NH + CO_2 = HNO + CO\ , \qquad \text{(HR2)}$$

and

$$NH + H_2O = HNO + H_2\ . \qquad \text{(HR3)}$$

The products were assigned based primarily on thermochemical considerations. However, considerable doubt has arisen. Lin and coworkers' thermostated reactor experiments on H_2/CO/NO mixtures (Diau et al. [*67*]) once again provide relevant tests. As mentioned in the previous N+CO_2 section, we (Anderson, unpublished, 1995) modeled this data shortly after it appeared, using a mechanism very similar to (a forerunner of) that in the appendices. Our modeling predicted overall reaction rates, e.g., of CO_2 growth, in good agreement with the experiments (see figure 2a of Anderson and Fontjin [*3*]). However, if either HR2 or HR3 is included with the Rohrig and Wagner rate constants, the rate is 10^3 or 10^4 times too fast (see figures 2c and 2d, respectively, of Anderson and Fontjin [*3*]). The error becomes cumulatively worse if the reactions are simultaneously added to the mechanism (not shown). In a second test

(not shown), we found when either or both of these reactions are included for DZ mixture predictions, the global chemical rates are so extremely fast—and thus τ_{DZ} and L_{DZ} shorter by several orders of magnitude—that were either of these reactions correct, no DZ would ever exist; that is clearly contrary to observations. We have therefore been excluding the reactions since about 1995. Two other independent experimental and modeling studies on H_2/CO/NO mixtures have recently been performed: (1) Glarborg et al., in flow reactor experiments, 1200–1800 K (*86*); and (2) Dagaut et al., in jet-stirred reactor experiments, 800–1400 K (*87*). Modeling in those works considered inclusion of one or both of HR2 and HR3. Those workers showed that predictions agree well with the experiment if the reactions are excluded, but, once again, the predicted overall reaction rates are far too fast if either is included. For all four tests, detailed chemical analysis of the solutions revealed that HR2 and HR3 reverse, providing a major radical source via the NH so produced, *in the models*. We determined this occurs because the reactions H + NO (+ M) = HNO (+ M) and H + HNO = H_2 + NO have very roughly equal forward and reverse rates, thus creating significant traces of HNO along with the abundant NO, H_2, and CO in DZ mixtures (see section 3), while there is little NH radical in the original mixtures. The differences vs. the four experiments were a strong suggestion of some error in Rohrig and Wagner (*85*).

Rohrig and Wagner had also reported on the following:

$$NH + H_2 = NH_2 + H \ . \qquad (–R124)$$

Therefore, to provide independent testing of the shock tube studies, we teamed with the Fontijn group to study NH + H_2 in HTP experiments (*88*). NH was produced by multiphoton photolysis of NH_3. Our results for –R124 were in excellent agreement with Rohrig and Wagner's; this suggests the problem with their results for HR3 and HR4 is unlikely to be with their novel NH production method and resulting reactant disappearance rate coefficients. It seems much more likely to be with their suggested products. Ab initio calculations on NH + CO_2 were therefore also made (*88*). These showed barriers to the HNO + CO product are far larger than the measured (*85*) disappearance reaction's activation energy, and no other bimolecular product channel is thermodynamically feasible. Therefore, a role for an as yet unidentified stable addition product seems indicated. The ab initio study suggested some possible adducts, but all were of low stability and would likely undergo further reactions. All three reactions, NH with H_2, H_2O, and CO_2, were also independently studied via quantum methods at about the same time by Mackie and Bacskay (*89*). Their results were supportive of present conclusions—namely, their rate constant expression for –R124 agrees reasonably with the previously mentioned experiments (*85, 88*), and no low-energy pathway to the HNO product channels could be found for the reaction of NH with either CO_2 or H_2O. For the H_2O reaction, Rohrig and Wagner pointed out the formation of two adducts, H_3NO and H_2NOH, is thermodynamically feasible. The barrier to these on the singlet surface, per Mackie and Bacskay, is also much larger than Rohrig and Wagner's measured E_a. However, the possibility that one of these adducts may be formed by a low-energy intersystem crossing may need further study. It seems unlikely the

reactions of NH with CO_2 or H_2O in the forward direction to any products would matter for propellant combustion because concentrations of NH are generally very low, especially for DZ conditions; thus, it seems justifiable to ignore them. Clearly, however, further study of these reactions is warranted, especially since they might impact NO_x emissions chemistry.

2.2.4 Reactions Related to HCN Consumption Pathways

As previously mentioned, HCN is very important in nitramine DZs. There is a significant controversy concerning the HCN chemistry which needs further study. Via ab initio-based rate coefficient estimates, Lin and coworkers (*90*) have suggested that the following H-atom shift isomerization reaction:

$$HCN + M = HNC + M \,, \qquad \text{(R194)}$$

followed by the reactions

$$HNC + O = NH + CO \,, \qquad \text{(R167)}$$

$$HNC + O = H + NCO \,, \qquad \text{(R168)}$$

and

$$HNC + OH = HNCO + H \,, \qquad \text{(R169)}$$

are very significant pathways for HCN consumption in combustion. However, Hanson and coworkers (*91*) have suggested that these may be unimportant and only

$$HCN + OH = CN + H_2O \qquad \text{(R75)}$$

need be considered. It is our current recommendation that the ab initio results are probably reasonable, and thus all these reactions should be considered. But the subject is clearly very important and needs further study. Formation of NCO and HNCO brings in considerable complexity because of competition between possible pathways and product-branching reactions:

$$HNCO + H = NH_2 + CO \,, \qquad \text{(R181)}$$

$$NH_2 + NO = NNH + OH \,, \qquad \text{(R147)}$$

$$NH_2 + NO = N_2 + H_2O \,, \qquad \text{(R148)}$$

$$HNCO + OH = H_2O + NCO \,, \qquad \text{(R178)}$$

$$NCO + NO = N_2O + CO \,, \qquad \text{(R101)}$$

and

$$NCO + NO = CO_2 + N_2 \,. \qquad \text{(R102)}$$

In fact, sensitivities to many of these reactions are high for nitramine DZ conditions, as will be shown in section 5.

2.2.5 Note on Possible HNOH and NH_2O Chemistry

We have assumed in the current work that the species HNOH and NH_2O, which have been included in some recent NO_x mechanisms (see, e.g., Dean and Bozzelli, DB00 [*81*]) are unimportant. Towards the end of the preparation of this manuscript, it occurred to us that this might be incorrect. Our thought was that these species might form via the two recombination reactions HNO + H + M = X + M, where X represents HNOH or NH_2O. Either species once formed might then react with H, namely X + H = NH_2 + OH. The NH_2 would then react with NO, producing predominantly NNH + OH (R147), and some N_2 + H_2O (R148). The sequence is chain-branching. Thus, although it seemed unlikely to us since the [HNO] is small, this had potential to shorten predicted τ_{DZ} values significantly. We have recently added 15 reactions of these two species to the mechanism of appendix B and run tests; these included reactions of HNOH and NH_2O with H, OH, O, and NH_2. The reactions and their kinetics parameters were obtained from DB00's recommendations (see their table 2.19). Reactions chosen were their numbers 37a, b, c1, c2, d, e, g, 38a, b1, b2, c1, c2, d, f1, and f3. For the three reactions involving nonreacting colliders, the low-pressure limit expressions were chosen. Note that DB00 assumed pure N_2 as the collider, so we inserted estimates for collider efficiencies of some other species: N_2O = 5.0, H_2O = 7.0, O_2 = 0.82, CO_2 = 2.0, NH_3 = 5.0, and NO_3 = 5.0. DB00 wrote some of the reactions in the reverse direction to that discussed here, and we used them in that form; as mentioned previously, our codes automatically compute and include reverse reactions. Thermodynamics for HNOH and NH_2O were also obtained from DB00, their table 2.2. Upon inclusion of this chemistry in our mechanism, the nitramine DZ delays were shortened by less than ~0.1%; the nitrate ester DZ delays were shortened by about 1%. Species and temperature profiles also were little affected. Tests included all of the retained experimental datasets that were at single pressures and several selected pressures across the full ranges of those wherein pressure was varied. Tiny traces of HNOH and NH_2O are predicted to form not only from the two HNO + H + M recombination reactions, as expected, but also from the two HNO + H_2 = X + H reactions. Thus, HNOH and NH_2O chemistry is found to be negligible, although apparently if it were about 10× faster, revisions to the current work might be necessary. This chemistry was therefore excluded.[*]

[*]It would be wise to also consider these species in future works. A version of our mechanism with the added reactions is available upon request. Please cite 040610.wHNOH. Note, though, that the recombination reactions are written for the low-pressure limit. For applications at very high (e.g., gun) pressures, and perhaps also at lower temperatures, falloff of these reactions might have to be considered.

3. Critical Selection of Experimental Datasets

In this section, we present our critical evaluation of experimental datasets available for testing DZ chemical kinetic models. Those that can be used are discussed. It is also explained why some promising looking datasets must be discarded.

To reiterate from section 2.1, to determine τ_{DZ} from the experimental literature, one needs the following measured data: DZ temperature, DZ length, and the solid propellant's density and burning rate at pressure of interest. To model the τ_{DZ} and then compare it to the experiment, one needs, in addition to pressure and initial DZ temperature, the measured initial species concentrations in the DZ. We performed a thorough literature search for acceptable datasets and find there are not many; this is no surprise since measurement of species and temperature in propellant flames is quite challenging. The list of accepted datasets is further restricted by several criteria we judge to be very important: (1) species and temperature profiles must be of large enough signal-to-noise ratio that they do not strongly vary due to random fluctuations within the DZ, thus allowing meaningful determination; (2) where possible to examine photographs, check that the flame appears one dimensional and laminar; (3) atomic mass balance within the DZ is reasonably preserved; and (4) if it is possible to perform an energy closure test, the results are self-consistent. Atomic mass balance means, of course, the atom ratios inferred from the measured species mixture in the DZ match those of the initial propellant mixture. Since major species and temperature gradients are small in the DZ, diffusion is also. Therefore, if only gaseous DZ components are present, the element ratios there must match those of the propellant. Energy closure testing means the enthalpy of the DZ mixture matches that of the initial propellant; this is tested by running the NASA-Lewis equilibrium code (*92*) to predict adiabatic flame temperatures (T_{AD}) of both the propellant and the measured DZ mixture to see if these match reasonably well. If tests (3) and (4) are not met, this indicates something is seriously internally wrong with the dataset and it cannot be trusted. Items (1) and (2) cannot be checked for all datasets we found because, in many cases, we only have species and temperature measured at "some position within the DZ," and many, perhaps most, publications did not include photos of "typical" flames. We did form a general impression of the comparative quality of the datasets—the nitrate ester DZ measurements typically have smaller error limits than the nitramine DZ measurements. One likely reason for this is flame flicker (unsteadiness), which, if strong, is an inherent quality of a given propellant that is difficult to avoid. B. E. Homan, an ARL colleague who has performed many strand burner experiments, has informed us (*93*) that there is at least mild flickering of virtually all propellant flames, probably much more than writings in the area and still photos of "typical" flames suggest. Furthermore, this flickering tends to be more pronounced for nitramine than for nitrate ester propellants. This tendency vs. propellant types may be the result of inherent heterogeneity of nitramine propellants (crystals of nitramine held within a binder), as opposed to the more homogeneous nitrate ester type, or

perhaps to the typically lower energy content of nitramine types, as evidenced by their lower adiabatic temperatures, which might lead to lower gaseous flame velocities and stability. Note, if flicker is strong, as suggested in a few discarded cases, probably the flame is, indeed, not strongly stabilized against the propellant surface.

In any case, as will be seen, not many published datasets meet all the previous criteria. The experiments to obtain the data are challenging and involved, and the required instrumentation is typically complex. There are more surviving datasets for nitrate ester than for nitramine propellant types. In the following two subsections, we discuss first nitrate esters, then nitramine propellants. Within each subsection, we first discuss all datasets that are retained, and then some that appeared promising but ultimately were discarded. Note that in most of the cases we have retained, we had to estimate at least one crucial datum that was not measured, frequently due to limitations of the diagnostics used. For example, one frequently missing datum is H_2O concentration. This species is always present. Its concentration could not be determined in some of the studies due to physical sample collection in cells or gas lines, where its condensation and/or adsorption on walls is notoriously problematic. If we had not made these estimates, almost none of the datasets could be retained, making this study impossible. However, we are reasonably comfortable with the estimates. We will not discuss discarded datasets for which the reason for their exclusion is obvious, such as missing key quantities that could not be estimated reliably. It should be noted that in some cases, the mole fractions in the tables do not total exactly 1.0, due either to slight measurement errors or our error in digitizing plots. In those cases, our codes automatically normalize the initially input mixture mole fractions.

3.1 Nitrate Ester DZ Datasets

Four nitrate ester studies provide information of sufficient detail for modeling and survive the various tests. Three of the studies provide pressure-dependent data so that our understanding of one of the most important factors affecting DZ structure can be examined. Details concerning these studies, and one which was discarded, form the rest of this section.

3.1.1 Heller and Gordon, Double-Base Propellants

Heller and Gordon (*94*) (HG55) studied the burning rates and flame structures of three double-base, NC/NG (nitrocellulose/nitroglycerine) propellant formulations in a strand burner over the pressure range 11.2–35.0 atm.* Their mixture, PL-673, which had NC/NG = 55/45 with 12.6% N in the NC, is selected as our primary focus because the % N was only mentioned for this case. However, HG55 obtained results for all three mixtures; the PL-673 results are well representative. Photography was used to determine burning rates and DZ thickness. Temperatures were measured using Pt/Pt-10%Rh thermocouples of three sizes. A few runs were made with embedded thermocouples of very small diameter wire—7.5 μm—to obtain the near-

*Note that Heller and Gordon used PSIG units, which is 1 atm below the absolute pressure and thus must be corrected by this amount, in most of their paper, but PSIA units, the absolute pressure, in one figure.

surface T profiles given in their figure 2. However, most of their runs were made with thermocouples of 25- or 75-μm wire initially held against the burning propellant surface by a 5-g mass, probably hanging on the thermocouple wire towards one side, and then the thermocouple was allowed to rise into the DZ (their paper is not entirely clear about the exact geometry and procedure). They thus obtained only two main T data each for most of the runs—at the surface and in the DZ plateau region (see their figure 4). Tests were made with either bare thermocouples or with a variety of coatings; lack of variation in results indicated no significant systematic problems were present due to surface catalysis. However, after several careful readings and deliberation, we are convinced that no radiative energy loss correction was made to the thermocouple measurements. Further discussion and implications of this are given later. Both the surface and DZ temperatures increase with pressure. Gas samples were extracted into evacuated flasks using Vycor probe tubes, treated with P_2O_5 to remove H_2O (which was thus not quantified), and analyzed by infrared absorption and mass spectrometric techniques. Mole fractions of the extracted DZ mixtures were determined. These mole fractions without H_2O sum to unity; this must be taken into account when using their results.

HG55 made important observations concerning trends vs. the three propellant formulations at various pressures. A plot of their L_{DZ} results from their table II is shown in our figure 3. As expected, L_{DZ} decreases monotonically vs. increasing P. Note that one of the points, lot PL-673 at "26.0 atm" and having L_{DZ} = 8.3 mm, falls far from the curve defined by the rest of the data. In their table II, this point appears with P = 367 PSIG (pounds per square inch gauge), which corresponds to 26.0 atm. However, all points in their table, except this one, are arranged in order of increasing pressure. The point appears roughly in the middle of the dataset, between entries for 250 and 300 PSIG. We believe HG55 had a transcription error for this entry, and that it was actually taken at 267 PSIG, which corresponds to 19.2 atm; we proceeded using this assumption. When this "special" point is replotted at 19.2 atm, it is in excellent agreement with the trend in the rest of their data, (see figure 3). HG55 concluded L_{DZ} does not vary much vs. the formulations (the three lots having NC/NG = 55/45, 57.5/40.9, 54.51/44.6, with % N of the NC not mentioned for the latter two); indeed it does not vary within the scatter. Note the scatter about the trend is roughly 1.5 mm, regardless of P; thus, the relative contribution of error in L_{DZ} to error of derived quantities increases vs. P. The values of L_{DZ} for PL-673 from HG55's table II were analyzed in combination with the other data described in the following paragraphs to obtain experimental τ_{DZ} values. Scatter in L_{DZ} was considered in the determination of, and was the main contributor to, the error limits.

Analysis of the gas-phase samples indicated the DZ is composed primarily of major species N_2, NO, H_2, CO, CO_2, 0.01 to 0.02 mole fractions of trace hydrocarbons CH_4 and C_2H_4, perhaps very small and uncertain traces of ~0.001 HCN and ~0.0005 C_2N_2, and, of course, the unmeasured major species H_2O (see HG55's figure 3 and table III). The HCN and C_2N_2 exhibit considerable relative scatter, but this is likely due to being near the limits of detection. The five detected major species and CH_4 do not vary much vs. P or propellant formulation. C_2H_4 has considerable

scatter but may decrease from about 0.013 to 0.008 mole fraction from the low to high P limits of the range of present interest (11.2–35.0 atm); except where it was removed for tests as noted, we used 0.01 for the present calculations. We discuss in section 4 the modest effects of CH_4 and C_2H_4, and negligible effects of HCN and C_2N_2 on predicted τ_{DZ} values (see section 4.2.1); except for this testing, initial HCN and C_2N_2 concentrations were assumed to be zero. Mole fractions extracted from HG55 figure 3 define the ratios of most of the DZ species; the mixture was then corrected for an H_2O concentration estimated as discussed later (see results in table 1). This mixture was one of the inputs used in our modeling presented in section 4.2.1. Note the unmeasured H_2O is listed in table 1 at 0.25 mole fraction. We inferred this value via assuming energy closure and that the DZ consisted only of gas-phase species and all except H_2O were detected. The unburnt propellant atomic ratios are C: H: N: O = 19.6: 27.4: 11.8: 41.2. HG55 suggested the mole fraction of H_2O is "about 30%" based on the respective element ratios of "17 : 28 : 12 : 38 for most of the samples" (which is 17.9 : 29.5 : 12.6 : 40.0 when normalized to 100) that this yields. However, we have determined that assuming 0.25 mole fraction H_2O yields ratios that also agree reasonably, the respective atomic ratios of the table 1 mixture being 17.5 : 30.8 : 12.1 : 39.6. The mole fraction used for H_2O was determined by comparing computed adiabatic flame temperatures of hypothetical DZ mixtures to those of the propellant at several pressures, while varying the assumed initial amount of H_2O in the former. Ratios of the other DZ components were preserved at their measured values and the mole fractions renormalized, while the T_{DZ} values used were obtained for each P as described in the next paragraph. The calculations were done at four pressures representative of the range, P = 11.2, 18.0, 22.1, and 35.0 atm. T_{AD} of the propellant is found to be 3047, 3086, 3102, and 3138 K, respectively. For the DZ mixtures in table 1 with 0.25 mole fraction H_2O, we obtain T_{AD} = 3013, 3074, 3107, and 3173 K, respectively. The agreement is excellent at the center, and ~35 K low or high at the limits, of the P range, which is good. Agreement becomes considerably worse at one of the limits for assumed 0.24 or 0.26 mole fraction H_2O. For 0.30 mole fraction H_2O, recommended by HG55, DZ mixture T_{AD}'s are considerably too low; probably they could not calculate T_{AD} accurately in 1955 due to lack of computers and/or accurate thermal data, so a better estimate was not possible. Since H_2O could not be measured by HG55, an energy closure test on the dataset is not possible; rather it is used to estimate H_2O concentration. However, the fact that the concentration thus derived yields reasonable element ratios is a reassuring cross-check on the internal consistency of the results. Note that our predicted τ_{DZ} values are only affected by a few percent vs. this change in H_2O concentration (not shown).

Values of r_b were extracted from HG55's figure 1 of r_b vs. P. Initial estimates of T_{DZ} were obtained from a fit to HG55's data in their figure 4 of T_{DZ} vs. P. However, as mentioned previously, HG55 apparently assumed the radiative correction to be unimportant. This would be true for the fine-wire thermocouples used to obtain the near-surface T profiles. However, we estimate the correction for the larger 25- and 75-μm wires used for their figure 4 data to be ~50 K, assuming a thermocouple bead size twice the wire diameter and using the techniques described in Venizelos and Sausa (*95*) and Martins et al. (*96*). Therefore, for each pressure, we

added 50 K to the initial T_{DZ} estimates taken from HG55's figure 4. Our predictions are very sensitive to this correction, as discussed in section 4.2.1; the possible error in estimating the exact correction, in addition to the scatter in the T_{DZ} vs. P plot, was considered in our error analyses. Note that HG55 cited Klein et al. (*97*) regarding how thermocouple measurements can be applied in burning propellants; that short paper discusses both surface catalysis and radiative loss effects, so HG55 apparently were aware of both possible issues. They only mentioned checking for catalysis effects, finding them to be negligible. They did not mention correcting for the radiative effect. Since corrections or checking for either effect require considerable effort, it seems they would have mentioned any that were done; it is therefore most reasonable to assume they also thought that effect to be negligible. Indeed, a correction of 50 K is fairly small, of the same order as the scatter in the data, and they may have ignored the effect on this basis. Alternatively, they may have noted the correction was negligible in Klein et al. and simply assumed this applied to their work as well; it did apply for their T-profile runs, for which very fine wires were used, but not for the larger thermocouples used for the bulk of their experiments. L_{DZ} results for the lot PL-673, for which the composition is best defined, are well representative of the three propellants, and therefore these are selected for our testing. The P, r_b, T_{DZ}, and L_{DZ} data are summarized in table 2. These data were combined in equation 3, along with an assumed ρ_s of 1.6 g/cm^3, which is appropriate for NC/NG mixtures (*24*), to extract experimental τ_{DZ} values (see table 2). HG55's mixture ratios and T_{DZ} values at the various pressures define initial conditions for the modeling calculations to obtain predicted τ_{DZ} values, as discussed in section 4.2.1. Despite its limitations, this excellent, pioneering contribution, based on old, simple techniques, remarkably remains one of the most informative available on solid propellant DZ structure and behavior.

3.1.2 Aoki and Kubota, Double-Base Propellant

Aoki and Kubota (*35*) (AK82) performed strand burner studies on 12 double-base propellants composed primarily of NC and NG with two additives—diethylphthalate (DEP) and 2-nitrodiphenylamine (2NDPA)—across the pressure range 2–80 atm. Photography and embedded thermocouple methods were used to measure r_b, T_{DZ}, and L_{DZ}. Similarly to HG55, when comparing at the same pressures, they found L_{DZ} to be invariant vs. composition, within error limits, for those propellants for which it was measured and for a wider range of compositions. Fine-wire thermocouples were used for temperature measurements, making radiative corrections unnecessary. They used the procedure and assumptions described in section 2 to extract measured τ_{DZ} values. No species measurements were made. However, the propellant they refer to as "EC-1" has small amounts of the additives and a formulation close to the PL-673 propellant of HG55 (see prior subsection): NC/NG/DEP/2NDPA = 53.0/40.5/4.0/2.5, with 12.2% N in the NC. As previously mentioned, the HG55 study indicated that at least for mild variations in double-base propellant formulation, the DZ mixture ratio does not vary. Along these lines, note that DZ mixture results for several propellants similarly composed primarily of NC and NG are gathered and compared in Miller and Anderson (*24*), table 9; most

are measured, albeit a few with only partial species information, while one is from a calculation (*24*) of the entire gas-phase flame structure. In addition, measured DZ mixtures for two rather dissimilar nitrate ester cases are discussed in the next two subsections: JA2 propellant and the pure ingredient BTTN (1-, 2-, 4-butane triol trinitrate). DZ mixture ratios for all of these cases are similar.* Also, we note that the two additives present in EC-1 in small amounts would likely not affect DZ mixture much; in particular, considering their molecular structure, we would not expect them to produce DZ molecules of identity different than those observed for a typical nitrate ester propellant, e.g., we do not expect they would produce N_2O or HCN as for a nitramine propellant (see section 3.2). Consequently, we believe it is justified to assume the initial AK82 DZ mixtures are nearly identical to those of the HG55 study. The assumption allows us to add a dataset to the few available for DZ model tests; note especially the attractive feature that a range of pressures was studied. Because of similarity of AK82's EC-1 to HG55's PL-673 propellant and satisfaction of the element closure test for the latter, it must also be satisfied for the former.

AK82 combined r_b, T_{DZ}, and L_{DZ} with an assumed ρ_s of 1.6 g/cm^3, which is appropriate for NC/NG mixtures (*24*), to extract experimental τ_{DZ} values for 10–32 atm; we also similarly digitized and analyzed data from their figures 2, 8, and 9, obtaining slightly differing results (see table 3). AK82 computed an adiabatic flame temperature of 2756 K for the propellant starting at 1 atm, 298 K. Using their measured T_{DZ} = 1323 K at 1 atm and the DZ mixture from table 1, we compute 2731 K with and 2745 K without the trace hydrocarbons. Either agrees well with AK82's propellant T_{AD}; thus, the dataset survives the energy closure test. Our predicted values of τ_{DZ} , based on the mixture that includes the trace hydrocarbons, are compared to the experimental results in section 4.2.2.

3.1.3 Vanderhoff and Coworkers, JA2 Propellant

Vanderhoff and coworkers (*53*, *98*) (VKMT-JA2) performed two studies on JA2, a nitrate ester propellant composed primarily of NC, NG, and DEGDN (diethylene-glycol dinitrate). Measurements from the studies can be combined to obtain a test case at 16 atm. Ultraviolet absorption spectroscopy was used to measure NO, some radical species concentrations, and temperature, while infrared absorption spectroscopy was used at 10 atm for NO, CO, CO_2, and H_2O concentrations. Measured mole fractions of these species at 10 atm are given in table 4. From Vanderhoff et al. (*53*), L_{DZ} for 16 atm is observed to be 0.9 ± 0.1 cm from NO and T vs. distance profiles in their figures 5 and 6, and T_{DZ} is 1500 ± 100 K from their figures 6 and 7. The HG55 results (see section 3.1.1) indicate major species concentrations in the DZs do not change much vs. pressure for NC/NG propellants, and figure 7 of Vanderhoff et al. for NO vs. P indicates this is also true for NO in the similar JA2 propellant. So, to obtain a test case at 16 atm, we assume the four measured mole fractions at 10 atm are also appropriate for 16 atm. N_2 and

*This, incidentally, likely has much to do with why HG55 and AK82 found L_{DZ} values to be invariant vs. propellant compositions.

H_2, which could not be measured by the techniques used, are expected by comparison with HG55 (see table 1) and Lengelle et al. (*40*) (see their table 4A, ONERA entry) to be present at about 0.03 and 0.08 mole fraction, respectively. The C : H : N : O ratio for the propellant is 20.7 : 30.5 : 10.5 : 38.3. Assuming the DZ is composed of the six species at the mentioned mole fractions, the element ratio is then 20.1 : 25.4 : 11.5 : 43.0, in fair agreement. The adiabatic flame temperatures at 16 atm are computed as 2866 K for JA2 and 2983 K for the DZ mixture, also in fair agreement. Curiously, though spectra through the JA2 DZ region suggest a small peak due to CH_4, it is concluded the concentration of CH_4 is negligible, while no mention is made of C_2H_4; were these species closer to 0.01 mole fraction, as in HG55's NC/NG propellant, and taken into account, the DZ mixture's computed adiabatic temperature would be slightly lower, in better agreement with that of the propellant. The possible effect of a trace of CH_4 on the predicted delay time is discussed in more detail in section 4.2.3. The solid propellant density is estimated as 1.56 g/cm^3 in Miller and Anderson, and the burning rate of 0.30 cm/s at 16 atm is obtained from unpublished strand burner experiments of M. S. Miller, 1993, as shown in figure 10 of Miller and Anderson (*24*). Combining the necessary data in equation 3 yields an experimental τ_{DZ} of 6.5 ± 0.8 ms. Our predicted τ_{DZ} value using the initial DZ mixture conditions is compared to this result in section 4.2.3.

3.1.4 Parr and Hanson-Parr, BTTN

Parr and Hanson-Parr (*99, 100*) (PHP-BTTN) studied BTTN, a nitrate ester propellant ingredient of molecular structure similar to NG, over the range 0.92–51.0 atm. A tube-type burner system with constantly fed liquid BTTN was used. Gas-phase species concentration profiles were measured by Raman spectroscopy, while temperature profiles were measured using thermocouples (radiative corrections were included, per T. Parr [*101*]) and/or Raman stokes/antistokes ratios on a number of the species. However, species and temperatures were only measured at 0.92 atm. The measured species concentrations in the DZ are given in table 5. We ignore five species for which only small measured upper limits were listed; these are highly unlikely to have significant effects. A more important point is that PHP-BTTN mention an unidentified peak, likely due to a hydrocarbon, was observed in the Raman spectrum in the DZ and may be the primary reason that the mole fractions of identified species sum to less than unity (~0.89–0.91). We assumed this and any other undetected species are negligible and renormalized the measured concentrations (see table 5). We also assumed the variation in DZ mixture ratios vs. P is negligible, as suggested by HG55 and VKMT-JA2 results presented for solid nitrate ester propellants previously. Both energy and element balance checks work out very well using this mixture (see next paragraph), suggesting concentration of any unknown species was small. Calculations on HG55 mixtures with and without trace hydrocarbons CH_4 and C_2H_4 suggest effects of any unidentified hydrocarbon trace species on the τ_{DZ} predictions for these similar BTTN mixtures would be small if it could be included (see section 4.2.1).

The measured T_{DZ} at 0.92 atm is 1200 K. Measured r_b and L_{DZ} values (*100*) are given in table 6; note that the P range of data useful for present DZ model test purposes is restricted to ~10–20 atm, the range at which L_{DZ} could be measured. T_{DZ} values at P higher than 0.92 atm had to be estimated by analogy; these values rise vs. P for HG55 (see table 2) and AK82 nitrate ester propellants (see table 3). The relative increase in T_{DZ} vs. P for BTTN was assumed to be similar to that in these analogous nitrate ester experiments (see our T_{DZ} estimates for higher P in table 6; see also the plot of HG55 and AK82 results in Lengelle et al.'s figure 19 [*40*], which was very helpful in making the estimates). It is quite plausible per combustion modeling results on BTTN in Puduppakkam et al. (*102–104*), however, that the T_{DZ} values at the highest pressures might be as much as 100 K larger than we have estimated.* Puduppakkam et al. cited $\Delta H^{\circ}_{f,298}$ (BTTN) values of –93.03 or –98.9 kcal/mol and recommended the former for use in their calculations, which we have therefore adopted, and ρ_s = 1.520 g/cm^3. We calculated adiabatic temperatures for the former BTTN enthalpy (see the dependence on P in table 7). The results are about 15–20 K smaller for the latter enthalpy (not shown). There is a stronger dependence upon pressure. Using the measured DZ mixture and T_{DZ} values at 0.92 atm and estimated T_{DZ} values for higher P, predicted adiabatic temperatures are in good agreement with those of the pure BTTN (see table 7). Finally, PHP-BTTN found the element ratios comparison check was excellent, even though having to ignore the species related to the unknown peak; the C : H : N : O ratios were 17.4 : 30.4 : 13.0 : 39.1 and 16.8 : 28.6 : 12.5 : 42.2 for BTTN and DZ mixture, respectively (*99, 100*). The experimental data are combined in equation 3 to yield measured τ_{DZ} values (see the next to last column of table 6). Predicted τ_{DZ} values based on these inputs are compared to these experimental values in section 4.2.4.

3.1.5 Discarded Nitrate Ester Dataset

Korobeinichev et al. (*105, 106*) studied several propellants using mass spectrometric and thermocouple techniques. The nitrate ester "propellant N" is of interest. They provided structure data for a 15-atm flame from which one apparently can derive a nearly complete DZ test dataset. However, (1) the exact propellant composition was not given, so we cannot test element conservation, (2) the H_2O was inferred from mass balance, and (3) r_b and ρ_s are not known. From Korobeinichev at al.'s profiles figure, the measured final flame temperature, which is typically very close to T_{AD} for nitrate ester propellants, was 1800 K. Using the measured DZ conditions from their figure of T_{DZ} = 1420 K and mole fractions CO : NO : H_2O : H_2 : CO_2 : N_2 = 0.37 : 0.065 : 0.08 : 0.25 : 0.15 : 0.095, we compute T_{AD} of the DZ mixture = 1953 K, which is uncomfortably high. The authors also note considerable soot formed, which was not quantified; this might have nonnegligible effects. T_{AD} for this propellant is very low compared to typical propellants (see prior subsections), suggesting the formulation is very different from others considered herein. Thus, it would be unwise to assume that r_b for this one is close to the others. For these several reasons, we concluded this dataset cannot be used for present tests.

* Also see, in particular, figure 18 of the solid propellant modeling review (ref *18*); this figure is credited to the study resulting in ref *104* but apparently appears only in ref *18*.

3.2 Nitramine DZ Datasets

Two nitramine propellant studies provide information of sufficient detail and survive various tests. Unfortunately, both were at only a single pressure. Also, the second of these presents an unusual issue that may create some doubt about its validity as a test meeting assumptions used in our model; this will be discussed in later sections. We also discuss reasons a number of cases have been discarded. It is particularly unfortunate that we have discovered a study that we modeled in some of our prior papers, which included pressure dependence, had to be discarded.

3.2.1 Parr and Hanson-Parr, HMX/GAP/BTTN Propellant

Parr and Hanson-Parr (*107–109*) (PHP-HMX) studied a propellant formulated of HMX/glycidyl azide polymer (GAP)/BTTN at 0.92 atm. Species and temperature profiles were measured by a combination of planar laser-induced fluorescence (PLIF), UV/VIS absorption, and laser Raman spectroscopies, and thermocouple techniques (radiative corrections were included, per T. Parr [*101*]), and, for a few of the species, atom balance considerations. The leading edge of the DZ was taken to be at ~0.15 cm, based on the NO profile; difficulty in defining this point makes initial DZ concentrations of N_2O, NO_2, and CH_2O rather uncertain since they vary in this region, so sensitivity of the modeling results to their initial concentrations is considered in section 4.3.1. The measured mixture at the leading edge of the DZ extracted from PHP-HMX's (*107–109*) figures is given in table 8. Since atom balance was used by the authors to derive the concentrations of several species, the elemental ratios were perfectly preserved by their assumption and therefore cannot provide a consistency cross-check of this aspect. However, the measured DZ species mole fractions in table 8 and T_{DZ} (discussed at the end of this section) seem reasonable upon comparison with other, partial datasets for nitramine propellants (*4*, *37*). The energy balance test is possible, however, and is reassuring. Chosen $\Delta H^{\circ}_{f,298}$ values of HMX and BTTN are 21.0 (*110*) and –93.0 (*102*) kcal/mol, respectively.* For GAP cured as described in PHP-HMX, we estimate a heat of formation of 0.184 kcal/g via the correlation developed in Puduppakkam and Beckstead (*112*) for the dependence on hexamethylene diisocyanate (HMDI) curing agent fraction. Using these data, we calculate an adiabatic flame temperature of 2809 K at 0.92 atm for the propellant. The measured burnt gas flame temperature from the OH PLIF measurements is about 2800 ± 100 K, in excellent agreement. For the measured DZ mixture with best measured T_{DZ}, we calculate an adiabatic flame temperature of 2789 K; with T_{DZ} set instead to the upper end of its measurement limit, we calculate 2830 K. The measured final temperature and calculated adiabatic flame temperatures agree reasonably well. The measured L_{DZ} and T_{DZ} from their figures are 0.28 ± 0.12 cm and 1450 ± 100 K, respectively, while the measured r_b is 0.0495 cm/s (*109*). ρ_s is estimated as 1.77 g/cm^3 using HMX, GAP, and BTTN

*For HMX, the heat of formation resulting from the critical review of Lyman et al. (*110*) is presently much more defensible than the often cited (e.g., Washburn et al. [*111*]) 17.9 kcal/mol value. However, the adiabatic flame temperature results are only affected by ~5–10 K vs. this choice.

densities of 1.90 (*111*), 1.27 (*112*), and 1.52 (*102–104*) g/cm^3, respectively. These data combined in equation 3 lead to $\tau_{DZ} = 0.64 \pm 0.28$ ms. Predicted τ_{DZ} values based on the DZ mixture conditions are compared to the experimental value in section 4.3.1.

3.2.2 Litzinger et al., RDX/BAMO Propellant

Litzinger et al. (*113*)* (LLT00) measured species concentration and temperature in atmosperhic pressure flames of several nitramine-energetic binder propellants using a triple quadrupole mass spectrometer with a quartz microprobe sampler and thermocouple techniques. (Note that radiative corrections were not included). Also, the availability of second and third quadrupole stages makes separation of species at identical m/e values possible (although this feature was not used in all their studies, for example some discussed in the next section). The propellant surface was heated using a steady CO_2 laser during the combustion; this is no small perturbation—if the heating were removed, the flames extinguished. Profiles were reported for three mixtures: RDX/GAP, HMX/GAP, and RDX/BAMO, all in mass ratio of 8:2, and at two CO_2 laser intensities each, resulting in datasets for six different flames [BAMO is 3,3 bis (azidomethyl)oxetane]. Unfortunately, only one of these, RDX/BAMO at 400 W/cm^2 CO_2 laser intensity, is found to be suitable for our DZ model testing purposes. For each of the rest, either some key piece of information was missing, such as r_b appropriate to the laser-assisted conditions or T_{DZ}, or in the RDX/BAMO 100 W/cm^2 case, the profiles indicated the second-stage flame did not form within the measurement distance, so L_{DZ} is indeterminate. Or, there was indication the flame was highly non-one-dimensional and, in some cases unsteady, which invalidates key assumptions in the present approach. See, e.g., Litzinger et al.'s figures 7 and 11 photos for RDX/GAP and HMX/GAP cases indicating that important heterogeneity, fluctuation/turbulence, and/or expansion of the flame above the propellant surface are present, and the text regarding observed unsteadiness of some of the flames. From LLT00's figure 3, for the retained RDX/BAMO 400 W/cm^2 case, the example flame photo indicates that there were some hot surface particles, and these may even intermittently lead to the formation of hot "streamers" in the gaseous flame. Despite this, and the fact that the photo is somewhat dark, the flow appears reasonably one-dimensional, with little area vs. height variation.

For this case, the DZ species mole fractions, temperature, and length were obtained from the profiles in LLT00's figures 5 and 6 and the propellant burning rate from their table 4. The beginning of the DZ was taken from the NO profile to be at about 0.1 cm, where the NO profile first hits its plateau level. The NO profile in this region is somewhat noisy, so determining exactly where the DZ begins is subject to a fair amount of uncertainty. It should be noted correlated fluctuations are observed in the species profiles.† By "correlated fluctuations," we

*Preliminary reports containing much of the data summarized in this final report appear in two earlier works: (*114*, *115*).

†Correlation in profile fluctuations vs. spatial position in measured profiles as introduced here is prominent in many nitramine flames, especially many of those studied by the Litzinger group. We believe the phenomenon is a likely indication of a weakly stabilized, flickering flame. We also believe the unsteady flame issue to be very important for many of the studies cited, beginning here and later in this subsection; many propellant flame studies exhibit this effect.

mean major reactant species (e.g., at the end of the DZ where the second-stage reaction is beginning these are NO and HCN) tend to exhibit upwards fluctuations, while major product species (e.g., at end of the DZ these are N_2 and CO) tend to exhibit downwards fluctuations, away from the general trends of the individual profiles, all at the same spatial locations, or vice versa.* It appears the correlated fluctuations are not merely random noise; rather, they are likely due to—hopefully mild in this case—flame flicker. Note that the spatial profiles were obtained by translating the burning propellant strands towards the mass spectrometer probe tip during the burns. Thus results at various distances were obtained at different times, so flame unsteadiness can be an issue (as in most, but not all, strand burner experiments). We believe correlated fluctuations in the species profiles are probably the result of usage of a diagnostic which results in groups of the species concentrations at each given distance being measured almost simultaneously and instantaneously as a nonsteady flame is pushed towards the mass spectrometer probe tip (exact groupings unknown). As regions of a nonsteady flame move back and forth vs. the probe tip, reactants and products measured almost simultaneously would naturally exhibit correlated fluctuations about the general trends in their individual profiles. Were the flame completely steady, we believe the profiles would look smoother. Because the fluctuations are correlated as we describe, we believe they are not merely strong, random noise. (Conversely, the H_2 species, present at trace levels in this flame, is very difficult to measure by this technique. Its profile exhibits much higher frequency fluctuation, which is probably due to random noise.) Not surprisingly, the fluctuations are most prominent in regions of strong gradient, e.g., at end of the first-stage and DZ regions. They make both the beginning and end positions of the DZ, and hence L_{DZ} and the species concentrations at beginning of the DZ, more uncertain than in most of our retained studies. It appears there are, in fact, correlated bumps in opposite directions in the NO_2 and NO profiles at about 0.08 cm, just ahead of the point we chose as beginning of the DZ, which contributes to the uncertainty in locating the beginning of the DZ. These species are directly connected chemically, the NO being the primary product of NO_2 consumption in the first-stage flame.

The species mole fractions at the beginning of the DZ are given in table 9. Two profiles from small signals at m/e = 41 and 43 were given and the authors suggested they may be ascribable to CH_3CHNH (43), CH_3CN (41), CH_2CNH (41), which are not in our mechanism, or HNCO (43); the issue of exact species yielding the signals at those m/e values was not resolved. These trace species profiles were ignored. A very small trace species profile ascribed to CH_3CHO (constant at ~0.001 mole fraction—seems strange it was constant) was also ignored. T_{DZ} was 1500 ± 150 K; the large error limits are due to strong fluctuation in the T profile that may be further evidence of flame fluctuation. For RDX, $\Delta H^{\circ}_{f,298}$ is taken as 14.69 kcal/mol (*58*), while for BAMO, it is estimated as equal to that of the monomer, 103.6 kcal/mol (*116*). Using these values, we calculate for the propellant at 1 atm an adiabatic flame temperature of 2627 K. The

*Note that whether a given major species is a reactant, product, or relatively inert can depend on position in the flame; e.g., NO is a product in the first-stage region (exhibits fluctuations correlated in opposition with those of its precursor NO_2 in this case) but a reactant in the second-stage region.

computed adiabatic temperature for the DZ mixture is 3045 K. Although these disagree, the CO_2 laser assist increases the energy available to the flame; thus the DZ mixture is expected to yield a considerably higher adiabatic temperature. The difference is in the correct direction and therefore does not disqualify the dataset. Furthermore, LLT00 checked the element ratios of flame mixture vs. the propellant and found reasonable agreement, although, in this case, the measured C fraction was somewhat low (see LLT00's figure 5). In spite of satisfying these tests, however, there is a strange feature, possibly of some concern, regarding this dataset. NO_2 and CH_2O usually tend to be confined to propellants' first-stage flame regions or to decay very rapidly at the leading edge of the DZ regions. Also, as we will see in section 4.3.2, N_2O is predicted to be completely consumed partway through the DZ region. In this case, these expectations are not met. The NO_2 decay extends about halfway through the DZ. The N_2O profile holds nearly constant over the entire length of the flame. The CH_2O mole fraction begins at 0.03 at the leading edge of the DZ region and actually rises slightly to 0.05 at the center of the DZ region. It then falls back to about 0.04 at the end of the observation region at 0.4 cm. The distance of 0.4 cm is well into the second-stage flame region, which, from trends in the NO, HCN, N_2, and CO profiles, appears to begin at ~0.33 cm and probably extends to slightly above 0.40 cm. Thus both N_2O and CH_2O concentrations remain very large and nearly constant throughout much of the flame, well into the second-stage region. That the gas-phase decay of these species is typically much more rapid than these results seem to suggest is quite well established; cf. PHP-HMX measurements cited in the prior subsection and our discussion of modeling both cases in section 4. Long decays or lack of decays in the NO_2, CH_2O, and N_2O profiles thus suggest something unusual is occurring. Perhaps the flow is not purely gas phase, e.g., a condensed aerosol or particulates are actually entrained in the flow in this case and are sources of these species. The photograph is too dark to help resolve this issue (and it might not be definitive even were the photograph better). Perhaps some large gas-phase molecule precursor that survives over a long distance went undetected. Perhaps the first-stage flame is rather stretched out (which might be expected when flickering effects are present). Alternatively, perhaps there is some problem in the measurements. Despite these issues, the dataset was modeled and the results are presented, partly because there are so few retained nitramine datasets, partly due to an interest to explore the role of the trace NH_3, which is present in no other case, and partly because of an interest in exploring predicted DZ chemical details when large traces of first-stage species remain, especially both CH_2O and NO_2. The two issues of, first, the nonluminous region possibly just being a stretched first-stage flame and, second, flickering, do not seem as prominent as in many of the cases that are discarded on these grounds (see the next section).

Densities (*117*) for RDX and BAMO are 1.816 and 1.30 g/cm^3, respectively, from which we estimate the propellant density as 1.7 g/cm^3. L_{DZ} and r_b were 0.27 ± 0.07 cm and 0.14 cm/s, respectively. Combining these data with T_{DZ} in equation 3, we obtain a measured τ_{DZ} of 0.24 ± 0.07 ms, where primary contributors to the error limits are L_{DZ} and T_{DZ}. This result is compared to predictions in section 4.3.2.

3.2.3 Discarded Nitramine Datasets

This section consists of a number of discarded nitramine datasets and describes reasons they are discarded. In the first subsection, we present a fairly large number of cases for which the reasons may be briefly described. In the second, we discuss a dataset that at first appears very promising but required us to "estimate" (guess) at concentrations of some important, unmeasured initial species. We have, in fact, modeled it in earlier studies (*4*, *7*) with results that were only moderately satisfying. Only recently, after thinking of a new, more logical approach to deriving the initial species concentrations, have we discovered the dataset apparently has internal consistency problems (at least when any possible amounts of the likely unmeasured species are added). Justification for discarding this case requires a considerably extended explanation.

3.2.3.1 Cases requiring brief discussions. In addition to the retained study on HMX/GAP/BTTN in section 3.2.1, Parr and Hanson-Parr also performed measurements at 0.92 atm on a similar RDX/GAP/BTTN propellant (*118–120*), this apparently being the first time they employed many newly developed diagnostic methods. The measured DZ mole fractions are presented in table 10. The measured T_{DZ} was 1250 ± 50 K. As in the HMX propellant study, atom balances were used by the authors to infer several species; the atom balances, thus, are nearly perfectly preserved but cannot provide an internal consistency cross-check. The authors' calculated adiabatic flame temperature of the propellant was ~2820 K (from their figure 9), in excellent agreement with their burnt gas flame temperature measured by OH PLIF, ~2820 ± 50 K (from the same figure). These results are in excellent agreement with our value, 2805 K, which was calculated using 14.69 kcal/mol for $\Delta H^{\circ}_{f,298}$ of RDX (*58*) and values cited for the other ingredients in section 3.2.1. However, we calculate an adiabatic flame temperature for the DZ mixture in table 10 of only 1895 K, in serious disagreement with the propellant's adiabatic temperature. We tried multiple input adjustments to no avail; none seemed both justifiable and to resolve the disagreement. We note that the mass fractions of nitramine : GAP : BTTN in the HMX vs. RDX propellants studied by this team were almost identical. However, comparing measured major DZ species concentrations for the two propellants, one of the biggest differences is that, whereas the N_2 concentrations are similar, the NO concentration is a factor of ~3 smaller for the RDX vs. the HMX propellant (compare tables 8 and 10). The measured surface temperatures of the RDX and HMX propellants were found to be ~605 and ~785 K, respectively (*107–109*, *118–120*). For RDX, pyrolysis experiments indicate that at 605 K, the branching ratio of pure RDX between the two main initial gaseous product paths, $HCN+NO_2$: CH_2O+N_2O, is ~1 : 1 (*13*, *14*). During combustion, at the end of the first-stage flame, though some traces may remain, one typically finds NO_2 to be primarily converted to NO, while N_2O is primarily converted to N_2. This leads to the expectation that the $N_2 + N_2O$: $NO + NO_2$ mole fraction ratio for these species surviving at the leading edge of the DZ should also be ~1 : 1. For the RDX propellant, that ratio is very much larger, ~4 : 1 (see table 10). Such a major difference in expected and observed ratios might be the result of a measured NO concentration that is, for unknown reasons, too low. Furthermore, NO is an oxidizer, and the propellants are fuel rich;

using an assumed input oxidizer concentration too low vs. its actual value in a fuel-rich case would lead to too small a predicted adiabatic flame temperature. These observations suggest suspicion regarding the NO concentration datum in the RDX/GAP/BTTN case. In fact, tests indicate increasing the assumed NO DZ concentration to a level similar to that observed for the HMX propellant would raise the DZ mixture's T_{AD} to about 200 K lower than that of the propellant (which is still a bit lower than we would like). However, justification for using such a change is not at all clear because this reasoning could be overly simplistic. The pyrolysis results might not directly apply to the more complicated combustion conditions. Furthermore, there may be a discrepancy for the HMX case vs. pyrolysis results as well, though perhaps not nearly as large. The measured $N_2 + N_2O : NO + NO_2$ ratio of ~5 : 4 for the HMX propellant (see table 8) may also be different than one might expect at 785 K based on the pyrolysis results; see figure 1 of Brill (*14*), where the $N_2O : NO_2$ ratio for HMX is ~0.8 at ~648 K and appears to be either trending downwards or reaching a plateau towards higher T (note the pyrolysis measurements end at 648 K for HMX and we are trying to draw a comparison by extrapolation of the pyrolysis results to temperatures well above the measurements, a possibly questionable procedure). Following communication of these points to T. Parr, he indicated that increasing the NO by as much as a factor of 3, and decreasing the H_2 by a similar amount, might be acceptable (*120*). We find changes slightly larger than these would yield an acceptable T_{AD}; however, the accompanying element ratios are inconsistent with the propellant (not shown), so we mutually concluded this adjustment must be rejected and also agreed that there appears to be no other reliable resolution. Whatever the cause of the energy inconsistency, we conclude it is serious. No justifiable changes leading to an acceptable DZ mixture could be found, and the RDX/GAP/BTTN dataset is therefore not retained for the present DZ model testing purposes.

Experiments indicate a DZ may form at subatmospheric to 1.0 atm pressures in the gas-phase flames above burning RDX if a CO_2 laser beam impinging on the surface is used to supply heat to support the combustion. However, no DZ is observed without the laser (see the YTLY06 [*37*] review and references therein). The Lee et al. study (*121*) is of particular interest. Techniques similar to those described in section 3.2.2 were used. Pressures were between 0.2 and 1.0 atm, and CO_2 laser fluxes used were 100 and 400 W/cm^2. The 0.5 atm, 400 W/cm^2 case is of interest because a T profile was provided that has a plateau one might ascribe to a DZ (their figure 18). The plateau is at ~720 K—considerably lower than the usual T_{DZ}. Above the 720 K region, the profile rises fairly smoothly beginning at about 0.2 cm—there is some minor slope fluctuation that may be due to noise or flame flicker—to a final T of ~2700 K, which is reached at about 0.36 cm above the surface; T holds at this final value between 0.36 and 0.5 cm, where the measurements cease. Note the final temperature is indicative of having reached the burnt gas region. There is no further plateau region beyond the end of the 720 K region. The plateau extends from about 0.02 to 0.2 cm. However, the corresponding species profiles (see their figure 15) indicate the first-stage flame is very long. The NO_2 and CH_2O profiles are nonzero at the surface, and their consumption takes place between about 0.15 and 0.35 cm. Presence of these species is indicative that from the surface to 0.2 or 0.3 cm is an extended first-stage, and/or

pre-first-stage, region of the flame; these species typically do not survive far into the DZ (*3*). The 720 K plateau is so unexpectedly cool it supports this idea. Such a long first-stage region suggests the flame was only weakly stabilized against the propellant. Further supporting the notion that this is simply a stretched first-stage region, the NO and HCN concentrations are small near the surface and only begin to rise between 0.2 to 0.3 cm to plateau levels. Some slight consumption of NO and HCN may start at about 0.4 cm, but their profiles indicate not much consumption occurs to as high as 0.5 cm above the surface, where the measurements end. Thus the T profile indicates the combustion is complete at 0.36 cm, whereas the species profiles indicate it is not yet complete even at the largest observation distance, 0.5 cm, a clear inconsistency. Correlated fluctuations are observed in the species profiles, suggesting flame flicker is prominent. The fluctuations hampered our efforts to analyze the dataset. Furthermore, flicker may be responsible for the strong inconsistency between T and species profiles since they were probably taken in different runs. To summarize, there is a lack of consistency between T and species profiles, strong noise in the profiles,[*] and a probability that the 720 K region is connected with a stretched out first-stage flame rather than the typical DZ region and mixture of interest to the current study. Therefore, we conclude that while Lee et al. (*121*) provides qualitative indications of conditions in the flames, it cannot be used for our quantitative DZ model test.

The Litzinger group has also published several other papers with relevant data discussed here (*45*, *46*, *122*, *123*). All of the techniques used were discussed in section 3.2.2. The studies concerned RDX and various RDX propellants, with the combustion assisted by CO_2 laser heating. In Fetherolf et al. (*45*), three RDX formulations, pure RDX, BLX39, and XM39, were studied. For BLX39 and XM39, the intermediates NO and HCN form and do not decay within the distances plotted and a corresponding T profile has a final T of ~1100 K, which, though indicative that the DZ has been reached, is clearly far below the adiabatic temperature; thus, the second-stage flame was not observed and L_{DZ} is unknown. For the pure RDX case, plateaus in some profiles occur between 0.0 and 0.06 cm; however, CH_2O and NO_2 are slowly decaying in this region, which, as noted in the preceding paragraph, is indicative of the first-stage flame rather than the DZ region. Also, no T profile is available. In Fetherolf et al. (*122*), XM39 and M43 were studied. N_2 and CO, which both occur at m/e = 38, were not separately identified in this early work by the group, which is problematic. In most of the flames, the HCN and NO profiles rise to plateau levels and do not decay, indicating the DZ is reached, but no second-stage flame occurs in the measured region; the corresponding T profiles reach plateaus at ~1150–1250 K, supporting this conclusion. In one case, M43 at 3 atm, 100 W/cm^2, the HCN and NO profiles decay but over most of the observed region of 0.5 cm and nearly in conjunction with the CH_2O decay; the corresponding NO_2 profile unexpectedly decays over a much narrower region near the surface than the CH_2O. Also, the T profile is not given for that case. In Tang et

[*] One could infer L_{DZ} values ranging over a factor of ~5 since the point where the typical DZ mixture begins is difficult to determine and where it ends is highly uncertain; the initial mixture to use is virtually indeterminate.

al. (*46*), XM39 and M43 were revisited. The profiles are once again indicative that regions where change is occurring are associated with the first-stage flame; the DZ intermediates form fairly far from the surface but do not decay in the measurement region, i.e., no second-stage flame was observed, so L_{DZ} is indeterminate. Also, no T profiles were given. In Kudva et al. (*123*), pure RDX and RDX-based propellants RDX/CAB and XM39 were studied. The NO_2 and CH_2O decays indicate the first stage was again observed extending far from the surface, with measurements ending in the DZ, and the second-stage flame was not observed, so L_{DZ} was indeterminate in most of these cases. One case (*123*), RDX/CAB at 3 atm, 400 W/cm^2, has species profiles that appear to define the traditional DZ region. However, the corresponding T profile is not given. A T profile is given for the same propellant at 1 atm, 400 W/cm^2 to 0.35 cm, that has a final T of ~2500 K, suggestive of final products being reached (their figure 4). The corresponding species profiles unfortunately end at 0.18 cm (their figure 2). The HCN and NO profiles end in plateaus, indicating the second-stage flame is not reached in the species figure. One could hope to combine the observed DZ species with DZ length extracted from the T profile. However, the T profile has a strange, multiple step-like appearance. Once again, it seems likely this unusual appearance is due to flame flicker. In fact, the authors mention the flame visually appeared to be unsteady, with standoff distance of the luminous region varying between 0.24 and 0.4 cm. It appears neither T_{DZ} nor L_{DZ} can be reliably obtained from the T profile. Also, the burning rate was not given.

Finally, the Litzinger group studied HMX flames at 100 and 300 W/cm^2 CO_2 laser-assisted heating using techniques similar to those discussed in the last paragraph (*124*). A picture of one typical flame (laser intensity unspecified) exhibits a domed appearance, which may create issues of applicability of our model due to not being close enough to one dimensional. But since there are so few nitramine cases, we attempted nevertheless to investigate this one further. Profiles of the 100 W/cm^2 case have no clear indication of separated first- and second-stage regions, but we at first thought the 300 W/cm^2 case might be retained. Unlike the RDX/BAMO case that was retained (see section 3.2.2), decays in the CH_2O and NO_2 profiles, indicative of the global reaction between them, are complete by about 0.22 cm; whereas the NO and HCN profiles plateau from this point to about 0.43 cm, then decay, indicating the end of a DZ. The temperature profile, however, indicates T_{DZ} is only ~900 K at 0.22 cm, which seems more appropriate to the near surface region. We have modeled the DZ mixture based on this initial temperature and find the modeled delay time is about 4 orders of magnitude too long compared to the experiment (not shown). Like the RDX/CAB case towards the end of the preceding paragraph, this HMX case also has a temperature profile with a somewhat step-like appearance, though perhaps not as pronounced as in the former case. The profile is curving upwards at 0.22 cm to about 0.33 cm, at which point the slope begins to diminish, possibly indicative of the beginning of a plateau region, but then it exhibits further steps upwards at 0.4 and 0.5 cm. We believe, similar to the RDX/CAB case at end of the preceding paragraph, there is in this case disagreement between the species profiles, which were probably taken simultaneously with each other, and the temperature profile, surely from a different burn, regarding the DZ position. Some

of the species profiles were obtained simultaneously by the mass spectral technique; thus they agree with each other on DZ position. The temperature profile was, however, obtained in several burns using thermocouples of materials for different T regimes; probably all those burns were separate from the species burn. Differing initial DZ positions from these profiles again suggest the presence of significant flame flicker. We have modeled the species mixture measured at 0.22 cm using instead the temperature ~1450 K, measured at the lowest bend downwards in the profile at 0.33 cm; this would be a somewhat reasonable combination assuming the DZ begins at these two different distances in separate burns due to flame flicker but is otherwise similar. The predicted τ_{DZ} time agrees well with that suggested by the species profiles. These results, however, will not be presented. The method of achieving them, in particular of determining T_{DZ} from a profile of unusual appearance, does not constitute a very satisfying test. The modeling results are extremely sensitive to the assumed T_{DZ}, and we feel it is not possible to obtain this value from the experimental profile in an unbiased fashion. There is also a problem that the temperature profile was not corrected for radiative emission losses; the correction, though surely not nearly 550K (1450–900 K), is very substantial compared to our model's sensitivity. While it would be of interest to discuss our analysis of the detailed chemistry, as we do for all the selected cases in subsequent sections, the DZ mixture is similar to that of the PHP-HMX case. Therefore, further discussion of this dataset is probably not particularly valuable.

We suspect many nitramine propellant flames exhibit considerable flicker, leading to strange looking, and sometimes very strong, fluctuations from expected trends in measured species and T profiles. The Litzinger group specifically mentioned it for one of their flames, and previously we have mentioned our strong suspicions that the effects are present in several of their other studies. As mentioned at the beginning of section 3, our ARL colleague, B. Homan, who performed strand burner experiments like this for many years, informed us this problem is typically most troublesome for nitramine propellants (*93*). In fact, Homan and Vanderhoff (*57*) focus on the issue in a "Snapshot Spectroscopy" study on XM39. Two successive frames, 0.033 s apart, of a video recording for a burn at 16 atm show the luminous flame's shape and position vary drastically within this short time, illustrating the unsteady, non-one-dimensional flame structure even at pressures well in excess of 1 atm. Our simple model is not applicable for such unsteady flames (and, indeed, currently available detailed chemistry, solid propellant models that include the entire flame structure are also not appropriate because all assume the flame is steady).

Mallery and Thynell (*125*, *126*) studied an XM39 flame at 21.7 atm. Species were measured by an infrared absorption technique (FTIR) and temperature by thermocouples and/or by infrared absorption on NO. The infrared method, of course, precludes detection of homonuclear species H_2 and N_2. The species profiles have a problem that due to experimental limitations, only data at a nearly point region, about 0.04 cm, and from 0.17 to about 0.4 cm, are available. The space between 0.04 and 0.17 cm could not be probed, possibly due to refractive beam steering into the

propellant surface. It appears likely that much of interest occurs within this region, e.g., there may be plateaus in the profiles ending at some undefined distance. The T profile measured by thermocouple has a plateau region at about 1100 K from 0.002 to 0.16 cm, sharply rises at 0.16 cm to about 1800 K, and then up to about 0.28 cm exhibits several extremely sharp downwards and then back upwards spikes—excursions over very short distances between, very roughly, 1200 and 1800 K. Above 0.28 cm, the temperature settles to about 1850 K, with a few much smaller downward spikes. It seems probable the spikes are due to flame flicker; see, e.g., the discussion of results from ref *57* for the same propellant at 16 atm in the preceding paragraph. L_{DZ} cannot be reliably determined from these data, and there is an important unprobed spatial region; therefore, the dataset cannot be used for present purposes.

Vanderhoff and coworkers performed several studies on XM39 (*55*, *98*, *127*). A compilation of mixture results from the three studies is given in table 1 of Vanderhoff et al. (*98*); L_{DZ} may be estimated from NO profiles in Teague et al. (*127*), suggesting the possibility of combining results to form a dataset (note that YTLY06 apparently incorrectly interpreted the infrared probe height of 0.15 cm given by us in table 1 of Vanderhoff et al. (*98*) as L_{DZ}). However, the C : O ratio of measured DZ species can be readily checked; note that H_2 and N_2 were not probed due to use of infrared absorption techniques, thus, they have to be estimated, which precludes checking H and N ratios. In the unburnt propellant, the C : O ratio is 0.75, while for the DZ mixture it is 0.59. The agreement is poor, and so long as one keeps ratios of the species that were measured constant, as seems to be the only justifiable approach, no amount of added H_2 or N_2 can affect it. The poor agreement may be due to flame flicker, which, as discussed in the two preceding paragraphs, may be especially troublesome for XM39; this would probably have adverse effects when attempting to combine results from different burns/studies. In any case, the poor element conservation necessitates discarding this dataset for the present purposes. We also note that even were there no unsteady flame issues, combining the sets in this way might induce a more subtle error. The mixture data fromVanderhoff et al. are for P ~10–12 atm, while L_{DZ} is only available from profiles in figure 13 of Teague et al., which is for P ~16–18 atm. There is no clear reason the DZ species ratios for nitramine propellants have to behave like those of the nitrate ester propellants and remain constant as P is varied. In fact, since pyrolysis studies on RDX and HMX show the ratio of HCN + NO_2 to CH_2O + N_2O produced varies vs. the solid's temperature (*13*, *14*), and the surface temperature of combusting propellants varies vs. pressure, there would be considerable concern such an assumption might be quite invalid. So perhaps discarding this dataset is for the best.

Vanderhoff and coworkers (*52*, *53*) studied the propellant "HMX2," and Kubota studied a number of HMX propellants (*128*). We have modeled the results of these datasets in our earlier efforts (*4*, *7*), in spite of some concerns about them, due to a paucity of well-defined experimental results for nitramine propellants at those times. We now have two complete nitramine DZ datasets available (PHP-HMX and LLT00). We have decided the reference *52*, *53* and *128* datasets should be discarded for our present study. Reasons for discarding the Kubota

data are discussed in the following subsection, 3.2.3.2. For the Vanderhoff HMX2 data, only the NO mole fraction was measured. The rest of the species mole fractions were "estimated" (guessed) in that early work by comparison to results from other studies on nitramine propellants that had no L_{DZ} data (see Vanderhoff et al. [*4*]). Furthermore, the results in Vanderhoff et al. suggest there may be energy closure problems (too high a predicted T_{AD} for the DZ mixture) if one assumes N_2O is present as a minor component, as many other studies suggest is likely. For these reasons, the Vanderhoff HMX2 data are discarded.

3.2.3.2 Kubota nitramine/binder propellants dataset. Kubota studied 80/20 mixtures of HMX with four nonenergetic binders at pressures from about 9 to 90 atm (*128*). Photography and thermocouple techniques were used to measure burning rates and temperature profiles. T_{DZ} and τ_{DZ}, the latter inferred by Kubota from measured L_{DZ} and other data using the approach discussed in section 2.1, were reported over the range ~10–30 atm for the formulations with the nonenergetic binders PA (a polyacetylene) and PE (a polyether). Gas-phase samples were withdrawn for these two formulations from both the DZ and luminous flame zones into a gas sampling system "via a thin suction probe" and analyzed to obtain mole fractions. The description of the analysis method, however, is unfortunately very sketchy, little more than presented here (possibly due to a manuscript length limit). This dataset is very unique among nitramine propellants in that it provided mixture data, both within the DZ and luminous flames, and P was varied. In two earlier papers, we have compared predictions using earlier versions of the present model with Kubota's results (*4*, *7*). We have always been concerned, however, that there might be a potentially serious problem with energy closure, see, e.g., Vanderhoff et al. (*4*), where the computed T_{AD} of propellant and the assumed DZ mixture are 1928 and 2585 K, respectively; the data were used in spite of this issue due to lack of other comprehensive nitramine studies. However, we have recently determined by a new approach that, in addition to this problem, there is a serious issue concerning element conservation, discussed in the next few paragraphs.

Kubota reported detecting the species in table 11 in the DZ regions of formulations HMX/PA and HMX/PE at 20 atm. Similar concentrations were observed for the two propellants. Notice that HCN and H_2O were not observed, and the mole fractions sum to well below 1.0. Kubota specifically mentions he did not include H_2O in the analysis; presumably, this was due to the typical troublesome condensation issues. The nonobservation of HCN, however, was not discussed; it is highly suspicious. For every other nitramine DZ study of which we know wherein species were probed, so long as the technique was sensitive to HCN, copious amounts of HCN were observed in both the near surface and DZ regions (see, e.g., refs *45*, *46*, *54–56*, *98*, *107*, *108*, *113*, and *118–126*). This is true whether or not CO_2 laser heating is used to assist the combustion. It seems highly probable that Kubota's nonobservation of HCN was due to using a diagnostic that was insensitive to HCN. For example, depending upon conditions, HCN could polymerize on sampling tube and/or vessel walls, or it might not pass easily through a gas chromatograph, were that the diagnostic, depending upon the column type used. In any case,

when we have previously modeled Kubota's data (*4*, *7*), we assumed some HCN, as well as H_2O, was actually present—the amount having been "estimated" (guessed) by comparison to similar propellants. This idea was retained in an attempt to uniquely determine the concentrations with a numerical approach, as documented next.

Note that the mole fractions of detected DZ species in table 11 sum to only 0.696. We attempted in a first approach to determine a unique DZ mixture assuming that the species concentrations listed in table 11 are correct and that HCN and H_2O were the only missing species from this list, and thus their mole fractions total to 0.304. Note that the presence of small traces of other components would not seriously affect the coming conclusions. We tried by adding hypothetical amounts of HCN and H_2O and using an iterative approach to find a mixture that preserves element ratios.* The results of this attempt are presented in table 12. We used data for the binder elemental compositions given in Kubota (*128*). The element ratios for HMX/PA and HMX/PE starting formulations, given in the first two rows of table 12, are found to be similar. The next five rows show the element ratios for five assumed DZ mixtures based on the measured species in table 11, combined with an assumed HCN ranging from 0.0 to 0.304 and H_2O appropriately adjusted to maintain the total mole fraction at 1.0. None of the computed element ratios for any of the five hypothetical mixtures comes close to those of the propellant formulations. The propellant C fraction of ~0.2 is most closely met for hypothetical DZ compositions with the least H_2O; in those cases, the O fraction matches the propellants well; however, the H and N agreement is extremely poor. The H and N ratios match better, though not extremely well, for 0.304 H_2O, 0.0 HCN, but the C and O agreement is then very poor. For completeness, we also tried Kubota's exact measured DZ mixture in table 11, i.e., with no H_2O or HCN and renormalizing, although it is highly doubtful that either is not present; the resulting element ratios are not at all satisfactory in this case either. We also ran energy closure tests for these assumed mixtures. The DZ mixture starting temperature of 1000 K was taken from the HMX/PE results in Kubota's figure 3; the temperature for HMX/PA is slightly higher, 1150 K, but these equilibrium calculations are not strongly sensitive to this variable (and, in any case, using the higher initial temperature makes the disagreement discussed later in this paragraph worse). For the propellants at 20 atm, we found, using Kubota's binder enthalpies (*128*), the highest computed T_{AD} for the starting formulations is 2237 K for HMX/PA. For the five hypothetical DZ mixtures, the computed T_{AD} values range from ~2750 to 3010 K (see table 12). Obviously, the hypothetical DZ mixture T_{AD}s are far too high, also a disqualifying result. In a second approach, since a number of nitramine DZ studies indicate fairly large traces of CH_2O and NO_2 might survive at the leading edge of the DZ (see, e.g., PHP-HMX and LLT00 cases discussed previously), we replaced a part of the HCN and H_2O assumed present in the mixtures with traces of these species instead, of course, having the sum of these four species' mole

*Several earlier attempts to solve for these concentrations via very involved, error-prone analytical algebraic approaches were made at various times over many years, but we were totally unsuccessful—probably because, as we show by this new approach, there is apparently no solution within the bounds of our assumptions.

fractions remain equal to 0.304. Kubota mentions shapes of the measured T profiles were indicative of a rapid first-stage reaction very near the propellant surfaces under all conditions he studied, so using much higher amounts of CH_2O and NO_2 would be incorrect. We tried a total of CH_2O and NO_2 mole fractions first of 0.1 and then of 0.2, with three cases each being first all one, then equal parts of each, then all the other; see tables 13, 14 (assumed mole fractions in some of these cases, of course, are large enough to qualify the CH_2O or NO_2 as a major species, but investigation of these examples amply covers the desired ranges). The H_2O and HCN were both decreased accordingly, but their ratios were chosen to match those in the five cases of table 12. Thus $2 \times 3 \times 5 = 30$ total hypothetical mixtures were considered. The resultant element ratios of all these have serious disagreement with the propellant element ratios. And the T_{AD} values of all are ~600 K or more too large vs. those of the propellants. There appear to be serious consistency errors in all these hypothetical DZ mixtures. From examination of the trends in the results, it appears that no hypothetical DZ mixture based on further variation of the four most likely species we tried, within the boundaries set by Kubota's measured concentrations, can match the element ratios of the propellants. Furthermore, the T_{AD} values are far too high. Unfortunately, we have concluded this enticing dataset must be discarded.

Two possible explanations of our difficulty determining a DZ mixture consistent with the propellants' properties have occurred to us. First, the present results obviously suggest the possibility of an error in the concentrations of the DZ species Kubota was able to detect. However, one further, puzzling point must be made if this is indeed the explanation. We compared Kubota's measurements of the luminous flame species to the equilibrium mixture computed for the propellants, which is another output of the equilibrium program used to calculate the adiabatic temperatures. Predicted equilibrium mole fractions for the HMX/PA propellant are given in table 15; results for HMX/PE are almost identical (not shown). The agreement is not excellent, especially for the relative predicted and observed amounts of CO_2, but Kubota's measured luminous flame species results are fairly close to the equilibrium mole fractions, as one would expect. We are at a loss to explain how, if Kubota's technique has some systematic error in measuring the DZ mixture, this does not also adversely affect his measured luminous flame composition—although perhaps there is an error confined to the two species NO and N_2O, which of course were only detected in the DZ. A decrease of these concentrations would reduce the T_{AD} of the DZ mixtures because they are rich; however, it probably would take an adjustment well outside the error limits, and this does not even address the issue of element ratios.[*] We see little justification for making such an adjustment. We are contemplating changing so many variables, with no clear idea whether one of the measured species might be in error and why, that this approach seems quite unsound. Therefore, we did not pursue this avenue further.

[*]Error limits were not stated. However, for stable major species such as these, most measurement techniques would yield error limits of about 10% of the absolute concentrations. A few tests we ran indicated it might require very large adjustments in the NO and/or N_2O concentrations to match T_{AD}.

A second possibility that could lead to inconsistencies for our hypothetical DZ mixtures is that some additional species other than the four just considered was/were present. Kubota mentions "hydrocarbon fragments" (an enigmatic phrase) and "solid carbon generated at the surface" (quite possibly not pure carbon, as a literal interpretation of that phrase implies) were present in the DZ mixture. In any case, our element and energy conservation tests show the approach of deriving the proper DZ mixture based on adding only HCN, H_2O, and possibly traces of CH_2O and NO_2, which seem on the basis of many other studies to be the most likely candidates, to Kubota's measured DZ species cannot be used for the present DZ modeling tests. However, we note in passing that Kubota's discussion seems to suggest the flames of these propellants were fairly steady, contrary to many of the other nitramine propellant flames discussed previously. This suggests if someone were to attempt to replicate and investigate those propellants' flame structures with appropriately species sensitive techniques, then in addition to providing new results, Kubota's excellent study might be salvaged for DZ model tests.

4. Modeling Results

4.1 Some Introductory Considerations

In this subsection, we discuss some important issues that affect all the modeling results in this work. We first present details of an example calculation, illustrating how τ_{DZ} is obtained. Then we explore the quality of some key assumptions made in the analysis to obtain τ_{DZ} from experiments and to obtain the modeled results. Finally, we discuss how sensitivity analysis was used to estimate, quantitatively, the precision limits of the computed τ_{DZ} values as implied by those of the input reaction rate coefficients.

For the example calculation, we chose the VKMT-JA2 case, which is for JA2 burning at 16 atm. Predictions using the initial mixture of table 4 at the measured T_{DZ} of 1500 K are presented in figures 4–7. Plots of temperature and total heat release rate vs. time are shown in figure 4, the corresponding major species profiles are given in figure 5, and three of the most important trace species in figures 6 and 7. Note that the profiles in figures 4 and 5 have relatively small gradients until about 8 or 9 ms, at which point gradients in the profiles become very steep, indicating a fast global reaction is occurring. Of course, one notes that the profiles, especially the temperature profile, are not nearly as flat during the delay time as caricatured in the idealization of figure 2; nevertheless, the general idea that there will be a delay during which radicals and temperature slowly build, and then a sudden, global runaway reaction occurs, is followed. When the runaway reaction finally does occur, the major reactant species undergo conversion—some of the H_2 and nearly all of the NO to H_2O and N_2, and some of the CO to CO_2 (figure 5). The H and OH rapidly rise at this point, while HNO is consumed (figures 6 and 7).

From figure 7, one notes that although [OH] is larger than [H] at equilibrium, for this case [H] is ~10× larger than [OH] throughout most of the DZ region. For this example, the radical concentrations are assumed initially to be zero. They very rapidly increase from 0.0 to reach small, less rapidly changing values just after t = 0. Note, e.g., the sharp rise from 0 to ~4.5 $\times 10^{-5}$ mole fraction in the HNO profile ([HNO] × 100 rises from 0 to 0.0045) between t = 0 and 0.1 ms (figures 6 and 7). Then [H] and [OH] both rise about 2 orders of magnitude throughout the DZ. We have determined that during the very early period, the small values they approach are steady-state concentrations, an important issue discussed later in this section. Some detailed examples and expanded plots of the early time profiles will be given. Returning to figures 4–7, a separate equilibrium calculation (not shown) indicates that just after the runaway reaction occurs at about 9 ms, the species go to nearly their equilibrium values and the temperature to nearly the adiabatic limit. It is difficult to know exactly what point in time to associate with the appearance of the luminous flame in the experiment. To obtain a well-defined point, we assume that the lower boundary of the luminous flame is coincident with the maximum in the single peak in the heat release profile associated with the steep gradient—in this case, at 9.3 ms (figure 4). There is probably some error associated with this assumption, but since the runaway global reaction occurs over a very short time, this error is probably of little consequence; it is clearly quite small compared to the experimental error in τ_{DZ}. All of the other nitrate ester cases result in plots qualitatively similar to figures 4–7, so further detailed profiles will not be shown for them. For the two nitramine cases, most of the ideas presented in this section pertain, but multiple heat release maxima occur. The complications this presents are discussed in detail in the specific subsections dealing with those cases (vide infra).

The plateau regions of T and major species profiles have smaller gradients, i.e., appear "flatter" at lower pressures and have somewhat steeper gradients at higher pressures (not shown), which is not at all surprising. In other words, the idealization made that T, and also ρ_g, are constant throughout the entire DZ region, which is used to derive equation 3 for extraction of τ_{DZ} from experimental data, is certainly not perfect; it is best at low pressures. There will be some systematic error associated with using this assumption in the experimental data analysis. We have estimated its magnitude by examining two cases from the Miller and Anderson study on nitrate ester propellant combustion (*24*). As mentioned in the Introduction, that model includes details of the entire propellant gas-phase flame structure. It uses a premixed laminar flame submodel for this purpose. In that work, two cases, JA2 at 16 atm and M9 at 17 atm, had their profiles studied and presented in detail because literature data on T and some species profiles were available for comparison; fair agreement was obtained. Since WRA has details on the solutions readily available and since the flame submodel includes a rigorous treatment of mass and heat transfer by conduction and diffusion, these cases provide us a means to examine the possible systematic error involved with the assumptions made in the data analysis. We do this by assuming that the full flame modeling profiles represent "experimental data" and applying the

analysis procedure described in section 2 to the results, via equation 3, to obtain an "experimental τ_{DZ}." We can also obtain for comparison a rigorous evaluation of τ_{DZ} by examining outputs of the premixed laminar flame submodel. In particular, it provides the gas-phase convective velocity profile, *v(x)*, as a function of distance, *x*, above the solid propellant surface. The time for convection from beginning to end of the DZ can be obtained rigorously from these data via the following:

$$\tau_{DZ} = \int_{x_1}^{x_2} [v(x)]^{-1} dx \ , \tag{4}$$

where x_1 and x_2 represent the DZ limits. Equation 4 was integrated numerically for the JA2 and M9 cases. Consider first the JA2 case. Analyzing plots from the full flame solution as an "experiment," we note the following results from the predicted profiles and burning rate: L_{DZ} ~1.21 cm, T_{DZ} ~1275 K at beginning of the DZ, r_b ~0.718 cm/s, and remind that ρ_s was estimated to be 1.56 g/cm^3 in Miller and Anderson (*24*). Obviously, some of these values agree only modestly well with the actual experiment. But to achieve consistency in this comparison, we combine them in equation 3 to obtain an "experimental" τ_{DZ} = 4.3 ms, from the solution. The result from the more rigorous integration of equation 4 is 3.3 ms. For the M9 case, similarly treating the solution as an "experimental" result, we obtain 1.8 ms, whereas the rigorous integration method yields 1.4 ms. In both cases, the "observed" value obtained via the simple analysis of equation 3 is about 25%–30% larger than the "actual" decay time observed in the more rigorously modeled flow. These results should be kept in mind when comparing the selected experimental observations to our predictions. The actual delay times in the experiments retained in section 3 are probably smaller than reported there by amounts similar to these. One would usually expect an error in this direction because T_{DZ} is taken at the leading edge of the DZ in the data analysis, and the typical slight rise in T vs. increasing height is ignored in equation 3. Note that one would expect the error to be smaller at lower pressures because the DZs are longer, leading to flatter profiles and vice versa. The systematic error is difficult to estimate in most cases since the more rigorous full flame models are not available and would require great effort to develop; one would expect them to provide only a moderately close match to conditions at the leading edge of the DZ in any case. However, we note that the random errors in the experimental results are of similar magnitude to these predicted systematic differences. Both random and systematic error, and other issues, restrict our ability to use the experimental results for a very rigorous kinetic test of the DZ mechanism—a point we will discuss in more detail in the Conclusions (section 6).

We also examined usage of the plug flow assumption for the modeling, as opposed to a full flame calculation, for the JA2 16 atm case; we note that it would likely be impossible to obtain the solution for a full flame calculation beginning with the DZ mixture because the gradients and heat feedback would be so small that it is extremely likely the solution could not be stabilized on a surface. We also note that this comparison was not possible for the M9 case because the files

containing the species profiles information for Miller and Anderson (*24*) results (from M. S. Miller) have been lost. However, for the JA2 case, we have the solution files and were able to obtain all species and temperature profiles from the flame calculation. Using the species concentrations from the Miller and Anderson solution beginning at the same point, ~1275 K, as described in the prior paragraph, we ran the calculations treating the mixture instead with plug flow assumptions (SENKIN code, as used herein). The Miller and Anderson flame calculation considered effects of diffusion, convection, and conduction, which is a more accurate approximation of the combustion experiment, so the comparison of results will yield a test of the plug flow assumption that ignores them. Of course, for the plug flow calculation, we switched back to the earlier version of the mechanism used in Miller and Anderson. It was found sufficient to keep all species of initial concentration above 1×10^{-6} mole fraction, and to retain three significant digits in input parameters. The result was $\tau_{DZ} = 3.3$ ms; when three digits are considered, the agreement is to within a few percent. The agreement with the full flame calculation is excellent, suggesting the plug flow assumption is very good. This is not surprising when one considers how gentle the gradients in the DZ are for this case. However, the assumption might not be so good for cases in which L_{DZ} is very short, for which steeper gradients might cause stronger diffusion effects.

Another important assumption made in our modeling is that all significant species in the initial DZ mixture have been included. It is unlikely that any major species have been missed in our tables of the experimental mixtures. But one wonders whether species present at trace levels might have gone undetected. These can be present as stable or radical species. Where universal diagnostic methods have been used, we believe the likelihood that significant amounts of stable trace species have been missed is small; a more important issue for some of these is accurate quantification, which is difficult for species at low levels. Along these lines, it is important to note whether the species considered is "kinetically active," i.e., whether it might lead to reactions that strongly affect the radical pool, as opposed to merely affecting the mixture equivalence ratio, hence its available energy. The former has a much stronger effect on DZ structure. NH_3 is an example of a kinetically active stable species, which we will discuss in detail later, since it was observed in one of the mixtures. The issue of radical trace species is considered in the next few paragraphs.

Over the years, several colleagues have suggested, and at one point we also considered, that radicals might be present in the initial DZ mixtures at trace levels, go undetected by most experimental methods, and have important effects. About 5–10 years ago, however, we determined that it is highly unlikely, for reasons having to do with the kinetic behavior of these mixtures, that any radical is present at high enough levels to have a significant effect on the predicted τ_{DZ} and DZ structure. Possible effects of hypothetical nonzero initial trace levels of radicals on DZ structure were, to our knowledge, first investigated by Fifer et al. (*36*). They predicted that the effects of several different radicals, present at assumed levels up to 0.001 mole fraction, would be small; the main effect was to rapidly, slightly raise the initial temperature, as

most of the radical assumed to be initially present is converted to stable species. τ_{DZ} was then slightly shortened, but this was apparently simply due to the concomitant, slightly increased initial temperature; runs starting instead with zero initial radical but with the higher initial temperature yielded nearly identically shortened delays. We confirmed that this was the case also (unpublished), using our more rigorously determined initial mixtures and more refined mechanism (especially in that ours does not contain the incorrect N + CO_2 reaction, HR1). The reason this occurs was, however, not understood; thus the possibility this issue could yet be a major source of error remained a concern until more recently. In about the mid 1990s, a collaboration between the Seshadri and ARL groups (*6–9*) developed reduced DZ mechanisms. This was done in two steps. First, unimportant reactions and species were removed from the full detailed mechanism to obtain a skeletal mechanism; this type of smaller mechanism is still used in a full finite-rate treatment, i.e., all the species' partial differential equations are retained and solved to obtain the time-dependent solution. Then, more pertinent to the present discussion, steady-state (SS) assumptions were found to be appropriate for the radicals in the remaining species list; making this assumption for each, one arrives at an even smaller, so-called "reduced" mechanism. The SS assumption, of course, means the partial differential equation for each of the radical species was set equal to zero. Doing so for the DZ model yields a rather complicated set of algebraic equations involving the species concentrations and rate coefficients, one for each radical for which an SS assumption was deemed appropriate, where the stable species and rate constants are known quantities. The reduced mechanism is utilized in the computations for each time point in a given calculation by first solving the algebraic equations to obtain all of the SS radical concentrations using a matrix technique; then the nonzero partial differential equations for the remaining, mostly majority, species are time stepped using the SS radical concentrations in the stable species partial differential equations. It was found that the predicted profiles using the detailed, skeletal, or reduced mechanism approaches are almost identical, except for the radicals at the very beginning of the calculation. In the full finite-rate calculations, the initial radical concentrations were assumed to be zero, whereas via the reduced mechanism the nonzero, SS concentrations are solved for and used even at t = 0. For the full finite-rate calculations, the radical concentrations start at zero and very rapidly relax to the finite-rate SS values. This led us towards the end of the 1990s to hypothesize that the reason why when one instead starts a calculation with a hypothesized, high concentration of radical(s) it rapidly decays and is converted to stable species is that, whatever one assumes for the initial radical concentrations, the kinetics will force them to rapidly approach their SS values as appropriate to the mixture conditions. We have more recently performed calculations using our full mechanism which convince us that this, in general, is indeed the case.

We find the kinetically driven SS effect on the radicals is very strong. To illustrate, the 16 atm JA2 case is again used, and we choose for this example to add H atom in various hypothetical amounts to the initial mixture in table 4. Results are shown in table 16, and compared to the prior result with zero initial radical concentrations. Three amounts of H-atom, 0.0001, 0.001, or

0.01 mole fraction, were added to the nominal initial mixture of table 4 and the model rerun, yielding the results for τ_{DZ} as shown in table 16. (Note that the values in table 4 total slightly larger than 1.0, and after the amounts of H atom shown were added, the totals were renormalized, so the initial H mole fractions were actually slightly less than indicated.) Note that 0.0001 mole fraction H produces an almost negligible change, 0.001 a modest change, and 0.01 a more substantial change. Also shown is the predicted temperature a very short time after the calculation is started, when we have determined an SS on the various radicals has just been reached. Whether an SS has been reached is determined by examination of the radical profiles for an early, rapid gradient change in the initial radical profiles, which is typically observed, and evaluation of an SS parameter, as described in the next paragraph. Also shown in table 16 are the three results where, instead of adding H atom to the mixture, we started with zero radical concentrations but changed the initial temperature to the temperatures at which SS was first reached in the three calculations where H atom was added. Note that the resulting τ_{DZ} values of the latter-type calculations are very close to those reached in the three corresponding calculations starting at 1500 K (the measured T_{DZ}, section 3.1.3), where various concentrations of H-atom were added. The equivalence of τ_{DZ} results from the two approaches is similar to the results of Fifer et al., as mentioned in the prior paragraph. These match well because in all cases, including those with zero initial radical, the SS radical concentrations are rapidly reached, and they are quite small. The temperature responds accordingly as recombination or dissociation to/from stable species occurs as required to achieve the early SS radical concentrations. Qualitatively, this result holds for all the DZ cases retained for study. Also, a wide variety of the available radicals was tested at hypothetical 0.001 mole fraction, which is a very large amount, and the result still holds.

The 16 atm JA2 cases with initial 0.0 or 0.0001 H mole fractions are discussed and compared in more detail to better illustrate these results. First, we found for the 0.0001 H case, the profiles are almost identical to those of figures 4–7, where the initial 0.0 H atom was used, except at very short times. There is a very slight shift of the steep gradients at 9.3 ms to a shorter time, as the results of table 16 suggest (not shown; the difference is difficult to see whether plotted in the same or side-by-side figures). A more important difference in the profiles for the two cases is most easily seen in expanded scale plots of the radical profiles at very short times. Three of the most important trace species profiles, H, OH, and HNO, are shown at short times for the two cases in figures 8–10. In figures 8 and 9, profiles for the two cases are compared on a timescale of 0.3 ms. The 0.0 H case has these profiles rising over the first ~0.05 ms, while for the 0.0001 H case, these profiles instead decay over about the same period. The concentrations of the three trace species in the two cases become nearly equal beginning at ~0.1 ms and remain so, leading us to hypothesize this occurs because SS on all is reached there, and the concentrations at 0.1 ms are the initial SS values; this was confirmed as described next. The 0.0001 H case is the more complex of the two because the profiles exhibit even more structure during an initial, very short period not readily noticed in figures 8 and 9 (see figure 10). During the first 0.5×10^{-6} s (0.0005 ms), the H atom assumed initially present is converted mainly to HNO and some OH.

To quantitatively analyze whether an SS applies, we define an "SS parameter" for species *k* (computed at selected time points in our postprocessing code) as follows:

$$SS_k \equiv (C - D)/(C + D) \ , \tag{5}$$

where *C* is the total rate of creation and *D* the total rate of destruction, of the species, summed over the various elementary reactions; note that forward and reverse directions of each elementary reaction are separately considered in the summations to obtain C and D. If the species is only being created, $SS_k = 1$, if only destroyed, $SS_k = -1$. When creation and destruction rates are equal, the species is in SS and $SS_k = 0$. Of course, SS_k is seldom exactly equal to zero, except when perfectly at equilibrium.* But for time periods in which SS_k is close to zero, an SS assumption is good, can be used in reduced mechanisms, and may have a primary influence on the mixture's kinetic behavior. Thus the numerical result for SS_k provides a quantitative test we have examined, though we will only qualitatively summarize our findings here. For the 0.0001 H case, during the first ~0.5×10^{-6}s, the three radicals shown have not reached SS; the SS_k values indicate overall H is being destroyed and HNO created, which agrees with gradients in the profiles in figure 10. From analysis of individual reaction rates, we find this is due primarily to H + NO (+M) → HNO (+M) (R3). HNO overshoots its SS value during this time. OH also overshoots via $H_2O + H \rightarrow OH + H_2$ (–R49). Next, considering the slower process from the end of this very brief time and up until ~0.05 ms, SS_k values indicate that overall HNO, H, and OH are being destroyed in the 0.0001 H case. For the 0.0 H case, beginning at 0 and up until ~0.05 ms, overall, these three species are instead being created. In both cases, the SS_k in results agree with the profiles in figures 8 and 9. From analysis of individual reaction rates in the 0.0001 H case, R3 continues to contribute to HNO formation over the longer time interval, but the destruction of HNO via $HNO + NO \rightarrow N_2O + OH$ (R19) becomes even faster, so HNO decreases. OH is produced in R19, but its destruction via $CO + OH \rightarrow CO_2 + H$ (R43) is faster yet, leading to decreasing OH. For the 0.0 H case, $H_2 + NO \rightarrow H + HNO$ (–R161) and H + NO + M → HNO (+M) (R3) contribute to HNO formation. At ~0.1 ms in both cases, the SS_k values of all radicals and some stable trace species, not just the three shown, become close to 0.0 and remain so throughout the DZ. The chemistry during the more important DZ delay time will be considered in detail in later sections. For the two cases of the initial H atom, predicted concentrations of the radicals become approximately equal at this point (see, e.g., figures 8 and 9). One would expect this result, given that the radicals are in SS with the major species. Depending on how much hypothetical radical is added, there are concomitant, but only very slight, changes in majority species concentrations when SS is reached. This analysis thus provides strong evidence that an SS controls the radicals' concentrations and, at the leading edge

*An exception would be at an extremum point in the species profile, where the sign of SS_k reverses. Note that SS_k being close to zero does *not* mean the concentration of species k is invariant. For example, as we shall discuss, an SS applies to the radicals and a few trace species throughout the DZ, yet their concentrations grow several orders of magnitude during the DZ delay. SS_k being nearly zero merely means a SS assumption can be used to solve for species *k* in terms of the non-SS species and mixture conditions.

of the DZ, causes them to be at values predetermined by the primary features of the mixture conditions—temperature, pressure, and majority species concentrations. We find the reactive trace species SS concentrations are all very small, typically less than 1×10^{-4} mole fraction, at this point. The fact that Fifer et al. (*36*) obtained qualitatively similar results using a mechanism made very different via the incorrect inclusion of HR1, which reverses and becomes the major, *hypothetical* radical source reaction *in their model*, suggests this behavior will be the case no matter what the actual mechanism is. Radical initiation or branching reactions tend to have barriers. Thus small formation rate constants typically pertain to radicals at low T. Radical recombination reactions instead tend to be fast at high P. Hence, no matter what the actual mechanism is, we believe radical concentrations are in SS in DZs, where T is still relatively low, and their concentrations tend to be very small. Furthermore, even if larger molecular radicals not considered in our mechanism are produced close to the propellant surface, probably these will be nearly completely consumed in the first-stage flame. Any that survive would likely be converted to smaller radicals such as H and OH, within a few, rapid, radical exchange reactions a very short distance into the DZ. It is therefore highly unlikely the measurements in any of the selected experiments were taken close enough to the first-stage flame for a high concentration of radicals to have survived. If a high concentration of any radical were to survive, it would be forced by the SS issue to recombine to stable species over an extremely short distance, causing T to rise. Several of the selected experimental results have provided spatial profiles, and the distances at which the results are digitized to obtain mixture conditions are where the profiles, including that of T, have reached plateaus; this suggests the radicals are already close to SS values. Our conclusion that the radical concentrations are negligible can probably never be totally assured, because we cannot ever be certain we have the exact mechanism. However, the sheer existence of dark zones is an argument that there cannot actually be an extremely large radical source reaction that would provide a very much larger SS concentration of some radical at the leading edge of the DZs than projected in the current predictions. We also note modeling studies of full propellant flame structures suggest radical concentrations in general are very small in the near surface region (see, e.g., Beckstead et al. (*18*) and Miller and Anderson [*24*]). These observations and results are a strong indication that the initial radical concentrations can, indeed, be treated as negligible; otherwise, DZs probably would not exist.

In section 5 on analysis of the detailed chemistry that has led to our modeling results, we include prioritized lists of sensitivities of the results to the input reactions' rate coefficients. Those results may be used to estimate precision limits of computed τ_{DZ} values as implied by error limits of the rate coefficients. We note that sensitivity coefficients for the τ_{DZ} parameter cannot be directly computed. Rather, we use temperature sensitivities at τ_{DZ} to indicate which reactions' rate coefficients most directly control the modeled result. To begin, note that the generalized form of an equation for precision in modeled dependent (i.e., solution) variables given in Smith et al. (*129*) suggests how this might be done:

$$U(F_j) = \left[\sum_i (S_{ji} \times \sigma k_i / k_i)^2\right]^{1/2} , \tag{6}$$

where F_j is a dependent variable such as temperature, U is its relative error limit, S_{ji} is a computed sensitivity parameter that has been logarithmically normalized as described in section 2.1, k_i is the rate coefficient of reaction i, and σk_i is its error limit. The sorted list of temperature sensitivities then directs us to those reactions whose rate coefficients are the most sensitive for τ_{DZ}. In section 5, we present results of brute force calculations of the response of τ_{DZ} to changes by a factor of ±2 in rate coefficients of the most sensitive reactions for temperature. Assuming the response to changes in the rate coefficients this large is linear, which should be accurate enough for precision estimates, a normalized sensitivity of τ_{DZ} to the rate coefficients can be calculated by dividing the relative change in τ_{DZ} by the relative change (factor of 2) in k_i. Equation 6 can then be used with these estimated τ_{DZ} sensitivity coefficients to obtain the precision limits for τ_{DZ} induced by the error limits in the input rate constants. We note that for all of the cases considered, only the highest ~1–3 reactions in the sensitivities list contribute noticeably to the result. Also, we note the error limits in k_i values are typically about a factor of 1.5 for bimolecular reactions. A few of the reactions involve a collider (+M). For these, the high- and low-pressure limit rate coefficient expressions have precision of about a factor of 1.5, but the collider efficiencies typically are poorly known for any colliders other than Ar; we estimate error limits for these are roughly a factor of 3. Note this calculation has just included the effects of the rate coefficients' error limits on the precision limits. There are other factors influencing precision of τ_{DZ} as well, especially the error limits in T_{DZ}. All of these are discussed in the following three subsections. We have not attempted to combine these into overall precision limits. Indeed, it is not entirely clear how to do this. Nonetheless, these can yield a rough estimate how, if two or more of these factors were to combine, the modeled result would be affected.

4.2 Nitrate Ester DZ Comparisons

4.2.1 Heller and Gordon, 1955

Experimental and predicted τ_{DZ} results for the HG55 dataset described in section 3.1.1 are presented in figure 11 and table 2. Both experimental and predicted DZ delay times, τ_{DZ}, decrease vs. increasing pressure. This result is expected due to increasing reaction rates vs. pressure. The values predicted using the "best" measured input parameters match experimental results reasonably well except at the lowest pressure, where the predicted time is somewhat longer than experimental. Also shown are predictions where the T_{DZ} input was increased or decreased by 50 K, the approximate error limits typical of such experiments. As can be seen, the predicted τ_{DZ} values are quite sensitive to the initial DZ temperature, and results can be made to match experiment by these modest changes in T_{DZ}. Precision in predicted τ_{DZ} attributable solely to rate coefficient sensitivities is about 40% at all pressures. These results suggest that the model may be properly describing the most important chemical mechanism features of the experiment.

We also examined sensitivity of the predictions to assumed initial concentrations of four stable species observed at trace levels in the experiment: CH_4, C_2H_4, HCN, and C_2N_2. Relative error

limits on these species are large, so this testing is desirable. We first tried removing CH_4 and C_2H_4, simultaneously, from the assumed initial mixture of table 1. Note that it is surely incorrect to remove these species entirely, thus, this test represents a much larger change than necessary. The result was that predicted τ_{DZ} decreased by about 4% at the lowest pressure and 1% at intermediate pressures, and increased 1% at the highest pressure. For the second set of tests, we started again with the mixture of table 1 and added HCN and C_2N_2 at 0.001 and 0.0005 mol fractions, respectively. The result was to decrease τ_{DZ} by about 1% or 2% across the pressure range studied. Thus possible errors induced by lack of precision on, or exclusion of, these trace species are small, especially compared to the error limits in the experiment. Also, the precision of the predictions is much more markedly affected by error limits in other input parameters, such as T_{DZ} (see prior paragraph) and certain rate constants (vide infra).

4.2.2 Aoki and Kubota, 1982

Experimental and predicted τ_{DZ} results for the AK82 dataset described in section 3.1.2 are presented in figure 12 and table 3. Behavior vs. pressure is similar to that of the HG55 dataset. Once again, agreement is best at the highest pressures, but predicted values are longer than experimental at the lower pressures. The disagreement is worst at the lowest pressures. We also examined the sensitivity of predictions to changes of T_{DZ} by 50 K, the approximate error limit in the measurement. Results with 50 K added agree reasonably for the higher pressures but not at the lowest pressure, 10 atm. Reasons for the discrepancy are not understood. Effects of changing the four stable trace species were examined, in similarity to what was done for HG55 (see prior subsection), and were again found to be negligible. Precision in computed τ_{DZ} due solely to sensitivity to the input rate coefficients is about 45%. A combination of these factors might explain the remaining discrepancies.

4.2.3 Vanderhoff and Coworkers, 1992 and 1997

The VKMT-JA2 dataset for JA2 at 16 atm described in section 3.1.3 was selected for presentation in detail to illustrate what the modeling results are and how they are interpreted; see section 4.1, where plots of the predicted species profiles, temperature, and heat release vs. time are given. The predicted result for τ_{DZ} using the nominally best measured input parameters is 9.3 ms. This result is somewhat larger than the experimental value, 6.5 ± 0.8 ms. However, upon adding the error limit of ~50 K to the measured T_{DZ} to obtain an initial value of 1550 K, the predicted τ_{DZ} becomes 7.0 ms, which agrees well with the experimental result. As mentioned in section 3.1.3, the best interpretation of the experiment seems to be that concentrations of hydrocarbons are negligible, but this is not entirely clear for CH_4 and, perhaps, C_2H_4. Therefore, we tried adding 0.01 mole fraction of CH_4 or C_2H_4. The effect of each was to increase τ_{DZ} by a few percent, which is negligible. Precision of the computed τ_{DZ} derived solely from sensitivities to the input kinetic rate constants is about 45%.

The concentration of OH in the luminous flame region was also measured in the experiment, affording another check on the model. From figure 6, the predicted OH concentration at

equilibrium for the DZ mixture is about 0.02 mole fraction. An equilibrium calculation for JA2 yields a 0.007 mole fraction and adiabatic flame temperature of 2866 K. The experiment yielded an OH concentration of only 0.002 mole fraction in the luminous flame region and a final flame temperature of only 2690 K. The measured OH concentration being lower than the equilibrium calculation may be due to the measured flame temperature being lower than adiabatic, which, in turn, may be due to heat losses. Obviously, the predicted OH concentration of our DZ model is much higher. This, in turn, is probably due to the adiabatic flame temperature, 2983 K, of the DZ mixture taken from the measurements being somewhat higher than that of the propellant.

We attempted to reduce the DZ mixture adiabatic flame temperature and equilibrium OH concentration via numerous, reasonable changes in the initial mixture conditions, as follows:

- Changes of 10%, the approximate error limit, in concentrations of the species that were measured (see table 4).
- Reducing the T_{DZ} by 100 K, twice the error limit, to 1400 K.
- Adding 0.01 mole fraction of CH_4 and/or C_2H_4.
- Factor of 2 changes in the H_2 and N_2 concentrations, which had to be estimated.

Mostly, these changes were only tested one parameter at a time. It was found that no such change of an individual parameter is large enough to result in the desired reduction of the adiabatic flame temperature or equilibrium OH concentration. Probably simultaneous changes to about three or four of these parameters would produce the desired effect. However, this seems like a major change, and there is no clear indication which combination of the inputs might be in error and properly be adjusted. Therefore, we have not pursued this idea further. The computed τ_{DZ} is, however, in fair agreement with the experiment, suggesting that the main features of the mechanism and model may still be correct. We also note the experiment indicates the OH radical concentration near the surface and in the DZ region is below the detection limit. Although no definitive statement of that limit was made in VKMT-JA2, clearly it is much less than the measured 0.002 mole fraction in the luminous flame. This result is supportive of our argument in section 4.1 that initial DZ radical concentrations are negligibly small.

4.2.4 Parr and Hanson-Parr, 2002

Experimental and predicted τ_{DZ} results for the PHP-BTTN dataset described in section 3.1.4 are presented in figure 13 and table 6. Even with the nominally best input parameters, the values at all pressures agree within the experimental error limits. The tendency is for the modeled τ_{DZ} results to be slightly larger than experimental at most of the pressures; therefore, for this dataset we only tested the effects of adding 50 K to the T_{DZ} values. The result is that predicted τ_{DZ} values are then all slightly below the experimental results, but results still agree within error limits. Note in this case, though, because of the manner in which we had to estimate them, the T_{DZ} values have much larger error limits than for all the other retained nitrate ester datasets,

especially for higher pressures (see section 3.1.4). The proper error limits are probably on the order of 100 K. Also, precision limits in τ_{DZ} arising from sensitivities to the kinetics rate constants are about 40%. This case is thus somewhat less convincing than the other nitrate ester datasets. Nonetheless, the agreement in magnitude and trend vs. pressure is encouraging. It should be noted that we also tested changing initial CH_4 and C_2H_4 concentrations, setting them to zero as for the three prior datasets, and found the results to be similarly insensitive.

4.3 Nitramine DZ Comparisons

4.3.1 Parr and Hanson-Parr, 2002 and 2004

Predicted profiles for the PHP-HMX dataset described in section 3.2.1 are shown in figures 14–17. Recall the experimental τ_{DZ} is 0.64 ± 0.28 ms. That result was estimated using L_{DZ} obtained from the measured species and temperature profiles from Parr and Hanson-Parr (*107–109*), in particular, the distances at which NO is formed and consumed. From figure 14, the predicted heat release profile has maxima at 0.02, 1.8, and 2.5 ms that make it quite clear that at least three exothermic, overall processes take place. The chemistry associated with these will be discussed in detail in a later section, but briefly, the first is due to CH_2O/NO_2 reaction, the second N_2O consumption, and the third occurs when the major reaction finally takes place and HCN and NO are converted to products; see also the species profiles, which support these assignments. Thus the proper one of these to associate with the measured τ_{DZ} is the third maximum in the heat release profile, 2.52 ms, where the NO decays. Obviously, this result is considerably longer than experimental. However, if we add 100 K, the error limit in T_{DZ}, to the initial T, the prediction becomes 0.99 ms, which is almost within error limits of experiment; testing instead a slightly larger addition of 150 K, the prediction becomes 0.66 ms, in good agreement. Returning to the nominally measured T_{DZ} and instead changing the initial N_2O from 0.05 to 0.06 mole fraction, the prediction becomes 1.81 ms. With T_{DZ} increased by 100 K and N_2O set to 0.06 mole fraction simultaneously, the prediction is 0.72 ms. Resetting other inputs to nominal values, we find changing NO_2 from 0.01 to 0.0125 yields 2.23 ms, while instead changing CH_2O from 0.03 to 0.02 likewise yields 2.23 ms. All these changes are within experimental tolerances. The precision limits in τ_{DZ} arising solely from the sensitivities to the kinetics rate constants are 50%. Clearly, a combination of changes within error limits of one or two key modeling inputs can lead to τ_{DZ} values well within tolerances of the experiment; these tests also reveal which are the most sensitive input parameters.

Experimental profiles vs. distance are available for most of the species measured in this dataset. Direct comparisons of measured and experimental profiles are not possible because the changes in T and gas convective velocity within the DZ cause some distortion of scales; that is, the modeling time is not directly proportional to distance in the experiment due to our data reduction assumptions not being perfect. Nevertheless, it seems reasonable to make some relevant, semiquantitative comments; the reader is referred to Parr and Hanson-Parr (*107–109*) to examine the experimental profiles, which are not herein reproduced. First, we note that CH_2O and NO_2

are predicted to react very rapidly at a short time (figure 16). This agrees with the experimental profiles, though the latter are perhaps somewhat more spread out. CH_2O is present in excess of NO_2, and its predicted profile exhibits a two-staged decay indicative of rapid reaction early while NO_2 is present, then a somewhat slower reaction once the NO_2 is consumed. The experimental CH_2O profile does appear to extend to larger distances than the NO_2 profile, in qualitative agreement; it is difficult to be completely certain of agreement regarding this detail, however, because of scatter in the experimental data. Shapes of the predicted major species profiles (figure 15) exhibit the same basic trends as in the experiment—those that undergo large changes at the global runaway point do so in both model and experiment and have similar magnitudes before and after the runaway reaction point, while those that do not undergo much change, e.g., H_2O and CO_2, agree both in magnitude and in that not much change occurs. Features such as mild peaks or bumps in the predicted profiles are computationally trustworthy for the tolerances used in the modeling; they are not the result of numerical errors and so are probably related to fine details in the chemistry. These cannot be discerned in the experimental profiles, but this could easily be attributable to scatter in the experimental data. Thus whether these predicted modest features are correct is unclear. The predicted N_2O profile decays slightly before the main global runaway. The experimental profile appears to agree, but it is difficult to be certain because of sparse data points (note the experimental points in figure 12 of Parr and Hanson-Parr [*107–109*], not the ad hoc fit to them). The NO and HCN decays at global runaway occur simultaneously in both the prediction and experiment.

Finally, the experiment provided profiles for a few radical species: OH, CN, and NH. These species are below detection limits in the near surface and DZ regions, which agrees with our aforementioned contention that radical concentrations are negligible in the initial DZ mixtures (section 4.1). Experimental CN and NH profiles are sharply peaked and occur near the global runaway point. Not much of either one exists away from that point, which agrees with the prediction (figure 17). CN appears slightly prior to NH in both experiment and theory. OH can first be detected at the runaway point and grows from that point onwards; it reaches the equilibrium plateau well after the CN and NH maxima. The predicted profiles (figures 16 and 17) agree regarding these points about positioning, although separation between CN and NH peaks is not nearly as large as in the experiment. The latter mild difference in relative peak placement, however, is not a major concern because these three profiles were measured by PLIF. Undoubtedly, each had to be done in a separate experiment to allow switching of laser dyes and wavelengths. A mild shift in optical instrumentation positioning, or slight flame flicker, could easily lead to the difference. A more important difference is that the predicted CN profile exhibits a small bump at its leading edge. There may be a similar leading bump in the experimental profile, but its size is not nearly as prominent relative to the maximum in the profile. Finally, we compare the absolute magnitudes of these three species. The predicted OH reaches about 0.012 mole fraction at equilibrium, while in the experiment it reaches about 0.011; it may still be climbing, slightly, at the distance where the measurements end. The agreement is

excellent. In the experiment, the maximum CN and NH concentrations are 1.5×10^{-4} and 1.7×10^{-4} mole fraction, while in the prediction they are 0.98×10^{-4} and 1.05×10^{-4} mole fraction, respectively. Were diffusion taken into account in the model, it would probably reduce predicted concentrations somewhat; thus the agreement is not quite as good as a first glance suggests. Nevertheless, we note experimental measurements on trace radicals such as these probably should be assigned error limits of about a factor of 2. See, e.g., the comparison of results from two highly regarded laboratories for these same two radicals in 1-atm flames of RDX (*25*). A factor of 2 difference in experimental results (*130*, *131*) for each of these radicals is observed. Such differences for radical concentrations are not uncommon in combustion studies, especially for the challenging environment of propellant flames. With this point in mind, we conclude the agreement between predicted and measured CN and NH concentrations is actually quite good.

In summary, comparison of predicted and measured species profiles is encouraging. Predicted and measured τ_{DZ} values differ somewhat when the nominally "best" measurements are used to determine the initial DZ mixture conditions to use in the model. However, changes in one or two mixture parameters by values equal to or slightly greater than experimental tolerances can yield predicted τ_{DZ} results in good agreement with the experiment. These results suggest that the model may be capturing the main features of the experiment.

4.3.2 Litzinger et al., 2000

Predicted profiles for the LLT00 dataset (*113*) described in section 3.2.2 are shown in figures 18–21. Recall the measured τ_{DZ} was 0.24 ± 0.07 ms. The L_{DZ} used to infer that delay time was obtained from the species profiles, in particular the points at which NO is formed and consumed. From figure 18, the predicted heat release profile has two maxima, at 0.008 and 0.107 ms. Again, extended discussion of the detailed chemistry is deferred to section 5.2.2. Briefly, the first maxima corresponds to the global CH_2O/NO_2 reaction and the second to the final runaway where HCN and NO are converted to final products (see figures 19 and 20). There is also a slight bump at 0.033 ms, to the side of the first peak, which may correspond to NO_2 consumption. The time to the second peak, where HCN and NO are consumed, thus is properly compared to the experimental τ_{DZ}. The computed 0.107 ms is smaller than the experimental result. Recall in this case the estimated error limit in T_{DZ} is 150 K. This fairly larger error limit is the result of fairly large fluctuations in the temperature profile from thermocouple measurements, which, in turn, may result from the likely flame fluctuation suggested in section 3.2.2. Subtracting 100 or 150 K from the assumed T_{DZ}, we obtain 0.185 or 0.254 ms, respectively, for τ_{DZ}. Either of these agrees with the measured τ_{DZ}, the latter exceptionally well. We also examined sensitivity to changes in some of the initial trace species concentrations, returning in each case first to the nominal measured input parameters prior to each of the following changes:

- NH_3 from 0.010 to 0.015 mole fraction leads to 0.097 ms, while removing it entirely yields 0.135 ms.

- CH_2O from 0.03 to 0.02 mole fraction yields 0.108 ms.
- N_2O from 0.04 to 0.03 mole fraction yields 0.126 ms.
- NO_2 from 0.07 to 0.05 mole fraction yields 0.163 ms.
- C_2H_4 from 0.004 to 0.008 mole fraction yields 0.117 ms, while removing it entirely yields 0.098 ms.
- Finally, H_2 from 0.015 to 0.0075 mole fraction yields a negligible change.

Most of these changes vs. trace species concentrations are small. The largest exception is NO_2; reduction by ~30%, which is probably within error limits, yields a τ_{DZ} which is nearly within error limits of the measured value. Though more modest, the responses to changes in initial N_2O and NH_3 concentrations are also significant. We will discuss why initial concentrations of these species are sensitive in the detailed chemistry section. The precision limit in computed τ_{DZ} arising solely from sensitivities to the kinetics rate constants is 45%. Once again, a combination of changes to only one or two input parameters within their experimental tolerances can yield τ_{DZ} in agreement with experiment.

The experiment also provided profiles of all the measured species vs. distance above the propellant surface. As mentioned in the prior subsection, direct comparisons of measured and experimental profiles are not possible because the changes in T and gas convective velocity within the DZ cause some distortion of scales; that is, the modeling time is not directly proportional to distance in the experiment due to our data reduction assumptions not being perfect. Semiquantitative comparisons are again discussed, and the reader is referred to Litzinger et al. (*113*) to examine the experimental profiles. Some of the following points about the experimental profiles were also made in more detail in section 3.2.2. First, the predicted CH_2O and NO_2 profiles decay very rapidly immediately at the leading edge of the DZ (see figure 20). The experimental NO_2 profile instead slowly decays to zero over nearly the entire DZ length. And the experimental CH_2O profile actually grows slightly throughout the DZ up until the point where the DZ ends; it just begins to decay as the conversion of HCN and NO to N_2 and CO begins. In the experiment, N_2O is nearly constant across the entire DZ length and well past the point where HCN and NO decays are occurring, with no hint of decay even at the largest distance examined. The computation indicates N_2O decays to zero beginning well ahead of the decays for HCN and NO (figures 19 and 20). Experimental C_2H_4 is nearly constant throughout most of the DZ; then it grows slightly across the region where a portion of the second-stage fast global reaction begins, which is very unexpected. Experimental NH_3 is nearly constant through most of the DZ region and into the fast global reaction region. Predictions for C_2H_4 and the initial NH_3 are that both are almost entirely consumed by about halfway through the DZ region (figure 21). A small amount of new NH_3 is predicted to temporarily form within the second-stage flame at 0.1 ms (figure 21) from secondary reactions subsequent to HCN reaction; this is discussed in section 5.2.2.

The experimental profiles end at 4 mm, just when the main second-stage conversion reaction is beginning. Unfortunately, only about 1/3 to 1/2 of the HCN and NO have been consumed at the distance where the measurements stopped. Thus comparison of the experimental and computed final equilibrium concentrations is not possible for any species. It appears there is some modest growth of the H_2 profile, in agreement with the computed profile, but the experimental result is very noisy for this challenging species. Comparative aspects about the profiles of some of the trace species, in particular CH_2O, NO_2, N_2O, C_2H_4, and NH_3, are not very satisfying (see prior paragraph). The chemical reactions that lead to predictions of more rapid consumption of some of these than observed are fairly well established. Thus either there are some errors in the measurements or some fundamental assumptions of the model are incorrect for this case. For example, we assume no large molecule major species, or condensed phase particulate matter, went undetected in the experiments. Such species or material flowing with the DZ gases could be a source of additional amounts of the smaller molecules as the gases flow. And perhaps the CO_2 laser heating of the propellant surface, not used in any of the other retained experiments, facilitates this, e.g., via inducing vigorous boiling. Were this correct, however, it would be strange that the production rate of several of the trace components would almost exactly balance their consumption rates. This seems a very fortuitous, thus unlikely, outcome. A possible source of systematic experimental error for some of these species might be problems separating signals from species having the same m/e values via the mass spectrometric technique, e.g., C_2H_4 and N_2, and N_2O and CO_2. The authors state that a triple quadruple mass spectrometer system was used, and that this allows proper analysis, so that this issue should not be a problem. One wonders, though, whether there might be subtle problems with this, especially for an experiment of such short duration (burn of a propellant strand). Perhaps instead, though, the flickering which seems to be present in this flame (see section 3.2.2) has a stronger effect than we hoped. And perhaps associated with this there is also stretching of the flame, and these effects somehow contribute to differences in the results.

Manipulation of the initial T_{DZ} within error limits can bring about agreement in predicted and experimental τ_{DZ} values; this is encouraging. We feel, though, that overall the comparisons in this case are the least convincing of all the datasets considered in this work regarding correctness of the model. It appears possible that some unexpected effect outside the limits set by our assumptions, such as discussed previously, may be important in the experiment. However, despite the issue of poor agreement of qualitative aspects of some experimental and predicted trace species profiles, we discuss and consider the predicted chemistry further in the next section. There are so few nitramine datasets that we feel this is desirable, and in addition, the DZ in this case initially contains traces of NH_3. This species was not observed in any of the other datasets, and its chemistry is of interest.

5. Discussion and Detailed Chemical Analysis

Comparisons of the results of the critically selected experiments and our predictions are close enough to suggest that the mechanism may be properly capturing the main chemical features of dark zones of both propellant types.* For nitrate esters, the data are more extensive and cover a range of modest pressures. The τ_{DZ} predictions exhibit the correct trends vs. changes in pressure and DZ composition, though the latter is not varied over a wide range. Low-pressure results do not agree well for the AK82 dataset, but agreement is reasonable at higher pressures in this case and for all conditions in the other three cases. For nitramines, we only have two experimental datasets, both near 1 atm. For these, agreement concerning predicted τ_{DZ} values is fair. Agreement regarding the qualitative behavior of species profile shapes is good for the first dataset, poor for the second. There may, however, be some physical consideration in the latter not accounted for in the present, simple modeling approach. Thus there is a reasonable hope that the detailed chemical mechanism used in the present work is basically correct; that is, it contains all the correct and important elementary reactions with approximately correct rate coefficients and accurate enough species thermodynamics where that factor is sensitive. The results are more extensive and convincing for nitrate esters; they are not as convincing, but still quite possibly correct, for nitramines. In both cases, further studies to test, develop, and establish the mechanism and DZ model are desirable. In the following two subsections, we discuss the chemistry for the two major propellant types that has led to the present modeling results. These analyses yield the best current insights about the main chemical reactions controlling propellant DZ structure. This chemistry is of interest in its own right; furthermore, these results should be a useful guide for future testing and development of the model. Recall that the numbering of reactions in the text follows that in appendix B, where the mechanism is documented.

In these discussions, we make extensive use of pathway diagrams. In the present paper, these portray for a given case how the major reactive fluxes involved at a selected point in time connect all of the species containing one of the elements. Those species are contained in boxes in the diagrams, and arrows between them indicate their connections as reactants and products. Relative width of the arrows indicates relative total reactive rate flux over all reactions between the connected species (the relative fluxes are sorted into such bands ranging by 15%, e.g., 0%–15%, 15%–30%, etc., prior to drawing). The other reactant(s) involved is (are) indicated next to the arrows, and relative flux through individual reactions, based on the reactant

*Of course, we must keep in mind that the results in section 4.1 suggest simplifying assumptions used in the data reduction methods typically applied to extract τ_{DZ} from the experimental data probably yield overestimates of the correct results. The size of the systematic error estimated in that section is roughly equivalent to the random error in the τ_{DZ} results.

disappearance rate, by a number up to 100 in parentheses next to the other reactant(s).* Second (and third) products are not shown (except in cases where both products of a given elementary reaction contain the focus element; then both appear somewhere in the boxes, and that elementary reaction can be identified on more than one arrow in the diagram). It should be noted that it is the relative net flux that is indicated for the elementary reactions (i.e., the flux in the predominant direction of the elementary reaction minus the less dominant); there are many examples of elementary reactions being net reversed. It is also possible for both forward and reverse fluxes of a given reaction to be very much larger than the net flux (a situation not evident from the diagrams that must be identified in other ways, and an indication that the reaction is in partial equilibrium). Also, since more than one elementary reaction can take part connecting reactant-product pairs, more than one reaction partner may be shown next to an arrow. Finally, a floor level of about 5 to 10 on the relative scale of 100 for highest flux reaction is typically used to reject reactions at low fluxes from portrayal; otherwise, most of the diagrams would be exceedingly cluttered.

5.1 Detailed Chemistry of Nitrate Ester Propellant Dark Zones

Much can be learned about chemical factors controlling the DZ length by an examination of chemical rates and sensitivity parameters prior to and at the global runaway reaction time. For the nitrate esters, we choose to present only the VKMT-JA2 case of JA2 at 16 atm in detail. Some qualitative comments about how the other cases differ will be mentioned. However, all of the nitrate ester DZ mixtures are rather similar in composition, and it was found from careful examination of cases representative of extremes in the various pressure regions of the experiments that the predominant chemistry is qualitatively very similar in all of the cases.

Pathway diagrams for the four elements present in the dark zone of the JA2 example are given in figures 22–26. Diagrams for the four elements in the order H, N, C, O are shown at 4.47 ms, a point approximately midway through the ignition delay, in figures 22–25. The relative rate of 100 in those diagrams corresponds to 8.5×10^{-4} mol/cm^3/s. Diagrams at most other times within the delay period are qualitatively very similar, though as one would expect the maximum rate to which 100 corresponds grows with increasing time. Towards the end of the delay period as the runaway is approached, the reaction diagrams change qualitatively because other reactions become feasible as the temperature increases (discussed later). At the maximum in the heat release profile at 9.33 ms, clearly at global runaway, the primary pathways are very different. This is principally due to changes in N-species reactions consuming NO, so a sufficient understanding may be obtained by perusal of the N-species pathway diagram at that time (see figure 26). The relative rate of 100 in that diagram corresponds to 2.19×10^{-2} mol/cm^3/s.

*Note that we could equally well have chosen to base the relative numbers on product appearance rates. Reactant disappearance and product appearance rates can differ due to differing stoichiometric coefficients in the elementary reaction(s) connecting them.

The preceding results indicate the chemical rates during the delay period are many orders of magnitude slower than at runaway and may vary greatly during that time; the main radicals H and OH concentrations also increase by several orders of magnitude during this time (see figure 7). Figures 22–25 show that during the delay, the main reactions that slowly occur are as follows:

$$CO + OH \rightarrow CO_2 + H \,, \tag{R43}$$

$$H_2O + H \rightarrow OH + H_2 \,, \tag{–R49}$$

$$H + NO\ (+M) \rightarrow HNO\ (+M) \,, \tag{R3}$$

$$H + HNO \rightarrow H_2 + NO \,, \tag{R161}$$

$$HNO + NO \rightarrow N_2O + OH \,, \tag{R19}$$

$$N_2O\ (+M) \rightarrow N_2 + O\ (+M) \,, \tag{R2}$$

$$N_2O + H \rightarrow N_2 + OH \,, \tag{R111}$$

and

$$O + H_2 \rightarrow OH + H \,. \tag{R51}$$

The main reaction that allows the strong N=O bond to ultimately be broken is R19; R19 forms N_2O, which, in turn, mostly reacts in R2 to form the final product N_2. Later, we will see that R19 is the most sensitive for controlling nitrate ester DZ structure (τ_{DZ} and thus L_{DZ}) and examine why. Note that during this time, the rate fluxes indicate a small amount of the H_2O, which is a major final equilibrium product, is actually converted to fuel species H_2 by –R49. Also see in figure 5 that in the 5–8.5 ms period, the effect becomes noticeable just prior to the global runaway, creating bumps in the H_2 and H_2O profiles; there are accompanying bumps in the CO and CO_2 profiles indicating a concurrent minor conversion of CO to final product CO_2. This curious early reversal of R49 occurs at all pressures for all the nitrate ester DZ cases except PHP-BTTN. A small amount of the CO and NO are also converted to final products CO_2 and N_2 during the DZ delay time. The primary effect of this chemistry is to build up the radical pool concentration and slightly increase temperature to the point where the second-stage flame runaway can occur.

During the runaway in the second-stage flame, the nitrogen chemistry becomes very different. The main nitrogen species reactions (see figure 26) are as follows:

$$NO + H \rightarrow N + OH \,, \tag{R165}$$

and

$$N + NO \rightarrow N_2 + O \,. \tag{R163}$$

As during the delay time, the CO conversion still primarily takes place via R43, while a high [O] from R163 leads to the H_2 conversion resulting primarily via R51, which, in turn, yields much of the OH for R43. A secondary H_2 consumption reaction is as follows:

$$OH + H_2 \rightarrow H_2O + H \,. \qquad \text{(R49)}$$

Note that the dominant direction of R49 switches between the DZ and the second-stage flame. R49 is primarily reversed in the DZ for most of the cases, which accounts for the conversion of a small amount of the H_2O to H_2 during the delay time. But R49 is always primarily forward at runaway, resulting in the more expected conversion of H_2 to final product H_2O. Note also the dominant radical is H during the delay period, but becomes OH sometime during and after the runaway. The shift in relative H and OH concentrations was pointed out in section 4.1 and is clearly evident in figure 7. Concentrations of these radicals are small at early times; however, they increase quickly just prior to and during the runaway, and [OH] clearly becomes much larger than [H] after ~9.0 ms. We focused on these two curious results with our postprocessing tools. We noticed that, whereas R43 is predominately forward—though with an important reverse contribution, about 40% of the forward rate—R49 is actually quite close to partial equilibrium. The forward and reverse rates of R49 are almost equal, typically differing by only ~2%, beginning very early in the DZ and continuing upwards through the rest of the flame. This behavior was confirmed for all the nitrate ester cases. Dominance of R49's equilibration is not surprising when one considers the forward rate is very rapid (see the rate constant in appendix B), and the reaction is only modestly exothermic (–14.6 kcal/mol at 298 K), so the reverse is also rapid at these temperatures. We find R49's unidirectional rates are considerably faster than those of the other reactions, again having checked all the nitrate ester cases. Thus, the large forward and reverse rates of R49 *cause* its partial equilibrium to occur and not some linear combination of other elementary reactions adding to the stoichiometry of R49. Hence, the [H]/[OH] ratio, and change in the dominant radical, must be determined by the R49 equilibrium constant and major species [H_2] and [H_2O]. To demonstrate, in this case, at 4.47 ms, T is 1636 K at which the equilibrium constant, K_{49}, is ~20, and the ratio [H_2O]/[H_2] is ~3 (see figure 5). Thus, if R49 drives itself into partial equilibrium at this time, this would cause [H]/[OH] to be ~ 20/3 = 7; this is what is predicted in figure 7. A similar estimate at the runaway, 9.93 ms, yields [H]/[OH] ~0.6, which is also what is predicted.* This important partial equilibrium of R49 applies for all the current nitrate ester DZ cases, beginning very early and extending all the way up through the second-stage flame into the burnt gases. For nitramine DZs, it only applies to the first of the two retained cases (PHP-HMX) and then only beginning about halfway through the DZ and upwards into the burnt gases (not discussed further).

Given that equilibrium of R49 is nearly achieved in nitrate ester DZs and second-stage flames, it is somewhat difficult to predict which direction might slightly dominate. However, in the VKMT-JA2 case, R43 has the largest net rate of any reaction in its DZ; and it rapidly converts

* The results are from numerical text files. They are difficult to read in the figures at runaway due to steep gradients.

OH to H in the DZ. One would expect that the tendency of R43 to deplete OH while forming H would drive the nearly equilibrated R49 to oppose this and be slightly reversed during the delay, thus converting some H_2O to H_2, as noticed in figure 5. In the runaway region, the net rate of R165 dominates, converting H to OH and driving R49 slightly in the forward direction instead; this, together with R51, results in the more expected, final conversion of H_2 to product H_2O.

The rise in T and increase in radical concentrations in the DZ causes R165 to become possible and take dominance over R19 just prior to runaway as the global reaction proceeds (explained later). The chain-branching nature of R165, together with the concurrent exothermic conversion of CO, NO, and H_2 to CO_2, N_2, and H_2O, drives the global reaction to occur abruptly at a very high rate. The unidirectional rates of R49 are the largest and are huge at runaway: tens of mol/cm^3-s for most of the cases studied and even hundreds at the highest pressures.

Other reactions of lesser, but substantial, importance to the pathways during runaway are R3,

$$H + OH + M \rightarrow H_2O + M \,, \qquad \text{(R61)}$$

and

$$H_2O + O \rightarrow OH + OH \,. \qquad \text{(–R56)}$$

HNO is produced via R3 and consumed via several reactions (figure 26) as follows:

$$H + HNO \rightarrow NH + OH \,, \qquad \text{(R116)}$$

$$H + HNO \rightarrow H_2 + NO \,, \qquad \text{(R161)}$$

and

$$HNO + OH \rightarrow NO + H_2O \,. \qquad \text{(R160)}$$

None of the individual rates of the last three reactions is very large, but together they account for most of the HNO consumption. The small trace of NH produced in R116 is consumed by three competing reactions with NO that individually have very small fluxes, only two of which are above the cutoff and appear in the diagram:

$$NH + NO \rightarrow N_2O + H \,, \qquad \text{(R108)}$$

$$NO + NH \rightarrow NNH + O \,, \qquad \text{(–R113)}$$

and

$$NH + NO \rightarrow N_2 + OH \,. \qquad \text{(R109)}$$

In the thin, second-stage flame, the above runaway chemistry rapidly converts most of the H_2 and NO to H_2O and N_2, while a substantial portion of the CO is converted to CO_2 (figure 5). Of course, there will be substantial concentrations of some, and traces of all, of the "reactant" species at equilibrium. The relative dominance of R19 in the DZ vs. R165 and R163 in the second-stage flame for the key breakage of the N=O bond occurs because of the comparative rate

expressions of R19 and R165. Note that R163 is not rate controlling in the second-stage flame because it has no barrier and proceeds at the collisional rate, even at room temperature, with one of the largest neutral species rate constants known; also, there is plenty of NO present to react immediately with any N atoms that may be formed. On the other hand, the rate of R165 is very slow at low temperatures, as in the DZ, because it has a substantial E_a, ~49 kcal/mol, due primarily to its endothermicity. R19 also has a fairly large E_a, ~30 kcal/mol, due to the barrier at its four center transition state (*66–68*), which leads to a slow overall reaction and DZ formation, but its much lower E_a nonetheless makes it comparatively much faster than R165 in the DZ. Note, though, that the A factor of R165 is 1 order of magnitude larger than that of R19. Also, at the second-stage runaway point, [H] becomes somewhat larger than [HNO], whereas in most of the DZ, [HNO] is much larger than [H] (see figures 6 and 7). The larger E_a of R165 means that k_{165} increases much more rapidly than k_{19} as T increases, and this aspect, in addition to the comparative A factors and reactant concentrations, causes R165 to dominate over R19 in the second-stage flame. R163 rapidly consumes the N-atom produced in R165 (e.g., see figure 26 that indicates the rate fluxes are almost identical); however, k_{163} is not found to be sensitive, because R165 is rate limiting. Reactions converting H_2 and CO to products H_2O and CO_2 occur mainly as these two reactions allow the N=O bond breakage, freeing the oxygen as OH and O. Note that R165 is radical chain branching thus causing rapid radical pool growth during the runaway; it is by far the fastest radical growth reaction in the second-stage flame.

Much information about the controlling chemistry can also be learned from sensitivity analysis. Tables 17 and 18 contain ordered lists of the largest temperature sensitivities, logarithmically normalized as described in section 2.1, at the same times as presented for pathway analysis previously, 4.47 and 9.33 ms. The most sensitive reaction by far is R19, despite not being nearly the fastest (a not at all unusual occurrence). This appears to be caused by two main factors. First, as mentioned previously, the reaction allows the strong N=O bond to ultimately be broken. Clearly the primary reason for DZ formation is lack of species that can both react readily with NO and yield products with the N=O bond broken and/or weakened such that subsequent reactions can break this bond, so that N_2 can form (that is, not merely a path that temporarily transforms NO but then leads back to NO, such as R3 followed by R160 or R161). R19 is the fastest such reaction under these conditions; it forms a product, N_2O, which readily undergoes reactions where the NO bond is broken, forming N_2. Second, R19 yields radical growth via OH formation; the subsequent R2 further enhances radical growth via O formation. Note that the other main DZ reaction consuming HNO is with H (R161, figures 22, 23, and 25), but this simply reforms NO and does not break that bond.

At the midway time, R2 is also among the most sensitive reactions and is positive because of the radical formation; but R2 is not rate limiting so its sensitivity is much lower than R19. R161 sensitivity is also important and negative because it destroys radicals but is much lower than R19, probably because of its smaller rate. Several other reactions have modest sensitivities, apparently for a variety of reasons having to do with radical growth and/or heat release, but none is nearly so dominant as R19.

As mentioned in the Introduction, reactions that control propellant DZ lengths at lower (rocket motor) pressures become very important to the near-surface flame structure (predicted gradients) and thus the burning rates at higher (gun) pressures. For example, for M10 propellant, which is composed primarily of the nitrate ester nitrocellulose, reactions R19 and R161 become highly sensitive at the highest pressures modeled in the work of Miller and Anderson (*24*). The directions and qualitative magnitudes are similar to those in table 17. Curiously, R2 is insensitive; perhaps for those conditions, there is no competing pathway for consumption of N_2O formed in R19, that is, the conversion to N_2 + O by R2 is nearly quantitative.

Returning to the VKMT-JA2 case, at the runaway time, although the order of reactions in the list changes slightly, all of the sensitive reactions from the midway point remain on the list, and a few new reactions appear. This is despite the fact that, e.g., the rate of R19 is virtually negligible at runaway. This occurs because the system retains a "memory" of what has happened at early times. That is, a change in the rate constant of R19 will greatly affect the computed T at 9.33 ms despite its slow rate at that time. For testing purposes, we performed calculations starting with the computed mixture at the beginning of the steep T runaway region, so that what happened earlier does not matter; we found the T sensitivity to R19 with those starting conditions is negligible (not shown). The sensitivity to R165 then dominates the list. Apparently, what this means is that the time to DZ ignition, τ_{DZ}, is most strongly affected by k_{19} and much less so by k_{165}. k_{165} controls the slope of the T profile (thus, the width of the second-stage flame) once the runaway begins occurring but not the point at which it starts. k_{19} controls the point at which it starts. The second-stage flame is very narrow, so the point at which it starts is much more important than its width. Thus, k_{165} has a much smaller sensitivity for T, and for τ_{DZ}, than k_{19}.

The sensitivities yield useful information about relative importance of the reactions, but to see more clearly how the rate constants of the sensitive reactions quantitatively affect τ_{DZ}, we performed some brute force tests in which the mechanism parameters were actually changed, and the results recomputed. The reactions were adjusted one at a time by selecting one from tables 17 or 18, multiplying its rate coefficient by a factor of 2.0 or 0.5, and repeating the calculation. The results in table 19 show that when k_{19} is multiplied by 2.0, τ_{DZ} is decreased by almost a factor of 2, while if k_{19} is multiplied by 0.5, τ_{DZ} is increased by almost a factor of 2. The DZ chemical rate is, as expected, increased by increases in $k_{19,}$ and vice versa. The results indicate a very strong, nearly inversely proportional response of the calculated τ_{DZ}. It should be kept in mind that the error limit in k_{19} is about a factor of 1.5, indicating that the computed τ_{DZ} has an important contribution to its error limits just due to limitations of input mechanism precision. The next largest sensitivity is for k_{161}; it is negative, apparently due to the fact it occurs predominantly in the forward direction through the DZ region and thus destroys radicals. So, increasing its rate coefficient retards the chemistry, increasing the DZ delay, and vice versa (table 19). However, the changes in τ_{DZ} are only ~10%, much less than for k_{19}, as one would expect based on the sensitivity coefficients. Changes for all the other reactions tested were much

smaller. Note that we also included one reaction that does not appear on either of the sensitivity lists, R50, $O_2 + H \rightarrow O + OH$, for demonstration purposes. This reaction is typically very sensitive in modeling situations involving air or O_2 oxidized combustion due to its radical chain branching. The responses to changes in k_{50} were negligible (fifth significant digit), which is not surprising since there is so little O_2 in the present conditions. This result is also, however, supportive that the sensitivity analysis has singled out all the important reactions to test.

We have performed the sensitivity analyses for all four of the retained nitrate ester datasets at a few pressures representative of the ranges studied for each. This included brute force testing of changes in rate coefficients. We find the results are qualitatively similar for all these datasets at all pressures. Of the most interest is that changes in k_{19} of a factor of 2 produced an inverse response by factors of 1.5 to 2.0 for all conditions of interest, strong evidence that the reaction is extremely important for nitrate ester DZ structure.

As mentioned in section 4.2, inclusion or exclusion of traces of CH_4 and C_2H_4 from the initial mixtures for all four datasets was found to be unimportant for predicting τ_{DZ}. For completeness, we discuss the main reactions of these species. When they are included, reactions of these species are prominent at early times in the pathway diagrams (not shown). The most important reactions consuming them for CH_4 are as follows:

$$H + CH_4 \rightarrow CH_3 + H_2 , \quad \text{(R225)}$$

$$CH_3 + NO \rightarrow HCN + H_2O , \quad \text{(R342)}$$

$$HCN + M \rightarrow HNC + M , \quad \text{(R194)}$$

$$HNC + OH \rightarrow HNCO + H , \quad \text{(R169)}$$

and

$$HNCO + H \rightarrow NH_2 + CO . \quad \text{(R181)}$$

For C_2H_4, they are as follows:

$$H + C_2H_4 \rightarrow C_2H_3 + H_2 , \quad \text{(R246)}$$

$$C_2H_3 (+M) \rightarrow H + C_2H_2 (+M) , \quad \text{(–R242)}$$

$$O+C_2H_2 \rightarrow H+HCCO , \quad \text{(R212)}$$

$$O+C_2H_2 \rightarrow CO+CH_2 , \quad \text{(R214)}$$

$$CH_2 + NO \rightarrow H + HNCO , \quad \text{(R336)}$$

$$HCCO + NO \rightarrow HCNO + CO , \quad \text{(R71)}$$

and

$$HCNO + H \rightarrow H + HNCO . \quad \text{(R344)}$$

The chemistry of HNCO and NH_2 is similar to that in nitramine DZs (see next two subsections). A few of these hydrocarbon decomposition reactions have modest sensitivities (not shown), but none is nearly as large as R19, even at early times, and none is particularly large by the midpoint of the respective DZs. Brute force testing was performed on a few of the largest of these, changing rate coefficients by factors of 2, as demonstrated previously for other reactions. Not surprisingly, the changes in predicted τ_{DZ} were no more than a couple of percent. None of these reactions has a strong effect on the radical pool or releases very much heat.

A final topic of interest for this section concerns the H_2/NO subsystem chemistry. Some of the key issues were first discussed in Anderson (*5*), including the roles of certain HNO reactions and of $\Delta H_f°(HNO)$. As mentioned in section 2.2.1, our results of modeling kinetics experiments on H_2/NO mixtures at intermediate temperatures (900–1430 K) indicated a strong dependence of results for predicted global reaction rates on $\Delta H_f°(HNO)$ (which we had expected based on the analysis in the next paragraph, leading us to critically review this parameter [*5*, *70*]). This observation also suggested testing the sensitivity of DZ modeling results to this input parameter. The currently accepted value, 25.6 kcal/mol (298 K) (*70*), was used in obtaining our prediction, τ_{DZ} = 9.33 ms, for the JA2 case at 16 atm (VKMT-JA2). Switching instead to the older recommendation (*69*), 23.8 kcal/mol, we obtain τ_{DZ} = 6.21 ms. The delay is shortened by a factor of about 1.5, a very strong sensitivity indeed. Despite better agreement of this result with the experimental value of 6.5 ms, we emphasize that we are *not* suggesting usage of the older heat of formation; to the contrary, there is very strong independent evidence that the newer value should be chosen (*70*). For the DZ model, in section 4.2.3, we showed that adjustment of inputs such as the temperature, within error limits, can also yield results for τ_{DZ} in better agreement with the experiment. Instead, the intent here is to emphasize the dependence of predicted τ_{DZ} for nitrate ester DZs on the HNO thermodynamics. With the lower heat of formation, τ_{DZ} values at all pressures are shortened by about the same factor for all three of the other nitrate ester DZ cases, indicating the predicted chemistry is much faster with the older value. Modeling of the H_2/NO mixtures in the kinetics experiments is similarly affected. Thus it appears similar underlying chemistry may influence both the H_2/NO and the DZ mixtures.

The chemistry of H_2/NO mixtures in earlier, intermediate temperature, static reactor experiments has been modeled by Wilde (*65*). He noted the significance of the following three key reactions:

$$H + HNO \rightarrow H_2 + NO \,, \qquad \text{(R161)}$$

$$H + NO\ (+M) \rightarrow HNO\ (+M) \,, \qquad \text{(R3)}$$

and

$$HNO + NO \rightarrow N_2O + OH \,. \qquad \text{(R19)}$$

To explain results, he assumed the first two to be in partial equilibrium during the global reaction. Our postprocessing analysis indicates for the DZ mixtures this is only very approximately correct (forward and reverse rates within about a factor of 2). Nonetheless, using these assumptions can yield interesting insights that explain the system's macroscopic behavior. By writing the rate equation for NO and substituting the equation for [HNO] implied by the equilibrium equations for the first two reactions, Wilde derived the following:

$$\frac{\partial[NO]}{\partial t} = -k_{19}\left(K_3 / K_{161}\right)^{1/2}[H_2]^{1/2}[NO]^2 \ . \tag{6}$$

It was observed in the intermediate temperature H_2/NO kinetics experiments that the initial rate of the global reaction exhibits approximately the orders in [H_2] and [NO] that this equation implies. Note that the term $(K_3 / K_{161})^{1/2}$ is equivalent to the equilibrium constant for the pseudoreaction ½H_2 + NO = HNO. Assuming R161 and R3 are equilibrated is equivalent to assuming this pseudoreaction is equilibrated because the pseudoreaction is a linear combination of the two, 1/2 (R3–R161). Using the well-known relation between equilibrium constant of reaction r and its thermodynamics, $K_r = \exp(-\Delta G_r^\circ / RT)$, one can understand why the predictions are sensitive to $\Delta H_f^\circ(HNO)$. Suppose we reduce the input $\Delta H_f^\circ(HNO)$ by an amount C. Then ΔG_{psu}° for the pseudoreaction will also be reduced by C, and K_{psu} will increase by the factor $\exp(C / RT)$; for fixed [H_2] and [NO], there will be an increase in the predicted equilibrium [HNO], as one would expect for a lowered enthalpy, and so the predicted rate of R19 will increase. Thus, for H_2/NO mixtures at ~1000 K, one expects that, for a reduction by 1.8 kcal/mol, the predicted NO consumption rates would increase by a factor of ~2.5. For the JA2 16 atm case at 1500 K, if the assumptions remain correct, one estimates the predicted rate would increase by a factor of ~1.8. This is approximately the reduction factor, 1.5, predicted for τ_{DZ} earlier.* The comparison for DZs is not expected to be exact because, besides the partial equilibrium assumptions being rather approximate, temperature varies during the delay time; furthermore, the DZ mixtures are more complex than the H_2/NO mixtures, especially considering presence of the CO → CO_2 conversion chemistry. These tests nonetheless reveal an important facet of the system.

5.2 Detailed Chemistry of Nitramine Propellant Dark Zones

5.2.1 Parr and Hanson-Parr, 2002 and 2004

As is evident from figure 14, the structure of the DZ region for the PHP-HMX case is much more complicated than for nitrate esters. In the latter case, the heat release profile (e.g., figure 4) has one peak, suggesting mainly one major process takes place, while for the former there are peaks at 0.020, 1.8, and 2.5 ms, suggesting at least three main processes occur. Positions of

* For rigorous kinetics study, one would more typically examine NO reaction rate at an early time, when the extent of reaction and change in conditions is small (but after the steady state is established, of course). However, the approach utilized is adequate for purposes of providing semiquantitative insight.

decays in the species profiles (see figures 15–17) relative to these peaks suggest they are due to CH_2O/NO_2 reaction, N_2O reaction, and HCN/NO conversion to final products, respectively. In this section, we dissect details of the chemistry along the DZ region, showing that these assignments are correct and establishing the most sensitive parameters. CH_2O and NO_2, and sometimes other aldehydes, are major components in the first-stage region of nitrate ester and nitramine propellant flames; their very rapid reaction is responsible for much of the near-surface heat release of those flames at moderate pressures (~1–100 atm) and, thus, is a main factor controlling the gasification and burning rates of such propellants under those conditions (see, e.g., refs *3*, *18*, *132*). To our knowledge, detailed analysis of the main steps involved in this important global reaction has never been presented; though CH_2O and NO_2 are only trace components of the mixture, their nonetheless very fast reaction is striking, and we may learn much from the analysis applicable to models of full propellant flame structure. Therefore, although the delay time to the second-stage flame was not found to be very sensitive to reactions in this region (vide infra), we present that chemistry in considerable detail. It is likely the most sensitive reactions at the time of the first peak in the figure 14 heat release profile are also highly sensitive for burning rates of solid propellants, at least for conditions where a dark zone exists, singling out reactions that may need study to improve propellant modeling in general.

The first peak occurs at 0.020 ms. Pathway diagrams at this time are shown in figures 27–30. The analysis confirms CH_2O and NO_2 are being converted to products, the main reactions being the following:

$$OH + CH_2O \rightarrow HCO + H_2O \,, \qquad \text{(R261)}$$

$$H + CH_2O \rightarrow HCO + H_2 \,, \qquad \text{(R229)}$$

$$CH_2O + NO_2 \rightarrow HCO + HONO \,, \qquad \text{(R349)}$$

$$HCO + M \rightarrow H + CO + M \,, \qquad \text{(R37)}$$

$$HCO + NO \rightarrow HNO + CO \,, \qquad \text{(R200)}$$

$$HNO + NO_2 \rightarrow HONO + NO \,, \qquad \text{(R21)}$$

$$HONO\ (+M) \rightarrow NO + OH\ (+M) \,, \qquad \text{(–R4)}$$

$$NO_2 + H \rightarrow NO + OH \,, \qquad \text{(R94)}$$

and

$$OH + H_2 \rightarrow H_2O + H \,. \qquad \text{(R49)}$$

These reactions are consistent with the overall process being conversion of $CH_2O + NO_2$ to $CO + NO + H_2O$; species profiles in this region (see figures 15 and 16) are also consistent with this conclusion, although the reader may at first find this difficult to discern because the slightly

rising portions of the NO and H_2O profiles between 0 and 0.04 ms are almost coincident with one another. This overall process is 44.3 kcal/mol exothermic and rapid, which is consistent with the associated sharp, positive heat release peak.

Besides these main processes, a few other processes occur to a lesser extent. The main ones are discussed here (see figures 27–30). A trace of the CO is converted to CO_2 via reactions with OH and NO_2. The trace of C_2H_4 begins to be converted to C_2H_3 and then C_2H_2 by similar processes as in the nitrate ester DZs (see prior section), except that OH is the main initial reactant with C_2H_4, rather than H; the process continues until C_2H_4 is completely consumed at about 1.7 ms. Finally, isomerization of HCN to HNC takes place (R194). This reaction rapidly becomes partially equilibrated in most combustion conditions and has nearly achieved that state at this time in this DZ situation, but is not quite there and its net forward rate is fast enough to include on the diagrams. The reaction of HNC with OH becomes very important later (vide infra), but the OH concentration is still so small at this point that the rate of that reaction is just below the cutoff used for the diagrams.

Table 20 contains ordered temperature sensitivity coefficients for the PHP-HMX case at 0.020 ms. The only major thing that has happened at this point is the CH_2O/NO_2 conversion is well underway, and so the sensitivities primarily reflect just which reactions' rate coefficients control that process. Despite R349 being much slower than many of the reactions, it has, by far, the largest sensitivity. R21 is also very high, and both of these are positive. Two reactions of HCO, having opposite signs, follow. These results can be understood by considering the interplay of these and other main reactions in figure 27. The initiation step R349, $CH_2O + NO_2$, leads to both HCO and HONO formation. HCO is a new radical directly formed, and HONO usually undergoes decomposition via –R4, with one product being another new radical, OH. Note that after it is formed, HCO usually decomposes to H, another radical, but frequently instead reacts with NO to form HNO. HNO is not nearly so reactive as H, so as these two reactions compete for HCO, R200 exhibits a negative sensitivity, while that of R37 is positive. Although HNO is less reactive than H, it nonetheless can react with NO_2, forming more HONO, which, in turn, leads to OH formation. Thus, R21 has a strongly positive sensitivity. R349 is intimately important in enhancement of the entire process, especially since it probably is the main cause for the formation of the initial radicals at the earliest times, which perhaps accounts for its sensitivity being higher even than R21. Note that CH_2O is present in excess of the NO_2. When the NO_2 is almost entirely consumed at ~0.05 ms, the rate of CH_2O decay, which had been very steep, is suddenly strongly diminished (see figure 16). It cannot be seen at the scale of the figure, but [OH] and [H] peak near 0.020 ms at 2.5×10^{-5} and 2.0×10^{-5} mole fraction, respectively. As the NO_2 is consumed, the rates of both R21 and R349 become negligible, and concentrations of these radicals fall by factors of 10 and 2, respectively, to minima; shortly after these minima occur, the concentrations begin to increase (concomitant with the next major process). Thus, the overall reaction greatly slows down. The decline in radical concentrations is apparently due to reactions of HNO with H or OH, primarily the former, resulting in NO and H_2

or H_2O, respectively, and the loss of radical centers. Though –R4 is very important, its sensitivity is well down the list, apparently because the reaction is fairly rapid and there are no strongly competing reactions for HONO. It is important to note that the overall CH_2O/NO_2 reaction is so fast in large part because the centrally important R349 and R21 both have fairly low E_a values (see appendix B) and, thus, rather large rate constants at this temperature; also, the HO-NO bond energy is only about 50 kcal/mol, so that, once formed, HONO can readily decompose at these temperatures.

As mentioned previously, when consumption of NO_2 is complete, about half of the CH_2O remains because it was present in excess. The decay rate drops considerably, probably largely because of the aforementioned drop in radical concentrations. This continuing decay overlaps into the region where N_2O decomposes, which is discussed in the next few paragraphs.

As suggested previously, the heat release peak at 1.8 ms (figure 14) is found to be associated with the reaction of N_2O. In fact, examination at a few points along the entire region from about 0.1 ms to just after 1.8 ms shows that N_2O reaction is one of the major processes occurring. A couple of other processes also are important. At the beginning of the region, CH_2O decomposition is finishing, more slowly than when significant NO_2 was present. Towards the end of the region, HCN decomposition also begins to contribute and when the N_2O is consumed takes over. An O-species pathway diagram at 0.90 ms (see figure 31) shows the situation when significant CH_2O is still present. R229 and R261 convert CH_2O to HCO, and the latter is converted to CO via R37 and R200. The N_2O decays, producing N_2, via the following:

$$N_2O + H = N_2 + OH \ , \qquad \text{(R111)}$$

and

$$N_2O \ (+M) = N_2 + O \ (+M) \ . \qquad \text{(R2)}$$

Though slower, R2 is found to have the highest sensitivity at this time, followed by R111, both being positive (not shown). R2 creates a new radical, explaining its high sensitivity. The O atom thus produced primarily reacts via the usual H/O system reaction with H_2 and via a reaction with the trace C_2H_4 as follows:

$$O + H_2 = OH + H \ , \qquad \text{(R51)}$$

and

$$O + C_2H_4 = CH_3 + HCO \ . \qquad \text{(R216)}$$

An N species pathway diagram at 1.8 ms, the second heat release peak, is given in figure 32. Decomposition of N_2O has taken over as the main process and still occurs by R2 and R111. The HCN/NO reaction is beginning, as seen towards the bottom of the figure. Details of the exact reactions will be discussed in the next paragraph. R111 is very exothermic (~63 kcal/mol). Sorted contributions to the total heat release show it is by far the largest contributor, yielding the

sharp peak at this point where the N_2O decay is strong. There are also minor contributions to the heat release from steps connected with the beginning HCN/NO reaction. That chemistry is discussed next.

Detailed analysis was conducted also at the minimum at 2.1 ms in the heat release profile between the maxima at 1.8 and 2.5 ms (diagrams not shown). The results indicate a growing increase in importance of HCN associated chemistry vs. N_2O chemistry. N_2O still plays a very significant role, but it is primarily N_2O newly formed along pathways of the HCN/NO reaction rather than the initial N_2O. This is evidenced by the fact that $[N_2O]$ at times greater than 2.0 ms is very small compared to its initial value (see figure 16). An N species pathway diagram (figure 33) depicts the situation at 2.52 ms, the point of maximum heat release taken herein as τ_{DZ}. Per figure 15, both HCN and NO consumption rates are very high at this time. The main reactions involved for HCN decomposition are as follows:

$$HCN + M = HNC + M \,, \qquad \text{(R194)}$$

$$HCN + O = NCO + H \,, \qquad \text{(R80)}$$

$$HNC + OH = HNCO + H \,, \qquad \text{(R169)}$$

$$HNCO + H = NH_2 + CO \,, \qquad \text{(R181)}$$

$$HNCO + H = NCO + H_2 \,, \qquad \text{(–R103)}$$

$$NCO + M = N + CO + M \,, \qquad \text{(R100)}$$

$$NCO + H = NH + CO \,, \qquad \text{(R96)}$$

$$NH_2 + H = NH + H_2 \,, \qquad \text{(R124)}$$

and

$$NH_2 + OH = NH + H_2O \,. \qquad \text{(R123)}$$

NO primarily reacts immediately with the NH_x species produced in the prior HCN decomposition paths via the following:

$$N + NO = N_2 + O \,, \qquad \text{(R163)}$$

$$NH + NO = N_2 + OH \,, \qquad \text{(R109)}$$

$$NH + NO = N_2O + H \,, \qquad \text{(R108)}$$

$$NO + NH = NNH + O \,, \qquad \text{(–R113)}$$

$$NH_2 + NO = N_2 + H_2O \,, \qquad \text{(R148)}$$

and

$$NH_2 + NO = NNH + OH \,. \qquad \text{(R147)}$$

The NNH produced immediately decomposes as follows:

$$NNH\ (+M) = N_2 + H\ (+M)\ . \qquad (R192)$$

And the N_2O thus produced by R108 reacts rapidly, as earlier in the flame, via R111 and R2. The reactions of NO with N, NH, and NH_2 all have very large rate coefficients because of low E_a values (see appendix B). In general, for nitramine propellant DZs, both HCN and NO are present; therefore, these will probably be the reactions that break the strong N=O bond, leading to N_2 formation. On the other hand, as we mentioned in the introduction, if an ingredient is present in a propellant that produces large quantities of any of these three species near the surface, that propellant probably would not develop a DZ even at low pressures. Also, apparently, were the NH_x species not produced in the HCN decomposition, the NO, and hence $\tau_{DZ,}$ would last much longer.

Our conclusion that the N_2O at 2.52 ms is primarily newly formed, rather than the initial N_2O, is further evidenced by its near equal total rates of production and consumption, as seen in the diagram (figure 33), the relative rate of production being 41 in R108 and the total rate of consumption 32 + 12 = 44 in R111 and R2. The total production and consumption rates of N_2O are actually even closer than this suggests because there are slight contributions from other reactions that have been suppressed from the diagram to reduce clutter (the foremost being NCO + NO = N_2O + CO, R101 producing N_2O at relative rate 2). Thus, the newly produced N_2O is actually in near steady state.

Curiously, there is not a substantial change in [H_2O] during the overall reaction; rather, elemental H in the reactants produces H_2 in the final products (see figure 15). The analysis near the heat release maximum indicates H_2 is produced primarily via R124, –R103, and

$$H_2O + H = OH + H_2\ , \qquad (–R49)$$

where –R49 is not shown on the N species diagram. R124 is by far the largest of these. Another curious result is that T reaches a maximum at about 2820 K just after the heat release maximum and then drops by about 30 or 40 K (see figure 14). Associated with the falling T is an endothermic trough in the heat release profile at 2.68 ms. This is unusual enough that one might wonder whether it is a numerical artifact. However, long experience with the code used, and testing of it via changes in gridding parameters, has convinced us that this code seldom produces such errors (and never with such smoothly varying curves). The result is quite reasonable, and sorted contributions of the reactions to the total heat release at the endothermic trough show that it is primarily due to decomposition of H_2O via the following very endothermic reaction:

$$H_2O + M = H + OH + M\ , \qquad (–R61)$$

which dominates the heat release just after the HCN is gone. Note that [H] and [OH] radicals are actually well below their equilibrium values at 2.6 ms (see figure 16), where HCN is gone, thus

explaining why the reaction proceeds in the direction shown. [H] and [OH] both rise considerably after 2.6 ms, accounting for the endotherm and drop of T. One may note there is also a slight trace of NO in excess of the HCN, which slowly decays at t >2.6 ms; however, that overall process is exothermic, though not large enough to overcome the endothermicity of –R61.

This nitramine DZ case is opposite that typical of air or O_2 supported combustion, e.g., with hydrocarbon fuels, where radical concentrations just after fuel consumption are usually *higher* than equilibrium and slowly decay via recombination reactions in the burnt gases – with an associated slight *increase* to final temperature. This so-called "radical overshoot" usually occurs via rapid radical growth due to the chain branching reactions:

$$O_2 + H = O + OH, \qquad \text{(R50)}$$

and/or

$$CH_3 + O_2 = O + CH_3O. \qquad \text{(R307)}$$

However, R50 and R307 contribute little when the oxidizer is a nitrogen oxide, e.g., NO, NO_2, N_2O, or N_2O_4, because negligible O_2 is present. Instead, for such oxidizers, radical concentrations typically are about equal to or below equilibrium values just after fuel consumption; when significantly below, a slight "temperature overshoot" above adiabatic is noticeable, as in figure 14.

Ordered temperature sensitivity coefficients for the PHP-HMX case at 2.52 ms are given in table 21. This indicates which rate coefficients would strongly affect computation of τ_{DZ}. Note that the largest of these, R2, is a major radical source for the system during decay of the initially present N_2O. Certain of the reactions involved in the HCN decomposition, such as R169, R147, and R148, are also very sensitive. R169 allows breakage of the double bond in HNCO via R181. Formation of NH_2 in R181 allows NH_x to form, which can react with NO. NH_2 and NO can then react with two product channels expressed in R147 and R148. These have strong sensitivities of opposite sign, the channel to NNH + OH being radical products that promote further reaction, the one to $N_2 + H_2O$ being to much less reactive, closed shell species which comparatively slows the reaction; thus they have strong positive and negative sensitivities, respectively. Note that the reaction

$$HNO + NO \rightarrow N_2O + OH\ , \qquad \text{(R19)}$$

which is so important for nitrate esters (see prior section), barely makes the cutoff used in this list. It is below the floor level used in the pathway diagrams but makes a minor contribution to the radical pool formation during the initial N_2O decay period. For nitramines, it is not nearly as sensitive as R2. It would probably be relatively more important were there less initial N_2O. Also note that the sensitivity of reactions involved in the initial, fast reaction of the CH_2O/NO_2 traces are not very large at the ignition time, so mildly changing their rate coefficients should not strongly affect τ_{DZ}.

Similarly to the nitrate ester results, we can also cite a case from recent combustion modeling of a nitramine pseudo-propellant with no DZ (see recent results on pure RDX by Anderson and Conner [*25*]). Combustion of pure RDX exhibits no DZ even at the lowest pressures, as long as there is no enhancement of combustion by surface heating as by a CO_2 laser (*37*). The modeling results at 0.5 atm show that, like the table 21 DZ results, although the ordering differs, the near-surface temperature sensitivities are largest to R169, R181, R147, R148, R2, and some other small molecule chemistry. Thus, when no DZ is present, the reactions that would be sensitive for structure of a nitramine DZ when one forms have instead a primary effect on the computed burning rates. Those results are much less sensitive to the larger molecule RDX decomposition reactions. As an aside, we note this suggests models of pure RDX combustion may be very forgiving regarding possibly major errors in the early decomposition pathways. Curiously, two mechanisms predicting very different initial RDX decomposition products yielded largely similar results, possibly due to similarity of the DZ kinetic subsets, which supports this notion. This might not remain the case, however, when a binder is used, as in RDX propellant formulations, because a DZ more typically forms, and the burning rate becomes insensitive to the spatially separated DZ and second-stage chemistry; the first-stage chemistry is then more important to the burning rate.

Returning to the PHP-HMX case, tests of the response of τ_{DZ} to changes by factors of 2 or 0.5 in selected sensitive rate coefficients are presented in table 22 (of course, for R2, which has pressure dependent k_2, both high- and low-pressure A factors were adjusted). The beginning of table 22 includes results of tests on all of the sensitive reactions at τ_{DZ} from table 21, and, at the end, test results for the two most sensitive reactions from table 20 at 0.020 ms, where the CH_2O/NO_2 reaction is occurring. The results indicate that the response to the changes is strong for the most sensitive reaction at τ_{DZ}, R2; a factor of 2 or 0.5 produces a decrease/increase in τ_{DZ} by about a factor of 1.5, respectively. The responses decrease, as one would expect, as one goes down the list of reactions suggested by table 21. Tests for the two most sensitive reactions for CH_2O/NO_2 conversion, shown at the end, result in negligible changes in τ_{DZ}, as the fact that they are absent from the sensitivities listing of table 21 suggested would happen. This is due to the fact that changing either of those rate coefficients affects the rate of the heat release due to that conversion process at a very early time; the process is so rapid that the time for it is very small compared to the time required for the later DZ processes. Thus, moderate changes in the CH_2O/NO_2 rate do not much affect τ_{DZ}. Actually, in expanded plots of the heat release peak at that early time (not shown), we noted that the time to that peak changes by about 25% for the factor of 2 changes that were made in R349; so the result at that early time is indeed very sensitive to that reaction, as table 20 indicates. In general, our brute force testing is assuring that the T sensitivity analysis at τ_{DZ} has indeed singled out all the important reactions controlling τ_{DZ}'s magnitude and can be used to indicate how error limits in the *k*'s affects precision of the computations.

Upon consideration of the chemistry involved, there is another input parameter to which τ_{DZ} could be very sensitive. Note that R194 is a major pathway in figures 32 and 33. This reaction is 13 kcal/mol endothermic. It is at first surprising this main initial step in the HCN decomposition is not very sensitive. Upon further analysis using our postprocessing tools, we find the reaction rapidly becomes partially equilibrated under DZ conditions. Thus the main effect of R194 is to set the [HNC] to [HCN] ratio at partial equilibrium according to its thermodynamics. Fast equilibration of R194 explains why the system is not very sensitive to k_{194}. The rate of HCN consumption along this main pathway is then controlled by the rate of R169; thus, k_{169} is very sensitive. However, what becomes immediately obvious upon further consideration is that the thermodynamic parameters controlling [HNC] in R194 probably would also be very sensitive since [HNC] is a main factor controlling the rate of R169. In particular, while the thermodynamics of HCN are precisely known, the thermodynamics of HNC are only known from quantum calculations. Those inputs are traced to calculations of mechanism parameters used for combustion modeling of nitramine propellants by C. F. Melius, based on the BAC-MP4 quantum method (*133*). Quantum methods typically establish entropy and heat capacity functions to high enough precision that errors in them do not strongly affect kinetic calculations. However, heats of formation are frequently more problematic. Accuracy of the method used is typically about ±2 kcal/mol. So, we tested how τ_{DZ} is affected by addition or subtraction of 2 kcal/mol to/from the nominal HNC heat of formation. Recall the nominal result is 2.52 ms. Adding/subtracting 2 kcal/mol yielded 2.80 or 2.33 ms, respectively. The results are clearly sensitive and in the expected directions, but though substantial, the change is not extremely large. Consideration of heat release plots (not shown) indicates the time to the maximum at 1.8 ms, where N_2O consumption occurs, is not strongly affected, while the time after that to the HCN/NO reaction is changed by about a factor of 1.5; this is not surprising, the HCN/NO chemistry is too slow to affect consumption of the initial N_2O very much. Thus, for the current mixture, the sensitivity to heat of formation of HNC is diminished by the fact that the HCN/NO conversion time is nominally only the last 25%–30% of τ_{DZ}. However, this might not be true in general (see next paragraph).

To close this subsection, we highlight some key points indicated by the previous results connected with the traces of CH_2O, NO_2, and N_2O in the initial mixture. First, the early CH_2O/NO_2 reaction does not strongly change the DZ mixture ratio of the product species CO, H_2, and NO it produces. Nonetheless, the reaction clearly has a profound influence on τ_{DZ} because it raises the temperature by about 40 K (see figure 14). As we have seen in section 4, computed τ_{DZ} of various mixtures, including this one, can change by nearly a factor of 2 for initial T changes of this magnitude, so the rapid exothermic reaction of these two trace species is clearly very important. Second, the sensitivity results show the initial N_2O is also having a profound influence on computed τ_{DZ} because of the reactions R2 and R111 its presence makes possible, especially the former since it is a radical initiation step. These results explain the strong sensitivity of the overall τ_{DZ} results to the initial concentrations of these trace species (see section 4). Finally, these results suggest that in a hypothetical case of a nitramine DZ mixture

that did not initially contain much of these three trace components, that mixture's τ_{DZ} would be controlled more exclusively by the HCN/NO chemistry. The result would then be much more sensitive to the heat of formation of HNC. The HCN/NO chemistry also plays a major role in RDX combustion under conditions where there is no DZ; HCN is present in the flames and so both R194 and R169 are important reactions; R169 is found to be highly sensitive for burning rate prediction of RDX (*25*), and probably would be for nitramine propellants in general. We therefore suggest further examination of both k_{169} and the heat of formation of HNC would be beneficial.

5.2.2 Litzinger et al., 2000

The structure of the LLT00 (*113*) DZ is even more complicated than that of PHP-HMX discussed in the preceding section. The duration is quite short, and processes are less well defined, i.e., they overlap more (see figures 18–21). For example, there is a much more rapid HCN decomposition established even at the early part of the DZ leading up to the region of sudden, sharp decay. Additionally, the presence of a trace of NH_3 has a strong accelerating effect; that was proven by the test in which we removed it, resulting in a significantly increased delay time (see section 4.3.2). It appears there are no studies where NH_3 has been detected in DZs (see reviews in Vanderhoff et al. [*4*] and Yang et al. [*37*]) besides the Litzinger group (e.g., reference *113*). And it is important to note that many of the other studies used diagnostics that should capably detect NH_3. It would appear the main difference is that many propellants studied by Litzinger's group used energetic binders, while most other groups did not. Most energetic binders contain azide functionalities, and these can decompose, leading to NH_x. With this consideration, it is curious that in the studies of Parr and Hanson-Parr using RDX or HMX mixed with GAP and BTTN no NH_3 was observed (*107–109, 118, 119*). Additionally, not all of the propellants using energetic binders studied by LLT00 produced NH_3. So, it appears energetic binders with azide functionalities can produce NH_3 but not all of them do, at least not for all conditions, or perhaps it is produced in those cases but does not survive into the DZ. We discuss in this section the changes NH_3 produces in the DZ chemistry vs. the PHP-HMX case. It is found, not surprisingly, that the chemistries in the two cases are rather similar except for presence of this species. We will also suggest why the computed delay in the LLT00 case is so much shorter, and the heat release profile consequently suggests more blending of main overall reactions; there is no long region with nearly zero heat release. The chemistry of the two cases is in many regards qualitatively very similar, and where this is so, results for the LLT00 case will not be shown in as much detail. We will further compare and contrast detailed chemistries of these two cases as we proceed.

Like the PHP-HMX case, the early peak in the heat release profile, here at 0.0078 ms, is found to be due to the overall CH_2O/NO_2 reaction (see figures 18 and 20). Although relative rates differ, the chemistry in the LLT00 case is found to be similar, so a pathway diagram at that point is not shown. The main difference is that NH_3 decay chemistry also begins (see figure 21) via the following reactions:

$$NH_3 + OH = NH_2 + H_2O \ , \qquad \text{(R149)}$$

$$NH_2 + NO = N_2 + H_2O \ , \qquad \text{(R148)}$$

$$NH_2 + NO = NNH + OH \ , \qquad \text{(R147)}$$

and

$$NNH\ (+M) = N_2 + H\ (+M) \ . \qquad \text{(R192)}$$

These are present at rates about 0.05 relative to the fastest reactions at this point, R94 and R261. Temperature sensitivities at this point are shown in table 23. The sensitive reactions at their respective CH_2O/NO_2 reaction times are mostly the same as those for the PHP-HMX case, except that R147, R148, and R149 are now on the list. The radical vs. stable molecule character of the R147 vs. R148 channels makes these particularly important. R147 is chain-branching; it appears radical growth due to this preferred product channel is what leads to the positive sensitivity of the results to the initial $[NH_3]$. These reactions continue through the entire region where the initial NH_3 decays, up to about 0.07 ms, in figure 21. There is a peak in the NH_3 profile, near the heat release maximum at 0.10 ms, due to newly formed NH_3; this peak will be discussed in a later paragraph. Incidentally, a plot of heat release from the test in which the initial NH_3 was removed indicated that the initial CH_2O/NO_2 decay position was not strongly affected, but the position of the strong heat release peak from HCN/NO consumption was, i.e., the two processes were more separated in time.

Comparing the PHP-HMX vs. LLT00 CH_2O/NO_2 decay regions, note that whereas in the initial mixtures $[CH_2O]$ is the same at 0.03 mole fraction, $[NO_2]$ for the former is 0.01, whereas in the latter it is 0.07 (see tables 8 and 9). CH_2O is in excess for the former; NO_2 in excess for the latter. This apparently is the cause of the striking difference in magnitudes of their τ_{DZ} values, 2.52 vs. 0.107 ms, respectively. The initial T values are similar, 1450 vs. 1500 K, respectively, so though this difference will tend to make the LLT00 chemistry somewhat faster, the effect is expected to be only about a factor of 2, not an order of magnitude. However, the dissimilarity of concentrations of trace species has a strong effect. In the former case, the CH_2O/NO_2 reaction leads to a fast initial T increase of only about 40 K. In the latter, the similarly fast initial T rise leads to about a 200 K jump in T to about 1700 K (see figure 18). This probably largely explains the much shorter τ_{DZ} and associated blending of initial reactant consumption ranges. Note that the excess CH_2O in the former case decays much more slowly than the excess NO_2 in the latter (see figures 16 and 20). That observation is probably due to the large A factor, nearly barrierless k_{94}, leading to the well-known rapidity of

$$NO_2 + H \rightarrow NO + OH \ . \qquad \text{(R94)}$$

R94 in fact plays the major role in NO_2 consumption after the CH_2O is gone. Since the comparative mixture ratios will allow 3× as much CH_2O/NO_2 to rapidly react in the latter case than the former, and since the NO_2 can continue reacting more rapidly in the latter, all processes

contributing to heat release, a rapid initial temperature rise about 5× larger in the latter is not surprising. Note in figure 18 there is a slight bump in the heat release profile at ~0.033 ms, to the right of the CH_2O/NO_2 associated maximum. The tail end of the NO_2 profile occurs at about the same point, strongly suggestive that consumption of the excess NO_2 is very fast at that time and causes the bump. Confirming evidence for this notion was obtained by examining the sorted heat contributions of the reactions to the total heat release at that point (not shown). R94 is exothermic and has a contribution ~3× larger than any other reaction there.

As can be seen in figure 20, the N_2O consumption becomes rapid right after the NO_2 consumption finishes. HCN consumption overlaps both of these processes (see figure 19 and also the shape of the HNCO intermediate profile, the main species produced as HCN is consumed). However, the processes are more blended than in the PHP-HMX case. There is no strong, separate maximum associated with N_2O consumption in the LLT00 case; that heat release is apparently overshadowed by the release associated with HCN/NO decay. But, note that the main heat release peak at 0.107 ms in figure 18 is very broad towards its shorter time side; this result is suggestive of a strong N_2O consumption contribution towards that side. N-species pathway diagrams at 0.075 ms, which is in that N_2O consumption region, and at 0.107 ms, the maximum, where HCN/NO reaction occurs, are given in figures 34 and 35. The main reactions are mostly identical to those of the PHP-HMX case, so we will not repeat them here. Sorted T sensitivities at τ_{DZ} are given in table 24. Most of the sensitive reactions for the LLT00 case are the same as those for PHP-HMX. However, the relative sensitivities of R147 and R148 are much larger for LLT00, and R149 is now on the list; these results are clearly due to the trace of NH_3 present in the initial LLT00 DZ mixture. Note that

$$NO + NH \rightarrow NNH + O \qquad (-R113)$$

is also new on the list. NH_2 and NH can result not only from H abstractions from NH_3 but also from the main pathway HCN → HNC → HNCO → NH_2 → NH (see figure 35). Therefore, it was initially unclear to us whether the comparative prominence of –R113 here is due to early NH production from the initial NH_3 or NH from HCN, with enhancement in this case due to some unnoticed factor. The reaction is, however, similarly prominent in the sensitivities list for the test case we ran with no initial NH_3 present (not shown), suggesting the NH responsible is primarily from HCN. Also for that test case with no NH_3 present, the relative ordering of R147 and R148 vs. other reactions is more similar to that of the PHP-HMX case, and R149 drops off the list, further confirming the importance of the initial NH_3. So for the LLT00 case, R147 and R148 are important due to NH_2 arising both from NH_3 and from HCN. Note also that R349 and R21, which are associated with the CH_2O/NO_2 decay, now appear on the list of reactions that remain sensitive at τ_{DZ}, in contrast to the PHP-HMX case. This result is apparently due to the fact that the CH_2O/NO_2 and HCN/NO processes occur much closer in time. The delay time to, and width of, the former process is more comparable to τ_{DZ} for LLT00 than for PHP-HMX.

As we mentioned a few paragraphs prior, there is a peak in the NH_3 profile at about 0.10 ms, near the heat release maximum (see figure 21). This curious peak has nothing to do with the initial NH_3; rather it is clearly due to NH_3 produced during the HCN decomposition along the pathway to NH_2. Just prior to the main heat release maximum, analysis of the reactions shows that this trace of newly produced NH_3 comes primarily from the following:

$$NH_2 + H_2O = NH_3 + OH \ . \qquad (-R149)$$

Apparently [NH_3] has fallen, and there is a major source of NH_2 from the HCN consumption path, so R149 temporarily reverses. At later times, [OH] is considerably larger, and HCN has been consumed, so there is no longer such a large source of NH_2. Then R149 reverts to the forward direction, and the new NH_3 is consumed. As we mentioned earlier, changes in direction of an elementary step can occur during an overall process, producing curious results; here, R149 changes net direction twice. Examination of the PHP-HMX case shows that a trace mole fraction of NH_3 of similar magnitude also forms near the DZ ignition point for the identical reason (not shown). Although the unusual shape of the predicted NH_3 profile for LLT00 catches the eye, the trace of NH_3 formed in the second-stage flames appears to be inconsequential.

Responses of τ_{DZ} to factors of 2 or 0.5 changes in rate constants of the sensitive reactions are shown in table 25. The changes are by about a factor of 1.3 for the most sensitive reactions. These changes are not as large as for the prior datasets but still indicate very important quantitative sensitivities. The response rapidly becomes smaller as one goes down the ordered list of sensitive reactions, similar to observations for the earlier datasets.

Note in figure 18 that there is a maximum in T just after the heat release maximum and an endotherm in the total heat release associated with the fall in T just after the peak. The reasons for these results are entirely similar to those for the PHP-HMX case.

We also tested the sensitivity of τ_{DZ} to changes in the heat of formation of HNC in similar fashion to the procedure used for the PHP-HMX case. Tests were performed via 2 kcal/mol addition or subtraction to/from the nominal HNC heat of formation. The nominal τ_{DZ} changed from 0.107 to 0.115 or 0.996 ms, respectively. Once again, the change is about 7%, which is not strong, but is significant. And once again, the position of the CH_2O/NO_2 related peak in the heat release profile is not strongly affected but that of the HCN/NO heat release maximum is.

6. Conclusions

A mechanism for modeling the structure of propellant DZs has been developed over the last ~20 years. This mechanism was tested against experimental data obtained from a comprehensive critical review of all available literature. Results of both the critical selection process and

modeling thereof are presented herein. This renewed effort to complete and extensively document our testing of the phenomenon was motivated not only by academic interest in the curious DZ formation, but also by realization via other recent modeling studies of full propellant flame structures and burning rates that testing of the mechanism is germane to the results of those more complicated models. The mechanism represents a core set of small molecule reactions that is centrally important in larger propellant mechanisms.

Not many datasets are available for DZ model tests because a fairly large number of parameters must be known; thus the experiments demand both complex instrumentation and intensive efforts. We required retained datasets to meet internal consistency testing on both energy and mass balance; thus a few promising datasets unfortunately had to be discarded. Both the method for extraction of τ_{DZ} from experimental data, utilized by many researchers previously, and usage of the plug flow reactor approach for predicting τ_{DZ} require several simplifying assumptions. By treating previous results for the flame structure predicted by a more complicated propellant nitrate ester model as if it were "experimental data," the present work includes the first quantitative examination of how well those assumptions perform. Assumptions used in the data extraction from experiments suggest the actual values are likely smaller than those extracted by about 25%–30%. The plug flow assumption used in the modeling appears to lead to insignificant systematic errors. The systematic error in experimental data extraction is significant, and one would like to correct for it were it known how; however, at present the precision of τ_{DZ} from both experiment and the simple model is typically limited to magnitudes even somewhat larger because of random errors from other sources. Errors of such magnitudes do not preclude usage of the data in DZ model tests but do diminish the claims that can be made regarding results. Main factors affecting those precision limits are, for the experiments, the determination of L_{DZ}, and for the model, the precision of the input T_{DZ} and some trace species concentrations from experiments and of the input reaction rate coefficients and a few thermodynamics parameters from other sources. Experimental and predicted τ_{DZ} values we obtained generally agree within the combined error limits of both. The results are encouraging that the mechanism we have developed hopefully includes all the salient species and reactions, described by thermodynamic and kinetics parameters that are reasonably close to reality. However, the reader will note that we have carefully refrained from claims of high certainty that the mechanism is in fact correct. The DZ phenomenon involves complex mixtures, the number of test datasets is small, and the precision limits from both the experiments and predictions are fairly large. We therefore advocate usage of our mechanism but also suggest further experimentation for testing is desirable.

In prior work, we developed reduced mechanisms for DZ modeling based on a much earlier version of the detailed mechanism (*6*–*9*). We have not revisited that work to see whether the current detailed mechanism would result in the same reactions being selected for retention in a skeletal mechanism. However, it seems likely that they would be for nitrate ester DZ modeling.

The initial nitrate ester mixtures have not undergone very drastic revisions; thus, with proper updates of the elementary reaction coefficients, it seems likely both skeletal and reduced mechanisms would be unchanged. This is not the case for the nitramine DZs considered herein, because in the more recent retained studies, new, important trace species such as CH_2O, NO_2, and NH_3 are included in the initial mixtures. Chemistry for these, of course, was not retained in the nitramine skeletal and reduced mechanisms.

We also have determined that a steady state pertains to the radicals even at very short times. An important ramification thereof is that the assumption that initial radical concentrations are negligible is almost certainly very good. That conclusion will likely apply even if significant changes to the mechanism eventually prove necessary.

This discussion leads naturally to the issue of what future work might be done to improve the testing, a subject we have considered extensively. The main possibilities appear to be a few further strand burner experiments and testing using kinetics methods that typically provide much more precise data. One notes the precision of the data from the strand burner experiments is not very high, limiting the value of the results for kinetics testing. It does not appear that any substantial improvement is readily possible. A further very important limitation is that strand experiments do not readily lend themselves to variation of fundamental mixture parameters, such as T_{DZ} and mixture ratio. These parameters currently can only be crudely controlled, if at all, via adding complication to an already complicated experiment, e.g., by varying initial T of the unburnt propellant or by changing its formulation. This is not to imply further strand experiments would not have much value—to the contrary, if carefully thought out, a few more experiments directed towards DZ structure elucidation could be very useful. Despite their limitations, the datasets currently available have provided invaluable information as to the initial T and mixture ratio conditions and data for quantitative testing that is at least moderately demanding. It appears that it would be useful to have perhaps one further dataset for nitrate esters and two for nitramines,* preferably studied over as wide a range of pressure as possible. Examination of the pressure dependence of mixture ratio is especially important for nitramines because (as discussed in section 3.2.3.1) pyrolysis experiments indicate the intermediate mixture produced may be surface temperature dependent (*13, 14*) and, thus, would be indirectly affected by pressure; no such nitramine datasets exist. If study of the DZ structure is to be a primary focus of such efforts, care should be taken on selection of the propellant(s) to choose from formulations with fairly steady, one-dimensional flames.

We mentioned previously that fundamental DZ mixture parameters are not easily controlled in strand burner experiments. These parameters are much more readily varied, and more precisely known, in typical gas-phase kinetics experiments; therefore, we would advocate studies directed towards DZ-representative mixtures. Probably the shock tube technique is the best currently available that would most readily be applied. Mixture ratios can be precisely varied, and T and P

*Further exploration of the presence and role of NH_3 vs. binder type might be important and suggest even more studies.

much more readily controlled and precisely known, in such apparatus. Obviously variation of T and P are important because they yield information on gross response of the system to fundamental physical parameters; variation of T indicates global activation energy, which can be a key factor in understanding what are the most important elementary reactions controlling the system response. However, variation of mixture ratio is also very important. The results can be designed to indicate the orders of reaction in the various mixture components, which typically provides some of the most stringent test data to develop mechanisms. It is relatively difficult for an important reaction to be completely overlooked for inclusion in a mechanism if precise data from experiments varying all of these parameters over wide ranges is available. We do realize that the mixtures being suggested for study are considerably more complicated than typically attempted in shock experiments, and that some of the components (H_2O, NO_2, CH_2O) are not easily handled; also, the need to work with high concentrations of reactants with little or no inert gas injects complications (e.g., possible safety and vibrational energy equilibration rate issues). However, it appears that much could be learned from initial studies on mixtures composed of less complicated subsets of the DZ components, building towards more and more complicated mixtures. Furthermore, the results would be applicable not only to DZ modeling but also to other phenomena, such as NO_x emissions modeling, because the important reactions in these areas heavily overlap.

The present results indicate predictions of L_{DZ} based on complex chemical mechanisms are much less precise than has been commonly realized. Without mentioning specific individuals, we have noted over the years that typically when preliminary models of propellant flame structures have missed predicting L_{DZ} by as much as 25%–50%, many modelers have become very concerned, perhaps properly considering prior status of understanding of some of the controlling factors. The present work indicates for two major propellant types what those factors are, and they include important sensitivities to input kinetics parameters. Those parameters typically are not known to much better than about 50%; indeed, it is very difficult in kinetics experiments to achieve precision of 20% and accuracy. (Critical reviewers typically assign larger error limits, even when a group makes claims to 20% and their results are retained, because so often several excellent groups studying the same reaction have achieved limits of that order but disagree in the absolute numbers by much larger amounts; the area is very demanding, and hidden pitfalls many.) Thus, solid propellant combustion modelers need to be aware of these sensitivities and, if they achieve agreement of L_{DZ} within 50%, realize the model may not be doing too badly. One suggests they might try variation of the sensitive rate constants for their particular conditions, if they have capability to determine them, or, if not, to try varying those of sensitive reactions suggested herein. If reasonable agreement can be achieved by variations within rate constant error limits, the model could then be declared qualitatively, and semiquantitatively, acceptable. The present work reveals there typically is also a strong sensitivity to initial mixture conditions, especially T_{DZ}. Therefore, it would seem prudent to consider that models of the full flame structure might well not predict the conditions at leading edge of the DZ sufficiently accurately to avoid a significant imprecision in predicted L_{DZ}.

To summarize, we have had an interest in measurements and modeling regarding the DZ structure of solid propellants for about 20 years. Our recent discovery that reactions controlling this phenomenon at low pressures (5–100 atm) are more important to the burning rates at high pressures than had been previously realized inspired us to complete an exhaustive critical review of the literature to select datasets for testing DZ mechanisms; model the resulting datasets; analyze the solutions obtained in order to understand which reactions control the DZ structure, in particular τ_{DZ} and L_{DZ} and how the species evolve; and write this extensive report documenting the results. This effort should prove to be very valuable to solid propellant modelers and formulators, providing insights into some of the most important chemical features in propellant flames; to suggest further strand burner experiments regarding issues that would benefit from further attention; and to guide kineticists and mechanism developers interested in studies relevant to DZ and solid propellant reactions and mechanisms.

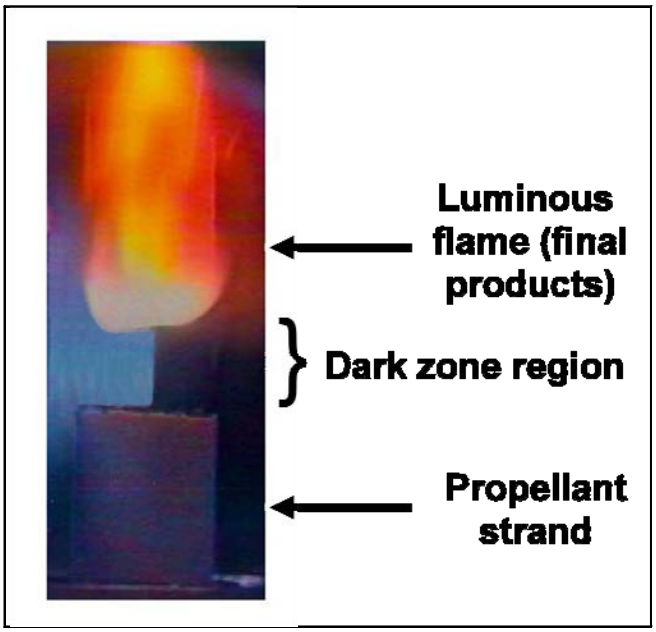

Figure 1. A strand of M43 propellant, an RDX-based propellant, burning in cigarette fashion at 15.5 atm. The strand is ~6-mm diameter. The picture has been edited in a photo editor to remove a shiny, distracting reflection from a window in the blue region to left and behind the strand and to brighten the strand for visibility.

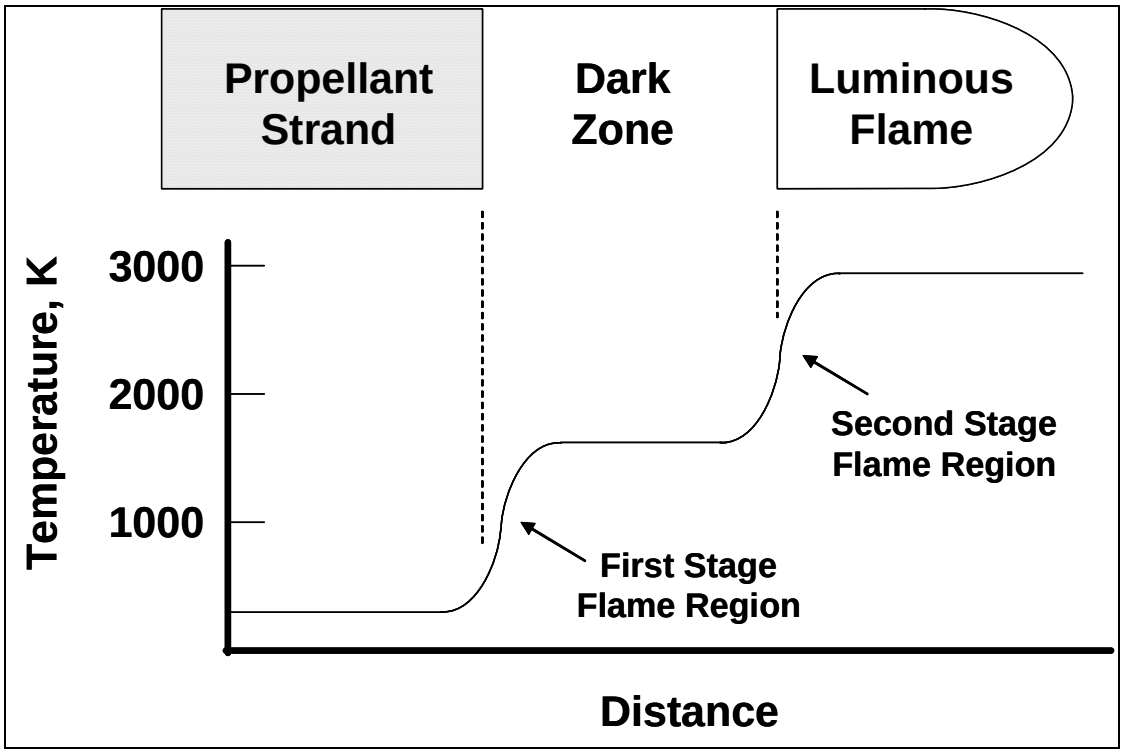

Figure 2. Idealized schematic of a solid propellant strand burning steadily, at constant pressure, with a dark zone. In typical experiments, the strand is oriented vertically, but it is shown here rotated 90° clockwise to make the correlation to the temperature profile clear.

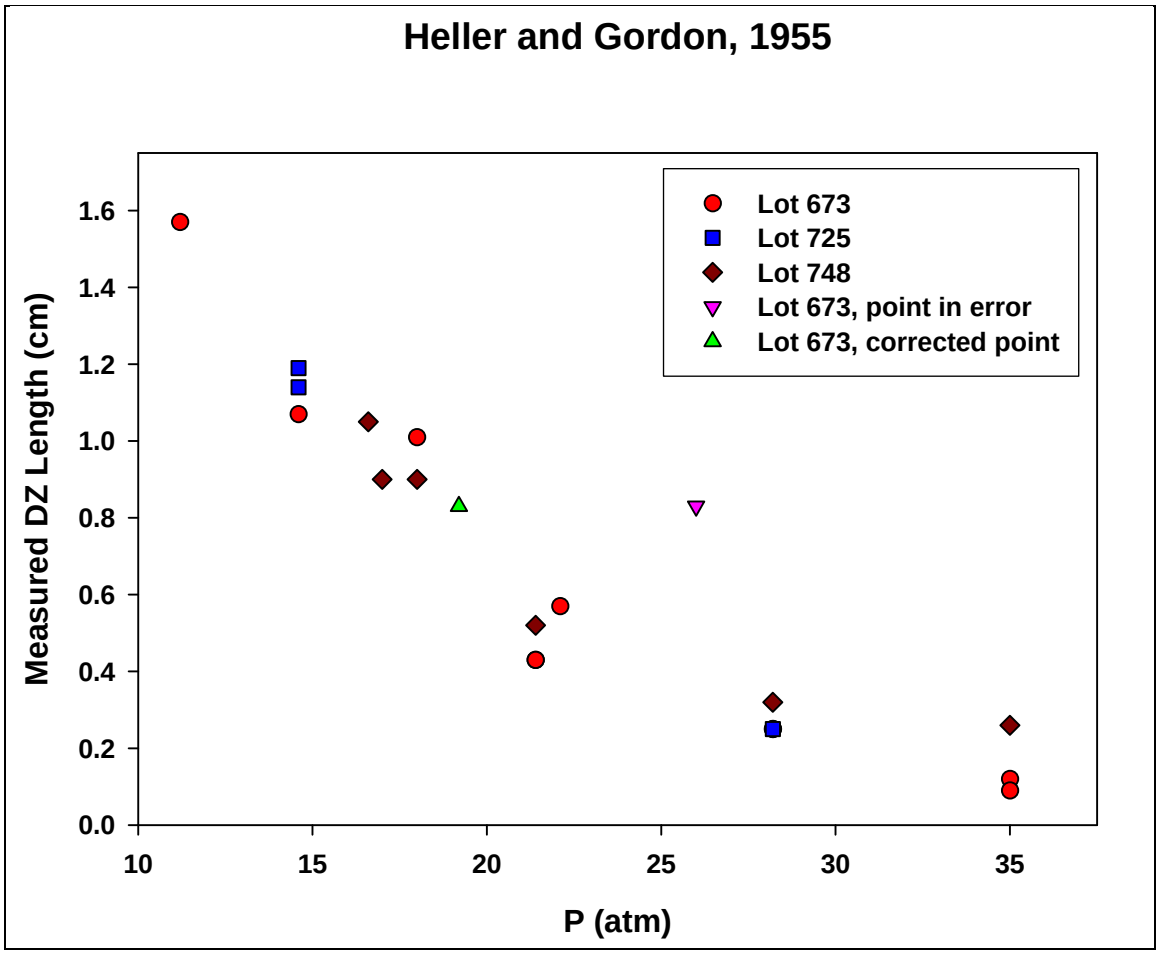

Figure 3. Measured dark zone length vs. pressure for Heller and Gordon (HG55) (*94*) NC-NG propellants. The "point in error" at 26.0 atm and our revision yielding the "corrected point" at 19.2 atm are explained in the text. Note that five of the points almost exactly overlap (same-valued), and this is not easy to indicate.

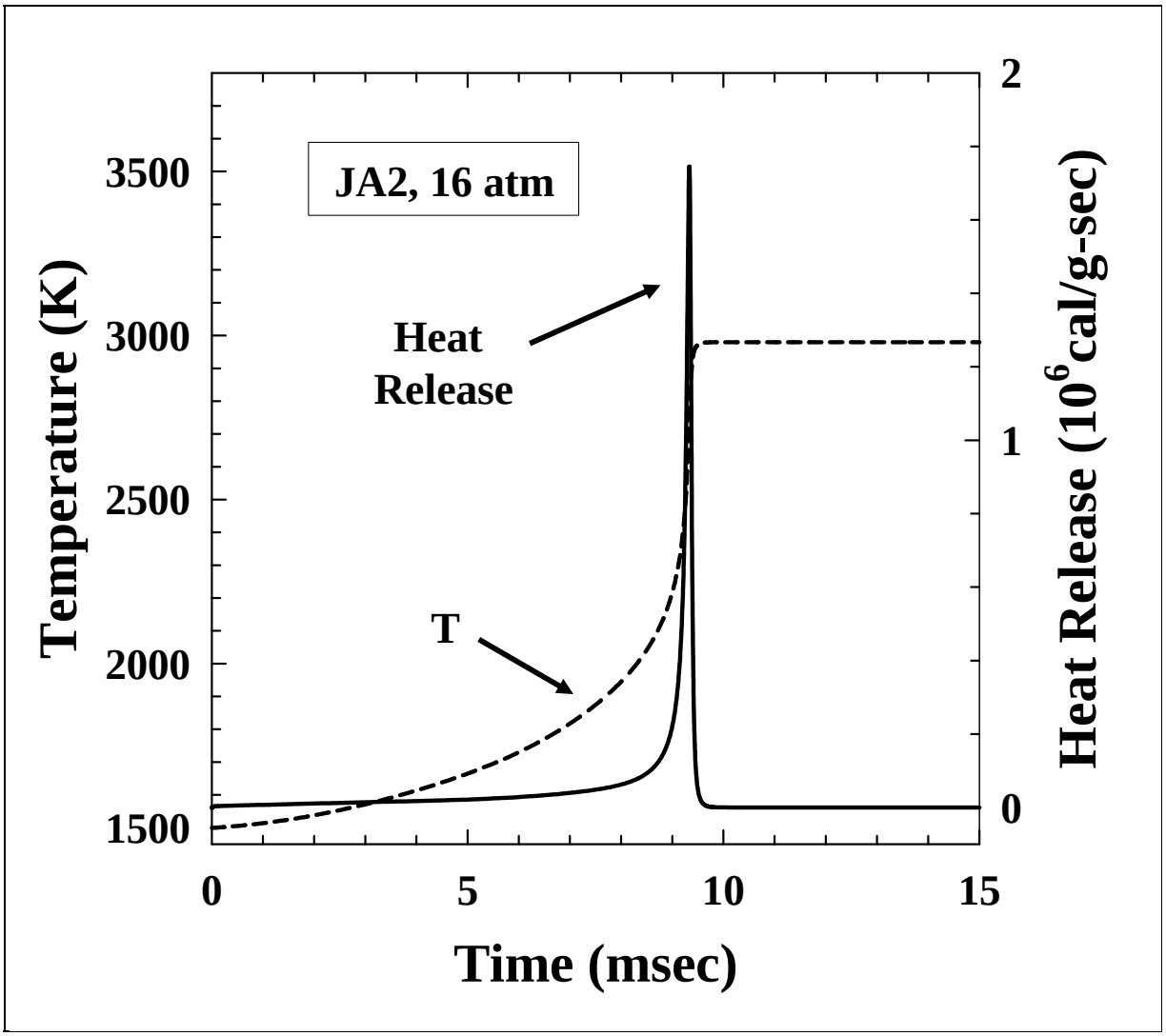

Figure 4. Predicted temperature and heat release profiles for the DZ of JA2 at 16 atm, studied experimentally in VKMT-JA2 (*53*, *98*).

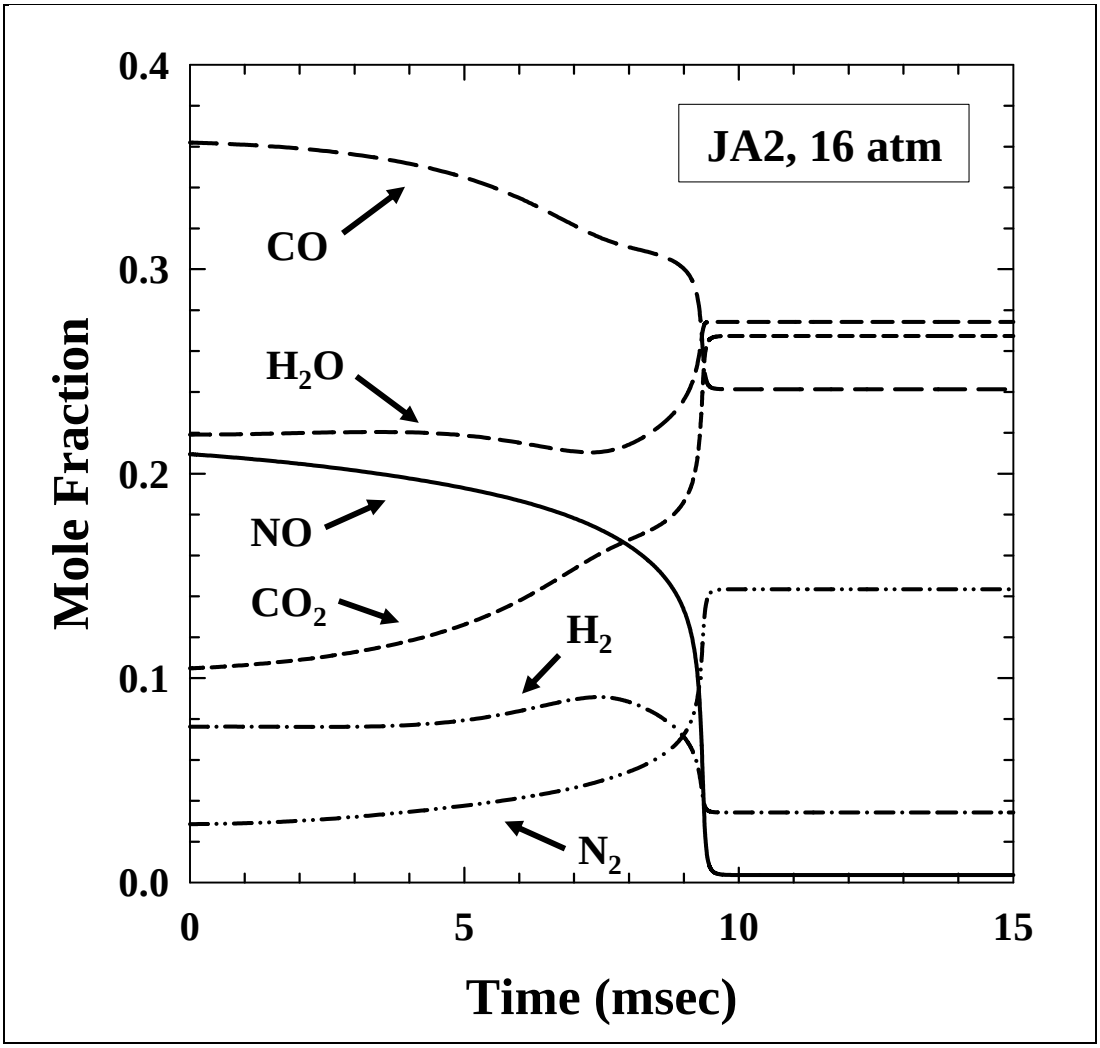

Figure 5. Predicted major species profiles for the DZ of JA2 at 16 atm, studied experimentally in VKMT-JA2 (*53*, *98*).

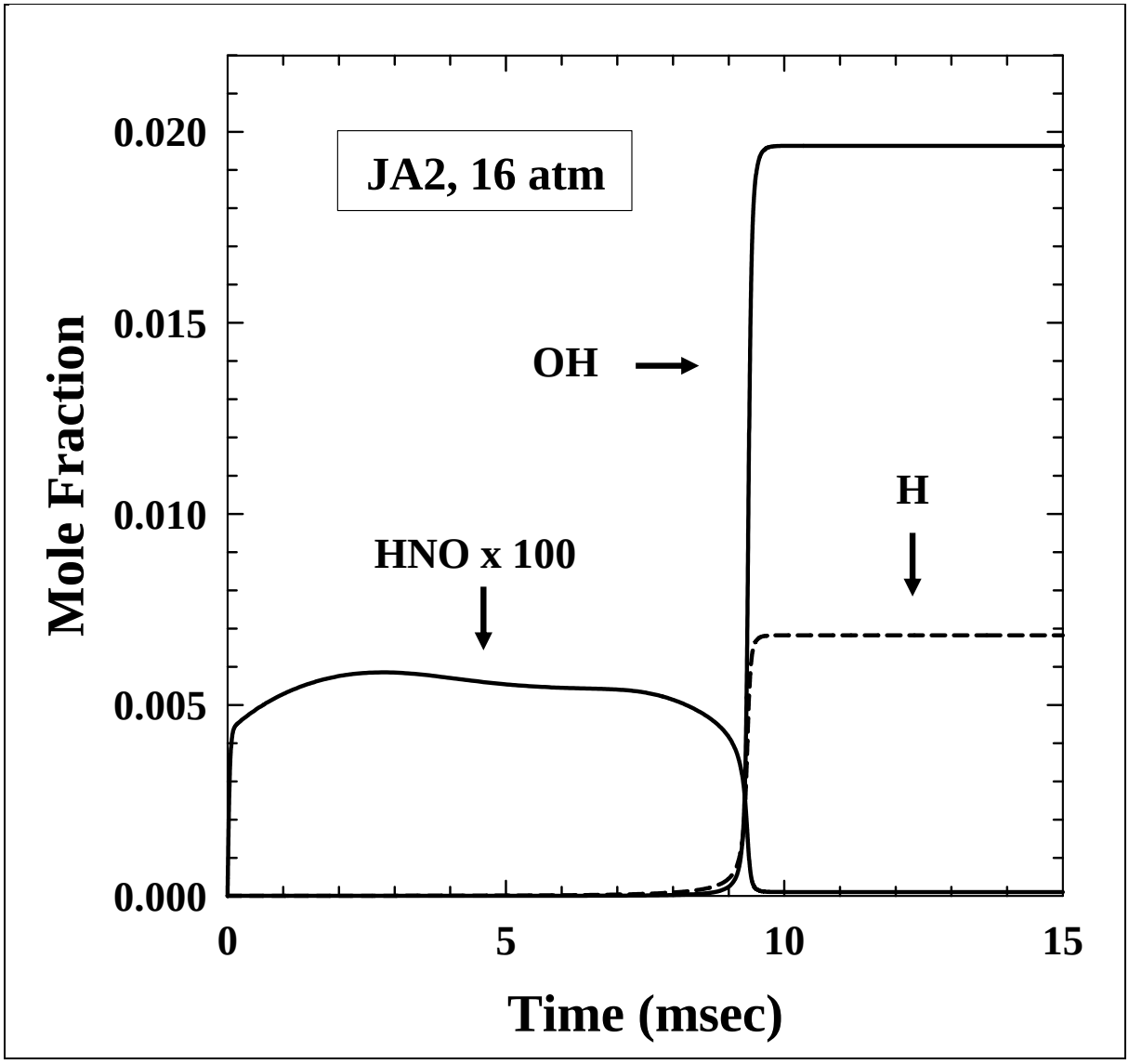

Figure 6. Predicted profiles of some important trace species for the DZ of JA2 at 16 atm, studied experimentally in VKMT-JA2 (*53*, *98*).

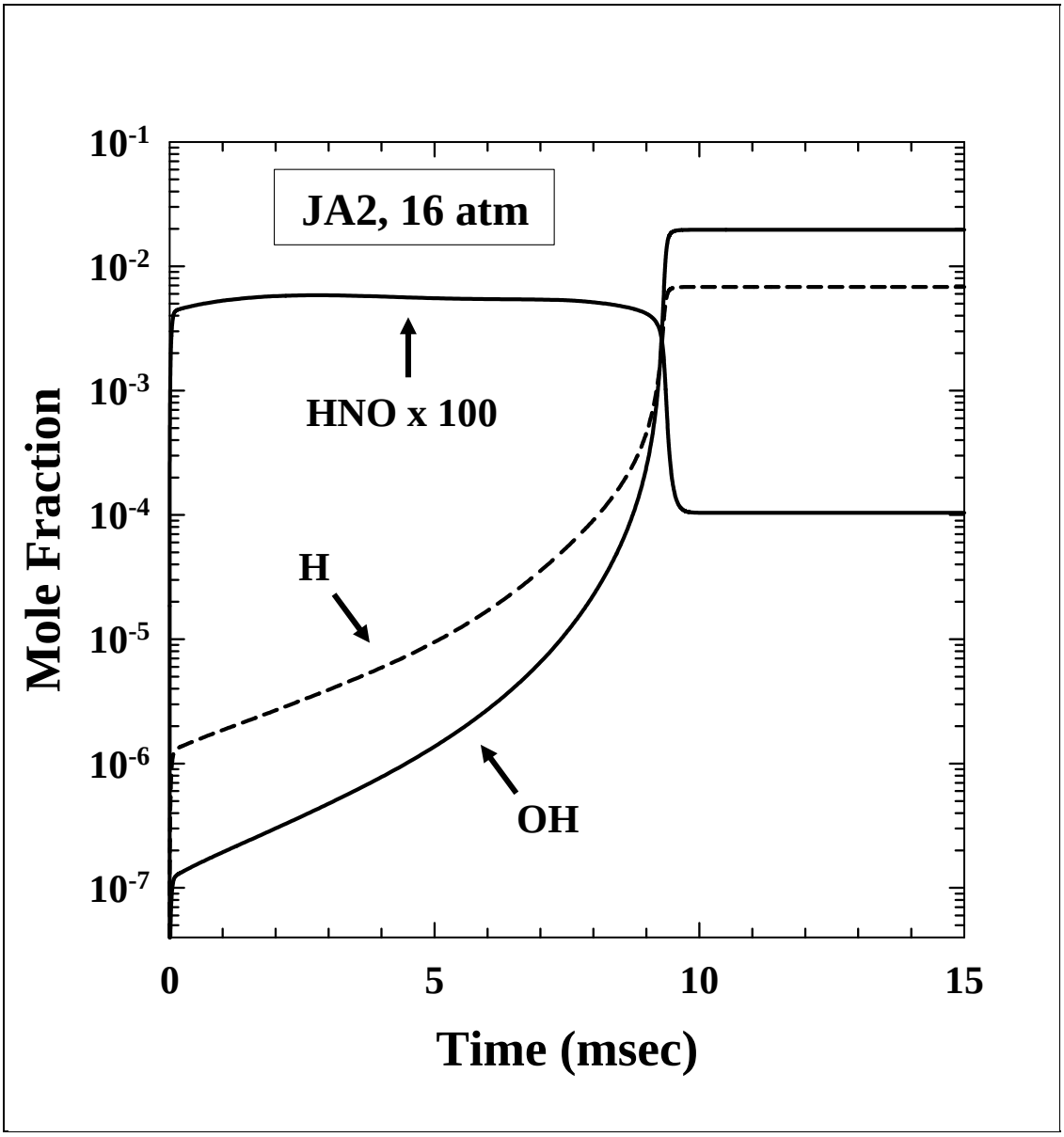

Figure 7. Predicted profiles of some important trace species, redrawn on log scale, for the DZ of JA2 at 16 atm, studied experimentally in VKMT-JA2 (*53*, *98*).

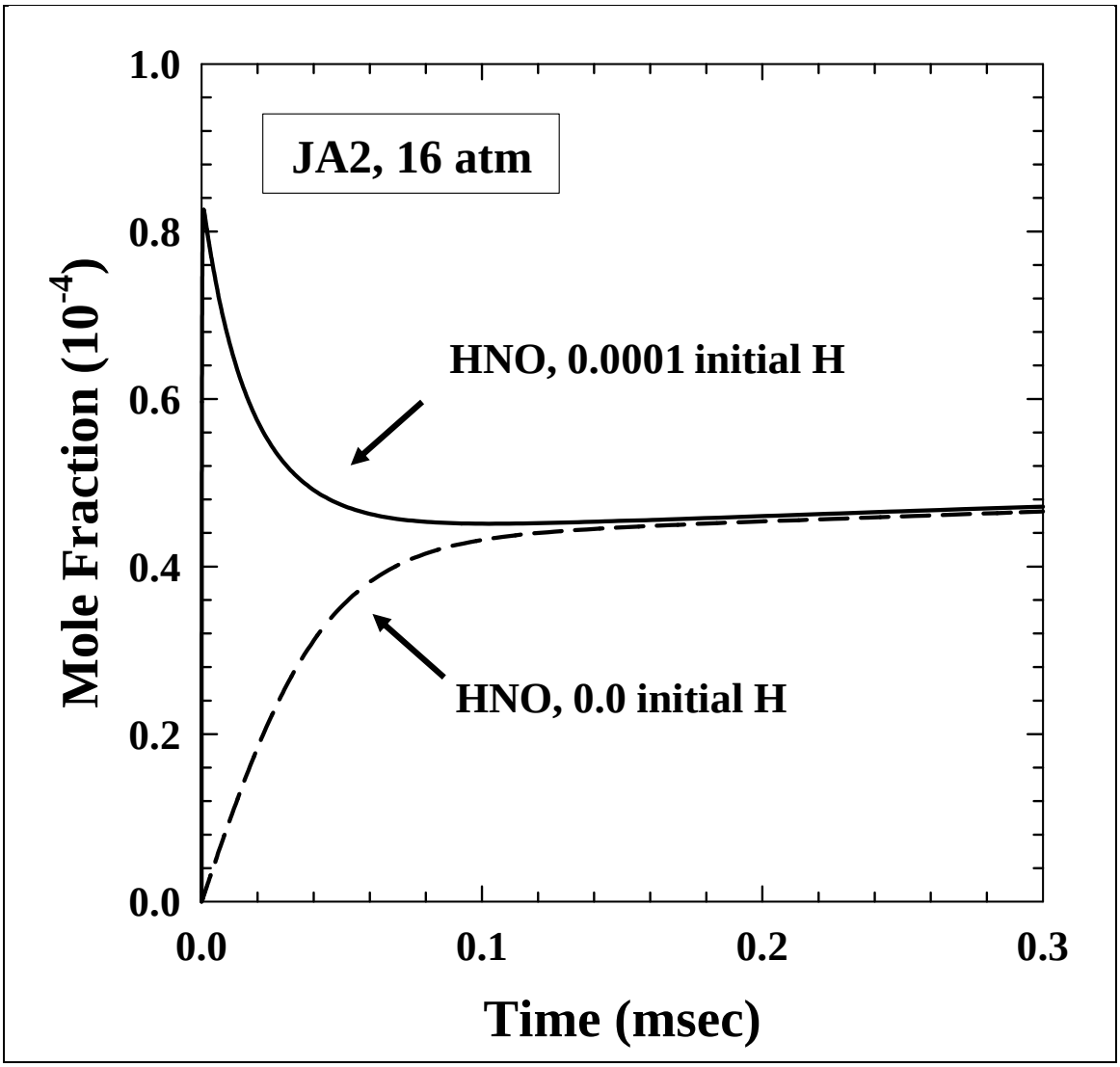

Figure 8. Predicted profiles of HNO in the DZ of JA2 at 16 atm during the time leading to steady state for two cases: (1) where all radical concentrations are assumed initially at 0.0 mole fraction and (2) where 0.0001 mole fraction of H is assumed present.

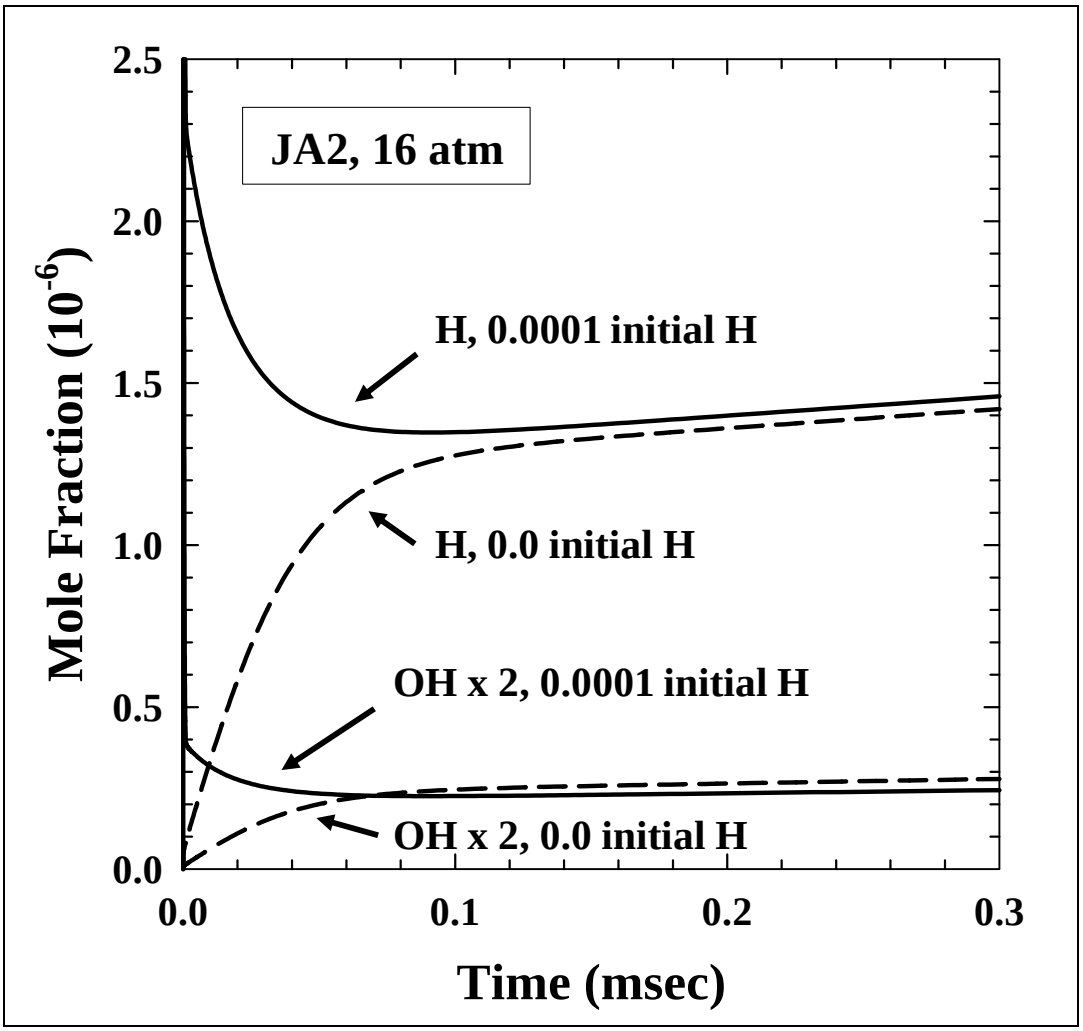

Figure 9. Predicted profiles of H and OH in the DZ of JA2 at 16 atm during the time leading to steady state for two cases: (1) where all radical concentrations are assumed initially at 0.0 mole fraction and (2) where 0.0001 mole fraction of H is assumed present.

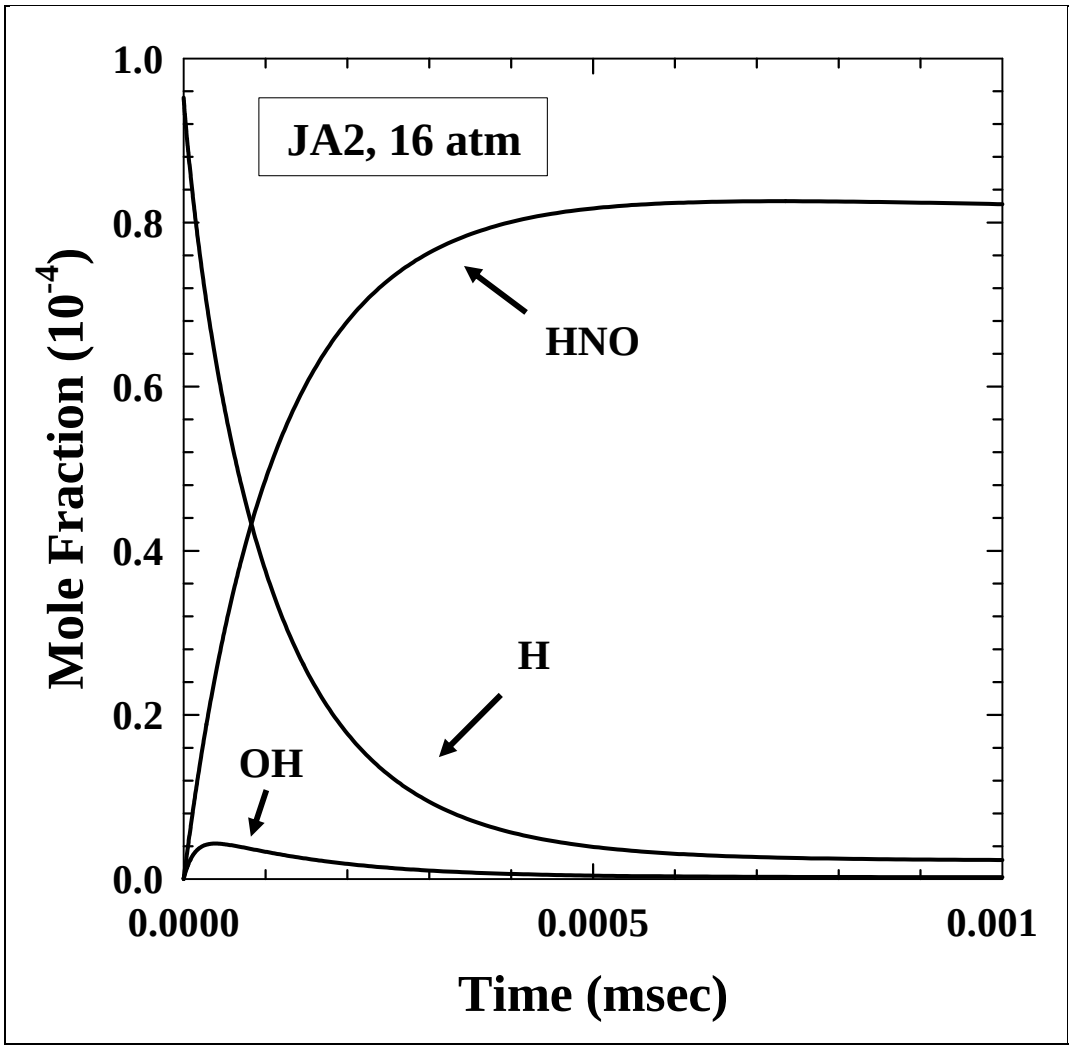

Figure 10. Predicted profiles of HNO, H, and OH in the DZ of JA2 at 16 atm for the case in which 0.0001 mole fraction of H is initially assumed present. This expands the region leading up to the decays in figures 7 and 8, showing that some extremely rapid processes initially take place.

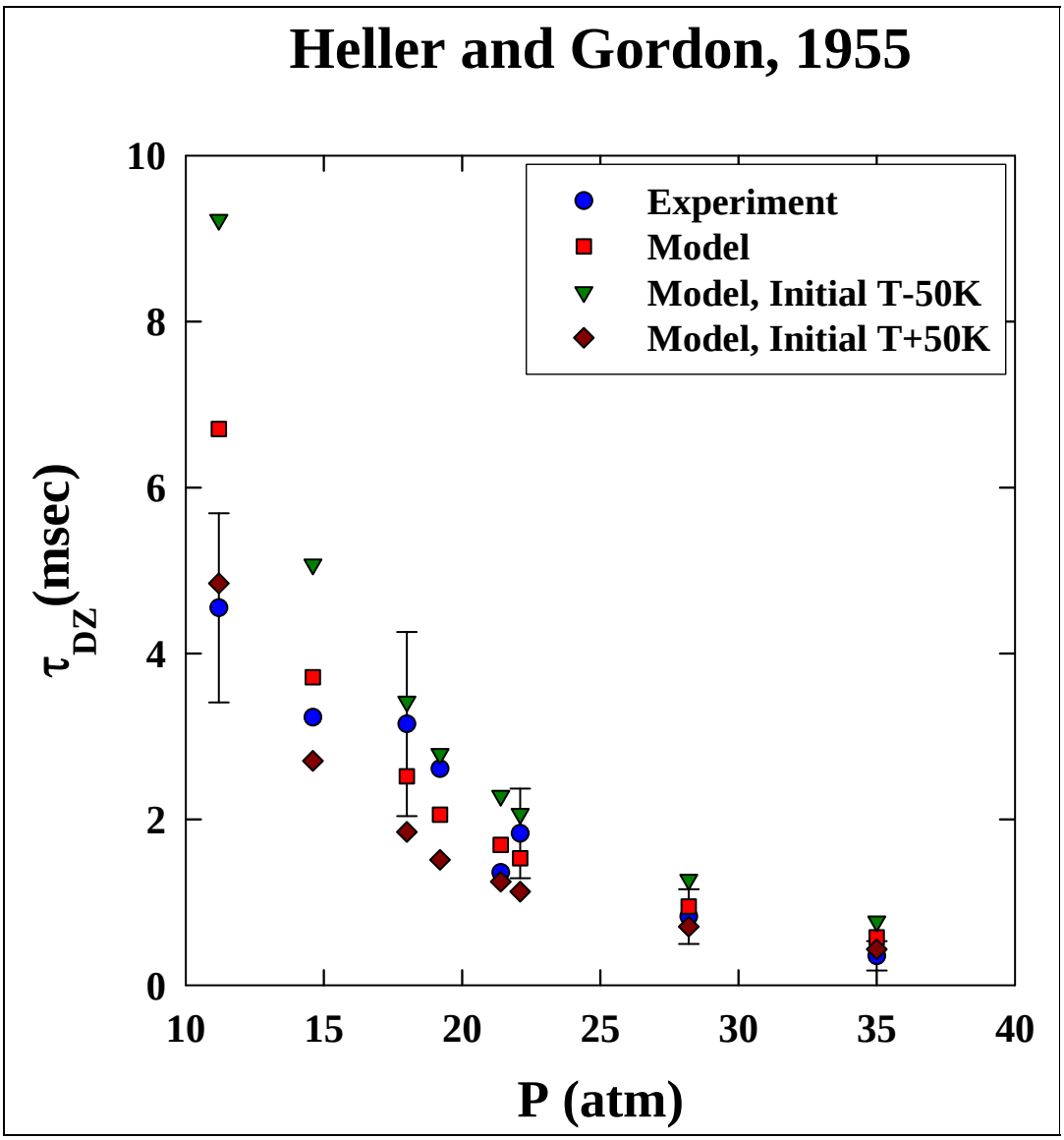

Figure 11. Comparison of experimental and predicted DZ ignition delay times for the HG55 dataset (*94*). Also shown are predictions resulting from increasing or decreasing T_{DZ} by 50 K.

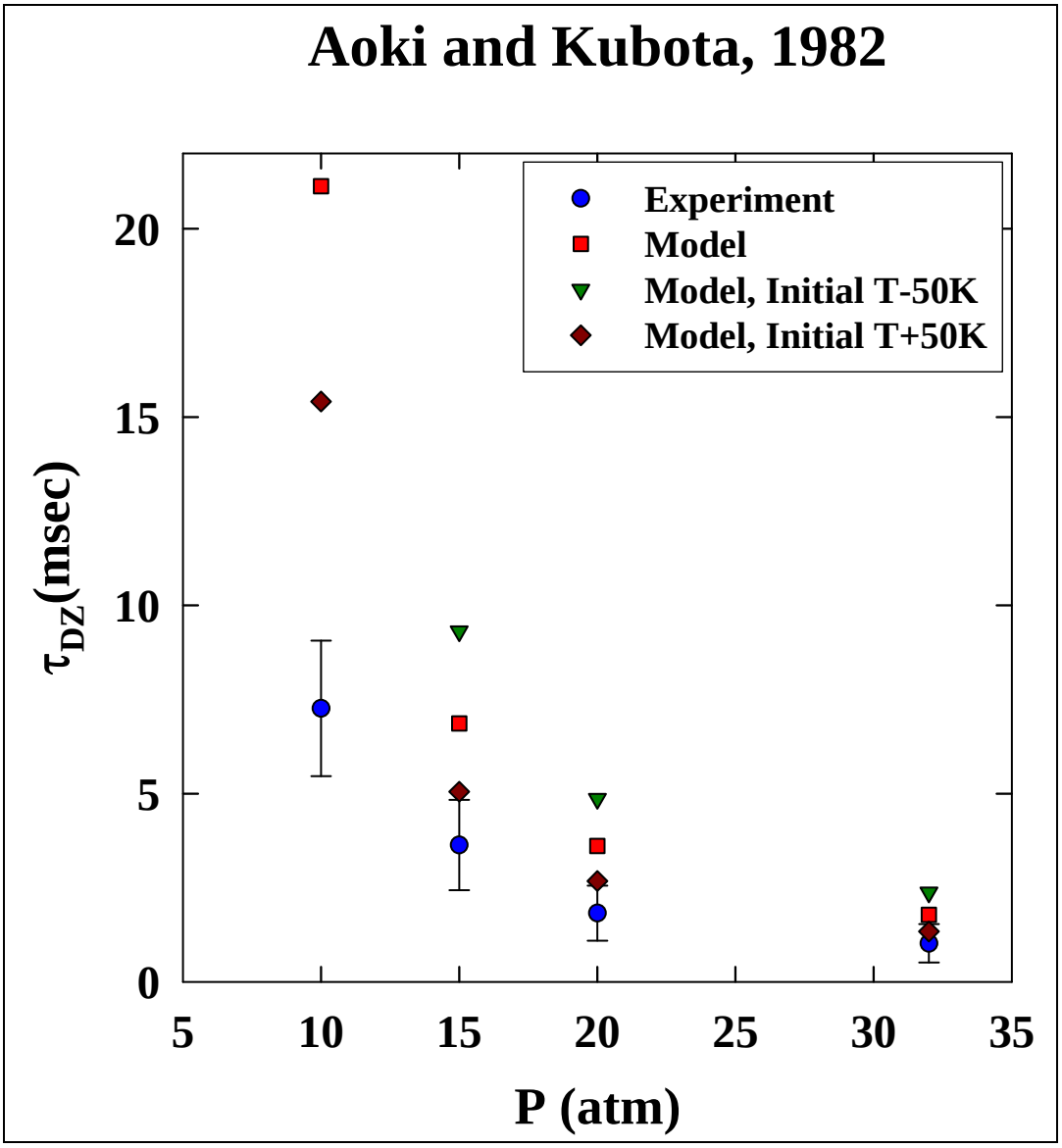

Figure 12. Comparison of experimental and predicted DZ ignition delay times for the AK82 dataset (*35*). Also shown are predictions resulting from increasing or decreasing T_{DZ} by 50 K.

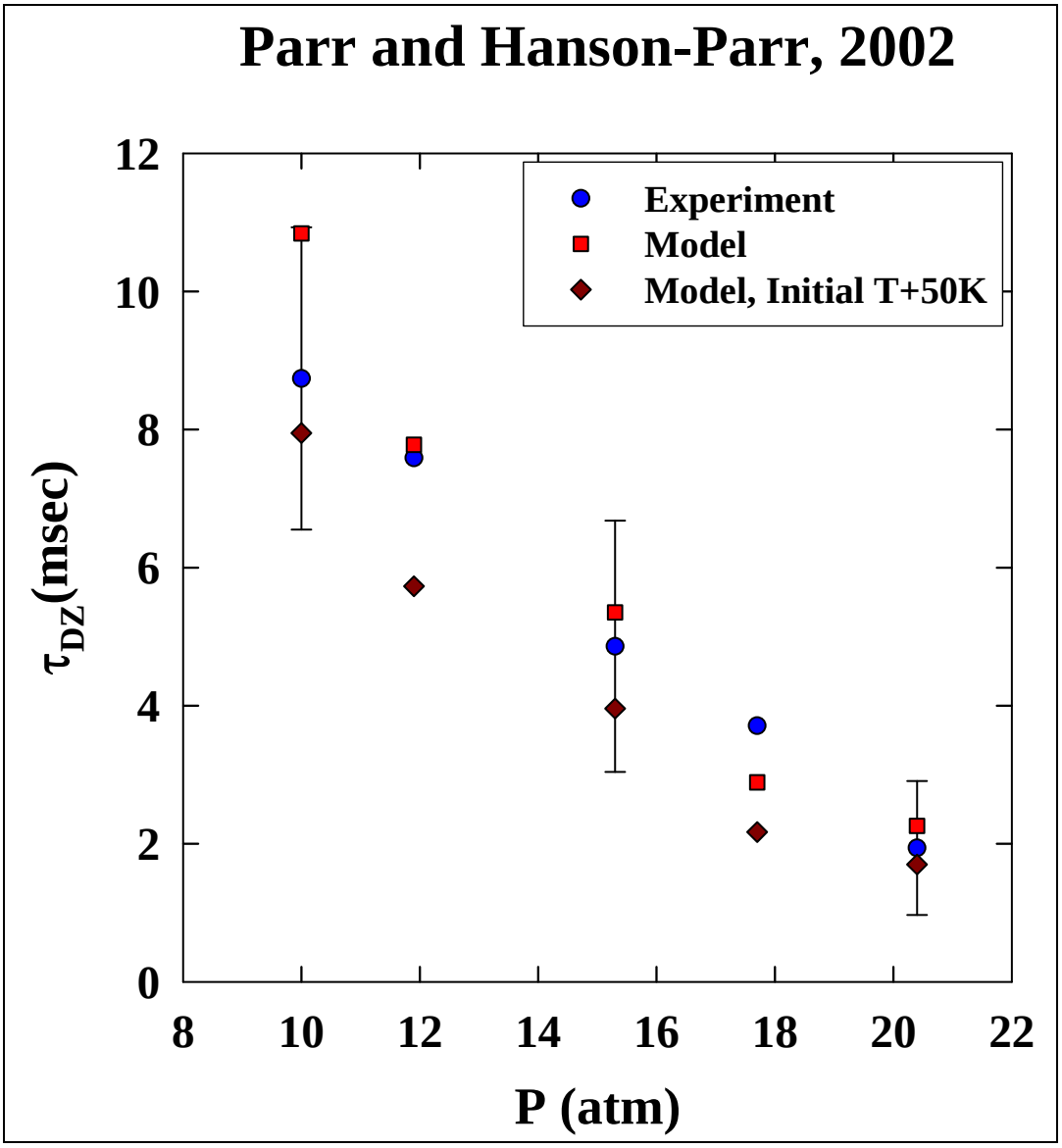

Figure 13. Comparison of experimental and predicted DZ ignition delay times for the PHP-BTTN dataset (*99*, *100*). Also shown are predictions resulting from increasing T_{DZ} by 50 K.

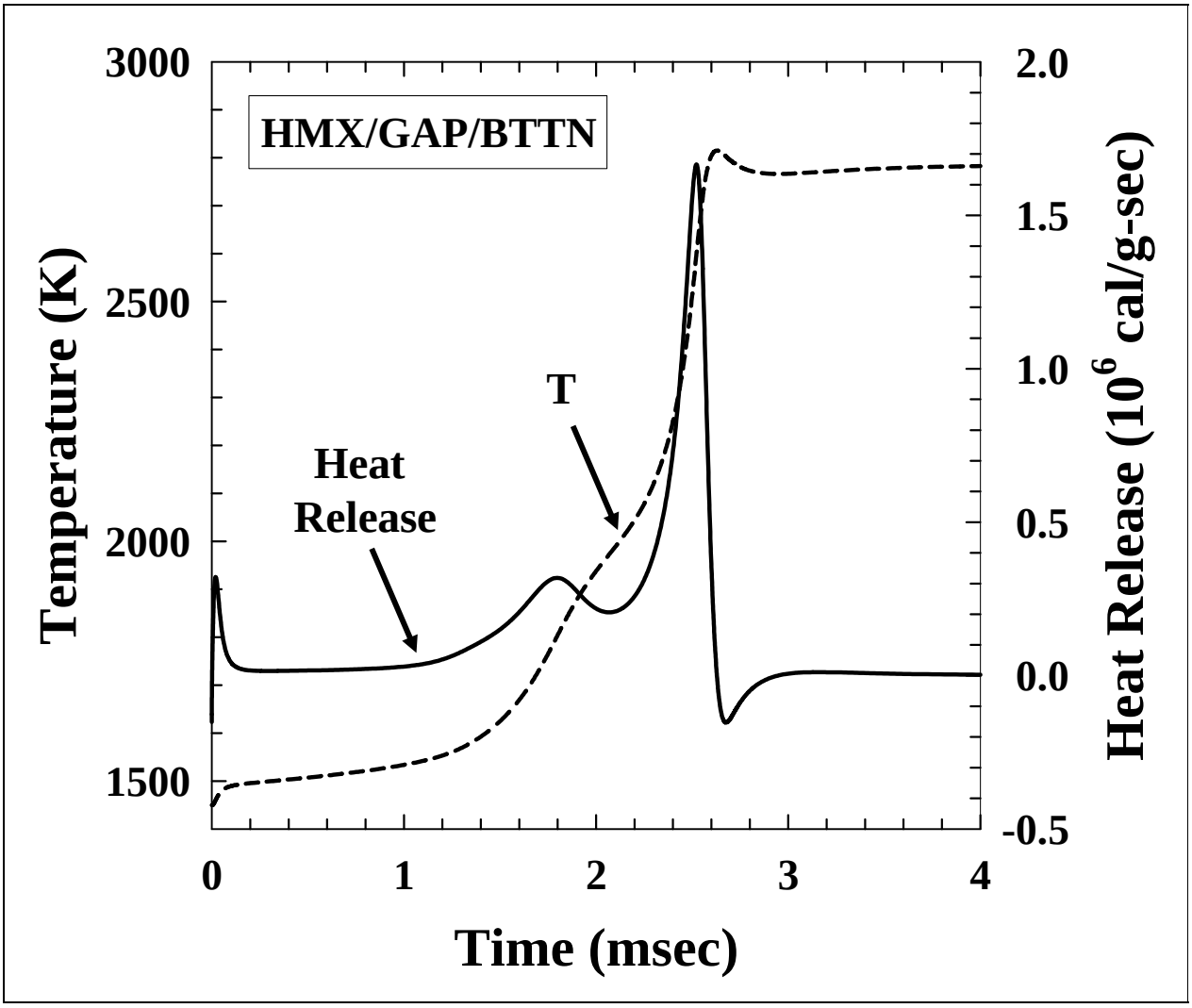

Figure 14. Predicted temperature and heat release profiles for the DZ of HMX/GAP/BTTN propellant at 0.92 atm, studied experimentally in PHP-HMX (*107–109*).

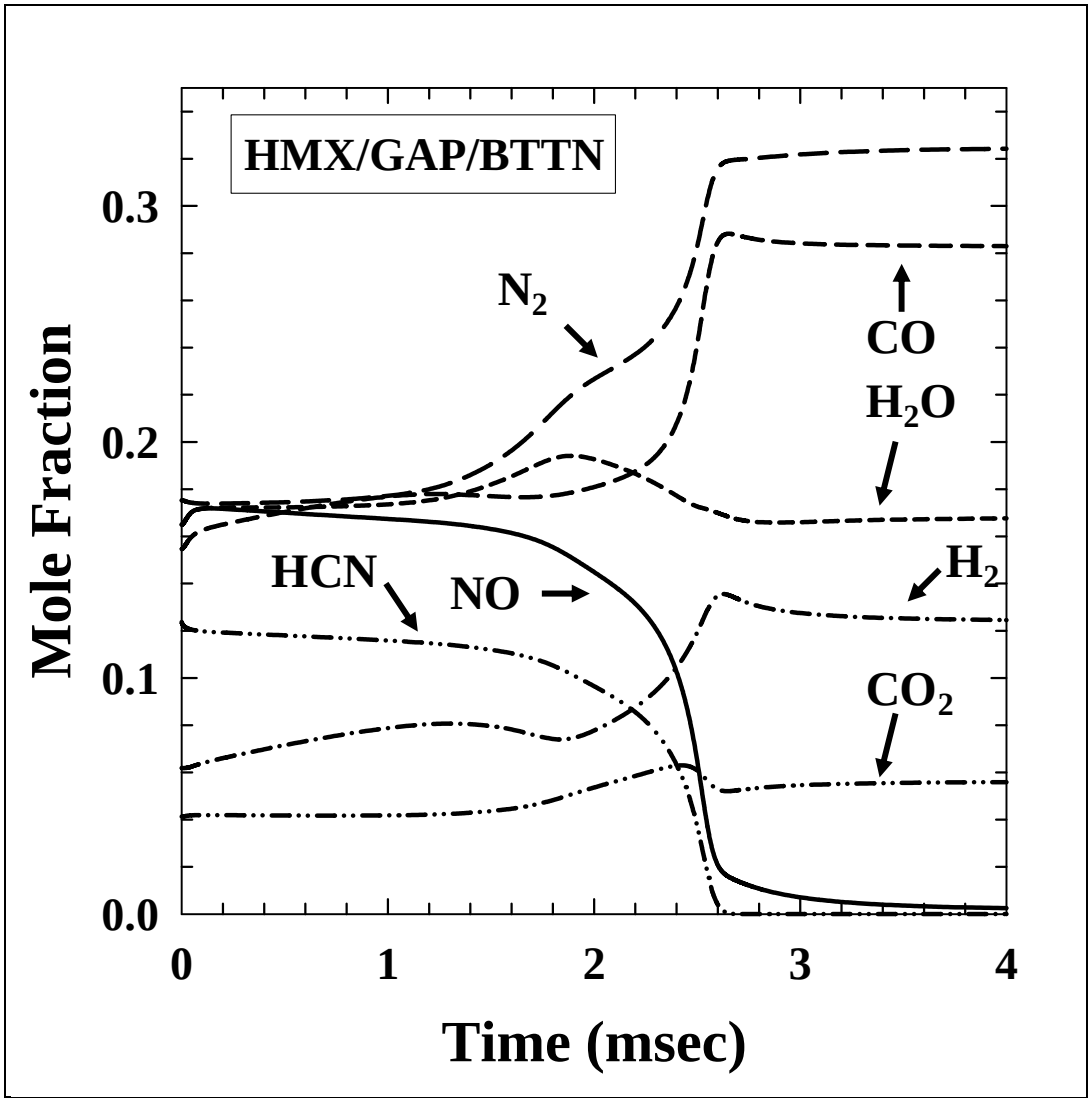

Figure 15. Predicted major species profiles for the DZ of HMX/GAP/BTTN propellant at 0.92 atm, studied experimentally in PHP-HMX (*107–109*).

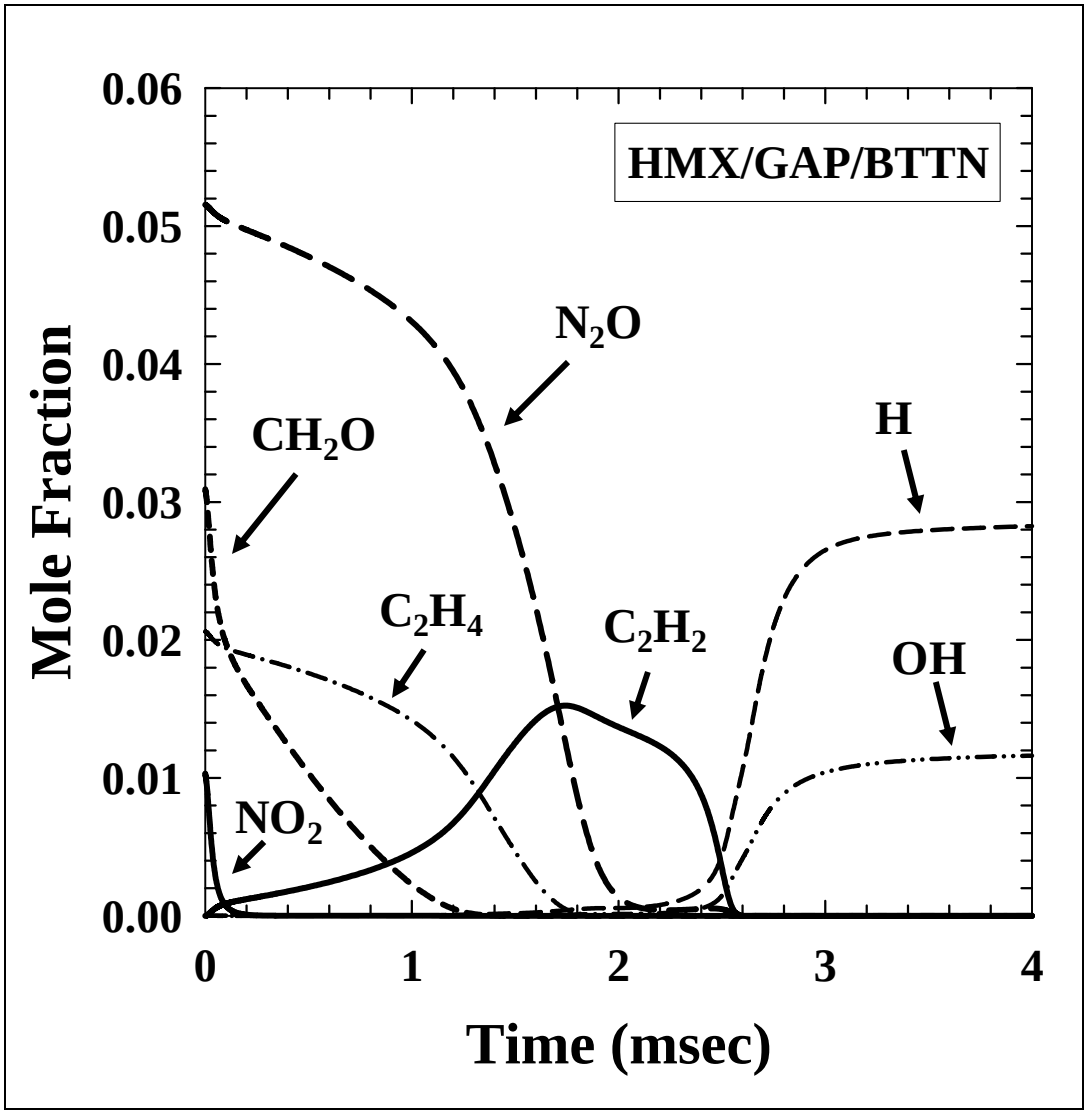

Figure 16. Predicted profiles of some trace species for the DZ of HMX/GAP/BTTN propellant at 0.92 atm, studied experimentally in PHP-HMX (*107–109*).

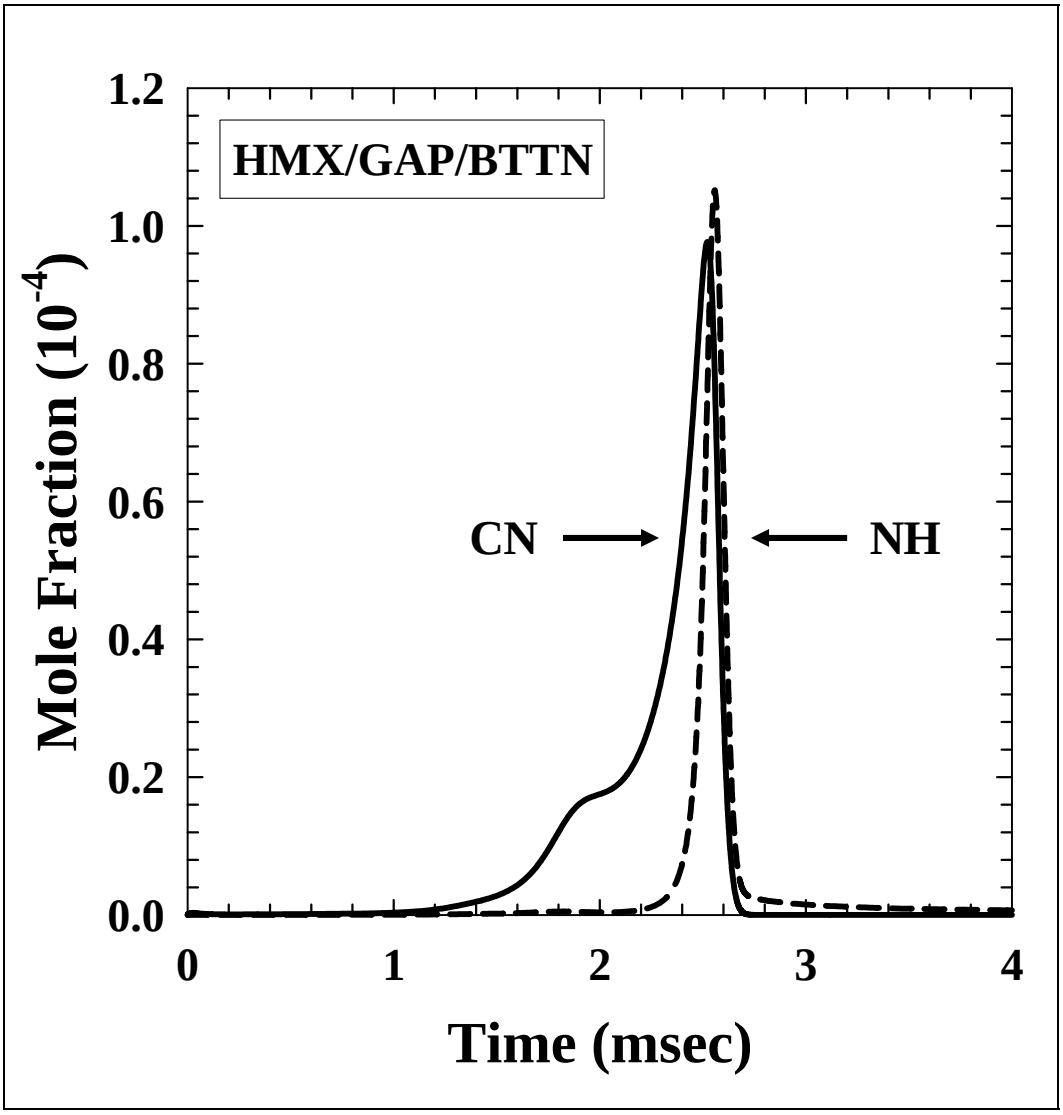

Figure 17. Predicted profiles of CN and NH trace species for the DZ of HMX/GAP/BTTN propellant at 0.92 atm, studied experimentally in PHP-HMX (*107–109*).

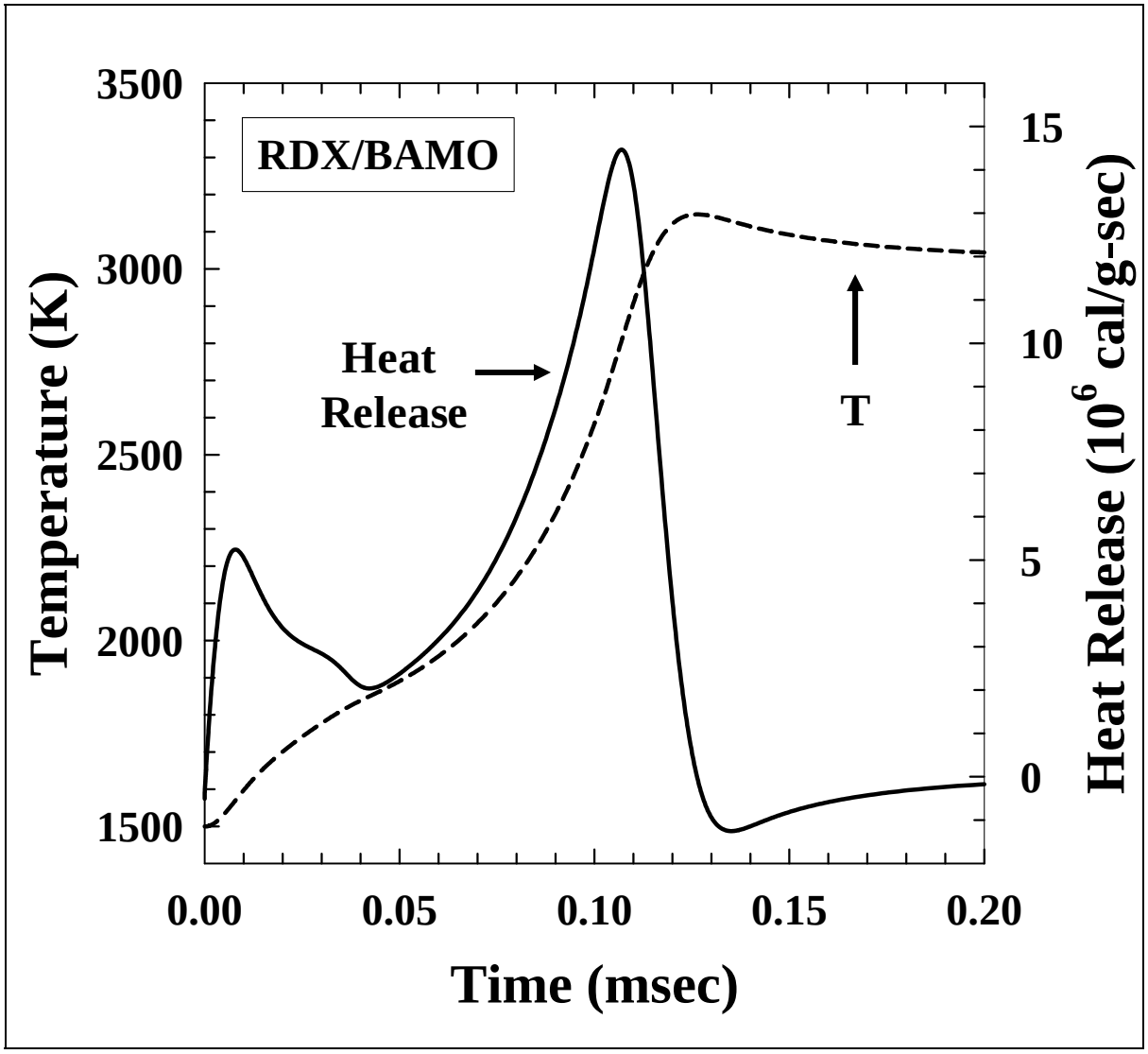

Figure 18. Predicted temperature and heat release profiles for the DZ of RDX/BAMO propellant at 1.0 atm, studied experimentally in LLT00 (*113*).

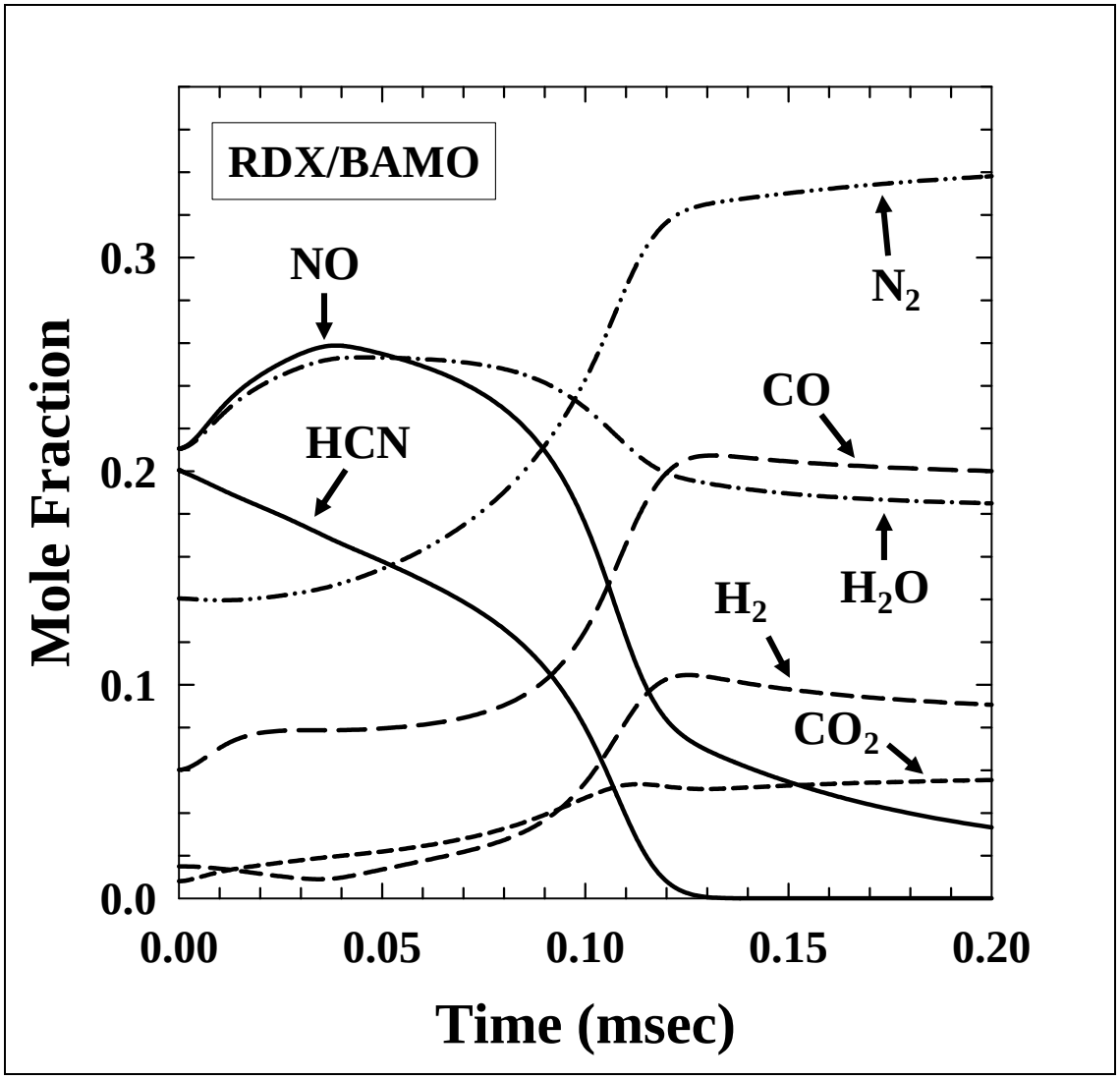

Figure 19. Predicted major species profiles for the DZ of RDX/BAMO propellant at 1.0 atm, studied experimentally in LLT00 (*113*).

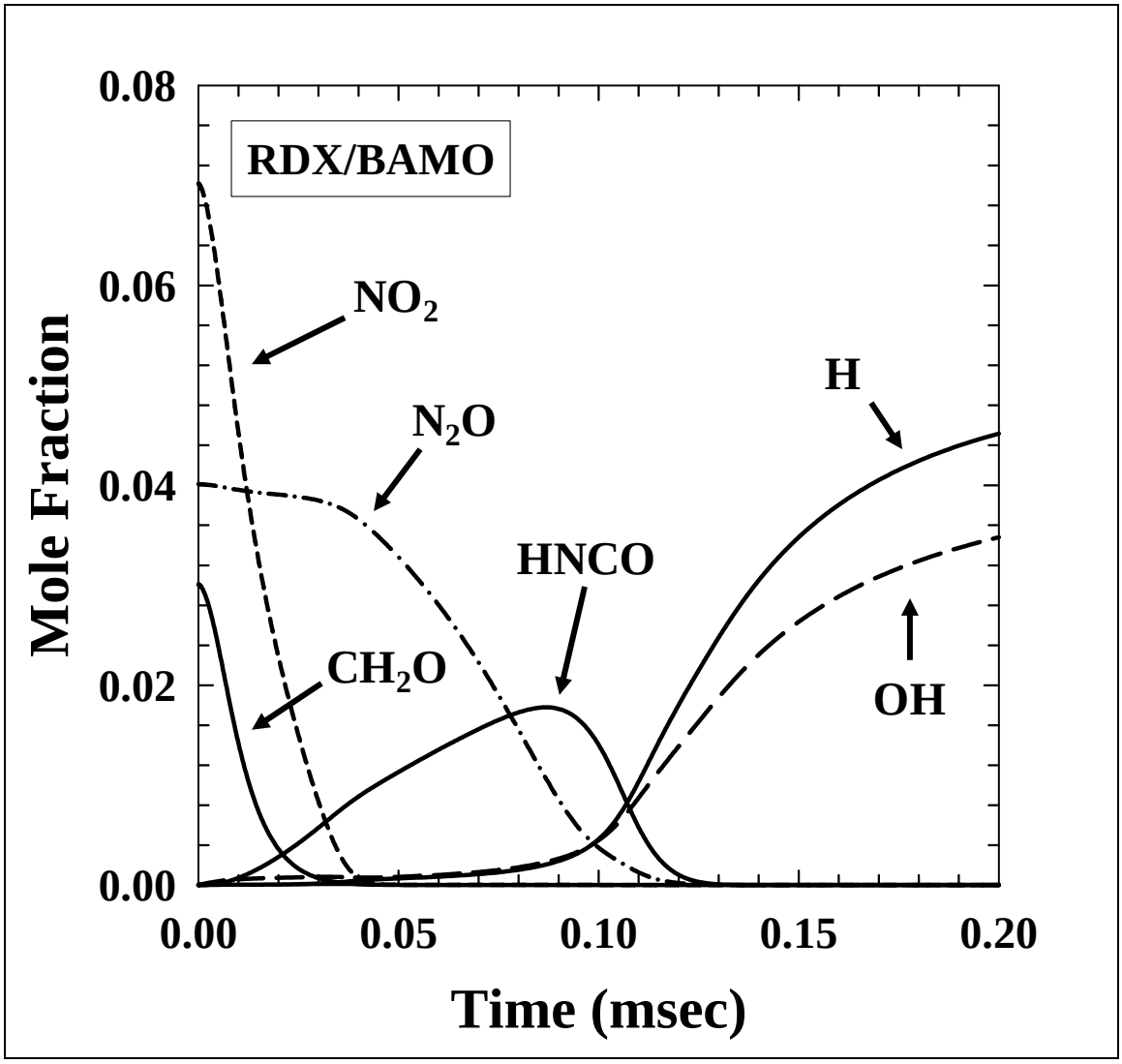

Figure 20. Predicted profiles of some modest concentration trace species for the DZ of RDX/BAMO propellant at 1.0 atm, studied experimentally in LLT00 (*113*).

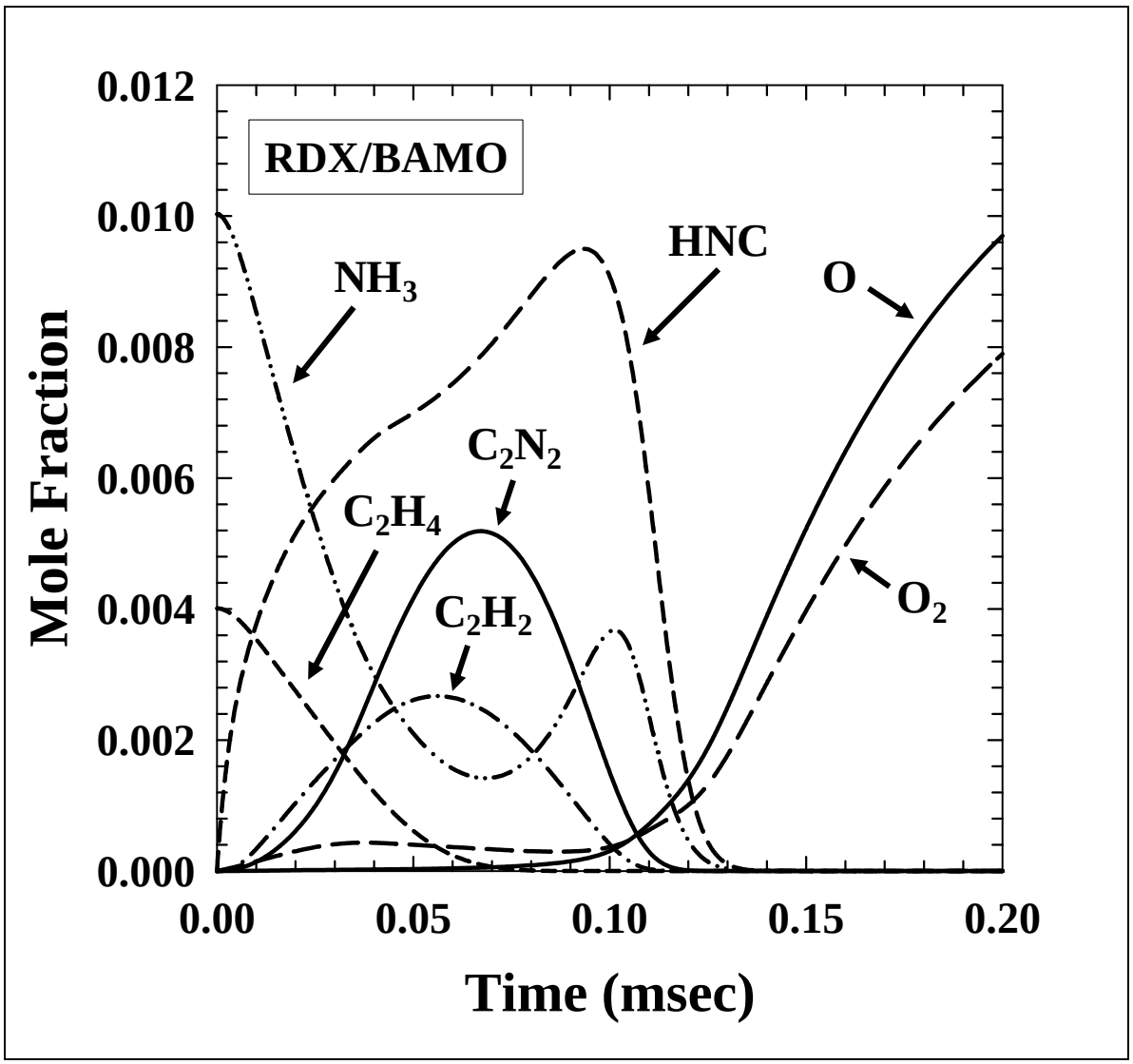

Figure 21. Predicted profiles of some low concentration trace species for the DZ of RDX/BAMO propellant at 1.0 atm, studied experimentally in LLT00 (*113*).

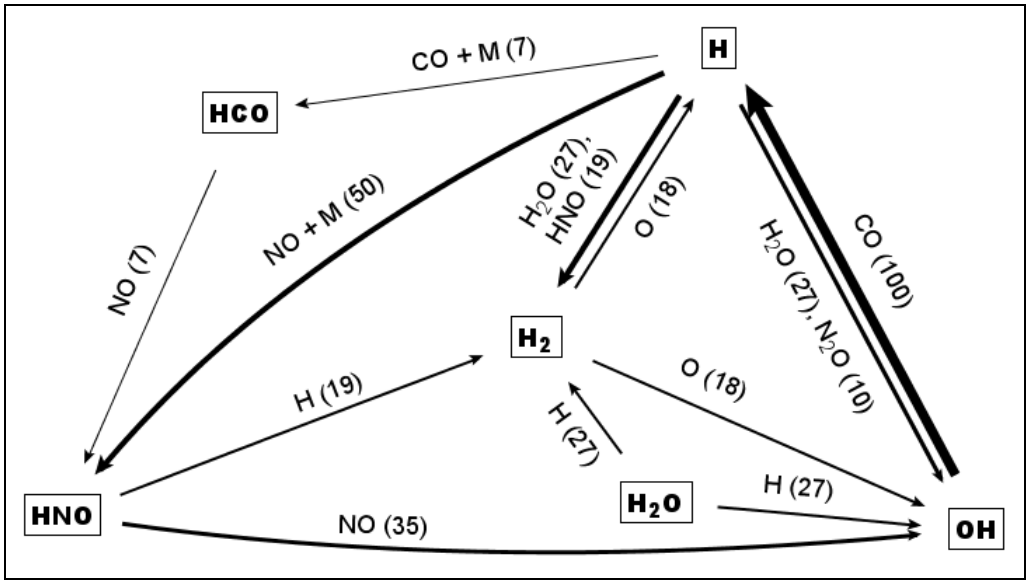

Figure 22. Predicted pathways connecting H-containing species in the 16 atm JA2 case (VKMT-JA2 [*53, 98*]) at 4.47 ms, a point about midway through the ignition delay period. The relative rate of 100 is 8.51×10^{-4} mol/cm^3/s.

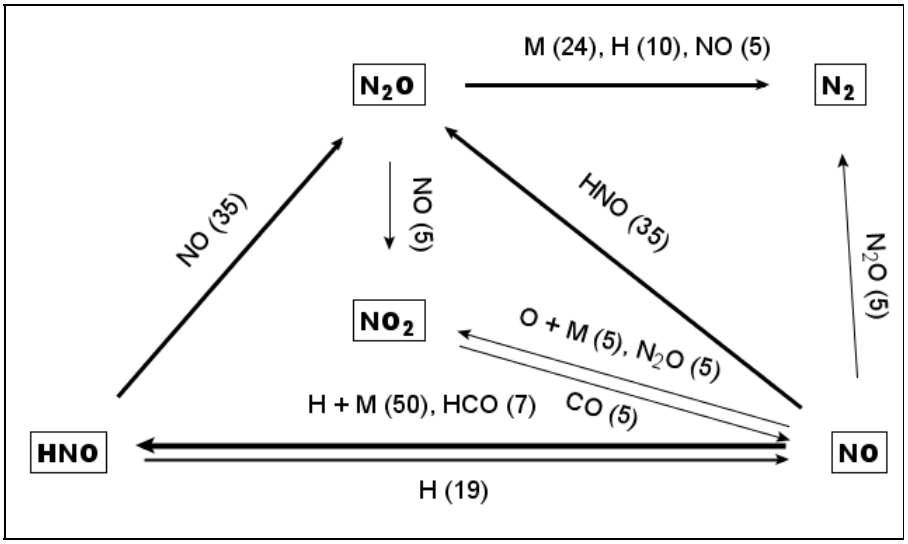

Figure 23. Predicted pathways connecting N-containing species in the 16 atm JA2 case (VKMT-JA2 [*53*, *98*]) at 4.47 ms, a point about midway through the ignition delay period. The relative rate of 100 is 8.51×10^{-4} mol/cm^3/s.

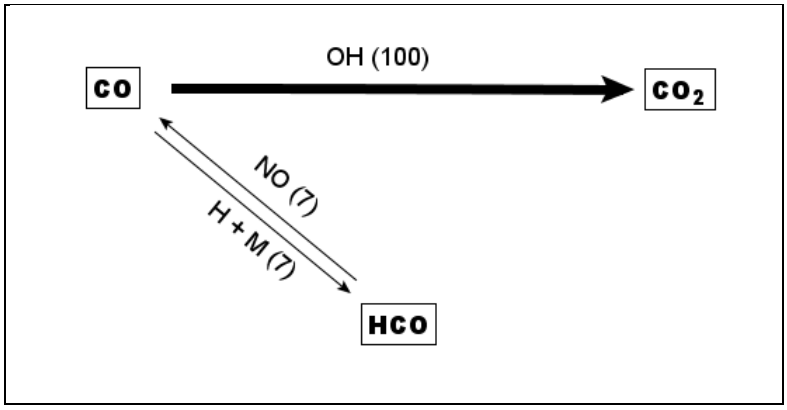

Figure 24. Predicted pathways connecting C-containing species in the 16 atm JA2 case (VKMT-JA2 [*53*, *98*]) at 4.47 ms, a point about midway through the ignition delay period. The relative rate of 100 is 8.51×10^{-4} mol/cm^3/s.

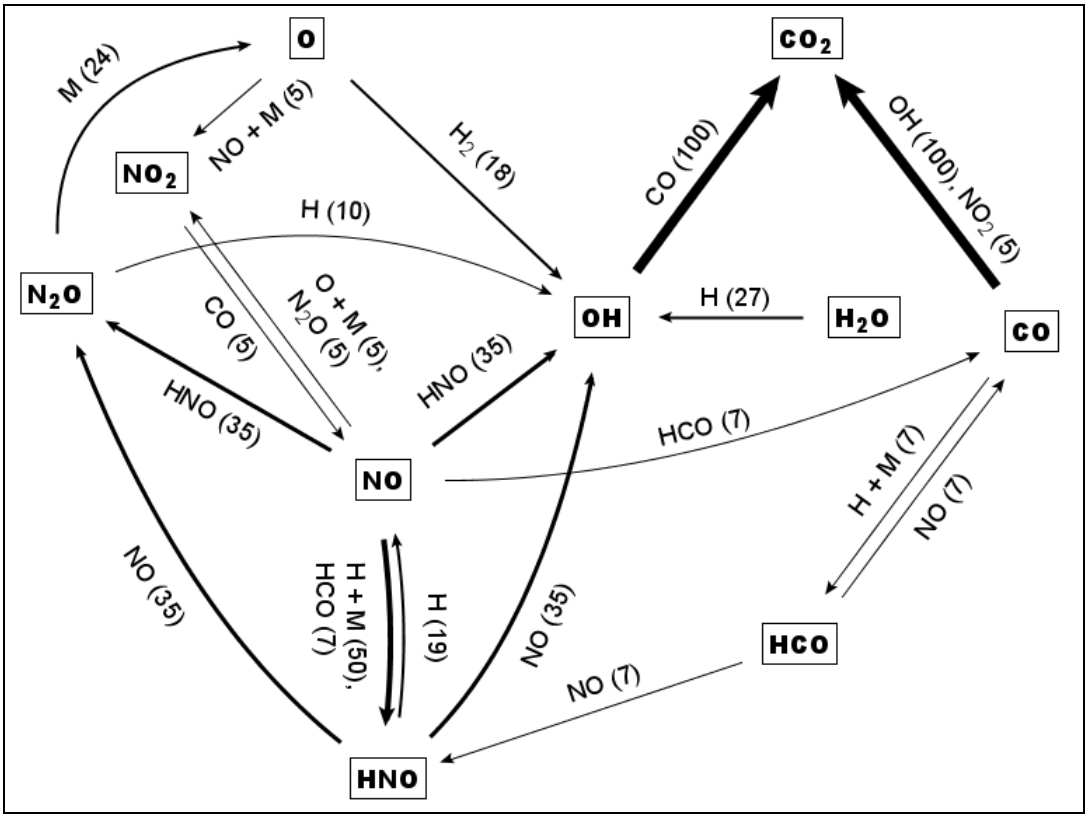

Figure 25. Predicted pathways connecting O-containing species in the 16 atm JA2 case (VKMT-JA2 [*53*, *98*]) at 4.47 ms, a point about midway through the ignition delay period. The relative rate of 100 is 8.51×10^{-4} mol/cm^3/s.

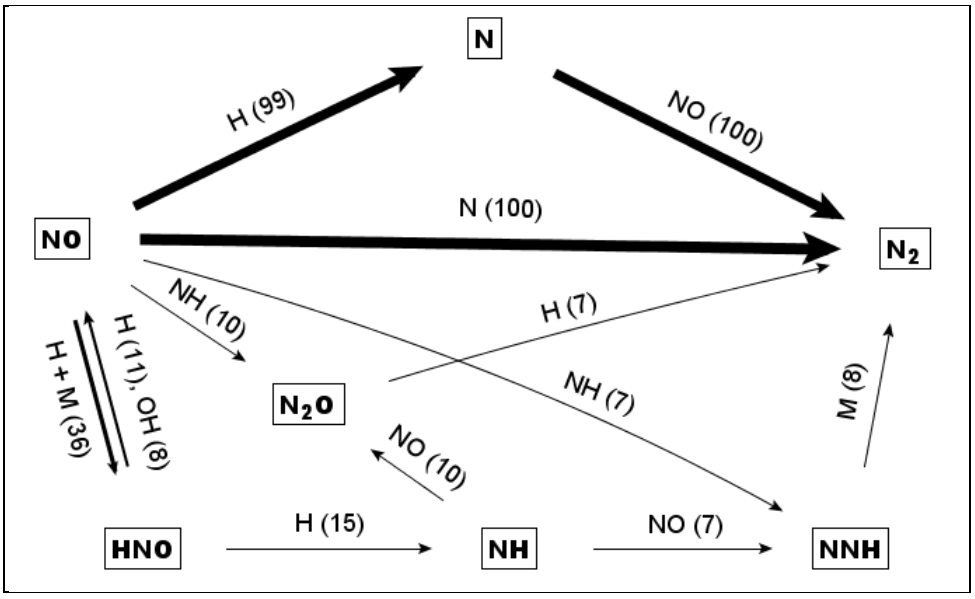

Figure 26. Predicted pathways connecting N-containing species in the 16 atm JA2 case (VKMT-JA2 [*53*, *98*]) at 9.33 ms, the point at which the DZ ignites. The relative rate of 100 is 2.19×10^{-2} mol/cm^3/s.

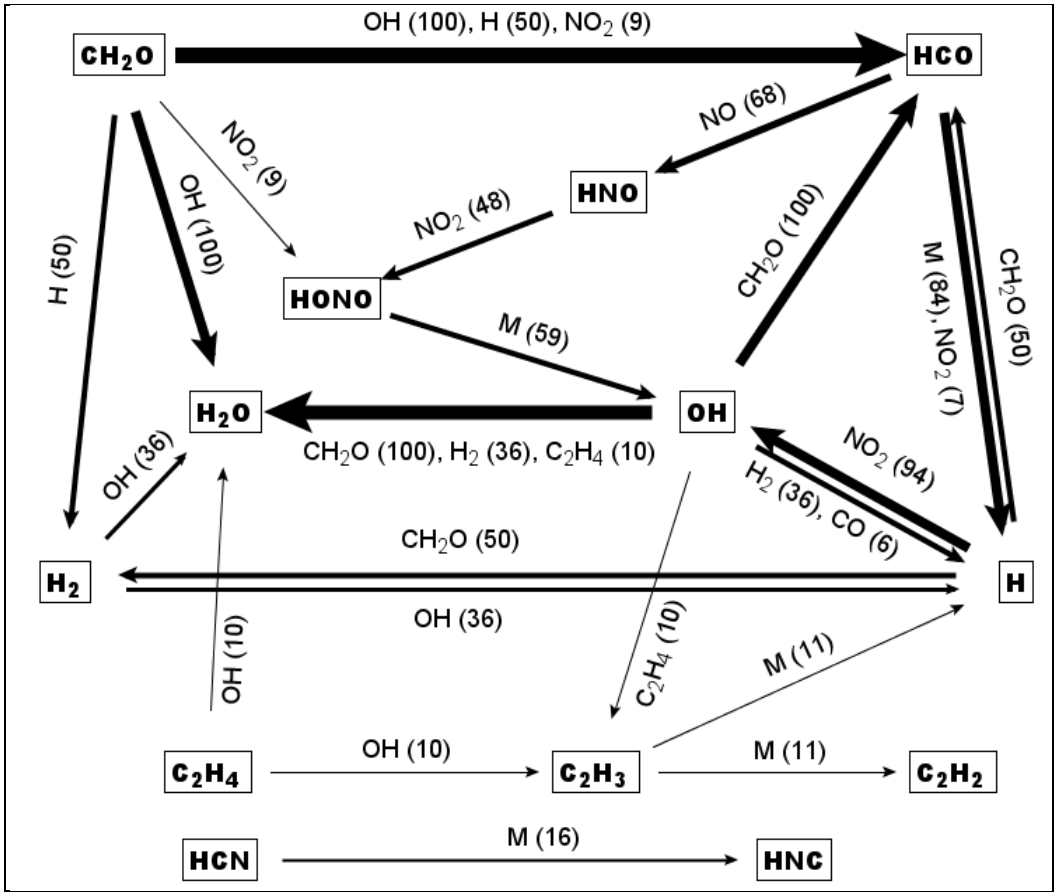

Figure 27. Predicted pathways connecting H-containing species in the 0.92 atm HMX/GAP /BTTN case (PHP-HMX [*107–109*]) at 0.020 ms, the point at which the traces of CH_2O and NO_2 are reacting. The relative rate of 100 is 9.05×10^{-4} mol/cm^3/s.

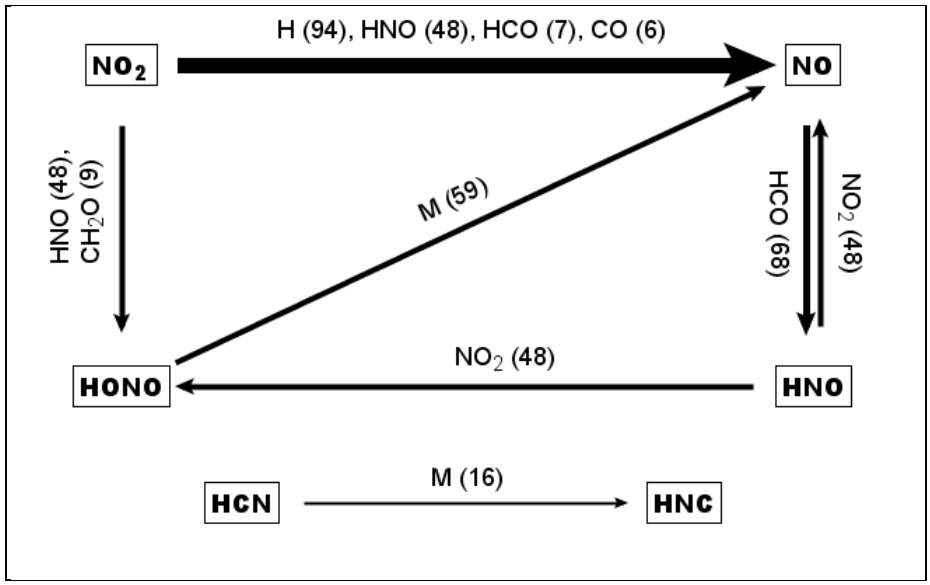

Figure 28. Predicted pathways connecting N-containing species in the 0.92 atm HMX/GAP/BTTN case (PHP-HMX [*107–109*]) at 0.020 ms, the point at which the traces of CH_2O and NO_2 are reacting. The relative rate of 100 is 9.05×10^{-4} mol/cm^3/s.

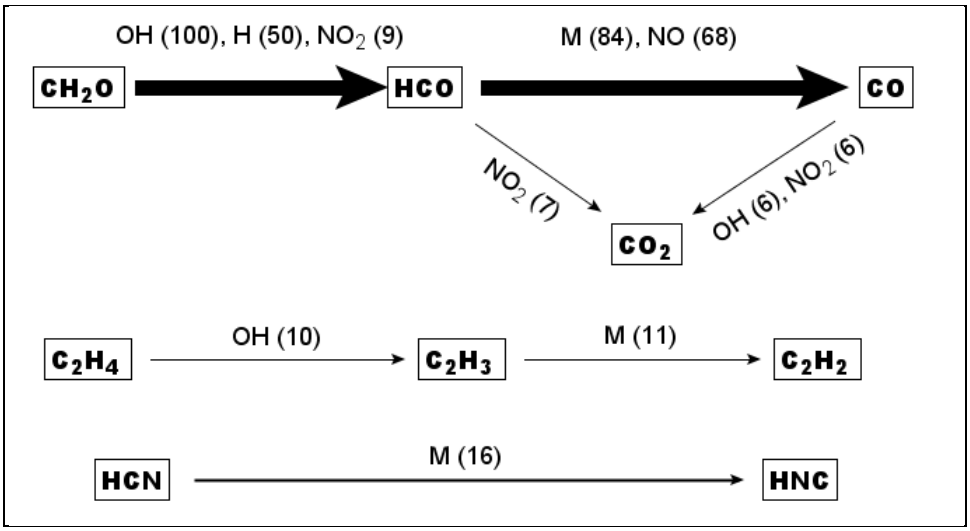

Figure 29. Predicted pathways connecting C-containing species in the 0.92 atm HMX/GAP/BTTN case (PHP-HMX [*107–109*]) at 0.020 ms, the point at which the traces of CH_2O and NO_2 are reacting. The relative rate of 100 is 9.05×10^{-4} mol/cm^3/s.

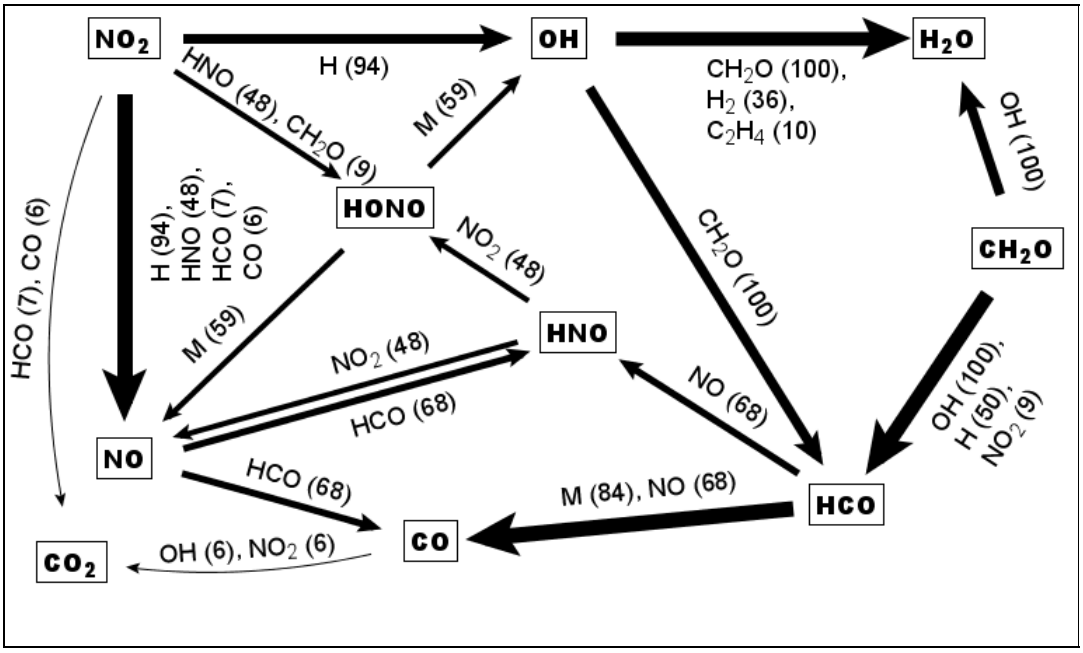

Figure 30. Predicted pathways connecting O-containing species in the 0.92 atm HMX/GAP/BTTN case (PHP-HMX [*107–109*]) at 0.020 ms, the point at which the traces of CH_2O and NO_2 are reacting. The relative rate of 100 is 9.05×10^{-4} mol/cm^3/s.

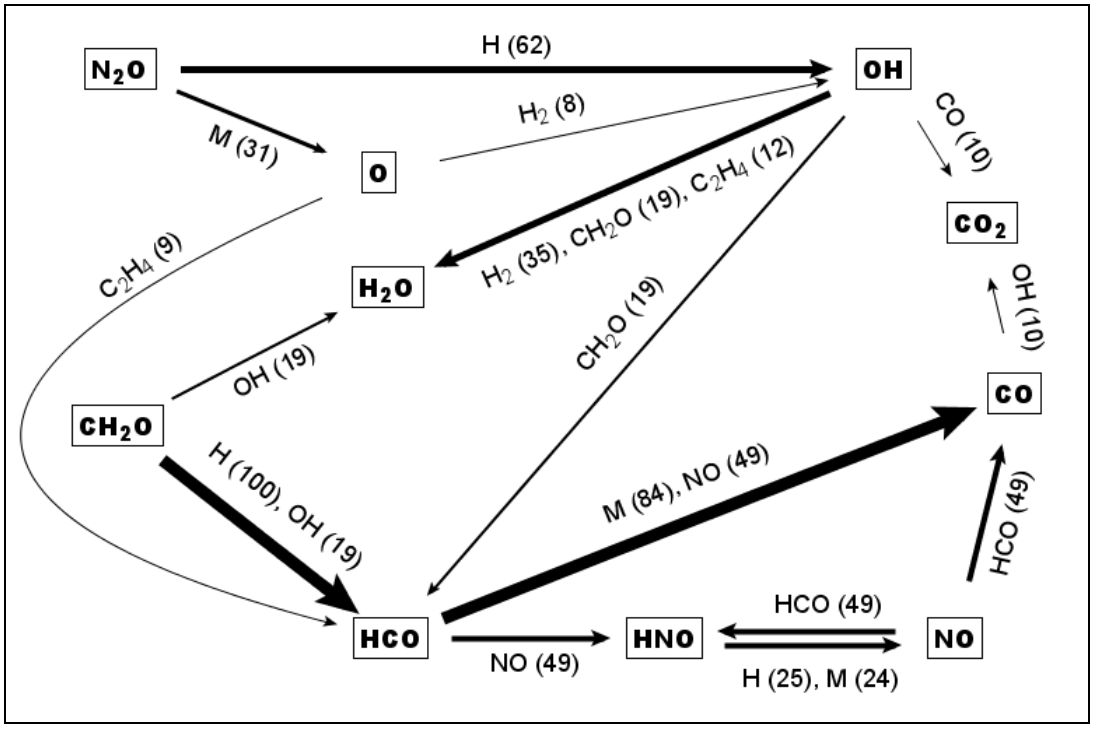

Figure 31. Predicted pathways connecting O-containing species in the 0.92 atm HMX/GAP/BTTN case (PHP-HMX [*107–109*]) at 0.90 ms, a point where the CH_2O decay is finishing and the N_2O reaction is starting. The relative rate of 100 is 8.15×10^{-5} mol/cm^3/s.

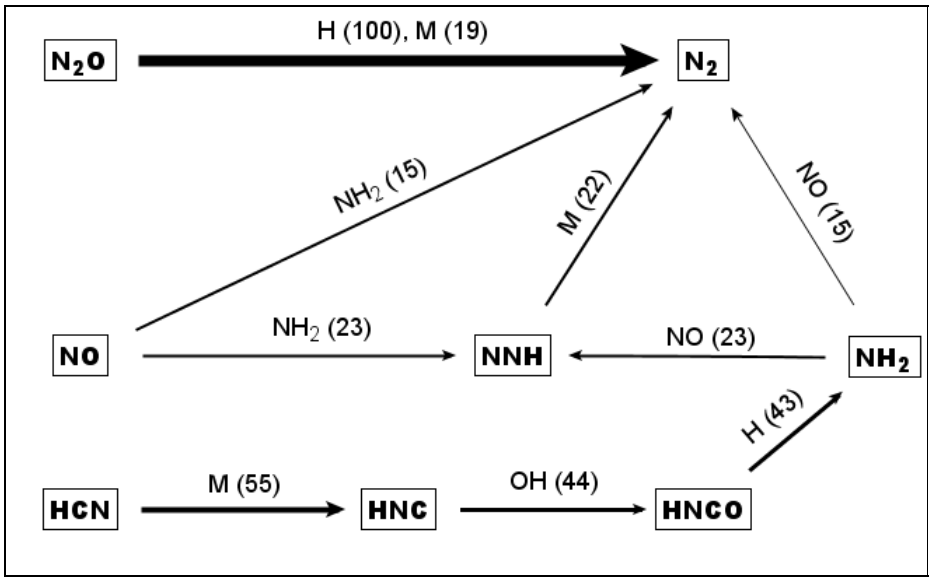

Figure 32. Predicted pathways connecting N-containing species in the 0.92 atm HMX/GAP/BTTN case (PHP-HMX [*107–109*]) at 1.8 ms, the point at which the heat release peak due to N_2O reaction occurs. The relative rate of 100 is 3.43×10^{-4} mol/cm^3/s.

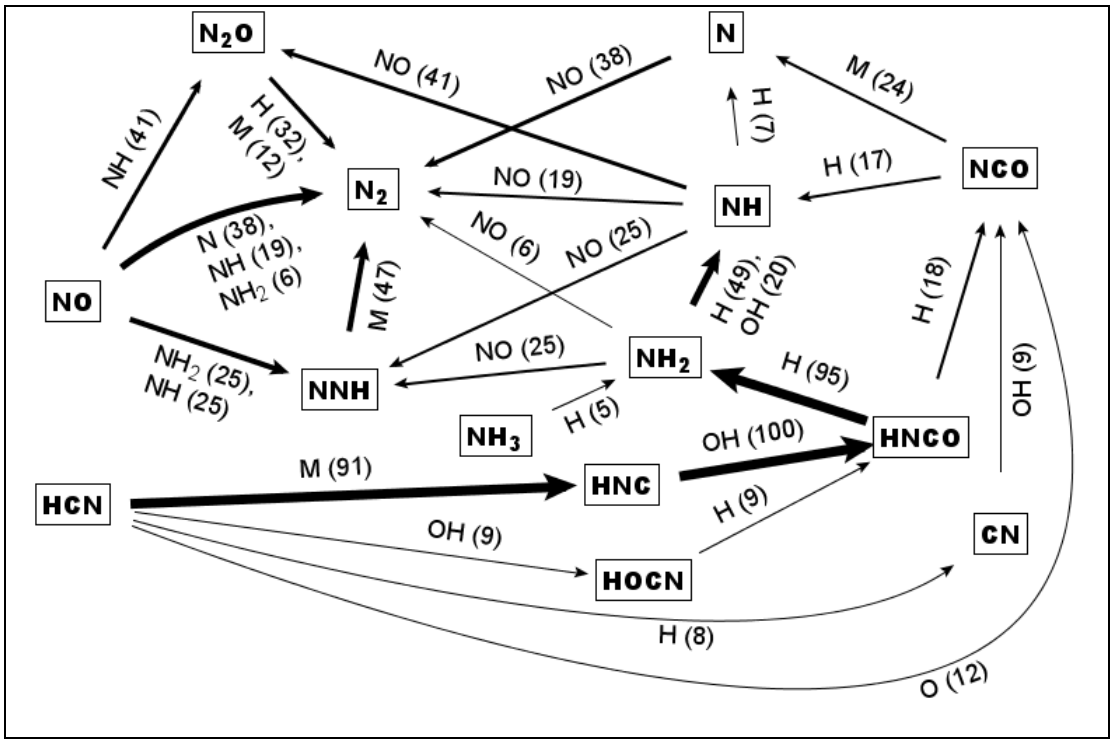

Figure 33. Predicted pathways connecting N-containing species in the 0.92 atm HMX/GAP/BTTN case (PHP-HMX [*107–109*]) at 2.52 ms, the point at which the DZ ignites. The relative rate of 100 is 1.39×10^{-3} mol/cm^3/s.

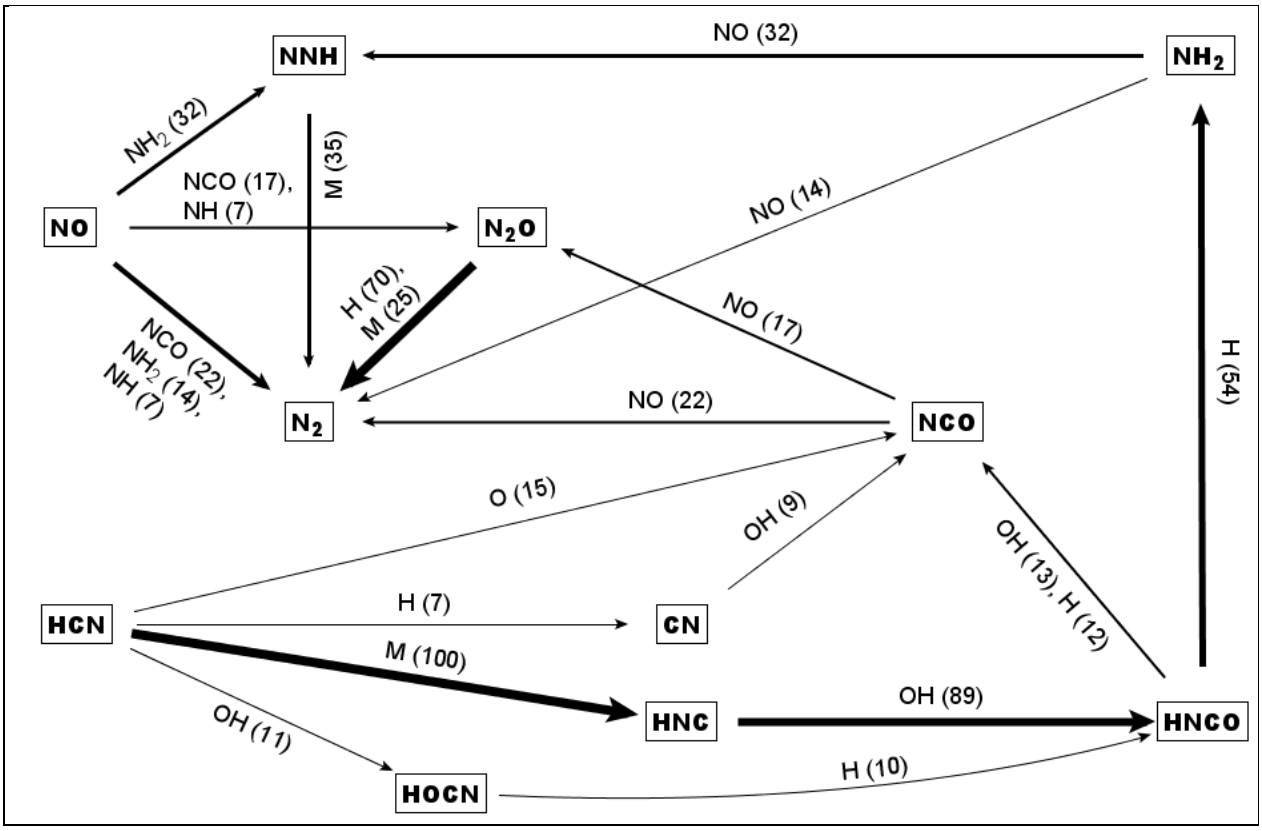

Figure 34. Predicted pathways connecting N-containing species in the 1.0 atm, 400 W/cm^2 laser-heated, RDX/BAMO case (LLT00 [*113*]) at 0.075 ms, a point slightly prior to the computed ignition delay time. The relative rate of 100 is 5.26×10^{-3} mol/cm^3/s.

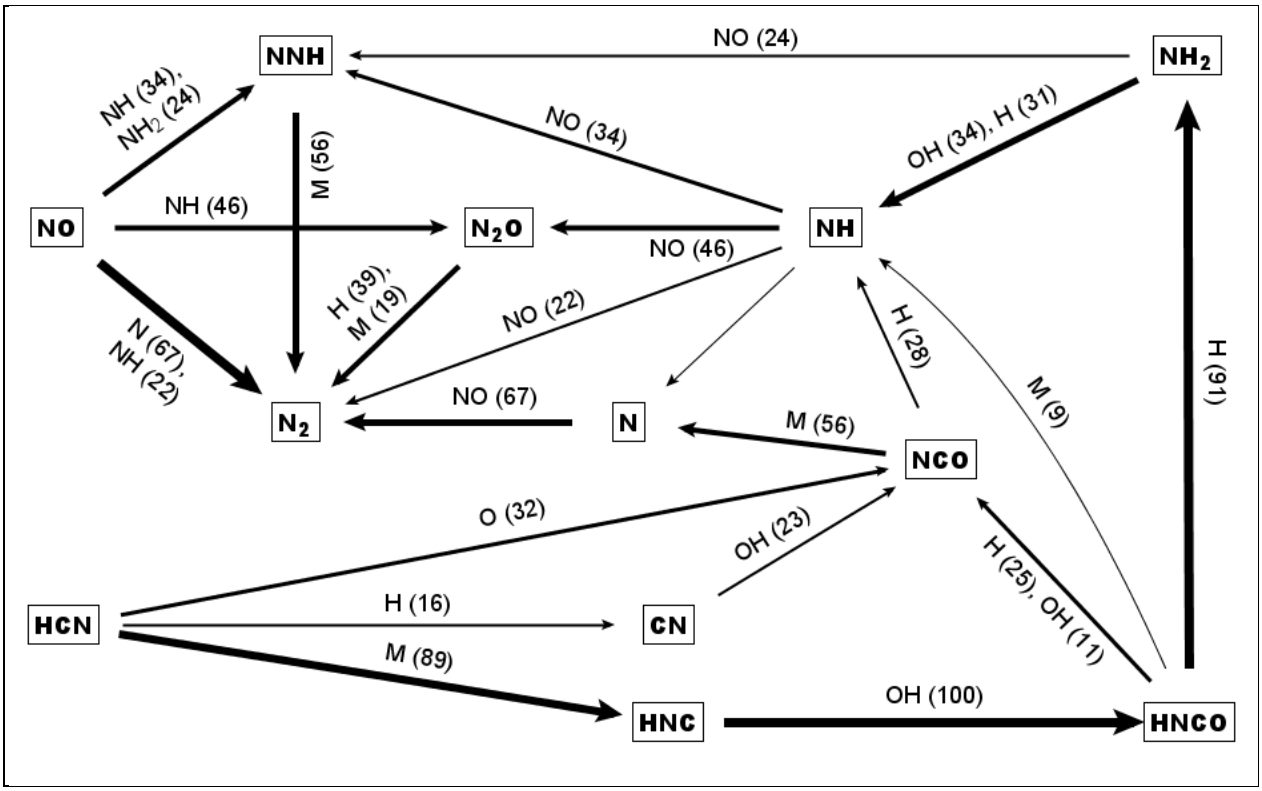

Figure 35. Predicted pathways connecting N-containing species in the 1.0 atm, 400 W/cm^2 laser-heated, RDX/BAMO case (LLT00 [*113*]) at 0.107 ms, the point at which the DZ ignites. The relative rate of 100 is 1.11×10^{-2} mol/cm^3/s.

Table 1. Measured dark zone species mole fractions of NC/NG lot PL-673 propellant flames studied by Heller and Gordon (HG55) (*94*).

Species	Mole Fraction
CO	0.31
CO_2	0.08
H_2	0.08
H_2O	0.25[a]
N_2	0.03
NO	0.23
CH_4	0.01
C_2H_4	0.01

[a]Value inferred in the present work via energy balance (see text).

Table 2. Physical data and inferred τ_{DZ} values for dark zones of NC/NG lot PL-673 propellant flames studied by Heller and Gordon (HG55) (*94*).

P (atm)	**r_b (cm/s)**	**T_{DZ} (K)**	**L_{DZ} (cm)**	**τ_{DZ} (ms) (Experimental)**	**τ_{DZ} (ms) (Model)**
11.2	0.478	1600	1.57	4.55	6.70
14.6	0.584	1640	1.07	3.23	3.71
18.0	0.689	1660	1.01	3.15	2.52
19.2	0.720	1680	0.83	2.61	2.06
21.4	0.794	1690	0.43	1.36	1.69
22.1	0.800	1700	0.57	1.83	1.53
28.2	0.975	1730	0.25	0.828	0.949
35.0	1.216	1770	0.11	0.354	0.578

Table 3. Physical data and inferred τ_{DZ} values for dark zones of nitrate ester lot EC-1 propellant flames studied by Aoki and Kubota (AK82) (*35*).

P (atm)	**r_b (cm/s)**	**T_{DZ} (K)**	**L_{DZ} (cm)**	**τ_{DZ} (ms) (Experimental)**	**τ_{DZ} (ms) (Model)**
10.0	0.325	1443	1.72	7.26	21.1
15.0	0.410	1535	0.770	3.64	6.86
20.0	0.495	1578	0.360	1.83	3.61
32.0	0.700	1593	0.180	1.02	1.78

Table 4. Measured dark zone species mole fractions of 16 atm JA2 propellant flame studied by Vanderhoff and coworkers (VKMT-JA2) (*53*, *98*).

Species	Mole Fraction
CO	0.38
CO_2	0.11
H_2	0.08[a]
H_2O	0.23
N_2	0.03[a]
NO	0.22

[a]Values estimated in this work via comparison to other nitrate ester propellants; see text.

Table 5. Measured dark zone species mole fractions[a] of 0.92 atm BTTN flame studied by Parr and Hanson-Parr (PHP-BTTN) (*99*, *100*).

Species	Mole Fraction
CO	0.336
CO_2	0.045
H_2	0.090
H_2O	0.232
N_2	0.000
NO	0.291
CH_4	0.003
C_2H_4	0.004

[a]Note, original mole fractions, which sum to 0.893, have been renormalized; see text.

Table 6. Physical data and inferred τ_{DZ} values for dark zones of BTTN flames studied by Parr and Hanson-Parr (PHP-BTTN) (*99*, *100*).

P (atm)	**r_b (cm/s)**	**T_{DZ} (K)**	**L_{DZ} (cm)**	**τ_{DZ} (ms) (Experimental)**	**τ_{DZ} (ms) (Model)**
10.0	0.250	1460	1.53	8.74	10.84
11.9	0.306	1475	1.38	7.59	7.78
15.3	0.370	1480	0.834	4.86	5.35
17.7	0.402	1550	0.627	3.71	2.89
20.4	0.444	1560	0.316	1.94	2.26

Table 7. Adiabatic flame temperatures of pure BTTN and dark zone mixtures appropriate to BTTN flames studied by Parr and Hanson-Parr (PHP-BTTN) (*99*, *100*).

P (atm)	**BTTN T_{AD} (K)**	**DZ Mixture T_{AD} (K)**
0.92	2885	2833
10.0	3122	3132
15.3	3163	3182
20.4	3191	3235

Table 8. Measured dark zone species mole fractions of 0.92 atm HMX/GAP/BTTN flame studied by Parr and Hanson-Parr (PHP-HMX) (*107–109*).

Species	**Mole Fraction**
CO	0.15
CO_2	0.04
H_2	0.06
H_2O	0.16
HCN	0.12
N_2	0.17
NO	0.16
N_2O	0.05
NO_2	0.01
CH_2O	0.03
C_2H_4	0.02

Table 9. Measured dark zone species mole fractions of 1.0 atm RDX/BAMO flame with 400 W/cm^2 CO_2 laser-heating assist studied by Litzinger et al. (LLT00) (*113*).

Species	**Mole Fraction**
CO	0.06
CO_2	0.008
H_2	0.015[a]
H_2O	0.21
HCN	0.20
N_2	0.14
NH_3	0.01
NO	0.21
N_2O	0.04
NO_2	0.07
CH_2O	0.03
C_2H_4	0.004

[a]This mole fraction is very uncertain, having error limits of nearly 100%, due to large relative noise for this difficult to measure species.

Table 10. Measured dark zone species mole fractions of 0.92 atm RDX/GAP/BTTN flame studied by Parr and Hanson-Parr (*118–120*).

Species	Mole Fraction
CO	0.20
CO_2	0.11
H_2	0.18
H_2O	0.12
HCN	0.12
N_2	0.18
NO	0.05
N_2O	0.035

Table 11. Measured dark zone species mole fractions of 20 atm HMX/PA and HMX/PE propellant flames studied by Kubota (*128*).

Species	Mole Fraction
CO	0.181
CO_2	0.073
H_2	0.067
N_2	0.098
NO	0.209
N_2O	0.068

Table 12. Element ratios and adiabatic flame temperatures for propellants studied by Kubota (*128*) compared to their dark zone mixtures with hypothetical amounts of H_2O and HCN.*

Mixture[a]	C	H	N	O	T_{AD} (K)[b]
HMX/PA	19.5	35.8	20.8	23.9	2237
HMX/PE	19.4	37.8	20.1	22.7	1928
A + 0.304 H_2O + 0.0 HCN	10.4	30.3	22.1	37.1	2756
A + 0.228 H_2O + 0.076 HCN	13.5	27.2	25.2	34.0	2962
A + 0.152 H_2O + 0.152 HCN	16.6	24.1	28.3	30.9	3010
A + 0.076 H_2O + 0.228 HCN	19.7	21.0	31.5	27.8	3011
A + 0.0 H_2O + 0.304 HCN	22.8	17.9	34.6	24.7	2994
A (assume no undetected species)	16.6	8.7	35.3	39.4	3157

[a]HMX/PA and HMX/PE were Kubota's acronyms for two propellant mixtures he used for the majority of his experiments. 'A' represents the mixture of mole fractions of species which he was able to detect in the dark zones at 20 atm (see table 11).

[b]At 20 atm.

* H_2O and HCN were not measured. Quantities presented in this table show the implications of an attempt to determine mole fractions to use for those two species under the assumption that they were the only significant undetected species (see text).

Table 13. Element ratios and adiabatic flame temperatures for propellants studied by Kubota (*128*) compared to their dark zone mixtures with hypothetical amounts of H_2O and HCN and 0.10 mole fraction total of trace CH_2O and NO_2.*

Mixture[a]	C	H	N	O	T_{AD} (K)[b]
HMX/PA	19.5	35.8	20.8	23.9	2237
HMX/PE	19.4	37.8	20.1	22.7	1928
A + 0.204 H_2O + 0.0 HCN + 0.1 CH_2O + 0.0 NO_2	13.9	29.2	21.3	35.7	2913
A + 0.204 H_2O + 0.0 HCN + 0.05 CH_2O + 0.05 NO_2	12.2	25.7	23.7	38.4	2967
A + 0.204 H_2O + 0.0 HCN + 0.0 CH_2O + 0.1 NO_2	10.4	22.2	26.2	41.2	2827
A + 0.153 H_2O + 0.051 HCN + 0.1 CH_2O + 0.0 NO_2	15.9	27.2	23.3	33.7	2943
A + 0.153 H_2O + 0.051 HCN + 0.05 CH_2O + 0.05 NO_2	14.2	23.7	25.7	36.4	3111
A + 0.153 H_2O + 0.051 HCN + 0.0 CH_2O + 0.1 NO_2	12.5	20.1	28.3	39.1	3078
A + 0.102 H_2O + 0.102 HCN + 0.1 CH_2O + 0.0 NO_2	17.9	25.1	25.3	31.7	2947
A + 0.102 H_2O + 0.102 HCN + 0.05 CH_2O + 0.05 NO_2	16.3	21.6	27.8	34.3	3204
A + 0.102 H_2O + 0.102 HCN + 0.0 CH_2O + 0.1 NO_2	14.6	18.0	30.4	37.1	3240
A + 0.051 H_2O + 0.153 HCN + 0.1 CH_2O + 0.0 NO_2	19.9	23.1	27.3	29.7	2940
A + 0.051 H_2O + 0.153 HCN + 0.05 CH_2O + 0.05 NO_2	18.3	19.6	29.8	32.3	3268
A + 0.051 H_2O + 0.153 HCN + 0.0 CH_2O + 0.1 NO_2	16.6	15.9	32.5	35.0	3362
A + 0.0 H_2O + 0.204 HCN + 0.1 CH_2O + 0.0 NO_2	21.9	21.1	29.3	27.7	2926
A + 0.0 H_2O + 0.204 HCN + 0.05 CH_2O + 0.05 NO_2	20.4	17.6	31.9	30.2	3314
A + 0.0 H_2O + 0.204 HCN + 0.0 CH_2O + 0.1 NO_2	18.7	13.8	34.6	32.9	3465

[a]HMX/PA and HMX/PE were Kubota's acronyms for two propellant mixtures he used for the majority of his experiments. "A" represents the mixture of mole fractions of species which he was able to detect in the dark zones at 20 atm (see table 11).
[b]At 20 atm.

* H_2O, HCN, CH_2O, and NO_2 were not measured. Quantities presented in this table show the implications of an attempt to determine mole fractions to use for those four species under the assumption that they were the only significant undetected species and that CH_2O and NO_2 total 0.10 mole fraction (see text).

Table 14. Element ratios and adiabatic flame temperatures for propellants studied by Kubota (*128*) compared to their dark zone mixtures with hypothetical amounts of H_2O and HCN and 0.20 mole fraction total of trace CH_2O and NO_2.*

Mixture[a]	C	H	N	O	T_{AD} (K)[b]
HMX/PA	19.5	35.8	20.8	23.9	2237
HMX/PE	19.4	37.8	20.1	22.7	1928
A + 0.104 H_2O + 0.0 HCN + 0.2 CH_2O + 0.0 NO_2	17.2	28.1	20.5	34.3	2887
A + 0.104 H_2O + 0.0 HCN + 0.1 CH_2O + 0.1 NO_2	13.9	21.3	25.2	39.6	3128
A + 0.104 H_2O + 0.0 HCN + 0.0 CH_2O + 0.2 NO_2	10.4	14.0	30.3	45.3	2868
A + 0.078 H_2O + 0.026 HCN + 0.2 CH_2O + 0.0 NO_2	18.1	27.1	21.4	33.3	2885
A + 0.078 H_2O + 0.026 HCN + 0.1 CH_2O + 0.1 NO_2	14.9	20.3	26.2	38.6	3200
A + 0.078 H_2O + 0.026 HCN + 0.0 CH_2O + 0.2 NO_2	11.5	12.9	31.4	44.3	3022
A + 0.052 H_2O + 0.052 HCN + 0.2 CH_2O + 0.0 NO_2	19.1	26.1	22.4	32.4	2880
A + 0.052 H_2O + 0.052 HCN + 0.1 CH_2O + 0.1 NO_2	16.0	19.3	27.2	37.6	3260
A + 0.052 H_2O + 0.052 HCN + 0.0 CH_2O + 0.2 NO_2	12.5	11.9	32.4	43.2	3144
A + 0.026 H_2O + 0.078 HCN + 0.2 CH_2O + 0.0 NO_2	20.1	25.1	23.4	31.4	2873
A + 0.026 H_2O + 0.078 HCN + 0.1 CH_2O + 0.1 NO_2	17.0	18.2	28.3	36.5	3314
A + 0.026 H_2O + 0.078 HCN + 0.0 CH_2O + 0.2 NO_2	13.6	10.8	33.5	42.1	3246
A + 0.0 H_2O + 0.104 HCN + 0.2 CH_2O + 0.0 NO_2	21.1	24.1	24.4	30.4	2866
A + 0.0 H_2O + 0.104 HCN + 0.1 CH_2O + 0.1 NO_2	18.0	17.2	29.3	35.5	3363
A + 0.0 H_2O + 0.104 HCN + 0.0 CH_2O + 0.2 NO_2	14.6	9.7	34.6	41.1	3334

[a]HMX/PA and HMX/PE were Kubota's acronyms for two propellant mixtures he used for the majority of his experiments. "A" represents the mixture of mole fractions of species which he was able to detect in the dark zones at 20 atm (see table 11).
[b]At 20 atm.

* H_2O, HCN, CH_2O, and NO_2 were not measured. Quantities presented in this table show the implications of an attempt to determine mole fractions to use for those four species under the assumption that they were the only significant undetected species and that CH_2O and NO_2 total 0.10 mole fraction (see text).

Table 15. Mole fractions of species measured by Kubota in the luminous flame regions of HMX/PA and HMX/PE propellants (*128*) compared to calculated equilibrium concentrations (this work).*

Species	Measured Mole Fractions	Predicted Equilibrium Mole Fractions
CO	0.422	0.391
CO_2	0.041	0.018
H_2	0.267	0.301
H_2O	—	0.073
N_2	0.228	0.217

[a]All results were at 20 atm. Predictions are for HMX/PA, but predictions for HMX/PE are within a few percent (relative). The detection methods were not sensitive to H_2O.

Table 16. Effects of assumed hypothetical added initial H atom on model for JA2 at 16 atm (VKMT-JA2 case [*53*, *98*]). Note, the mole fractions of H shown are added to the mole fractions of table 4, which total slightly greater than 1.0, and then renormalized; thus, the added mole fractions are actually slightly less than shown.

Mole Fraction H Added	Assumed T_{DZ} (K)	Predicted τ_{DZ} (ms)	Predicted T at SS (K)
0.0	1500	9.34	—-
—	—	—	—
0.0001	1500	9.26	1501.5
0.001	1500	8.9	1505.3
0.01	1500	6.7	1553.7
—	—	—	—
0.0	1501.5	9.25	—
0.0	1505.3	9.0	—
0.0	1553.7	6.8	—

* All results were at 20 atm. Predictions are for HMX/PA, but predictions for HMX/PE are within a few percent (relative). The detection methods were not sensitive to H_2O.

Table 17. Ordered temperature sensitivities for the JA2 16 atm case of VKMT-JA2 (*53*, *98*) at 4.47 ms, a point about midway through the DZ ignition delay time; computed T = 1636 K.

Reaction Number	Reaction	Sensitivity Coefficient	Relative Ranking
19	$HNO + NO = N_2O + OH$	7.20E-02	100.
161	$H + HNO = H_2 + NO$	–1.43E-02	–19.9
2	$N_2O(+ M) = N_2 + O(+ M)$	9.88E-03	13.7
43	$CO + OH = CO_2 + H$	5.00E-03	6.94
51	$O + H_2 = OH + H$	3.89E-03	5.40
1	$NO_2(+ M) = NO + O(+ M)$	–3.75E-03	–5.21
3	$H + NO(+ M) = HNO(+ M)$	3.44E-03	4.77
111	$N_2O + H = N_2 + OH$	–1.43E-03	–1.99
116	$H + HNO = NH + OH$	8.48E-04	1.18
170	$N_2O + NO = N_2 + NO_2$	–6.48E-04	–0.900
99	$NCO + OH = NO + CO + H$	5.82E-04	0.809
115	$N_2O + O = NO + NO$	5.07E-04	0.704
160	$HNO + OH = NO + H_2O$	–4.35E-04	–0.604
188	$H_2 + NO_2 = HONO + H$	3.65E-04	0.507

Table 18. Ordered temperature sensitivities for the JA2 16 atm case of VKMT-JA2 (*53*, *98*) at 9.33 ms, the time of the maximum in the predicted heat release profile, which is taken to be the DZ ignition delay time; computed T = 2741 K.

Reaction Number	Reaction	Sensitivity Coefficient	Relative Ranking
19	$HNO + NO = N_2O + OH$	11.6	100.0
161	$H + HNO = H_2 + NO$	–2.02	–17.3
2	$N_2O(+ M) = N_2 + O(+ M)$	1.01	8.64
43	$CO + OH = CO_2 + H$	0.777	6.68
116	$H + HNO = NH + OH$	0.748	6.43
165	$NO + H = N + OH$	0.717	6.16
3	$H + NO(+ M) = HNO(+ M)$	0.472	4.05
51	$O + H_2 = OH + H$	0.417	3.58
1	$NO_2(+ M) = NO + O(+ M)$	–0.399	–3.43
111	$N_2O + H = N_2 + OH$	–0.354	–3.04
115	$N_2O + O = NO + NO$	0.224	1.92
99	$NCO + OH = NO + CO + H$	0.171	1.47
170	$N_2O + NO = N_2 + NO_2$	–0.120	–1.03
120	$NH_2 + O = HNO + H$	9.99E-02	0.859
160	$HNO + OH = NO + H_2O$	–8.25E-02	–0.709

Table 19. Modeled τ_{DZ} for the JA2 16 atm case of VKMT-JA2 (*53*, *98*) when k_i of the chosen reaction is multiplied by 2.0 or 0.5. The reader is reminded that the result with the nominal mechanism is 9.33 ms. Also note that the last reaction, R50, does not appear on the sensitivity lists; it was included as a control (see text).

Reaction Number	Reaction	τ_{DZ} (ms) for 2.0 × k_i	τ_{DZ} (ms) for 0.5 × k_i
19	$HNO + NO = N_2O + OH$	5.05	16.70
161	$H + HNO = H_2 + NO$	10.12	8.20
2	$N_2O(+ M) = N_2 + O(+ M)$	8.89	9.83
43	$CO + OH = CO_2 + H$	8.99	9.74
51	$O + H_2 = OH + H$	9.16	9.56
1	$NO_2(+ M) = NO + O(+ M)$	9.56	9.17
3	$H + NO(+ M) = HNO(+ M)$	9.16	9.62
111	$N_2O + H = N_2 + OH$	9.54	9.19
116	$H + HNO = NH + OH$	8.87	9.61
165	$NO + H = N + OH$	8.95	9.64
50	$O_2 + H = O + OH$	9.33	9.33

Table 20. Ordered temperature sensitivities for the HMX/GAP/BTTN 0.92 atm case of PHP-HMX (*107–109*) at 0.020 ms, the time where the early overall reaction of the traces of CH_2O and NO_2 quickly occurs; computed T = 1460 K.

Reaction Number	Reaction	Sensitivity Coefficient	Relative Ranking
349	$CH_2O + NO_2 = HCO + HONO$	2.48E-03	100.0
21	$HNO + NO_2 = HONO + NO$	1.52E-03	61.3
200	$HCO + NO = HNO + CO$	–1.32E-03	–53.3
37	$HCO + M = H + CO + M$	1.03E-03	41.6
94	$NO_2 + H = NO + OH$	9.65E-04	38.9
229	$H + CH_2O = HCO + H_2$	–5.90E-04	–23.8
49	$OH + H_2 = H_2O + H$	4.32E-04	17.4
351	$HCO + NO_2 = H + CO_2 + NO$	3.58E-04	14.5
2	$N_2O(+ M) = N_2 + O(+ M)$	2.94E-04	11.9
4	$NO + OH(+ M) = HONO(+ M)$	2.56E-04	10.3
186	$CO + NO_2 = NO + CO_2$	2.41E-04	9.72

Table 21. Ordered temperature sensitivities for the HMX/GAP/BTTN 0.92 atm case of PHP-HMX (*107–109*) at 2.52 ms, the time of the third maximum in the predicted heat release profile, which is taken to be τ_{DZ}; computed T = 2597 K.

Reaction Number	Reaction	Sensitivity Coefficient	Relative Ranking
2	$N_2O(+ M) = N_2 + O(+ M)$	1.99	100.
147	$NH_2 + NO = NNH + OH$	0.953	48.0
169	$HNC + OH = HNCO + H$	0.760	38.3
148	$NH_2 + NO = N_2 + H_2O$	–0.680	–34.3
161	$H + HNO = H_2 + NO$	–0.554	–27.9
181	$HNCO + H = NH_2 + CO$	0.518	26.1
111	$N_2O + H = N_2 + OH$	0.404	20.3
37	$HCO + M = H + CO + M$	0.320	16.1
200	$HCO + NO = HNO + CO$	–0.311	–15.7
19	$HNO + NO = N_2O + OH$	0.215	10.8
229	$H + CH_2O = HCO + H_2$	0.206	10.4
246	$H + C_2H_4 = C_2H_3 + H_2$	–0.188	–9.48

Table 22. Modeled τ_{DZ} for the HMX/GAP/BTTN 0.92 atm case of PHP-HMX (*107–109*) when k_i of the chosen reaction is multiplied by 2.0 or 0.5. The reader is reminded that the result with the nominal mechanism is 2.52 ms. The first 12 reactions are those exhibiting large temperature sensitivities at 2.52 ms (see table 21), while the last two are highly sensitive at 0.020 ms where the CH_2O/NO_2 reaction occurs (see table 20).

Reaction Number	Reaction	τ_{DZ} (ms) for 2.0 × k_i	τ_{DZ} (ms) for 0.5 × k_i
2	$N_2O(+ M) = N_2+O(+ M)$	1.69	3.68
147	$NH_2 + NO = NNH + OH$	2.16	3.13
169	$HNC + OH = HNCO + H$	2.21	2.97
148	$NH_2 + NO = N_2 + H_2O$	3.01	2.29
161	$H + HNO = H_2 + NO$	2.80	2.26
181	$HNCO + H = NH_2 + CO$	2.33	2.85
111	$N_2O + H = N_2 + OH$	2.40	2.80
37	$HCO + M = H + CO + M$	2.36	2.66
200	$HCO + NO = HNO + CO$	2.66	2.36
19	$HNO + NO = N_2O + OH$	2.38	2.60
229	$H + CH_2O = HCO + H_2$	2.41	2.57
246	$H + C_2H_4 = C_2H_3 + H_2$	2.62	2.44
349	$CH_2O + NO_2 = HCO + HONO$	2.49	2.55
21	$HNO + NO_2 = HONO + NO$	2.52	2.52

Table 23. Ordered temperature sensitivities for the RDX/BAMO 1.0 atm, 400 W/cm^2 laser heated case of LLT00 (*113*) at 0.0078 ms, the time where the early overall reaction of the traces of CH_2O and NO_2 quickly occurs, along with some NH_3 consumption; computed T = 1568 K.

Reaction Number	Reaction	Sensitivity Coefficient	Relative Ranking
349	$CH_2O + NO_2 = HCO + HONO$	0.0143	100.
200	$HCO + NO = HNO + CO$	–0.00545	–38.0
261	$OH + CH_2O = HCO + H_2O$	0.00523	36.5
351	$HCO + NO_2 = H + CO_2 + NO$	0.00519	36.2
21	$HNO + NO_2 = HONO + NO$	0.00438	30.5
147	$NH_2 + NO = NNH + OH$	0.00263	18.4
4	$NO + OH(+ M) = HONO(+ M)$	0.00240	16.7
37	$HCO + M = H + CO + M$	0.00177	12.4
148	$NH_2 + NO = N_2 + H_2O$	–0.00152	–10.6
49	$OH + H_2 = H_2O + H$	0.00127	8.88
149	$NH_3+OH=NH_2+H_2O$	0.00124	8.68
94	$NO_2 + H = NO + OH$	0.00121	8.46

Table 24. Ordered temperature sensitivities for the RDX/BAMO 1.0 atm, 400 W/cm^2 laser-heated case of LLT00 (*113*) at 0.107 ms, the time to the second maximum in the predicted heat release profile, which is taken to be τ_{DZ}; computed T = 2802 K.

Reaction Number	Reaction	Sensitivity Coefficient	Relative Ranking
147	$NH_2 + NO = NNH + OH$	0.404	100.
2	$N_2O(+ M) = N_2 + O(+ M)$	0.372	92.1
148	$NH_2 + NO = N_2 + H_2O$	–0.258	–63.9
169	$HNC + OH = HNCO + H$	0.202	50.2
181	$HNCO + H = NH_2 + CO$	0.153	37.9
349	$CH_2O + NO_2 = HCO + HONO$	0.101	25.1
113	$NNH + O = NO + NH$	0.0668	16.6
21	$HNO + NO_2 = HONO + NO$	0.0577	14.3
200	$HCO + NO = HNO + CO$	–0.0567	–14.0
149	$NH_3 + OH = NH_2 + H2O$	0.0542	13.4
100	$NCO + M = N + CO + M$	0.0521	12.9
37	$HCO + M = H + CO + M$	0.0486	12.0
160	$HNO + OH = NO + H_2O$	–0.0460	–11.4
178	$HNCO + OH = H_2O + NCO$	–0.0418	–10.4

Table 25. Modeled τ_{DZ} for the RDX/BAMO 1.0 atm, 400 W/cm^2 laser-heated case of LLT00 (*113*) when k_i of the chosen reaction is multiplied by 2.0 or 0.5. The reader is reminded that the result with the nominal mechanism is 0.107 ms. The reactions are those exhibiting large temperature sensitivities at that time (see table 24).

Reaction Number	**Reaction**	**τ_{DZ} (ms) for 2.0 × k_i**	**τ_{DZ} (ms) for 0.5 × k_i**
147	$NH_2 + NO = NNH + OH$	0.083	0.136
2	$N_2O(+ M) = N_2 + O(+ M)$	0.084	0.135
148	$NH_2 + NO = N_2 + H_2O$	0.127	0.093
169	$HNC + OH = HNCO + H$	0.095	0.121
181	$HNCO + H = NH_2 + CO$	0.097	0.117
349	$CH_2O + NO_2 = HCO + HONO$	0.101	0.113
113	$NNH + O = NO + NH$	0.101	0.111
21	$HNO + NO_2 = HONO + NO$	0.104	0.111
200	$HCO + NO = HNO + CO$	0.111	0.104
149	$NH_3 + OH = NH_2 + H_2O$	0.104	0.111
100	$NCO + M = N + CO + M$	0.102	0.111
37	$HCO + M = H + CO + M$	0.104	0.110
160	$HNO + OH = NO + H_2O$	0.111	0.105
178	$HNCO + OH = H_2O + NCO$	0.110	0.105

7. References

1. Vanderhoff, J. A. U.S. Army Research Laboratory: Aberdeen Proving Ground, MD, unpublished experimental results, 1985.

2. Kubota, N. Survey of Rocket Propellants and Their Combustion Characteristics. In *Fundamentals of Solid Propellant Combustion*; Kuo, K. K., Summerfield, M., Eds.; Progress in Astronautics and Aeronautics Vol. 90, American Institute of Aeronautics and Astronautics: New York, 1984; Chapter 1.

3. Anderson. W. R.; Fontijn, A. Gas-Phase Kinetics for Propellant Combustion Modeling: Requirements and Experiments. In *Overviews of Recent Research on Energetic Materials*; Shaw, R. W., Brill, T. B., Thompson, D. L., Eds.; Advanced Series in Physical Chemistry Vol. 16, World Scientific: London, August 2005; Chapter 7.

4. Vanderhoff, J. A.; Anderson, W. R.; Kotlar, A. J. Dark Zone Modeling of Solid Propellant Flames. *29th JANNAF Combustion Subcommittee Meeting*, CPIA Publication No. 593, 1992; Vol. II; p 225.

5. Anderson, W. R. The Chemical Mechanism of H_2/NO Combustion at Intermediate Temperatures and Its Relation to the Dark Zone of Propellants. *30th JANNAF Combustion Subcommittee Meeting*, CPIA Publication No. 606, 1993; Vol. II; p 205.

6. Anderson, W. R.; Ilincic, N.; Seshadri, K. Studies of Reactions Pertaining to and Development of a Reduced Mechanism for the Double Base Propellant Dark Zone. *31st JANNAF Combustion Subcommittee Meeting*, CPIA Publication No. 620, 1994; Vol. II; p 387.

7. Anderson, W. R.; Ilincic, N.; Meagher, N. E.; Seshadri, K.; Vanderhoff, J. A. Detailed and Reduced Chemical Mechanisms for the Dark Zones of Double Base and Nitramine Propellants in the Intermediate Temperature Regime. *32nd JANNAF Combustion Subcommittee Meeting and 1995 Propulsion Systems Hazards Subcommittee Meeting, Joint Sessions*, CPIA Publication No. 638, 1995; Vol. I; p 197.

8. Ilincic, N.; Anderson, W. R.; Seshadri, K.; Meagher, N. E. Simplified Chemical-Kinetic Mechanisms for Characterizing the Structure of the Dark Zones of Double Base and Nitramine Propellants. *Proc. Combust. Inst.* **1996**, *26* (2), 1997–2006.

9. Ilincic, N.; Anderson, W. R.; Seshadri, K.; Meagher, N. E. *Reduced Chemical Kinetic Mechanisms for the Dark Zones of Double Base and Nitramine Gun Propellants*; ARL-TR-1352; U.S. Army Research Laboratory: Aberdeen Proving Ground, MD, May 1997.

10. Anderson, W. R. Propellant Dark Zone Chemistry: Detailed and Reduced Mechanisms for Interior Ballistic Applications. In *U.S. Army Workshop on Solid-Propellant Ignition and Combustion Modeling*; Miller, M. S., Shaw, R. W., Mann, D. M., Eds.; ARL-TR-1411; U.S. Army Research Laboratory: Aberdeen Proving Ground, MD, July 1997.

11. Korobeinichev, O. P.; Kubida, L. V.; Paletsky, A. A.; Shmakov, A. G. Molecular-Beam Mass-Spectrometry to Ammonium Dinitramide Combustion Chemistry Studies. *J. Prop. Power* **1998**, *14*, 991–1000.

12. Liau, Y.-C.; Yang, V.; Lin, M. C.; Park, J. Analysis of Ammonium Dinitramide (ADN) Combustion with Detailed Chemistry. *35th JANNAF Combustion Subcommittee and 17th Propulsion System Hazards Subcommittee Meeting*, CPIA Publication No. 685, 1998; pp 13–30.

13. Brill, T. B.; Brush, P. J. Condensed Phase Chemistry of Explosives and Propellants at High Temperature: HMX, RDX, and BAMO. *Phil. Trans. R. Soc. London* **1992**, *A339*, 377–385.

14. Brill, T. B. Multiphase Chemistry Considerations at the Surface of Burning Nitramine Monopropellants. *J. Prop. Power* **1995**, *11*, 740–751.

15. Beckstead, M. W. Brigham Young University, Provo, UT. Private communications, 1995 and 2007.

16. Davidson, J. E.; Beckstead, M. W. Improvements to Steady-State Combustion Modeling of Cyclotrimethylenetrinitramine. *J. Prop. Power* **1997**, *13*, 375–383.

17. Liau, Y.-C.; Kim, E. S.; Yang, V. A Comprehensive Analysis of Laser-Induced Ignition of RDX Monopropellant. *Combust. Flame* **2001**, *126*, 1680–1698.

18. Beckstead, M. W.; Puduppakkam, K.; Thakre, P.; Yang, V. Modeling of Combustion and Ignition of Solid-Propellant Ingredients. *Prog. Energy Combust. Sci.* **2007**, *33*, 497–551.

19. Kooker, D. E. U.S. Army Research Laboratory, Aberdeen Proving Ground, MD. Private communications, 1992–1995.

20. Kooker, D. E.; Chang, L. M.; Howard, S. L. *Flamespreading in Granular Solid Propellant: Design of an Experiment*; ARL-MR-80; U.S. Army Research Laboratory: Aberdeen Proving Ground, MD, June 1993.

21. Kooker, D. E.; Chang, L. M.; Howard, S. L. *Flamespreading in Granular Solid Propellant: Initial Results*; ARL-TR-446; U.S. Army Research Laboratory: Aberdeen Proving Ground, MD, June 1994.

22. Kooker, D. E.; Howard, S. L.; Chang, L. M. Flamespreading in Granular Solid Propellant: Influence of Propellant Composition. *32nd JANNAF Combustion Subcommittee Meeting*, CPIA Publication No. 631, 1995; Vol. I; pp 397–408.

23. Nusca, M. J. U.S. Army Research Laboratory, Aberdeen Proving Ground, MD. Private communication, 2009.

24. Miller, M. S.; Anderson, W. R. Burning-Rate Predictor for Multi-Ingredient Propellants: Nitrate-Ester Propellants. *J. Prop. Power* **2004**, *20*, 440–454; author's note, **2005**, *21*, 576.

25. Anderson W. R.; Conner, C. B. Comparison of Gas-Phase Mechanisms Applied to RDX Combustion Model. *Proc. Combust. Inst.* **2009**, *32* (2), 2123–2130.

26. Anderson, W. R.; Conner, C. B.; da Silva, G.; Bozzelli, J. W. Theoretical Study of the Combustion and Thermal Decomposition of RDX, Part I: Kinetic Modeling, *Eastern States Section Fall Technical Meeting of the Combustion Institute,* October 2007, Paper A-01.

27. da Silva, G. J.; Bozzelli, W.; Conner C. B.; Anderson, W. R. Theoretical Study of the Combustion and Thermal Decomposition of RDX, Part II: Detailed Kinetics on Initial Reaction Paths. Presented at Eastern States Section Fall Technical Meeting of the Combustion Institute, Charlottesville, VA, October 2007; Paper A-02.

28. Anderson, W. R.; Conner, C. B.; da Silva, G.; Asatryan, R.; Bozzelli, J. W. Revised Model for Combustion of RDX. *JANNAF 55th Propulsion, 42nd Combustion, 30th Airbreathing Propulsion, 30th Exhaust Plume Technology, 24th Propulsion Systems Hazards, and 12th Spirits User Group Joint Subcommittee Meeting*, Newton, MA, May 2008; Paper CS-2Q-9.

29. Anderson, W. R.; Conner, C. B.; da Silva, G.; Asatryan, R; Bozzelli, J. W. Revised Model for RDX Combustion. *Proceedings 24th International Symposium on Ballistics*, New Orleans, LA, September 2008; Paper IB151, Vol. 1, p 304.

30. Yetter, R. A.; Dryer, F. L.; Allen, M. T.; Gatto, J. L. Development of Gas Phase Reaction Mechanism for Nitramine Combustion. *J. Prop. Power* **1995**, *11*, 683–697.

31. Chakraborty, D.; Muller, R. P.; Dasgupta, S.; Goddard, W. A., III. The Mechanism for Unimolecular Decomposition of RDX (1,3,5-Trinitro-1,3,5-triazine), an ab Initio Study. *J. Phys. Chem.* **2000**, *A 104*, 2261–2272.

32. Chakraborty, D.; Muller, R. P.; Dasgupta, S.; Goddard, W. A., III. A Detailed Model for the Decomposition of Nitramines: RDX and HMX. *J. Computer-Aided Materials Design* **2001**, *8*, 203–212.

33. Chakraborty, D.; Muller, R. P.; Dasgupta, S.; Goddard, W. A., III. Chemical Simulation of Energetic Materials (see also http://www.wag.caltech.edu/home/rpm/projects/hedm/).

34. Sotter, J. G. Chemical Kinetics of the Cordite Explosion Zone. *Proc. Combust. Inst.* **1965**, *10*, 1405–1411.

35. Aoki, I.; Kubota, N. Combustion Wave Structures of High- and Low-Energy Double-Base Propellants. *AIAA J.* **1982**, *20*, 100–105; Paper AIAA-80-1165R.

36. Fifer, R. A.; Kotlar, A. J.; Miller, M. S.; Morris, J. B. Dark Zone Modeling for Delayed Ignition Kinetics. *27th JANNAF Combustion Subcommittee Meeting*, CPIA Publication No. 557, November 1990; Vol. I; pp 95–104.

37. Yang, R.; Thakre, P.; Liau, Y.-C.; Yang, V. Formation of Dark Zone and Its Temperature Plateau in Solid-Propellant Flames: A Review. *Combust. Flame* **2006**, *145*, 38–58.

38. Crawford, B. L., Jr.; Huggett, C.; McBrady, J. J. The Mechanism of the Burning of Double-Base Propellants. *J. Phys. Chem.* **1950**, *54*, 854–862.

39. Klein, R.; Mentser, M.; von Elbe, G.; Lewis, B. Determination of the Thermal Structure of a Combustion Wave by Fine Thermocouples. *J. Phys. Chem.* **1950**, *54*, 877–889.

40. Lengelle, G.; Bizot, A.; Duterque, J.; Trubert, J. F. Steady-State Burning of Homogeneous Propellants. In *Fundamentals of Solid Propellant Combustion*; Kuo, K. K., Summerfield, M., Eds.; Progress in Astronautics and Aeronautics Vol. 90; Summerfield, M., Series Ed. American Institute of Aeronautics and Astronautics: New York, 1984; pp 361–407.

41. Liiva, P. M.; Fetherolf, B. L.; Litzinger, T. A. Thermal and Chemical Structure of the Preparation and Reaction Zones for M9 and JA2. *28th JANNAF Combustion Subcommittee Meeting*, CPIA Publication No. 573, October–November 1991; Vol. II; pp 553–562.

42. Korobeinichev, O. P.; Kubida, L. V.; Paletsky, A. A.; Cherov, A. A. Study of Solid Propellant Flame Structure. *Combust. Sci. Tech.* **1996**, *113–114*, 557–571.

43. Kubota, N. Physicochemical Processes of HMX Propellant Combustion. *Proc. Combust. Inst.* **1982**, *19*, 777–785.

44. Teague, M. W.; Vanderhoff, J. A. *Spectral Studies of Solid Propellant Combustion III. Emission and Absorption Results for HMX2 Propellant*; BRL-MR-3911; U.S. Army Ballistics Research Laboratory: Aberdeen Proving Ground, MD, May 1991.

45. Fetherolf, B. L.; Liiva, P. M.; Litzinger, T. A.; Kuo, K. K. Thermal and Chemical Structure of the Preparation and Reaction Zones for RDX and RDX Composite Propellants. *28th JANNAF Combustion Subcommittee Meeting*, CPIA Publication No. 573, October–November 1991; Vol. II; pp 379–386.

46. Tang, C.-J.; Lee, Y. J.; Litzinger, T. A. A Study of Gas-Phase Processes During the Deflagration of RDX Composite Propellants Using a Triple Quadrupole Mass Spectrometer. *31st JANNAF Combustion Subcommittee Meeting*, CPIA Publication No. 620, October 1994; Vol. II; pp 307–316.

47. Mallery, C. F.; Thynell, S. T. Species and Temperature Profiles of Propellant Flames Obtained from FTIR Absorption Spectroscopy. *31st JANNAF Combustion Subcommittee Meeting*, CPIA Publication No. 620, 1994; Vol. II; pp 291–305.

48. Mallery, C. F.; Thynell, S. T. Further Improvement to FTIR Absorption Spectroscopy of Propellant Flames for Profiling of Species and Temperature. *31st JANNAF Combustion Subcommittee Meeting*, CPIA Publication No. 631, 1995; Vol. I; pp 449–460.

49. Lu, Y.-C.; Ulas, A.; Kuo, K. K.; Freyman, T. M. Absorption Spectroscopy of Solid Propellant Flames. AIAA 95-2713; *AIAA J.* **1995**, 1–9.

50. Lu, Y.-C.; Freyman, T. M.; Kuo, K. K. UV/Visible Absorption Spectroscopy of Dark Zones in Solid-Propellant Flames. *Combust. Flame* **1997**, *109*, 342–352.

51. Mallery, C. F.; Thynell, S. T. Line-of-Sight Profiling of Temperature and Species in Propellant Flames Using FTIR Spectroscopy. AIAA-1998-3827; *AIAA J.* **1998**, 1–13.

52. Vanderhoff, J. A.; Teague, M. W.; Kotlar, A. J. *Absorption Spectroscopy Through the Dark Zone of Solid Propellant Flames*; BRL-TR-3334; U.S. Army Ballistics Research Laboratory: Aberdeen Proving Ground, MD, April 1992.

53. Vanderhoff, J. A.; Teague, M. W.; Kotlar, A. J. Determination of Temperature and NO Concentrations Through the Dark Zone of Solid-Propellant Flames. *Proc. Combust. Inst.* **1992**, *24*, 1915–1922.

54. Modiano, S. H.; Vanderhoff, J. A. *Multichannel Infrared (IR) Absorption Spectroscopy Applied to Solid Propellant Flames*; ARL-TR-900; U.S. Army Research Laboratory: Aberdeen Proving Ground, MD, December 1995.

55. Vanderhoff, J. A.; Modiano, S. H.; Homan, B. E.; Teague, M. W. Overtone Absorption Spectroscopy of Solid Propellant Flames: CO and N_2O Concentrations. *Proceedings of the Fourth International Symposium on Special Topics in Chemical Propulsion*, Stockholm, Sweden, 27–31 May 1996.

56. Vanderhoff, J. A.; Modiano, S. H.; Teague, M. W.; Homan, B. E. *Temperatures and Species Concentration in Propellant Dark Zones via Fitting Infrared (IR) Spectral Absorption Data*; ARL-TR-1366; U.S. Army Research Laboratory: Aberdeen Proving Ground, MD, June 1997.

57. Homan, B. E.; Vanderhoff, J. A. *Spatially Resolved Combustion Species and Temperatures of Solid Propellant Flames Using Snapshot Spectroscopy*; ARL-TR-2060; U.S. Army Research Laboratory: Aberdeen Proving Ground, MD, October 1999.

58. Miller, M. S.; Anderson, W. R. Energetic-Material Combustion Modeling With Elementary Gas-Phase Reactions: A Practical Approach. In *Solid Propellant Chemistry, Combustion, and Motor Interior Ballistics*; Yang, V., Brill, T. B., Ren, W. Z., Eds.; *Progress in Astronautics and Aeronautics*, Vol. 185; Zarchan, P., Ed.; American Institute of Aeronautics and Astronautics: Reston, VA, 2000; Chapter 2.12.

59. Anderson, W. R.; Meagher, N. E.; Vanderhoff, J. A. Updated Critical Study of the Dark Zones of Combusting Solid Propellants. *JANNAF 55th Propulsion, 42nd Combustion, 30th Airbreathing Propulsion, 30th Exhaust Plume Technology, 24th Propulsion Systems Hazards, and 12th Spirits User Group Joint Subcommittee Meeting*, Newton, MA, May 2008; Paper CS-3O-3.

60. Anderson, W. R.; Meagher, N. E.; Vanderhoff, J. A. Critical Evaluation and Modeling of Solid Propellant Dark Zone Experiments. *Proceedings of the 26th Army Science Conference*, Orlando, FL, December 2008; Paper DP-03.

61. Lutz, A. E.; Kee, R. J.; Miller, J. A. *SENKIN: A Fortran Program for Predicting Homogeneous Gas Phase Chemical Kinetics with Sensitivity Analysis*; SAND 87-8248; Sandia National Laboratories: Albuquerque, NM, October 1988.

62. Kee, R. J.; Rupley, F. M.; Miller, J. A. *Chemkin-II: A Fortran Chemical Kinetics Package for the Analysis of Gas-Phase Chemical Kinetics*; SAND 89-8009; Sandia National Laboratories: Albuquerque, NM, September 1989.

63. Miller; J. A.; Bowman, C. T. Mechanism and Modeling of Nitrogen Chemistry in Combustion. *Prog. Eng. Combust. Sci.* **1989**, *15*, 287–338.

64. Smith, G. P.; Golden, D. M.; Frenklach, M.; Moriarty, N. W.; Eiteneer, B.; Goldenberg, M.; Bowman, C. T.; Hanson, R. K.; Song, S.; Gardiner, W. C., Jr.; Lissianski, V. V.; Qin, Z. GRI-Mech, version 2.11 (see also http://www.me.berkeley.edu/gri_mech/).

65. Wilde, K. A. The Role of HNO in the H_2 – NO Reaction. *Combust. Flame* **1969**, *13*, 173–180.

66. Bunte, S. W.; Rice, B. M.; Chabalowski, C. F. An Ab Initio QCISD Study of the Potential Energy Surface for the Reaction HNO + NO → N_2O + OH. *J. Phys. Chem. A* **1997**, *101*, 9430–9438.

67. Diau, E. W.; Halbegewachs, M. J.; Smith, A. R.; Lin, M. C. Thermal Reduction of NO by H_2 : Kinetic Measurement and Computer Modeling of the HNO + NO Reaction. *Int. J. Chem. Kinet.* **1995**, *27*, 867–881.

68. Diau, E. W.-G.; Lin, M. C.; He, Y.; Melius, C. F. Theoretical Aspects of H/N/O-chemistry Relevant to the Thermal Reduction of NO by H_2. *Prog. Eng. Combust. Sci.* **1995**, *21*, 1–23.

69. Chase, M. W., Jr.; Davies, C. A., Downey, J. R., Jr.; Frurip, D. J.; McDonald, R. A.; Syverud, A. N. JANAF Thermochemical Tables, Third Edition. *J. Phys. Chem. Ref. Data* **1985**, *14*, Suppl. 1.

70. Anderson, W. R. Heats of Formation of HNO and Some Related Species. *Combust. Flame* **1999,** *117*, 394–403.

71. Glarborg, P.; Østberg, M.; Alzueta, M. U.; Dam-Johansen, K.; Miller, J. A. The Recombination of Hydrogen Atoms With Nitric Oxide at High Temperatures. *Proc. Combust. Inst.* **1998**, *27*, 219–226.

72. Burcat, A.; Ruscic, B. Third Millennium Ideal Gas and Condensed Phase Thermochemical Database for Combustion with Updates from Active Thermochemical Tables, TAE 960 (see also http://garfield.chem.elte.hu/Burcat/burcat.html).

73. Smith, G. P.; Golden, D. M.; Frenklach, M.; Moriarty, N. W.; Eiteneer, B.; Goldenberg, M.; Bowman, C. T.; Hanson, R. K.; Song, S.; Gardiner, W. C., Jr.; Lissianski, V. V.; Qin, Z. GRI Mechanism Version 3.0 (see also http://www.me.berkeley.edu/gri_mech/).

74. Lin, M. C. Emory University, Atlanta, GA. Private communication, 1995.

75. Avramen'kov, L. I.; Krasnen'kov, V. M. Reactions of Nitrogen Atoms Communication 6. Rate Constant and Mechnism of the Elementary Reaction of Nitrogen Atoms With Carbon Dioxide. *Izvestiya Akademii Nauk SSSR, Seriya Kimicheskaya* **1967**, *3*, Eng. Trans. 501–503, 516–519.

76. Herron, J. T.; Huie, R. E. On the Reaction of Atomic Nitrogen with Carbon Dioxide. *J. Phys. Chem.* **1968**, *72*, 2235–2236.

77. Rawlins, W. T.; Kaufman, F. The Reaction of CO_2 with Active Nitrogen. *J. Chem. Phys.* **1976**, *64*, 1128–1133.

78. Manaa, M. R.; Chabalowski, C. F. A Theoretical Treatment of the Intersystem Crossing in the Spin-Forbidden Reaction: $NO(X^2\Pi) + CO(X^1\Sigma^+) \rightarrow N(^4S) + CO_2\ (X^1\Sigma_g^+)$. *Chem. Phys. Lett.* **1999**, *300*, 619–625.

79. Fernandez, A.; Goumri, A.; Fontijn, A. Kinetics of the Reactions of $N(^4S)$ Atoms With O_2 and CO_2 Over Wide Temperature Ranges. *J. Phys. Chem. A* **1998**, *102*, 168–172.

80. Lindackers, D.; Burmeister, M.; Roth, P. High-Temperature Kinetics of the Reaction CN + CO_2. *Combust. Flame* **1990**, *81*, 251–259.

81. Dean, A. M.; Bozzelli, J. W. Combustion Chemistry of Nitrogen. In *Gas-Phase Combustion Chemistry*; Gardiner, W. C., Jr., Ed.; Springer: New York, 2000; Chapter 2.

82. Sulzmann, K. G. P.; Leibowitz, L.; Penner, S. S. Shock-Tube Studies on Mixtures of NO, CO, and Ar. *Proc. Combust. Inst.* **1971**, *13*, 137–146.

83. Miller, J. A.; Bowman, C. T. Kinetic Modeling of the Reduction of Nitric Oxide in Combustion Products by Isocyanic Acid. *Int. J. Chem. Kinet.* **1991**, *23*, 289–313.

84. Glarborg, P.; Alzueta, M. U.; Dam-Johansen, K.; Miller, J. A. Kinetic Modeling of Hydrocarbon/Nitric Oxide Interactions in a Flow Reactor. *Combust. Flame* **1998**, *115*, 1–27.

85. Rohrig, M.; Wagner, H. G. The Reactions of NH($X^3\Sigma^-$) With the Water Gas Components CO_2, H_2O, and H_2. *Proc. Combust. Inst.* **1994**, *25*, 975–981.

86. Glarborg, P.; Kristensen, P. G.; Dam-Johansen, K.; Alzueta, M. U.; Millera, A.; Bilbao, R. Nitric Oxide Reduction by Non-Hydrocarbon Fuels. Implications for Reburning With Gasification Gases. *Energy and Fuels* **2000**, *14*, 828–838.

87. Dagaut, P.; Lecomte, F.; Mieritz, J.; Glarborg, P. Experimental and Kinetic Modeling Study of the Effect of NO and SO_2 on the Oxidation of CO-H_2 Mixtures. *Int. J. Chem. Kinet.* **2003**, *35*, 564–575.

88. Fontijn, A.; Shamsuddin, S. M.; Crammond, D.; Marshall, P.; Anderson, W. R. Kinetics of the NH Reaction With H_2 and Reassessment of HNO Formation From NH + CO_2, H_2O. *Combust. Flame* **2006**, *145*, 543–551.

89. Mackie, J. C.; Bacskay, G. B. Quantum Chemical Study of the Mechanism of Reaction Between NH ($X^3\Sigma^-$) and H_2, H_2O, and CO_2 Under Combustion Conditions. *J. Phys. Chem. A* **2005**, *109*, 11967–11974.

90. Lin, M. C.; He, Y.; Melius, C. F. Implications of the HCN → HNC Process to High-Temperature Nitrogen-Containing Fuel Chemistry. *Int. J. Chem. Kinet.* **1992**, *24*, 1103–1107.

91. Woolridge, S.T.; Hanson, R. K.; Bowman, C. T. Simultaneous Laser-Absorption Measurements of CN and OH in a Shock-Tube Study of HCN + OH → Products. *Int. J. Chem. Kinet.* **1995**, *27*, 1075–1087.

92. Svehla R. A.; McBride, B. J. *Fortran IV Computer Program for Calculation of Thermodynamic and Transport Properties of Complex Chemical Systems*; NASA-TN-D-0756; National Aeronautics and Space Administration: Washington, DC, January 1973.

93. Homan, B. E. U.S. Army Research Laboratory, Aberdeen Proving Ground, MD. Private communication, 2003.

94. Heller, C. A.; Gordon, A. S. Structure of the Gas-Phase Combustion Region of a Solid Double Base Propellant. *J. Phys. Chem.* **1955**, *59*, 773–777.

95. Venizelos, D. T.; Sausa, R. C. Laser-Induced Fluorescence, Mass Spectrometric, and Modeling Studies of Neat and NH_3 Doped H_2/N_2O/Ar Flames. *Combust. Flame* **1998**, *115*, 313–326.

96. Martins, C. A.; Pimenta, A. P.; Carvalho, J. A., Jr.; Ferreira, M. A.; Caldeira-Pires, A. A. CH and C_2 Radicals Characterization in Natural Gas Turbulent Diffusion Flames. *J. Braz. Soc. Mech. Sci. Eng.* **2005**, *27*, 110–118.

97. Klein, R.; Menster, M.; von Elbe, G.; Lewis, B. Determination of the Thermal Structure of a Combustion Wave by Fine Thermocouples. *J. Phys. Chem.* **1950**, *34*, 877–884.

98. Vanderhoff, J. A.; Kotlar, A. J.; Modiano, S. H.; Teague, M. W. Propellant Combustion Diagnostics Via Multichannel Absorption Spectroscopy. In *Challenges in Propellants and Combustion: 100 Years After Nobel*; Kuo, K. K., Brill, T. B., Pesce-Rodriguez, R. A., Eds.; Begell House: New York, 1997; pp 807–822.

99. Parr, T.; Hanson-Parr, D. BTTN Flame Structure. *JANNAF Combustion Subcommittee Meeting*, CPIA Publication No. 712, April 2002; Vol. I; pp 43–49.

100. Parr T.; Hanson-Parr, D. Flame Structure of TMETN, BTTN, and Cured GAP/BTTN Gumstock; unpublished memorandum, Naval Air Warfare Center, China Lake, CA, 2002.

101. Parr, T. Naval Air Warfare Center, China Lake, CA. Private communication, 2009.

102. Puduppakkam, K. V.; Beckstead, M. W.; Hecker, W. C. Combustion Modeling of Butanetriol Trinitrate With Detailed Kinetics. Proceedings of the 40th JANNAF Combustion Subcommittee Meeting, CPIAC Publication No. JSC-CD-39, June 2005.

103. Puduppakkam, K. V.; Beckstead, M. W. Combustion Modeling of Nitrate Esters With Detailed Kinetics. Proceedings of the 40th JANNAF Combustion Subcommittee Meeting, CPIAC Publication No. JSC-CD-39, June 2005.

104. Puduppakkam, K. V.; Beckstead, M. W. Combustion Modeling of Nitrate Esters With Detailed Kinetics. 41st AIAA/ASME/SAE/ASEE Joint Propulsion Conference and Exhibit, AIAA-2005-3770; *AIAA J.* **2005**.

105. Korobeinichev, O. P.; Kubida, L. V.; Paletsky, A. A.; Chernov, A. A. Study of Propellant Flame Structure by Mass-Spectrometric Sampling. *Combust. Sci. Tech.* **1996**, 113–4, 557–571.

106. Korobeinichev, O. P. Flame Structure of Solid Propellants. *In Solid Propellant Chemistry, Combustion, and Motor Interior Ballistics*; Yang, V., Brill, T. B., Ren, W. Z., Eds.; *Progress in Astronautics and Aeronautics*, Vol. 185, Zarchan, P., Ed.; American Institute of Aeronautics and Astronautics: Reston, VA, 2000; Chapter. 2.3.

107. Parr, T.; Hanson-Parr, D. HMX/GAP/BTTN Propellant Flame Structure. 38th JANNAF Combustion Subcommittee Meeting, CPIA Publication No. 712, 2002; Vol. I; pp 129–142.

108. Parr, T.; Hanson-Parr, D. Cyclotetramethylene Tetranitramine/Glycidy Azide Polymer/Butanetriol Trinitrate Propellant Flame Structure. *Combust. Flame* **2004**, 137, 38–49.

109. Hanson-Parr, D. Naval Air Warfare Center, China Lake, CA. Private communication, 2005.

110. Lyman, J. L.; Liau, Y.-C.; Brand. Thermochemical Functions for Gas-Phase 1,3,5,7-Tetranitro-1,3,5,7-tetraazacyclooctane (HMX), Its Condensed Phases, and Its Larger Reaction Products. *Combust. Flame* **2002**, 130, 185–203.

111. Washburn, E. B.; Beckstead, M. W.; Gross, M. L. Condensed-Phase Model for HMX Decomposition. 38th JANNAF Combustion Subcommittee Meeting, CPIA Publication No. 712, 2002; Vol. I, pp 33–42.

112. Puduppakkam, K. V.; Beckstead, M. W. Combustion Modeling of Glycidyl Azide Polymer with Detailed Kinetics. *Combust. Sci. Tech*. **2005**, 177, 1661–1697.

113. Litzinger, T. A.; Lee, Y.; Tang, C.-J. Experimental Studies of Nitramine/Azide Propellant Combustion. In Solid Propellant Chemistry, Combustion, and Motor Interior Ballistics; Yang, V., Brill, T. B., Ren, W. Z., Eds.; *Progress in Astronautics and Aeronautics*, Vol. 185, P. Zarchan, Ed.; American Institute of Aeronautics and Astronautics: Reston, VA, 2000; Chapter 2.4.

114. Tang, C. -J.; Lee, Y. J.; Litzinger, T. A. The Chemical and Thermal Processes of GAP/Nitramine Pseudo-Propellants Under CO_2 Laser Heating. 34th JANNAF Combustion Subcommittee Meeting, CPIA Publication 662, 1997, Vol. II, pp 491–504.

115. Lee, Y. J.; Kudva, G.; Tang, C. -J.; Litzinger, T. A. Thermal Decomposition of BAMO and RDX/BAMO Pseudo-Propellants. 33rd JANNAF Combustion Subcommittee Meeting, CPIA Publication 653, 1996, Vol. II, pp 79–85.

116. Schmidt, R. D.; Manser, G. E. Heats of Formation of Energetic Oxetane Monomers and Polymers. Proceedings 32nd International Annual Conference of Institute of Chemical Technologies, Karlsruhe, Germany, July 2001.

117. Miller, M. S.; Anderson, W. R. *Prediction of Advanced Nitramine Propellant Burning Rates With the CYCLOPS Code*; ARL-MR-552; U.S. Army Research Laboratory: Aberdeen Proving Ground, MD, March 2003.

118. Parr, T.; Hanson-Parr, D. RDX/GAP Propellant Flame Studies. 37th JANNAF Combustion Subcommittee Meeting, CPIA Publication No. 701, 2000; Vol. I, pp 391–402.

119. Parr, T.; Hanson-Parr, D. RDX/GAP/BTTN Propellant Flame Studies. *Combust. Flame* **2001**, 127, 1895–1905.

120. Parr, T. Naval Air Warfare Center, China Lake, CA. Private communication, 2009.

121. Lee, Y. J.; Tang, C.-J.; Litzinger, T. A. A Study of the Chemical and Physical Processes Governing CO_2 Laser-Induced Pyrolysis and Combustion of RDX. *Combust. Flame* **1999**, 117, 600–628.

122. Fetherolf, B. L.; Litzinger, T. A.; Lu, Y-C.; Kuo, K. K. A Comparison of the Physical and Chemical Processes Governing the CO_2 Laser-Induced Pyrolysis and Deflagration of XM39 and M43. 30th JANNAF Combustion Subcommittee Meeting, CPIA Publication No. 606, November 1993; Vol. II, pp 183–193.

123. Kudva, G.; Tang, C.-J.; Lee, Y. J.; Litzinger, T. A. Study of Laser-Assisted Combustion of RDX-CAB Pseudo Propellants at Various Operating Conditions. 33rd JANNAF Combustion Subcommittee Meeting, CPIA Publication No. 653, November 1996; Vol. II, pp 569–578.

124. Tang, C.-J.; Lee, Y. J.; Kudva, G.; Litzinger, T. A. A Study of the Gas-Phase Chemical Structure During CO_2 Laser Assisted Combustion of HMX. *Combust. Flame* **1999**, 117, 170–188.

125. Mallery, C. F.; Thynell, S. T. Species and Temperature Profiles of Propellant Flames Obtained From FTIR Absorption Spectroscopy. 31st JANNAF Combustion Subcommittee Meeting, CPIA Publication No. 620, 1994; Vol. II, pp 291–305.

126. Mallery, C. F.; Thynell, S. T. Further Improvements to FTIR Absorption Spectroscopy of Propellant Flames for Profiling of Species and Temperature. 32nd JANNAF Combustion Subcommittee Meeting, CPIA Publication No. 631, 1995; Vol. I; pp 449–460.

127. Teague, M. W.; Singh, G.; Vanderhoff, J. A. *Spectral Studies of Solid Propellant Combustion IV: Absorption and Burn Rate Results for M43, XM39, and M10 Propellants*; ARL-TR-180; U.S. Army Research Laboratory: Aberdeen Proving Ground, MD, August 1993.

128. Kubota, N. Physicochemical Processes of HMX Propellant Combustion. *Proc. Combust. Inst*. **1982**, 19, 777–785.

129. Smith, G. P.; Dubey, M. K.; Kinnison, D. E.; Connell, P. S. Assessing Effects of Rate Parameter Changes on Ozone Models Using Sensitivity Analysis. *J. Phys. Chem. A* **2001**, 105, 1449–1455.

130. Parr, T. P.; Hanson-Parr, D. M. Solid Propellant Flame Structure. *In Decomposition, Combustion and Detonation Chemistry of Energetic Materials*; Brill, T. B., Russell, T. P., Tao, W. C., Wadle, R. B., Eds. Materials Research Society Symposium Proceedings, Vol. 418, Materials Research Society: Pittsburgh, PA, 1996; pp 207–219.

131. Homan, B. E.; Miller, M. S.; Vanderhoff, J. A. Absorption Diagnostics and Modeling Investigations of RDX Flame Structure. *Combust. Flame* **2000**, 120, 301–317.

132. Fifer, R. A. Chemistry of Nitrate Ester and Nitramine Propellants. *In Fundamentals of Solid Propellant Combustion*; Kuo, K. K., Summerfield, M. Eds.; *Progress in Astronautics and Aeronautics*, Vol. 90, Summerfield, M., Series Ed.; American Institute of Aeronautics and Astronautics: New York, 1984; pp 177–237.

133. Melius, C. F. Thermochemical Modeling: II Application to Ignition and Combustion of Energetic Materials. In *Chemistry and Physics of Energetic Materials*; Bulusu, S., Ed., NATO ASI309, 51–78, 1990.

Appendix A. Thermochemical Data Used in the Mechanism

Table A-1 shows the species used in the chemical mechanism, their thermodynamics parameters, and sources of the thermodynamics data. The relevant data are the heat of formation, $\Delta H^{\circ}_{f,298}$; the entropy, S°_{298}; and the heat capacity function, $C^{\circ}_{P}(T)$. For simplicity in the table headers, we have abbreviated the nomenclature to HF(298), S(298), and, e.g., for $C^{\circ}_{P}(300K)$, CP300. It should be noted that in all cases, we actually use 14-parameter polynomial fits to the thermodynamics functions in our computer codes, as developed and popularized in the 1970s by B. J. McBride and coworkers of NASA (*1*). Two important points should be made. First, what is given in table A-1 is not the 14-parameter fits we used but rather the output of a simple code that provides easily understood thermodynamics values to which the fits correspond (we used the THERMLST submodule from the THERM code of Ritter and Bozzelli [*2*]). Thus the fitted thermodynamics functions rather than the originally fitted data are given. In some cases, e.g., N_2H_2, we obtained the raw thermodynamic functions S°_{298} and $C^{\circ}_{P}(T)$ as tabulated in a reference source and fitted the data and our choice for $\Delta H^{\circ}_{f,298}$ to the 14-parameter function ourselves. In those cases, the fitted polynomials will differ slightly from the source data. Thus the output in table A-1 may reflect minor fitting errors, differing slightly from the referenced source; one should therefore not be concerned about small differences. In some other cases, e.g., NH, the source cited actually contains the 14-parameter fits; we sometimes decided in cases where those were available to use the S°_{298} and $C^{\circ}_{P}(T)$ functions as defined by those fits but to change $\Delta H^{\circ}_{f,298}$ to a value of our choice. Then, we simply retained the exact coefficients of their fits except that the 6th and 13th were appropriately revised to reflect our new selection for $\Delta H^{\circ}_{f,298}$; those two parameters correspond to the two b_1 coefficients for the two temperature ranges of the fits, which set the enthalpy baseline. See, e.g., McBride et al. (*1*) for a detailed explanation of the coefficients. Second, note that in a few cases, no $C^{\circ}_{P}(T)$ values are given above 4000 K; the limit is even lower in a couple of cases, e.g., as low as 3000 K for CH_3O. The reason is that the $C^{\circ}_{P}(T)$ data fitted by the authors for those species was limited to lower T, and the THERMLST output reflects this. The point is that we watch whether our modeling includes T above the region fitted. Users of fits thus limited should be careful the T range of the application does not much exceed that indicated in the fits. If it does, one is then extrapolating the fits beyond the region to which they were constrained. Polynomial fits sometimes behave wildly outside the region constrained by fitting, which could cause serious error.

Modeling results can be much more sensitive to assumed thermodynamics parameters than many people realize; thus it is important that we have specified this part of the chemical mechanism. Entropy and heat capacity functions can usually be readily computed from spectroscopic data via statistical mechanics. It is unusual for accepted values of these functions to change much. Older

works sometimes have missed the significance of internal rotations for which the statistical mechanical expressions are more complicated than harmonic, or anharmonic, oscillator expressions that may have been improperly used, and revision for that factor can cause some modest change. Also, significant changes to these functions can occur when our knowledge regarding low-lying electronic structure is improved and taken into account, especially for species of only a few atoms. By comparison, though, accepted values of enthalpies have varied more considerably over time, especially for trace species because they can be hard to isolate, quantify, and study. Sensitivities to chosen enthalpies of formation can be very important, e.g., as discussed for HNO and HNC species in section 5 of this report. The reader will find upon scanning the notes to table A-1 that we have spent considerable effort on some species critically reviewing the literature to select the best current values. A few of these are highly sensitive for the present DZ model; perhaps most are not. A concise description of the sources and reasons for selection is given, however, in all cases.

Finally, in many of the cases where we critically selected the "best" enthalpy data, several results are considered equally valid. We frequently used an average of the selected data that is weighted to place the most emphasis on results of highest precision, i.e., having the smallest error limits—a so-called "weighted average." For convenience, we recount the relevant equations here, e.g., as presented in reference (*3*). The weighted average is defined as the following:

$$\bar{x} \equiv \sum_i a_i x_i \ , \tag{A-1}$$

where

$$a_i = (1/\sigma_i^2) / \sum_i (1/\sigma_i^2) \ , \tag{A-2}$$

x_i is the *i*th datum, and σ_i is the error limit (one standard deviation) of the *i*th datum. Unless otherwise stated, for the error limit of the weighted average we use its standard deviation, $\sigma(\bar{x})$, from statistics theory. $\sigma(\bar{x})$ is readily obtained via the variance as follows:

$$Var(\bar{x}) = \left[\sum_i (1/\sigma_i^2) \right]^{-1} \ , \tag{A-3}$$

whence

$$\sigma(\bar{x}) = \left[Var(\bar{x}) \right]^{1/2} \ . \tag{A-4}$$

Table A-1. Species thermochemical data. Heats of formation are in kcal/mol, entropy and heat capacities in cal/K-mol.[a] (Notes to table A-1 appear following the table.)

SPECIES	HF(298)	S(298)	CP300	CP400	CP500	CP600	CP800	CP1000	CP1500	Source
			CP2000	CP2500	CP3000	CP3500	CP4000	CP5000		
C	171.31	37.76	4.98	4.98	4.97	4.97	4.97	4.97	4.97	(4)
			5.01	5.08	5.17	5.26	5.34	5.46		
CH	142.01	43.72	6.95	7.00	7.05	7.11	7.37	7.78	8.75	(4)
			9.36	9.72	9.90	9.98	10.02	10.14		
CHOCHO	-50.66	66.89	14.64	17.31	19.50	21.29	23.91	25.63	27.92	b
			29.05	29.68	29.99	30.15	30.27	30.50		
CH2	92.49	46.72	8.25	8.55	8.88	9.23	9.93	10.57	11.74	(4)
			12.54	13.00	13.22	13.35	13.58			
CH2(S)	101.51	45.10	8.07	8.30	8.60	8.98	9.85	10.61	11.83	(4)
			12.64	13.09	13.28	13.39	13.64			
CH2CO	-12.40	57.79	12.43	14.17	15.67	16.91	18.79	20.24	22.44	(4)
			23.78	24.52	24.89	25.07	25.18	25.54		
CH2O	-25.95	52.28	8.47	9.36	10.44	11.52	13.37	14.82	17.01	(11)
			18.10	18.66	19.02	19.22				
CH2OH	-4.10	58.88	11.32	12.94	14.38	15.62	17.54	18.79	20.95	(4)
			22.40	23.23	23.60	23.82	24.27			
CH3	34.82	46.38	9.23	10.09	10.83	11.52	12.87	14.12	16.27	(4)
			17.55	18.29	18.71	18.98	19.19	19.40		
CH3O	3.90	54.61	9.08	10.79	12.43	13.98	16.63	18.60	21.51	(4)
			23.26	24.21	24.67					
CH3OH	-48.06	57.28	10.51	12.40	14.25	16.01	19.07	21.40	25.02	(4)
			27.25	28.51	29.16	29.47	29.67	30.27		
CH4	-17.90	44.47	8.43	9.84	11.14	12.41	15.00	17.25	20.63	(4)
			22.58	23.65	24.23	24.60	24.90	25.17		
CN	104.01	48.41	6.97	7.03	7.15	7.32	7.71	8.02	8.49	(4)
			9.01	9.54	10.03	10.45	10.76	10.99		
CO	-26.42	47.21	6.95	7.03	7.14	7.27	7.61	7.95	8.41	(4)
			8.67	8.81	8.89	8.96	9.01	9.09		
CO2	-94.06	51.08	8.91	9.86	10.65	11.31	12.32	12.99	13.93	(4)
			14.44	14.71	14.86	14.99	15.12	15.28		
C2H	135.01	49.56	8.90	9.63	10.22	10.72	11.54	12.18	13.31	(4)
			14.12	14.77	15.31	15.75	15.99			
C2H2	54.20	48.02	10.62	11.99	13.08	13.95	15.27	16.31	18.27	(4)
			19.52	20.30	20.82	21.21	21.55	22.05		
C2H3	68.42	55.33	9.57	11.19	12.78	14.31	16.98	18.75	21.26	(4)
			23.07	24.19	24.74	24.89	24.88	25.74		
C2H4	12.54	52.38	10.23	12.79	14.94	16.83	20.05	22.51	26.22	(4)
			28.33	29.46	30.07	30.46	30.79	31.07		
C2H5	28.02	60.14	11.32	13.60	15.95	18.29	22.58	25.50	29.56	(4)
			32.45	34.24	35.09	35.30	35.27	36.66		
C2H6	-20.04	54.73	12.58	15.69	18.62	21.30	25.82	29.30	34.61	(4)
			37.92	39.83	40.88	41.48	41.93			
C2N2	73.88	57.73	13.63	14.71	15.59	16.32	17.45	18.24	19.41	(4)
			20.02	20.31	20.44	20.54	20.63	20.67		
H	52.10	27.39	4.97	4.97	4.97	4.97	4.97	4.97	4.97	(4)
			4.97	4.97	4.97	4.97	4.97	4.97		
HCCO	42.45	60.74	12.65	13.47	14.23	14.92	16.07	16.83	17.98	(4)
			18.74	19.14	19.30	19.39	19.64			
HCCOH	20.43	58.71	13.22	14.78	16.16	17.35	19.15	20.30	22.29	(4)
			23.62	24.37	24.71	24.90	25.32			

SPECIES	HF(298)	S(298)	CP300	CP400	CP500	CP600	CP800	CP1000	CP1500	Source
			CP2000	CP2500	CP3000	CP3500	CP4000	CP5000		
HCN	31.89	48.24	8.59	9.36	9.97	10.48	11.31	12.01	13.20	c
			13.94	14.38	14.64	14.79	14.91	15.11		
HCNO	38.43	53.80	11.63	13.05	14.25	15.22	16.56	17.33	18.68	(4)
			19.56	20.03	20.21	20.31	20.61			
HCO	10.04	53.62	8.27	8.72	9.24	9.78	10.74	11.49	12.54	(1)
			13.16	13.49	13.67	13.78	13.89	14.13		
HNC	45.20	49.20	8.60	9.32	9.94	10.47	11.34	12.02	13.18	(14)
			13.82	14.19	14.39	14.50	14.57	14.71		
HNCO	-28.22	56.94	10.79	12.11	13.14	13.97	15.20	16.14	17.59	c
			18.45	18.93	19.18	19.32	19.42	19.62		
HNNO	55.39	60.56	10.73	12.13	13.29	14.25	15.72	16.72	18.14	(6)
			18.83	19.21	19.40	19.49	19.56	19.70		
HNO	25.60	52.80	8.10	8.48	8.98	9.54	10.56	11.40	13.28	(15)
			14.69	15.65	16.19	16.38	16.29	15.72		
HOCN	-3.53	59.26	10.56	11.45	12.27	13.02	14.26	15.19	16.55	(4),d
			17.39	17.89	18.14	18.29	18.51			
HOCO	-46.29	60.12	10.78	12.19	13.34	14.29	15.67	16.57	17.70	(4)
			18.16	18.43	18.56	18.62	18.72			
HONO	-18.34	59.59	10.88	12.27	13.39	14.31	15.67	16.56	17.89	(4)
			18.64	19.03	19.25	19.39	19.51	19.60		
HO2	3.30	54.76	8.35	8.89	9.46	9.99	10.77	11.38	12.48	e
			13.33	13.95	14.38	14.66	14.80	14.83		
H2	.00	31.21	6.90	6.96	7.00	7.02	7.07	7.21	7.73	(4)
			8.18	8.56	8.87	9.13	9.35	9.77		
H2CN	59.11	53.60	9.16	10.32	11.42	12.47	14.24	15.42	17.13	(4)
			18.25	18.84	19.07	19.19	19.55			
H2O	-57.80	45.10	8.00	8.23	8.44	8.67	9.22	9.87	11.26	(4)
			12.22	12.88	13.33	13.64	13.87	14.20		
H2O2	-32.53	55.66	10.41	11.44	12.34	13.11	14.29	15.21	16.85	(4)
			17.88	18.49	18.86	19.09	19.26	19.47		
N	112.96	36.61	4.97	4.97	4.97	4.97	4.97	4.97	4.97	(4)
			4.97	4.98	5.01	5.09	5.21	5.61		
NCN	107.60	54.77	10.58	11.50	12.22	12.78	13.52	13.96	14.45	(4)
			14.64	14.74	14.79	14.81	14.85			
NCNO	78.09	63.84	12.93	13.89	14.77	15.56	16.82	17.56	18.53	(24)
			19.14	19.43	19.51	19.55	19.77			
NCO	31.30	55.51	9.59	10.49	11.23	11.84	12.75	13.35	14.08	f
			14.46	14.64	14.71	14.73	14.76	14.89		
NH	85.50	43.31	6.98	6.98	7.00	7.05	7.22	7.47	8.07	g
			8.51	8.87	9.18	9.47	9.76	10.27		
NH2	45.20	46.60	8.09	8.31	8.60	8.93	9.64	10.36	11.81	(1,26)
			12.84	13.57	14.11	14.51	14.83	15.31		
NH3	-10.97	46.04	8.48	9.33	10.08	10.80	12.21	13.53	15.90	(4)
			17.40	18.32	18.86	19.16	19.33	19.31		
NNH	58.57	53.63	8.32	8.83	9.36	9.88	10.85	11.52	12.44	(4)
			13.04	13.36	13.48	13.55	13.74			
NO	21.81	50.37	7.14	7.16	7.29	7.46	7.83	8.12	8.54	(1)h
			8.78	8.91	8.98	9.03	9.08	9.24		
NO2	7.91	57.34	8.83	9.64	10.33	10.93	11.89	12.49	13.17	(4)
			13.51	13.65	13.71	13.75	13.80	13.81		
NO3	17.00	60.37	11.31	13.32	14.90	16.10	17.59	18.27	19.10	(4)
			19.48	19.62	19.66	19.70	19.77	19.76		

SPECIES	HF(298)	S(298)	CP300	CP400	CP500	CP600	CP800	CP1000	CP1500	Source
			CP2000	CP2500	CP3000	CP3500	CP4000	CP5000		
N2	.00	45.77	6.95	7.01	7.08	7.19	7.50	7.83	8.32	(4)
			8.60	8.76	8.85	8.91	8.97	9.05		
N2H2	45.70	52.18	8.41	9.26	10.32	11.43	13.44	15.08	18.24	i
			20.08	21.04	21.43	21.53	21.51	21.49		
N2H3	52.80	54.63	10.50	12.29	13.84	15.18	17.35	18.98	21.51	j
			22.81	23.53	23.90	24.09	24.23	24.49		
N2H4	22.79	57.03	12.20	14.76	16.83	18.52	21.12	23.04	26.33	(4)
			28.28	29.38	30.02	30.43	30.75	31.06		
N2O	19.61	52.55	9.27	10.18	10.94	11.56	12.51	13.12	13.94	(4)
			14.36	14.54	14.63	14.69	14.75	14.78		
O	59.56	38.47	5.23	5.14	5.08	5.05	5.02	5.00	4.98	(4)
			4.98	4.98	5.01	5.04	5.09	5.21		
OH	8.89	43.88	7.15	7.10	7.07	7.06	7.13	7.33	7.87	k
			8.28	8.57	8.78	8.94	9.05	9.26		
O2	.00	49.01	7.01	7.22	7.44	7.65	8.07	8.35	8.72	(4)
			9.03	9.29	9.52	9.72	9.90	10.19		

Notes to Table A-1

a. The file containing the 14-parameter polynomial fits used to create this table is available upon request.

b. $\Delta H^{O}_{f,298}$ was determined using the glyoxal heat of combustion obtained from Fletcher and Pilcher (*4*) and heats of formation of the combustion products from Kee et al. (*5*); note Fletcher and Pilcher referenced the heat of combustion to $H_2O_{(l)}$ product. The resulting $\Delta H^{O}_{f,298}$ is in excellent agreement with the quantum estimate of Melius, –50.4 kcal/mol (*6*). S^{O}_{298} and $C_P^{O}(T)$ were determined by standard statistical mechanical calculations. The calculations took into account that the lowest vibrational mode is a hindered internal rotation about the C-C bond. Rotational moments of inertia were obtained from Birss et al. (*7*), while vibrational frequencies were taken from Pebay Peyroula and Jost (*8*) and Cole and Osborne (*9*). Those data and assignments also agree well with quantum estimates of Melius (*6*). For the hindered rotation, key potential energy features (barrier height and cis-trans splitting) were obtained from Durig et al. (*10*).

c. $\Delta H^{O}_{f,298}$ from East and Allen (*12*), in concurrence with the recommendation in Glarborg and Miller (*13*). S^{O}_{298} and $C_P^{O}(T)$ from McBride et al. (*1*).

d. The data of Fletcher and Pilcher (*4*) were used without revision. $\Delta H^{O}_{f,298}$ from that source is within 0.02 kcal/mol of East and Allen (*12*), a negligible difference. As with HCN and HNCO, we concur with the recommendation of Glarborg and Miller (*13*) that East and Allen are the best source for that datum.

e. S^{O}_{298} and $C_P^{O}(T)$ from McBride et al. (*1*). $\Delta H^{O}_{f,298}$ = 3.3 ± 0.4 kcal/mol is the weighted average from experimental results selected in a critical review (Anderson, unpublished, 2000). The present DZ modeling is not sensitive to this datum, nor are most solid propellant studies, because fuel rich, high-temperature conditions prevail and [HO_2] is then typically negligible. However, the result is significantly larger than most previous recommendations. Our selected values were 3.3 ± 0.8 kcal/mol from Litorja and Ruscic (*16*); 3.2 ± 0.8 from Hills and Howard (*17*) (result corrected by +0.16 kcal/mol due to a revision of the ancillary $\Delta H^{O}_{f,298}$ [ClO] per Gurvich et al. [*18*], and error limit increased because ×3 precision in the measured K_{eq} is judged to be more reasonable for combined error limits derived from forward and reverse rates of the key reaction ClO + OH = HO_2 + Cl than that claimed in Hills and Howard [*17*]; cf. recommended error limits in DeMore et al.[*19*] with which we concur); 3.5 + 1/–0.5 kcal/mol (±0.8 kcal/mol was used in the weighted average) from the review of results prior to 1983, Shum and Benson (*20*); and 3.2 ± 1.2 kcal/mol from

Fisher and Armentrout (*21*) (as corrected in Litorja and Ruscic for updates to ancillary thermal data). Note that we have revised $\Delta H^{O}_{f,298}$(OH) downward vs. most recommendations (see later in the table). That revision occurred considerably after our review on HO_2. Until the preparation of this manuscript, it was overlooked that the OH revision would also affect the interpretation of Hills and Howard results. Our recommended $\Delta H^{O}_{f,298}$(OH), 8.89 kcal/mol, is 0.43 kcal/mol lower than the value used by Hills and Howard. Thus, their result for $\Delta H^{O}_{f,298}(HO_2)$ must be further corrected, and we now obtain 2.7 ± 0.8 kcal/mol. With this newly revised result, the weighted average of selected values becomes 3.2 ± 0.4 kcal/mol. We recommend usage of this newer, slightly smaller, result and will be changing to it in future work. The results of two high-level theoretical calculations, 2.8 ± 0.5 kcal/mol, Bauschlicher and Partridge (*22*), and "between 2.70 and 2.90 kcal/mol," Karkach and Osherov (*23*), agree well with our recommended value.

f. S^{O}_{298} and $C^{O}_{P}(T)$ from McBride et al. (*1*). $\Delta H^{O}_{f,298}$ = 31.3±0.5 kcal/mol from a weighted average of the results 31.5±0.5 kcal/mol, East and Allen (*12*), and 30.5±1 kcal/mol, Cyr et al. (*25*).

g. S^{O}_{298} and $C^{O}_{P}(T)$ from McBride et al. (*1*). $\Delta H^{O}_{f,298}$ (NH) was reviewed in Anderson (*26*), resulting in a recommendation of 85.4 ± 0.3 kcal/mol. This recommendation was based primarily on critically selected results, 85.2 ± 0.4 and 85.8± 0.6 kcal/mol, from Gibson et al. (*27*) and Ervin and Armentrout (*28*), respectively. Since that time, we have performed two further updates (Anderson, unpublished, 1990, 2000), yielding only very slightly revised results but noting new supporting studies. Shortly after Anderson (*26*) was published, we became aware that Marquette et al. (*29*) had concurrently reported on ion-molecule reaction experiments similar to those in Ervin and Armentrout, with the result 85.3 ± 0.3 kcal/mol. Including this value in the weighted average of the then three best results, we obtained 85.3 ± 0.2 kcal/mol, which we used and recommended privately for about a decade. In 2000, we performed a further update review. References *27–29* first involve measures of $\Delta H^{O}_{f,298}$(NH^+), and, thus, IP(NH) is very important in determining $\Delta H^{O}_{f,298}$(NH). The $\Delta H^{O}_{f,298}$ values given previously were based on IP(NH) = 13.49 ± 0.01 eV from Dunlavey et al. (*30*). A more precise determination has since appeared, 13.476 ± 0.002 eV, from de Beer et al. (*31*). The above $\Delta H^{O}_{f,298}$(NH) results are therefore revised upward by the difference, 0.32 kcal/mol, to 85.5 ± 0 .3, 86.0 ± 0.6, and 85.7 ± 0.1 kcal/mol, for refs *27–29*, respectively (the revisions in two of the three cases appear to not exactly equal 0.32 kcal/mol due to round-off). Upper limits to $\Delta H^{O}_{f,298}$ (NH) also became available from experiments on the reactions $N^+ + H_2 = NH^+ + H$ and $N^+ + D_2 = ND^+ + D$ by Tosi and coworkers (*32*, *33*). The latter reaction yielded $\Delta H^{O}_{f,298}(NH) \leq 85.30 \pm 0.14$; following similar algebraic manipulations, we

derive $\Delta H^{\circ}_{f,298}$ (NH) ≤85.54 ± 0.11 kcal/mol from data they presented on the former reaction. There is some controversy between Ervin and Armentrout (*28*) and Marquette et al. (*29*) vs. Tosi et al. (*32*, *33*) regarding whether there is a slight barrier of a few tenths kcal/mol for these ion-molecule reactions, the latter suggesting that there is and thus accounting for the fact those authors only provided upper limit results; however, it appears most likely to us that there is not. Thus we recommend using a weighted average of these five best results, 85.5 kcal/mol. However, it is unsettling that there remains some unresolved controversy regarding the possibility of a barrier, and that the lower of the two results from Tosi does not quite agree within error limits with the revised Marquette result. Because of their comparatively small error limits, the result from Marquette and the two from Tosi have the primary influence on the weighted average. For these reasons, we recommend using a conservative error limit, 0.2 kcal/mol, which is about a factor of 3 larger than that resulting from the weighted averaging procedure. Several new theoretical results for $\Delta H^{\circ}_{f,298}$ (NH) have also appeared (*33–40*). These are, in general, about 0.5–1.0 kcal/mol larger than the recommended value. This is within typical limits of theoretical accuracy, and an error of 1.0 kcal/mol in such a trace species would not adversely affect modeling applications in any but the most sensitive of situations. But it is noteworthy, and perhaps reason for further study, that most of these high-level theoretical results are somewhat larger than those from the best experiments.

h. See Anderson (*15*) for a detailed discussion.

i. $\Delta H^{\circ}_{f,0}$ from Ruscic and Berkowitz (*41*). Correction to 298 K identical per Gurvich et al. (*18*) and Chase et al. (*42*). The selected value is strongly supported by the quantum result of Pople and Curtiss (*43*). S°_{298} and $C^{\circ}_{P}(T)$ from Gurvich et al. (*18*).

j. $\Delta H^{\circ}_{f,0}$ from Ruscic and Berkowitz (*41*). Correction to 298 K was performed using $H–H_0(298\ K)$ = 2.63 kcal/mol from the quantum estimate of Armstrong et al. (*44*), and the similar functions for the elements from Chase et al. (*42*). The result is in reasonable agreement with the quantum result of Armstrong et al. S°_{298} and $C^{\circ}_{P}(T)$ from Dean and Bozzelli (*45*).

k. $\Delta H^{\circ}_{f,298}$ = 8.89 ± 0.09 kcal/mol from Ruscic (*46*). S°_{298} and $C^{\circ}_{P}(T)$ from McBride et al. (*1*).

References

1. McBride, B. J.; Gordon, S.; Reno, M. A. *Coefficients for Calculating Thermodynamic and Transport Properties of Individual Species*; NASA-TM-4513; NASA Glenn Research Center: Sandusky, OH, October 1993.

2. Ritter, E. R.; Bozzelli, J. W. THERM – Thermodynamic Property Estimation for Gas-Phase Radicals and Molecules. *Int. J. Chem. Kinetics* **1991**, *23*, pp. 767–778.

3. Meyer, S. L. *Data Analysis for Scientists and Engineers*. John Wiley: New York, 1975; p 146.

4. Fletcher, R. A.; Pilcher, G. Measurements of Heats of Combustion by Flame Calorimetry. *Trans. Faraday Soc.* **1970**, *66*, 794–799.

5. Kee, R. J.; Rupley, F. M.; Miller, J. A. *The Chemkin Thermodynamic Database*; SAND87-8215; Sandia National Laboratories: Livermore, CA, April 1987.

6. Melius, C. F. Thermochemical Modeling: II. Application to Ignition and Combustion of Energetic Materials. In *Chemistry and Physics of Energetic Materials*, NATO ASI-309, Bulusu, S., Ed.; Kluwer Academic Publishers: Norwell, MA, 1990; pp 51–78.

7. Birss, F. W.; Brown, J. M.; Cloe, A. R. H.; Lofthus, A.; Krishnam, S. L.; Osborne, G. A.; Paldus, J.; Ramsay, D. A.; Watmann, L. 4550 A Band System of Glyoxal. 2. Vibration-Rotational Analyses for 12 Bands of $C_2H_2O_2$. *Can. J. Phys.* **1970**, *48*, 1230–1241.

8. Pebay Peyroula, E.; Jost, R. $S_1 \leftarrow S_0$ Laser Excitation Spectra of Glyoxal in a Supersonic Jet: Vibrational Analysis. *J. Molec. Spectrosc.* **1987**, *121*, 177–188.

9. Cole A. R. H.; Osborne, G. A. Vibrational Spectra of Glyoxal, Monodeuteroglyoxal, and Dideuteroglyoxal. *Spectrochim. Acta* **1971**, *27A*, 2461–2490.

10. Durig, J. R.; Tong, C. C.; Li, Y. S. Microwave Spectrum of cis-Glyoxal. *J. Chem. Phys.* **1972**, *57*, 4425–4427.

11. Bowman, C. T.; Hanson, R. K.; Davidson, D. F.; Gardiner, W. C., Jr.; Lissianski, V.; Smith, G. P.; Golden, D. M.; Frenklach, M.; Goldenberg, M. GRI-Mech, version 2.11 (see also http://www.me.berkeley.edu/gri_mech/).

12. East, A. L. L.; Allen, W. D. The Heat of Formation of NCO. *J. Chem. Phys.* **1993**, *99*, 4638–4650.

13. Glarborg, P.; Miller, J. A. Mechanism and Modeling of Hydrogen Cyanide Oxidation in a Flow Reactor. *Combust. Flame* **1994**, *99*, 475–483.

14. Lin, M. C. Emory University, Atlanta, GA. Private communication regarding the quantum calculations of C. F. Melius, as in ref *6*, 1992.

15. Anderson, W. R. Heats of Formation of HNO and Some Related Species. *Combust. Flame* **1999**, *117*, 394–403.

16. Litorja, M.; Ruscic, B. A Photoionization Study of the Hydroperoxyl Radical, HO_2, and Hydrogen Peroxide, H_2O_2. *J. Electron Spectrosc.* **1998**, *97*, 131–146.

17. Hills, A. J.; Howard, C. J. Rate Coefficient Temperature Dependence and Branching Ratio for the OH + ClO Reaction. *J. Chem. Phys.* **1984**, *81*, 4458–4465.

18. Gurvich, L. V.; Veyts, I. V.; Medvedev, V. A.; Khachkuruzov, G. A.; Yungman, V. S.; Bergman, G. A.; Iorish, V. S.; Yurov, G. N.; Gorbov, S. I.; Kuratova, L. F.; Trishcheva, N. P.; Przheval'skiy, I. N.; Leonidov, V. Y.; Ezhov, Y. S.; Tomberg, S. E.; Nazarenko, I. I.; Rogatskiy, A. L.; Dorofeyeva, O. V.; Demidova, M. S. *Thermodynamic Properties of Individual Substances*, 4th ed.; Hemisphere: New York, 1989; Vol. 1, Parts 1 and 2.

19. DeMore, W. B.; Golden, D. M.; Hampson, R. F.; Howard, C. J.; Kurylo, M. J.; Molina, M. J.; Ravishankara, A. R.; Sander, S. P. *Chemical Kinetics and Photochemical Data for Use in Stratospheric Modeling*, Evaluation Number 8; JPL Publication 87–41; NASA Jet Propulsion Laboratory: Pasadena, CA, September 1987.

20. Shum, L. G. S.; Benson, S. W. Review of the Heat of Formation of the Hydroperoxyl Radical. *J. Phys. Chem.* **1983**, *87*, 3479–3482.

21. Fisher, E. R.; Armentrout, P. B. Heat of Formation of HO_2. A Direct Determination From Guided Ion Beam Studies of $O_2^+(^2\Pi_g, v=0) + CH_4$. *J. Phys. Chem.* **1990**, *94*, 4396–4398.

22. Bauschlicher, C. W., Jr.; Partridge, H. An Accurate Determination of the HO_2 Heat of Formation. *Chem. Phys. Lett.* **1993**, *208*, 241–246.

23. Karkach, S. P.; Osherov, V. I. Ab Initio Analysis of the Transition States on the Lowest Triplet H_2O_2 Potential Surface. *J. Chem. Phys.* **1999**, *110*, 11918–11927.

24. Prasad, K. R.; Yetter, A.; Smooke, M. D. An Eigenvalue Method for Computing the Burning Rates of RDX Propellants. *Combust. Sci. Tech.* **1997**, *124*, 35–82.

25. Cyr, D. R.; Continetti, R. E.; Metz, R. B.; Osborn, D. L.; Neumark, D. M. Fast Beam Studies of NCO Free Radical Photodissociation. *J. Chem. Phys.* **1992**, *97*, 4937–4947.

26. Anderson, W. R. Oscillator Strengths of NH_2 and the Heats of Formation of NH and NH_2. *J. Phys. Chem.* **1989**, *93*, 530–536.

27. Gibson, S. T.; Greene, J. P.; Berkowitz, J. Photoionization of the Amidogen Radical. *J. Chem. Phys.* **1985**, *83*, 4319–4328.

28. Ervin, K. M.; Armentrout, P. B. Energy Dependence, Kinetic Isotope Effects, and Thermochemistry of the Nearly Thermoneutral Reactions $N^+(^3P) + H_2$ (HD, D_2) → NH^+ (ND^+) + H (D). *J. Chem. Phys.* **1987**, *86*, 2659–2673.

29. Marquette, J. B.; Rebrion, C.; Rowe, B. R. Reactions of $N^+(^3P)$ ions with Normal, Para, and Deuterated Hydrogens at Low Temperatures. *J. Chem. Phys.* **1988**, *89*, 2041–2047.

30. Dunlavey, S. J.; Dyke, J. M.; Jonathan, N.; Morris, A. Vacuum Ultraviolet Photoelectron-Spectroscopy of Transient Species. 11. $NH_2(X^2B_1)$ Radical. *Mol. Phys.* **1980**, *39*, 1121–1135.

31. de Beer, E.; Born, M.; de Lange, C. A.; Westwood, N. P. C. A Rotationally Resolved REMPI-PES Study of the NH Radical. *Chem. Phys. Lett.* **1991**, *186*, 40–46.

32. Tosi, P.; Dmitriev, O.; Bassi, D.; Wick, O.; Gerlich, D. Experimental Observation of the Energy Threshold in the Ion-Molecule Reaction $N^+ + D_2 \rightarrow ND^+ + D$. *J. Chem. Phys.* **1994**, *100*, 4300–4307.

33. Tarroni, R.; Palmieri, P.; Mitrushenkov, A.; Tosi, P.; Bassi, D. Dissociation Energies and Heats of Formation of NH and NH^+. *J. Chem. Phys.* **1997**, *106*, 10265–10272.

34. Pople, J. A.; Curtiss, L. A. Theoretical Thermochemistry. 2. Ionization Energies and Proton Affinities of AH_n Species (A = C to F and Si to Cl); Heats of Formation of Their Cations. *J. Phys. Chem.* **1987**, *91*, 155–162.

35. Martin, J. M. L.; François, J. P.; Gijbels, R. Accurate Ab Initio Predictions of the Dissociation Energy and Heat of Formation of First-Row Hydrides. *Chem. Phys. Lett.* **1989**, *163*, 387–391.

36. Peterson, K. A.; Kendall, R. A.; Dunning, T. H., Jr. Benchmark Calculations With Correlated Molecular Wave Functions. II. Configuration Interaction Calculations on First Row Diatomic Hydrides. *J. Chem. Phys.* **1993**, *99*, 1930–1944.

37. Espinosa-Garćia, J.; Corchado, J. C.; Fernández, J.; Marquez, A. Theoretical Values of the Enthalpies of Formation of the NH_x (x = 1,2,3) Compounds. Importance of the Core-Correlation Effects. *Chem. Phys. Lett.* **1995**, *233*, 220–226.

38. Nicolaides, A.; Rauk, A.; Glukhovtsev, M. N.; Radom, L. Heats of Formation from G2, G2(MP2), and G2(MP2,SVP) Total Energies. *J. Phys. Chem.* **1996**, *100*, 17460–17464.

39. Luchow, A.; Anderson, J. B. First-Row Hydrides: Dissociation and Ground State Energies Using Quantum Monte Carlo. *J. Chem. Phys.* **1996**, *105*, 7573–7578.

40. Jursic, B. S. Computational Studies of Bond Dissociation Energies, Ionization Potentials, and Heats of Formation for NH and NH+. Are Hybrid Density Functional Theory Methods as Accurate as Quadratic Complete Basis Set and Gaussian-2 Ab Initio Methods? *Theoretical Chemistry Accounts* **1998**, *99*, 171–174.

41. Ruscic, B.; Berkowitz, J. Photoionization Mass-Spectrometric Study of N_2H_2 and N_2H_3: N-H, N=N Bond Energies and Proton Affinity of N_2. *J. Chem. Phys.* **1991**, *95*, 4378–4384.

42. Chase, M. W., Jr.; Davies, C. A.; Downey, J. R., Jr.; Frurip, D. J.; McDonald, R. A.; Syverud, A. N. JANAF Thermochemical Tables, 3rd Ed. *J. Phys. Chem. Ref. Data* **1985**, *14*, Suppl. 1.

43. Pople, J. A.; Curtiss, L. A. The Energy of N_2H_2 and Related Compounds. *J. Chem. Phys.* **1991**, *95*, 4385–4388.

44. Armstrong, D. A.; Yu, D.; Rauk, A. Gas Phase and Aqueous Thermochemistry of Hydrazine and Related Radicals and the Energy Profiles of Reactions with H^- and OH: An Ab Initio Study. *J. Phys. Chem. A* **1997**, *101*, 4761–4769.

45. Dean, A. M.; Bozzelli, J. W. Combustion Chemistry of Nitrogen. In *Gas-Phase Combustion Chemistry*; Gardiner, W. C., Jr., Ed.; Springer: New York, 2000; Chapter 2.

46. Ruscic, B.; Feller, D.; Dixon, D. A.; Peterson, K. A.; Harding, L. B.; Asher, R. L.; Wagner, A. F. Evidence for a Lower Enthalpy of Formation of Hydroxyl Radical and a Lower Gas Phase Bond Dissociation Energy of Water. *J. Phys. Chem. A* **2001**, *105*, 1–4.

Appendix B. Documentation of Elementary Gas Phase Reaction Mechanism and Sources

The elementary reactions and kinetics parameters used are given in table B-1. The rate constants for the simplest reactions, wherein only three parameters are specified, are determined as follows:

$$k_i = AT^n \exp(-E_a / RT) \cdot \tag{B-1}$$

The symbol M appearing in a particular reaction, which one might think indicates some particular species, instead indicates participation of a generalized nonreactive collider (candidates being all species present). Catalytic efficiencies, η_i, of the various species as colliders for a given reaction are assumed to be 1.0 except where specified "enhanced by. ..." The effective concentration of colliders is then given by the following:

$$C_M = [P / RT] \sum_i X_i \eta_i \ , \tag{B-2}$$

where the X_i represent the species mole fractions.

Reactions containing the string "(+ M)" have rate constants that are pressure dependent, with more complicated expressions. These are calculated as follows:

$$k_i = F k_\infty k_0 C_M / (k_\infty + k_0 C_M) \ . \tag{B-3}$$

F is the so-called "broadening factor" specified according to the fitting approach (and level of theory) used for the individual reaction (explained just below). Here, k_∞ is the high pressure limit, and k_0 the low pressure limit, rate constants. These are specified via the usual three parameter rate constant expression, as in equation B-1. In these cases, the three parameters on the first line for the reaction specify k_∞, and those after the string "low-pressure limit" on the second line specify k_0. In the case of a simple Lindemann type falloff expression, there is no string of parameters on a line between k_0 and enhancement factors (if the latter are used); see, e.g., R2. In those cases, $F = 1$. Two other types of falloff expressions were used, namely the Tsang and Herron (*1*) and Troe types (*2*). The former are identified as such in the third line for the former type reaction by the string "T&H," see, e.g., R1, and for the latter type by "TROE," see, e.g., R222. For T&H reactions, F is specified as follows:

$$\log_{10} F = \log_{10} F_C / \{1 + [\log_{10}(k_0 C_M / k_\infty)]^2\} \quad , \tag{B-4}$$

where $F_c = a_0 + a_1 T + a_2 T^2$, and the polynomial a_i parameters are given, in order, after the T&H string; the second and/or third terms are omitted if their higher level constants are not indicated. For the TROE type expressions, F is specified as follows:

$$\log_{10} F = \{1 + [\frac{L_{\mathrm{Pr}} + c}{n - d(L_{\mathrm{Pr}} + c)}]^2\}^{-1} \log_{10} F_C \ . \tag{B-5}$$

where

$$L_{\mathrm{Pr}} = \log_{10}(k_0 M / k_\infty) \ , \tag{B-6}$$

$$c = -0.4 - 0.67 \log_{10} F_C \ , \tag{B-7}$$

$$n = 0.75 - 1.27 \log_{10} F_C \ , \tag{B-8}$$

and

$$d = 0.14 \ . \tag{B-9}$$

In the Troe formalism, F_C is as follows:

$$F_C = (1 - a) \exp(-T / T^{***}) + a \exp(-T / T^{*}) + \exp(-T^{**} / T) \ . \tag{B-10}$$

The four parameters a, T^{***}, T^{*}, and T^{**} are specified in the table, in that order, after the string "TROE;" note that the fourth parameter, and its associated term, is often not used.

Finally, note that in some cases, e.g., R121 and R122, the string "Declared duplicate reaction" appears after two (or more) entries of seemingly identical reactions. Any number of reasons can lead to a purposeful entry of a reaction more than once, and we will not further discuss reasons here. It suffices to say, whether the reaction indeed occurs by more than one geometric pathway (from which one could argue the paths actually represent different reactions), or usage of the functional form is done merely for the sake of fitting convenience, we number the instances and count them as separate reactions in the list. The overall rate constant is then treated as the sum of the two (or more) individual rate constant expressions.

For each reaction, A is specified in mol-cm-s-K units as appropriate for the individual reaction's order, n is dimensionless, and E_a is in cal/mol.

Table B-1. Reactions and their kinetics parameters used in the mechanism. (Notes to table B-1 appear at the end of table.)

No.	REACTION	A	n	E_a	Source[a]
R 1.	NO2(+M)=NO+O(+M)	7.600E+18	-1.27	73290.0	b
	Low pressure limit: 0.24700E+29 -0.33700E+01 0.74800E+05				
	T&H VALUES 0.95000E+00 -0.10000E-03				
	N2O Enhanced by 1.500E+00				
	H2O Enhanced by 4.400E+00				
	N2 Enhanced by 1.000E+00				
	CO2 Enhanced by 2.300E+00				
R 2.	N2O(+M)=N2+O(+M)	1.260E+12	0.00	62620.0	c
	Low pressure limit: 0.59700E+15 0.00000E+00 0.56640E+05				
	N2O Enhanced by 5.000E+00				
	H2O Enhanced by 7.500E+00				
	N2 Enhanced by 1.000E+00				
	CO2 Enhanced by 3.200E+00				
	O2 Enhanced by 8.200E-01				
R 3.	H+NO(+M)=HNO(+M)	1.520E+15	-0.41	0.0	d
	Low pressure limit: 0.40000E+21 -0.17500E+01 0.00000E+00				
	N2O Enhanced by 5.000E+00				
	H2O Enhanced by 5.000E+00				
	N2 Enhanced by 1.000E+00				
R 4.	NO+OH(+M)=HONO(+M)	1.988E+12	-0.05	-721.0	e
	Low pressure limit: 0.50800E+24 -0.25100E+01 -0.67600E+02				
	T&H VALUE 0.62000E+00				
	N2O Enhanced by 5.000E+00				
	H2O Enhanced by 8.300E+00				
	N2 Enhanced by 1.000E+00				
	CO2 Enhanced by 1.500E+00				
R 5.	HCN(+M)=H+CN(+M)	8.300E+17	-0.93	123800.0	f
	Low pressure limit: 0.35700E+27 -0.26000E+01 0.12490E+06				
	T&H VALUES 0.95000E+00 -0.10000E-03				
	N2O Enhanced by 5.000E+00				
	H2O Enhanced by 5.000E+00				
	N2 Enhanced by 1.000E+00				
	CO2 Enhanced by 1.600E+00				
R 6.	CN+CN(+M)=C2N2(+M)	5.660E+12	0.00	0.0	g
	Low pressure limit: 0.34300E+26 -0.26100E+01 0.00000E+00				
	T&H VALUE 0.50000E+00				
	N2O Enhanced by 5.000E+00				
	H2O Enhanced by 5.000E+00				
	N2 Enhanced by 1.000E+00				
	CO2 Enhanced by 1.600E+00				
R 7.	HNCO(+M)=NH+CO(+M)	6.000E+13	0.00	99800.0	g
	Low pressure limit: 0.21700E+29 -0.31000E+01 0.10190E+06				
	T&H VALUES 0.90000E+00 -0.20000E-03				
	N2O Enhanced by 5.000E+00				
	H2O Enhanced by 5.000E+00				
	N2 Enhanced by 1.000E+00				
	CO2 Enhanced by 1.600E+00				
R 8.	HCN+H(+M)=H2CN(+M)	3.310E+13	0.00	4844.0	f
	Low pressure limit: 0.16000E+25 -0.27300E+01 0.76600E+04				
	T&H VALUES 0.95000E+00 -0.10000E-03				
	N2O Enhanced by 5.000E+00				
	H2O Enhanced by 5.000E+00				
	N2 Enhanced by 1.000E+00				
	CO2 Enhanced by 2.000E+00				

```
R  9. CN+NO(+M)=NCNO(+M)              3.980E+13    0.00        0.0         g
      Low pressure limit:  0.15600E+37 -0.62000E+01  0.48780E+04
      T&H VALUE  0.65000E+00
         N2O              Enhanced by    5.000E+00
         H2O              Enhanced by    5.000E+00
         N2               Enhanced by    1.000E+00
         CO2              Enhanced by    2.000E+00
R 10. CN+M=C+N+M                       2.500E+14    0.00   141100.0         h
         N2               Enhanced by    1.500E+00
         CO2              Enhanced by    2.400E+00
R 11. NO+M=N+O+M                       1.400E+15    0.00   148430.0         i
         N2               Enhanced by    1.000E+00
         H2               Enhanced by    2.200E+00
         H2O              Enhanced by    6.700E+00
         CO2              Enhanced by    3.000E+00
         N2O              Enhanced by    2.200E+00
R 12. N2+M=N+N+M                       3.710E+21   -1.60   225000.0        (3)
R 13. N2O+N=N2+NO                      1.000E+13    0.00    19870.0     Est. (10)
R 14. NO2+N=N2O+O                      5.010E+12    0.00        0.0       (10)
R 15. NO2+N=NO+NO                      3.980E+12    0.00        0.0       (10)
R 16. NO2+NO2=NO+NO+O2                 1.630E+12    0.00    26120.0        (1)
R 17. NO2+NO2=NO+NO3                   9.640E+09    0.73    20920.0        (1)
R 18. NO2+NO3=NO+NO2+O2                1.400E+11    0.00     3180.0        (3)
R 19. HNO+NO=N2O+OH                    1.700E+13    0.00    29590.0         j
R 20. HNO+O2=HO2+NO                    1.000E+13    0.00    25000.0        (7)
R 21. HNO+NO2=HONO+NO                  4.420E+04    2.64     4042.0       (11)
R 22. HONO+O=OH+NO2                    1.200E+13    0.00     5961.0        (1)
R 23. HONO+OH=H2O+NO2                  1.270E+10    1.00      135.0        (1)
R 24. HNO+O=OH+NO                      3.610E+13    0.00        0.0        (1)
R 25. NH+O=NO+H                        5.500E+13    0.00        0.0       (12)
R 26. NH+O=N+OH                        3.720E+13    0.00        0.0       (12)
R 27. NH+NH=N2+H+H                     5.100E+13    0.00        0.0       (13)
R 28. NH+M=N+H+M                       2.650E+14    0.00    75510.0       (13)
R 29. CH+O2=HCO+O                      3.300E+13    0.00        0.0        (7)
R 30. CH+O=CO+H                        5.700E+13    0.00        0.0        (7)
R 31. CH+OH=HCO+H                      3.000E+13    0.00        0.0        (7)
R 32. CH+CO2=HCO+CO                    3.400E+12    0.00      690.0        (7)
R 33. CH+H=C+H2                        1.500E+14    0.00        0.0        (7)
R 34. C+O2=CO+O                        2.000E+13    0.00        0.0        (7)
R 35. C+OH=CO+H                        5.000E+13    0.00        0.0        (7)
R 36. HCO+OH=H2O+CO                    1.000E+14    0.00        0.0        (7)
R 37. HCO+M=H+CO+M                     2.500E+14    0.00    16802.0        (7)
         CO               Enhanced by    1.900E+00
         H2               Enhanced by    1.900E+00
         CO2              Enhanced by    3.000E+00
         H2O              Enhanced by    5.000E+00
R 38. HCO+H=CO+H2                      1.190E+13    0.25        0.0        (7)
R 39. HCO+O=CO+OH                      3.000E+13    0.00        0.0        (7)
R 40. HCO+O=CO2+H                      3.000E+13    0.00        0.0        (7)
R 41. HCO+O2=HO2+CO                    3.300E+13   -0.40        0.0        (7)
R 42. CO+O(+M)=CO2(+M)                 1.800E+10    0.00     2380.0         k
      Low pressure limit:  0.13500E+25 -0.27900E+01  0.41900E+04
      T&H VALUE  0.10000E+01
         H2O              Enhanced by    1.200E+01
         H2               Enhanced by    2.500E+00
         CO               Enhanced by    1.900E+00
         CO2              Enhanced by    3.800E+00
         N2O              Enhanced by    5.000E+00
R 43. CO+OH=CO2+H                      1.510E+07    1.30     -758.0        (7)
```

R 44.	CO+O2=CO2+O		2.530E+12	0.00	47688.0	(15)
R 45.	HO2+CO=CO2+OH		5.800E+13	0.00	22934.0	(7)
R 46.	O+HCCO=H+2CO		1.000E+14	0.00	0.0	(7)
R 47.	HCCO+O2=2CO+OH		1.600E+12	0.00	854.0	(7)
R 48.	H2+O2=2OH		1.700E+13	0.00	47780.0	(7)
R 49.	OH+H2=H2O+H		2.160E+08	1.50	3430.0	(16)
R 50.	O2+H=O+OH		3.520E+16	-0.70	17070.0	(17)
R 51.	O+H2=OH+H		5.060E+04	2.67	6290.0	(18)
R 52.	H+O2+M=HO2+M		3.610E+17	-0.72	0.0	(7)
	H2O	Enhanced by	1.860E+01			
	CO2	Enhanced by	4.200E+00			
	H2	Enhanced by	2.900E+00			
	CO	Enhanced by	2.100E+00			
	N2	Enhanced by	1.300E+00			
R 53.	OH+HO2=H2O+O2		7.500E+12	0.00	0.0	(7)
R 54.	H+HO2=2OH		1.690E+14	0.00	874.0	(15)
R 55.	O+HO2=O2+OH		1.400E+13	0.00	1073.0	(7)
R 56.	OH+OH=H2O+O		3.570E+04	2.40	2112.0	(19)
R 57.	2H+M=H2+M		1.000E+18	-1.00	0.0	(7)
	H2	Enhanced by	0.000E+00			
	H2O	Enhanced by	0.000E+00			
	CO2	Enhanced by	0.000E+00			
R 58.	2H+H2=2H2		9.200E+16	-0.60	0.0	(7)
R 59.	2H+H2O=H2+H2O		6.000E+19	-1.25	0.0	(7)
R 60.	2H+CO2=H2+CO2		5.490E+20	-2.00	0.0	(7)
R 61.	H+OH+M=H2O+M		1.600E+22	-2.00	0.0	(7)
	H2O	Enhanced by	5.000E+00			
R 62.	H+O+M=OH+M		6.200E+16	-0.60	0.0	(7)
	H2O	Enhanced by	5.000E+00			
R 63.	O+O+M=O2+M		1.890E+13	0.00	-1788.0	(7)
R 64.	H+HO2=H2+O2		6.630E+13	0.00	2126.0	(15)
R 65.	2HO2=H2O2+O2		1.800E+12	0.00	0.0	(15)
R 66.	H2O2+H=HO2+H2		4.820E+13	0.00	7948.0	(15)
R 67.	H2O2+OH=H2O+HO2		1.750E+12	0.00	318.0	(15)
R 68.	CH+N2=HCN+N		3.000E+11	0.00	13600.0	(7)
R 69.	CN+N=C+N2		1.040E+15	-0.50	0.0	(7)
R 70.	C+NO=CN+O		6.600E+13	0.00	0.0	(7)
R 71.	HCCO+NO=HCNO+CO		2.000E+13	0.00	0.0	(7)
R 72.	HCNO+H=HCN+OH		1.000E+14	0.00	12000.0	(7)
R 73.	CH+N=CN+H		1.300E+13	0.00	0.0	(7)
R 74.	HCCO+N=HCN+CO		5.000E+13	0.00	0.0	(7)
R 75.	HCN+OH=CN+H2O		3.900E+06	1.83	10290.0	(20)
R 76.	OH+HCN=HOCN+H		5.850E+04	2.40	12500.0	(7)
R 77.	OH+HCN=HNCO+H		1.980E-03	4.00	1000.0	(7)
R 78.	OH+HCN=NH2+CO		7.830E-04	4.00	4000.0	(7)
R 79.	HOCN+H=HNCO+H		1.000E+13	0.00	0.0	(7)
R 80.	HCN+O=NCO+H		1.380E+04	2.64	4980.0	(7)
R 81.	HCN+O=NH+CO		3.450E+03	2.64	4980.0	(7)
R 82.	HCN+O=CN+OH		2.700E+09	1.58	26600.0	(7)
R 83.	CN+H2=HCN+H		3.610E+08	1.55	3000.0	(9)
R 84.	CN+O=CO+N		2.050E+13	0.00	417.0	(9)
R 85.	CN+O2=NCO+O		2.600E+14	-0.50	0.0	(21)
R 86.	CN+OH=NCO+H		4.000E+13	0.00	0.0	(9)
R 87.	CN+HCN=C2N2+H		1.510E+07	1.71	1530.0	(9)
R 88.	CN+NO2=NCO+NO		6.160E+15	-0.752	344.0	(22)
R 89.	CN+CO2=NCO+CO		3.670E+06	2.16	26900.0	(23)
R 90.	CN+N2O=NCN+NO		6.000E+13	0.00	15360.0	l
R 91.	C2N2+O=NCO+CN		4.570E+12	0.00	8880.0	(7)
R 92.	C2N2+OH=HOCN+CN		1.860E+11	0.00	2900.0	(7)

R 93.	NO+HO2=NO2+OH		2.110E+12	0.00	-479.0	(10)
R 94.	NO2+H=NO+OH		1.300E+14	0.00	361.0	(25)
R 95.	NO2+O=NO+O2		3.900E+12	0.00	-238.0	(26)
R 96.	NCO+H=NH+CO		5.400E+13	0.00	0.0	(9)
R 97.	NCO+O=NO+CO		4.520E+13	0.00	0.0	(9)
R 98.	NCO+N=N2+CO		2.000E+13	0.00	0.0	(7)
R 99.	NCO+OH=NO+CO+H		2.000E+13	0.00	7500.0	Est.
R100.	NCO+M=N+CO+M		1.140E+23	-1.95	59930.0	g
	N2O	Enhanced by	5.000E+00			
	H2O	Enhanced by	5.000E+00			
	N2	Enhanced by	1.000E+00			
	CO2	Enhanced by	1.500E+00			
R101.	NCO+NO=N2O+CO		8.800E+17	-1.78	790.0	m
R102.	NCO+NO=CO2+N2		1.130E+18	-1.78	790.0	m
R103.	NCO+H2=HNCO+H		2.070E+06	2.00	6020.0	(9)
R104.	NCO+NO2=CO2+N2O		1.950E+13	-0.258	-620.0	n
R105.	NCO+NO2=CO+NO+NO		1.770E+12	-0.258	-620.0	n
R106.	NH+O2=HNO+O		4.610E+05	2.00	6500.0	(37)
R107.	NH+O2=NO+OH		1.280E+06	1.50	100.0	(37)
R108.	NH+NO=N2O+H		3.500E+14	-0.46	16.1	(37,38) o
R109.	NH+NO=N2+OH		2.160E+13	-0.23	0.0	(37)
R110.	N2O+OH=N2+HO2		1.290E-02	4.72	36561.0	(39)
R111.	N2O+H=N2+OH		1.300E+11	0.938	15210.0	p
R112.	NNH+O=N2O+H		1.400E+14	-0.40	477.0	(48)
R113.	NNH+O=NO+NH		3.300E+14	-0.23	-1013.0	(48)
R114.	N2O+O=N2+O2		3.692E+12	0.00	15940.0	(49)
R115.	N2O+O=NO+NO		9.155E+13	0.00	27680.0	(49)
R116.	H+HNO=NH+OH		3.000E+14	0.00	18000.0	q
R117.	NH+OH=N+H2O		5.000E+11	0.50	2000.0	(7)
R118.	NH+N=N2+H		3.000E+13	0.00	0.0	(7)
R119.	N+H2=NH+H		2.330E+14	0.00	30830.0	(51)
R120.	NH2+O=HNO+H		4.600E+13	0.00	0.0	(47)
R121.	NH2+O=NH+OH		7.000E+12	0.00	0.0	(47)
	Declared duplicate reaction...					
R122.	NH2+O=NH+OH		3.330E+08	1.50	5077.0	(47)
	Declared duplicate reaction...					
R123.	NH2+OH=NH+H2O		4.000E+06	2.00	1000.0	(7)
R124.	NH2+H=NH+H2		4.000E+13	0.00	3650.0	(52)
R125.	NH2+NH=N2H2+H		1.500E+15	-0.50	0.0	(52)
R126.	NH2+N=N2+H+H		7.200E+13	0.00	0.0	(7)
R127.	NH2+O2=HNO+OH		4.500E+12	0.00	25000.0	(7)
R128.	NH2+NH2=NH+NH3		5.000E+13	0.00	10000.0	(52)
R129.	NH2+NH2=N2H3+H		1.790E+13	-0.35	11320.0	r
R130.	NH2+NH2+M=N2H4+M		2.980E+47	-9.44	9680.0	r
R131.	NH+NO2=N2O+OH		4.000E+12	0.00	0.0	s
R132.	NH+NO2=NO+HNO		5.700E+12	0.00	0.0	s
R133.	N2H4+H=N2H3+H2		5.500E+12	0.00	2268.0	t
R134.	N2H4+OH=N2H3+H2O		4.800E+06	2.00	-646.0	(47)
R135.	N2H4+O=N2H3+OH		6.700E+08	1.50	2851.0	(47)
R136.	N2H3+H=N2H2+H2		2.400E+08	1.50	-10.0	(47)
R137.	N2H3+OH=N2H2+H2O		1.200E+06	2.00	-1192.0	(47)
R138.	N2H3+O=NH2+HNO		3.000E+13	0.00	0.0	(47)
R139.	N2H3+O=N2H2+OH		1.700E+08	1.50	-646.0	(47)
R140.	N2H2+M=NNH+H+M		5.000E+16	0.00	50000.0	(7)
	H2O	Enhanced by	1.500E+01			
	O2	Enhanced by	2.000E+00			
	N2	Enhanced by	2.000E+00			
	H2	Enhanced by	2.000E+00			
R141.	N2H2+H=NNH+H2		5.000E+13	0.00	1000.0	(7)

```
R142. N2H2+O=NH2+NO                    1.000E+13    0.00        0.0        (7)
R143. N2H2+O=NNH+OH                    2.000E+13    0.00     1000.0        (7)
R144. N2H2+OH=NNH+H2O                  1.000E+13    0.00     1000.0        (7)
R145. N2H2+NH=NNH+NH2                  1.000E+13    0.00     1000.0        (7)
R146. N2H2+NH2=NH3+NNH                 1.000E+13    0.00     1000.0        (7)
R147. NH2+NO=NNH+OH                    2.290E+10    0.425    -815.0       (60)
R148. NH2+NO=N2+H2O                    2.770E+20   -2.65     1258.0       (60)
R149. NH3+OH=NH2+H2O                   2.040E+06    2.04      566.0        (7)
R150. NH3+H=NH2+H2                     5.420E+05    2.40     9917.0       (61)
R151. NH3+O=NH2+OH                     9.400E+06    1.94     6460.0       (62)
R152. NH3(+M)=NH2+H(+M)                5.500E+15    0.00   107792.0         u
      Low pressure limit:  0.22000E+17  0.00000E+00  0.93470E+05
R153. HONO+NH2=NO2+NH3                 9.200E+05    1.94     1920.0       (47)
R154. NH3+CN=NH2+HCN                   5.750E+12    0.00     -505.0         v
R155. NNH+NO=N2+HNO                    2.000E+13    0.00        0.0       Est.
R156. NNH+H=N2+H2                      1.000E+14    0.00        0.0        (7)
R157. NNH+OH=N2+H2O                    5.000E+13    0.00        0.0        (7)
R158. NNH+NH2=N2+NH3                   5.000E+13    0.00        0.0        (7)
R159. NNH+NH=N2+NH2                    5.000E+13    0.00        0.0        (7)
R160. HNO+OH=NO+H2O                    1.295E+07    1.884    -958.0       (65)
R161. H+HNO=H2+NO                      4.460E+11    0.72      655.0       (66)
R162. HNO+NH2=NH3+NO                   2.000E+13    0.00     1000.0        (7)
R163. N+NO=N2+O                        3.270E+12    0.30        0.0        (7)
R164. O+NO=N+O2                        3.800E+09    1.00    41375.0        (1)
R165. NO+H=N+OH                        1.700E+14    0.00    48800.0       (10)
R166. HNO+HNO=N2O+H2O                  3.630E-03    3.98     1190.0       (67)
R167. HNC+O=NH+CO                      5.440E+12    0.00        0.0       (68)
R168. HNC+O=H+NCO                      1.600E+01    3.08     -224.0       (68)
R169. HNC+OH=HNCO+H                    2.800E+13    0.00     3696.0       (68)
R170. N2O+NO=N2+NO2                    4.290E+13    0.00    47130.0         w
R171. NO+NO+NO=N2O+NO2                 1.070E+10    0.00    26800.0       (74)
R172. HOCO+M=OH+CO+M                   2.190E+23   -1.89    35270.0       (75)
R173. HNC+OH=CN+H2O                    1.500E+12    0.00     7680.0       (68)
R174. HNC+NO2=HNCO+NO                  1.000E+12    0.00    32000.0     (68b) x
R175. HNCO+O=CO2+NH                    1.950E+14   -0.34    13020.0       (76)
R176. HNCO+O=NCO+OH                    6.670E-04    4.55    -1770.0       (76)
R177. HNCO+O=HNO+CO                    1.490E+08    1.57    44010.0       (76)
R178. HNCO+OH=H2O+NCO                  4.790E+05    2.00     2560.0         y
R179. HNCO+OH=NH2+CO2                  1.600E+05    2.00     2560.0         y
R180. HNCO+NH=NH2+NCO                  2.000E+13    0.00    19300.0       Est.
R181. HNCO+H=NH2+CO                    2.250E+07    1.70     3800.0       (78)
R182. CH+NO=HCN+O                      1.100E+14    0.00        0.0        (7)
R183. CN+NO=NCO+N                      5.500E+12    0.00    30620.0       (79)
R184. CN+NO=N2+CO                      3.900E+11    0.00    27820.0       (79)
R185. CN+NO=NCN+O                      1.800E+13    0.00    38190.0       (79)
R186. CO+NO2=NO+CO2                    9.040E+13    0.00    33780.0        (1)
R187. CH+NO2=HCO+NO                    1.010E+14    0.00        0.0       (80)
R188. H2+NO2=HONO+H                    1.300E+04    2.76    29770.0       (81)
R189. HONO+H=HNO+OH                    5.630E+10    0.86     4969.0       (82)
R190. HONO+H=H2O+NO                    8.130E+06    1.89     3847.0       (82)
R191. 2HONO=NO+NO2+H2O                 3.490E-01    3.64    12140.0       (83)
R192. NNH(+M)=N2+H(+M)                 4.100E+09    1.13     5186.0         z
      Low pressure limit:  0.10000E+14  0.50000E+00  0.30600E+04
         N2O              Enhanced by    5.000E+00
         H2O              Enhanced by    9.000E+00
         N2               Enhanced by    1.000E+00
         O2               Enhanced by    8.200E-01
      Declared duplicate reaction...
R193. NNH=N2+H                         3.000E+08    0.00        0.0         z
```

```
      Declared duplicate reaction...
R194. HCN+M=HNC+M                       4.360E+26   -3.34    50194.0        aa
R195. HNO+NO+NO=HNNO+NO2                1.700E+11    0.00     2100.0       (85)
R196. HNNO+NO=NNH+NO2                   3.200E+12    0.00      270.0       (85)
R197. HNNO+NO=N2+HONO                   2.600E+11    0.00      810.0       (85)
R198. HNNO+M=H+N2O+M                    2.200E+15    0.00    21600.0       (85)
R199. HNNO+M=N2+OH+M                    1.000E+15    0.00    25600.0       (85)
R200. HCO+NO=HNO+CO                     7.230E+12    0.00        0.0        (1)
R201. O+CH2<=>H+HCO                     8.000E+13    0.00        0.0       (86)
R202. O+CH2(S)<=>H2+CO                  1.500E+13    0.00        0.0       (86)
R203. O+CH2(S)<=>H+HCO                  1.500E+13    0.00        0.0       (86)
R204. O+CH3<=>H+CH2O                    8.430E+13    0.00        0.0       (86)
R205. O+CH4<=>OH+CH3                    1.020E+09    1.50     8600.0       (86)
R206. O+CH2O<=>OH+HCO                   3.900E+13    0.00     3540.0       (86)
R207. O+CH2OH<=>OH+CH2O                 1.000E+13    0.00        0.0       (86)
R208. O+CH3O<=>OH+CH2O                  1.000E+13    0.00        0.0       (86)
R209. O+CH3OH<=>OH+CH2OH                3.880E+05    2.50     3100.0       (86)
R210. O+CH3OH<=>OH+CH3O                 1.300E+05    2.50     5000.0       (86)
R211. O+C2H<=>CH+CO                     5.000E+13    0.00        0.0       (86)
R212. O+C2H2<=>H+HCCO                   1.020E+07    2.00     1900.0       (86)
R213. O+C2H2<=>OH+C2H                   4.600E+19   -1.41    28950.0       (86)
R214. O+C2H2<=>CO+CH2                   1.020E+07    2.00     1900.0       (86)
R215. O+C2H3<=>H+CH2CO                  3.000E+13    0.00        0.0       (86)
R216. O+C2H4<=>CH3+HCO                  1.920E+07    1.83      220.0       (86)
R217. O+C2H5<=>CH3+CH2O                 1.320E+14    0.00        0.0       (86)
R218. O+C2H6<=>OH+C2H5                  8.980E+07    1.92     5690.0       (86)
R219. O+CH2CO<=>OH+HCCO                 1.000E+13    0.00     8000.0       (86)
R220. O+CH2CO<=>CH2+CO2                 1.750E+12    0.00     1350.0       (86)
R221. O2+CH2O<=>HO2+HCO                 1.000E+14    0.00    40000.0       (86)
R222. H+CH2(+M)<=>CH3(+M)               2.500E+16   -0.80        0.0       (86)
      Low pressure limit:  0.32000E+28 -0.31400E+01  0.12300E+04
      TROE centering:      0.68000E+00  0.78000E+02  0.19950E+04  0.55900E+04
         H2               Enhanced by    2.000E+00
         H2O              Enhanced by    6.000E+00
         CH4              Enhanced by    2.000E+00
         CO               Enhanced by    1.500E+00
         CO2              Enhanced by    2.000E+00
         C2H6             Enhanced by    3.000E+00
R223. H+CH2(S)<=>CH+H2                  3.000E+13    0.00        0.0       (86)
R224. H+CH3(+M)<=>CH4(+M)               1.270E+16   -0.63      383.0       (86)
      Low pressure limit:  0.24770E+34 -0.47600E+01  0.24400E+04
      TROE centering:      0.78300E+00  0.74000E+02  0.29410E+04  0.69640E+04
         H2               Enhanced by    2.000E+00
         H2O              Enhanced by    6.000E+00
         CH4              Enhanced by    2.000E+00
         CO               Enhanced by    1.500E+00
         CO2              Enhanced by    2.000E+00
         C2H6             Enhanced by    3.000E+00
R225. H+CH4<=>CH3+H2                    6.600E+08    1.62    10840.0       (86)
R226. H+HCO(+M)<=>CH2O(+M)              1.090E+12    0.48     -260.0       (86)
      Low pressure limit:  0.13500E+25 -0.25700E+01  0.14250E+04
      TROE centering:      0.78240E+00  0.27100E+03  0.27550E+04  0.65700E+04
         H2               Enhanced by    2.000E+00
         H2O              Enhanced by    6.000E+00
         CH4              Enhanced by    2.000E+00
         CO               Enhanced by    1.500E+00
         CO2              Enhanced by    2.000E+00
         C2H6             Enhanced by    3.000E+00
R227. H+CH2O(+M)<=>CH2OH(+M)            5.400E+11    0.454    3600.0       (86)
```

```
      Low pressure limit:  0.12700E+33 -0.48200E+01  0.65300E+04
      TROE centering:      0.71870E+00  0.10300E+03  0.12910E+04  0.41600E+04
         H2               Enhanced by    2.000E+00
         H2O              Enhanced by    6.000E+00
         CH4              Enhanced by    2.000E+00
         CO               Enhanced by    1.500E+00
         CO2              Enhanced by    2.000E+00
         C2H6             Enhanced by    3.000E+00
R228. H+CH2O(+M)<=>CH3O(+M)            5.400E+11    0.454    2600.0       (86)
      Low pressure limit:  0.22000E+31 -0.48000E+01  0.55600E+04
      TROE centering:      0.75800E+00  0.94000E+02  0.15550E+04  0.42000E+04
         H2               Enhanced by    2.000E+00
         H2O              Enhanced by    6.000E+00
         CH4              Enhanced by    2.000E+00
         CO               Enhanced by    1.500E+00
         CO2              Enhanced by    2.000E+00
         C2H6             Enhanced by    3.000E+00
R229. H+CH2O<=>HCO+H2                  2.300E+10    1.05     3275.0       (86)
R230. H+CH2OH(+M)<=>CH3OH(+M)          1.800E+13    0.00        0.0       (86)
      Low pressure limit:  0.30000E+32 -0.48000E+01  0.33000E+04
      TROE centering:      0.76790E+00  0.33800E+03  0.18120E+04  0.50810E+04
         H2               Enhanced by    2.000E+00
         H2O              Enhanced by    6.000E+00
         CH4              Enhanced by    2.000E+00
         CO               Enhanced by    1.500E+00
         CO2              Enhanced by    2.000E+00
         C2H6             Enhanced by    3.000E+00
R231. H+CH2OH<=>H2+CH2O                2.000E+13    0.00        0.0       (86)
R232. H+CH2OH<=>OH+CH3                 1.200E+13    0.00        0.0       (86)
R233. H+CH2OH<=>CH2(S)+H2O             6.000E+12    0.00        0.0       (86)
R234. H+CH3O(+M)<=>CH3OH(+M)           5.000E+13    0.00        0.0       (86)
      Low pressure limit:  0.86000E+29 -0.40000E+01  0.30250E+04
      TROE centering:      0.89020E+00  0.14400E+03  0.28380E+04  0.45569E+05
         H2               Enhanced by    2.000E+00
         H2O              Enhanced by    6.000E+00
         CH4              Enhanced by    2.000E+00
         CO               Enhanced by    1.500E+00
         CO2              Enhanced by    2.000E+00
         C2H6             Enhanced by    3.000E+00
R235. H+CH3O<=>H+CH2OH                 3.400E+06    1.60        0.0       (86)
R236. H+CH3O<=>H2+CH2O                 2.000E+13    0.00        0.0       (86)
R237. H+CH3O<=>OH+CH3                  3.200E+13    0.00        0.0       (86)
R238. H+CH3O<=>CH2(S)+H2O              1.600E+13    0.00        0.0       (86)
R239. H+CH3OH<=>CH2OH+H2               1.700E+07    2.10     4870.0       (86)
R240. H+CH3OH<=>CH3O+H2                4.200E+06    2.10     4870.0       (86)
R241. H+C2H(+M)<=>C2H2(+M)             1.000E+17   -1.00        0.0       (86)
      Low pressure limit:  0.37500E+34 -0.48000E+01  0.19000E+04
      TROE centering:      0.64640E+00  0.13200E+03  0.13150E+04  0.55660E+04
         H2               Enhanced by    2.000E+00
         H2O              Enhanced by    6.000E+00
         CH4              Enhanced by    2.000E+00
         CO               Enhanced by    1.500E+00
         CO2              Enhanced by    2.000E+00
         C2H6             Enhanced by    3.000E+00
R242. H+C2H2(+M)<=>C2H3(+M)            5.600E+12    0.00     2400.0       (86)
      Low pressure limit:  0.38000E+41 -0.72700E+01  0.72200E+04
      TROE centering:      0.75070E+00  0.98500E+02  0.13020E+04  0.41670E+04
         H2               Enhanced by    2.000E+00
         H2O              Enhanced by    6.000E+00
```

```
         CH4              Enhanced by    2.000E+00
         CO               Enhanced by    1.500E+00
         CO2              Enhanced by    2.000E+00
         C2H6             Enhanced by    3.000E+00
R243. H+C2H3(+M)<=>C2H4(+M)             6.080E+12    0.27      280.0       (86)
      Low pressure limit:  0.14000E+31 -0.38600E+01  0.33200E+04
      TROE centering:      0.78200E+00  0.20750E+03  0.26630E+04  0.60950E+04
         H2               Enhanced by    2.000E+00
         H2O              Enhanced by    6.000E+00
         CH4              Enhanced by    2.000E+00
         CO               Enhanced by    1.500E+00
         CO2              Enhanced by    2.000E+00
         C2H6             Enhanced by    3.000E+00
R244. H+C2H3<=>H2+C2H2                  3.000E+13    0.00        0.0       (86)
R245. H+C2H4(+M)<=>C2H5(+M)             1.080E+12    0.454    1820.0       (86)
      Low pressure limit:  0.12000E+43 -0.76200E+01  0.69700E+04
      TROE centering:      0.97530E+00  0.21000E+03  0.98400E+03  0.43740E+04
         H2               Enhanced by    2.000E+00
         H2O              Enhanced by    6.000E+00
         CH4              Enhanced by    2.000E+00
         CO               Enhanced by    1.500E+00
         CO2              Enhanced by    2.000E+00
         C2H6             Enhanced by    3.000E+00
R246. H+C2H4<=>C2H3+H2                  1.325E+06    2.53    12240.0       (86)
R247. H+C2H5(+M)<=>C2H6(+M)             5.210E+17   -0.99     1580.0       (86)
      Low pressure limit:  0.19900E+42 -0.70800E+01  0.66850E+04
      TROE centering:      0.84220E+00  0.12500E+03  0.22190E+04  0.68820E+04
         H2               Enhanced by    2.000E+00
         H2O              Enhanced by    6.000E+00
         CH4              Enhanced by    2.000E+00
         CO               Enhanced by    1.500E+00
         CO2              Enhanced by    2.000E+00
         C2H6             Enhanced by    3.000E+00
R248. H+C2H5<=>H2+C2H4                  2.000E+12    0.00        0.0       (86)
R249. H+C2H6<=>C2H5+H2                  1.150E+08    1.90     7530.0       (86)
R250. H+HCCO<=>CH2(S)+CO                1.000E+14    0.00        0.0       (86)
R251. H+HCCOH<=>H+CH2CO                 1.000E+13    0.00        0.0       (86)
R252. H2+CO(+M)<=>CH2O(+M)              4.300E+07    1.50    79600.0       (86)
      Low pressure limit:  0.50700E+28 -0.34200E+01  0.84350E+05
      TROE centering:      0.93200E+00  0.19700E+03  0.15400E+04  0.10300E+05
         H2               Enhanced by    2.000E+00
         H2O              Enhanced by    6.000E+00
         CH4              Enhanced by    2.000E+00
         CO               Enhanced by    1.500E+00
         CO2              Enhanced by    2.000E+00
         C2H6             Enhanced by    3.000E+00
R253. 2OH(+M)<=>H2O2(+M)                7.400E+13   -0.37        0.0       (86)
      Low pressure limit:  0.23000E+19 -0.90000E+00 -0.17000E+04
      TROE centering:      0.73460E+00  0.94000E+02  0.17560E+04  0.51820E+04
         H2               Enhanced by    2.000E+00
         H2O              Enhanced by    6.000E+00
         CH4              Enhanced by    2.000E+00
         CO               Enhanced by    1.500E+00
         CO2              Enhanced by    2.000E+00
         C2H6             Enhanced by    3.000E+00
R254. OH+CH2<=>H+CH2O                   2.000E+13    0.00        0.0       (86)
R255. OH+CH2<=>CH+H2O                   1.130E+07    2.00     3000.0       (86)
R256. OH+CH2(S)<=>H+CH2O                3.000E+13    0.00        0.0       (86)
R257. OH+CH3(+M)<=>CH3OH(+M)            6.300E+13    0.00        0.0       (86)
```

```
      Low pressure limit:  0.27000E+39 -0.63000E+01  0.31000E+04
      TROE centering:      0.21050E+00  0.83500E+02  0.53980E+04  0.83700E+04
         H2                Enhanced by    2.000E+00
         H2O               Enhanced by    6.000E+00
         CH4               Enhanced by    2.000E+00
         CO                Enhanced by    1.500E+00
         CO2               Enhanced by    2.000E+00
         C2H6              Enhanced by    3.000E+00
R258. OH+CH3<=>CH2+H2O                   5.600E+07    1.60     5420.0       (86)
R259. OH+CH3<=>CH2(S)+H2O                2.501E+13    0.00        0.0       (86)
R260. OH+CH4<=>CH3+H2O                   1.000E+08    1.60     3120.0       (86)
R261. OH+CH2O<=>HCO+H2O                  3.430E+09    1.18     -447.0       (86)
R262. OH+CH2OH<=>H2O+CH2O                5.000E+12    0.00        0.0       (86)
R263. OH+CH3O<=>H2O+CH2O                 5.000E+12    0.00        0.0       (86)
R264. OH+CH3OH<=>CH2OH+H2O               1.440E+06    2.00     -840.0       (86)
R265. OH+CH3OH<=>CH3O+H2O                6.300E+06    2.00     1500.0       (86)
R266. OH+C2H<=>H+HCCO                    2.000E+13    0.00        0.0       (86)
R267. OH+C2H2<=>H+CH2CO                  2.180E-04    4.50    -1000.0       (86)
R268. OH+C2H2<=>H+HCCOH                  5.040E+05    2.30    13500.0       (86)
R269. OH+C2H2<=>C2H+H2O                  3.370E+07    2.00    14000.0       (86)
R270. OH+C2H2<=>CH3+CO                   4.830E-04    4.00    -2000.0       (86)
R271. OH+C2H3<=>H2O+C2H2                 5.000E+12    0.00        0.0       (86)
R272. OH+C2H4<=>C2H3+H2O                 3.600E+06    2.00     2500.0       (86)
R273. OH+C2H6<=>C2H5+H2O                 3.540E+06    2.12      870.0       (86)
R274. OH+CH2CO<=>HCCO+H2O                7.500E+12    0.00     2000.0       (86)
R275. HO2+CH2<=>OH+CH2O                  2.000E+13    0.00        0.0       (86)
R276. HO2+CH3<=>O2+CH4                   1.000E+12    0.00        0.0       (86)
R277. HO2+CH3<=>OH+CH3O                  2.000E+13    0.00        0.0       (86)
R278. HO2+CH2O<=>HCO+H2O2                1.000E+12    0.00     8000.0       (86)
R279. C+CH2<=>H+C2H                      5.000E+13    0.00        0.0       (86)
R280. C+CH3<=>H+C2H2                     5.000E+13    0.00        0.0       (86)
R281. CH+H2<=>H+CH2                      1.107E+08    1.79     1670.0       (86)
R282. CH+H2O<=>H+CH2O                    1.713E+13    0.00     -755.0       (86)
R283. CH+CH2<=>H+C2H2                    4.000E+13    0.00        0.0       (86)
R284. CH+CH3<=>H+C2H3                    3.000E+13    0.00        0.0       (86)
R285. CH+CH4<=>H+C2H4                    6.000E+13    0.00        0.0       (86)
R286. CH+CO(+M)<=>HCCO(+M)               5.000E+13    0.00        0.0       (86)
      Low pressure limit:  0.26900E+29 -0.37400E+01  0.19360E+04
      TROE centering:      0.57570E+00  0.23700E+03  0.16520E+04  0.50690E+04
         H2                Enhanced by    2.000E+00
         H2O               Enhanced by    6.000E+00
         CH4               Enhanced by    2.000E+00
         CO                Enhanced by    1.500E+00
         CO2               Enhanced by    2.000E+00
         C2H6              Enhanced by    3.000E+00
R287. CH+CH2O<=>H+CH2CO                  9.460E+13    0.00     -515.0       (86)
R288. CH+HCCO<=>CO+C2H2                  5.000E+13    0.00        0.0       (86)
R289. CH2+O2<=>OH+HCO                    1.320E+13    0.00     1500.0       (86)
R290. CH2+H2<=>H+CH3                     5.000E+05    2.00     7230.0       (86)
R291. 2CH2<=>H2+C2H2                     3.200E+13    0.00        0.0       (86)
R292. CH2+CH3<=>H+C2H4                   4.000E+13    0.00        0.0       (86)
R293. CH2+CH4<=>2CH3                     2.460E+06    2.00     8270.0       (86)
R294. CH2+HCCO<=>C2H3+CO                 3.000E+13    0.00        0.0       (86)
R295. CH2(S)+N2<=>CH2+N2                 1.500E+13    0.00      600.0       (86)
R296. CH2(S)+O2<=>H+OH+CO                2.800E+13    0.00        0.0       (86)
R297. CH2(S)+O2<=>CO+H2O                 1.200E+13    0.00        0.0       (86)
R298. CH2(S)+H2<=>CH3+H                  7.000E+13    0.00        0.0       (86)
R299. CH2(S)+H2O(+M)<=>CH3OH(+M)         2.000E+13    0.00        0.0       (86)
      Low pressure limit:  0.27000E+39 -0.63000E+01  0.31000E+04
```

```
      TROE centering:      0.15070E+00  0.13400E+03  0.23830E+04  0.72650E+04
         H2               Enhanced by    2.000E+00
         H2O              Enhanced by    6.000E+00
         CH4              Enhanced by    2.000E+00
         CO               Enhanced by    1.500E+00
         CO2              Enhanced by    2.000E+00
         C2H6             Enhanced by    3.000E+00
R300. CH2(S)+H2O<=>CH2+H2O              3.000E+13    0.00        0.0       (86)
R301. CH2(S)+CH3<=>H+C2H4               1.200E+13    0.00     -570.0       (86)
R302. CH2(S)+CH4<=>2CH3                 1.600E+13    0.00     -570.0       (86)
R303. CH2(S)+CO<=>CH2+CO                9.000E+12    0.00        0.0       (86)
R304. CH2(S)+CO2<=>CH2+CO2              7.000E+12    0.00        0.0       (86)
R305. CH2(S)+CO2<=>CO+CH2O              1.400E+13    0.00        0.0       (86)
R306. CH2(S)+C2H6<=>CH3+C2H5            4.000E+13    0.00     -550.0       (86)
R307. CH3+O2<=>O+CH3O                   2.675E+13    0.00    28800.0       (86)
R308. CH3+O2<=>OH+CH2O                  3.600E+10    0.00     8940.0       (86)
R309. CH3+H2O2<=>HO2+CH4                2.450E+04    2.47     5180.0       (86)
R310. 2CH3(+M)<=>C2H6(+M)               2.120E+16   -0.97      620.0       (86)
      Low pressure limit:  0.17700E+51 -0.96700E+01  0.62200E+04
      TROE centering:      0.53250E+00  0.15100E+03  0.10380E+04  0.49700E+04
         H2               Enhanced by    2.000E+00
         H2O              Enhanced by    6.000E+00
         CH4              Enhanced by    2.000E+00
         CO               Enhanced by    1.500E+00
         CO2              Enhanced by    2.000E+00
         C2H6             Enhanced by    3.000E+00
R311. 2CH3<=>H+C2H5                     4.990E+12    0.10    10600.0       (86)
R312. CH3+HCO<=>CH4+CO                  2.648E+13    0.00        0.0       (86)
R313. CH3+CH2O<=>HCO+CH4                3.320E+03    2.81     5860.0       (86)
R314. CH3+CH3OH<=>CH2OH+CH4             3.000E+07    1.50     9940.0       (86)
R315. CH3+CH3OH<=>CH3O+CH4              1.000E+07    1.50     9940.0       (86)
R316. CH3+C2H4<=>C2H3+CH4               2.270E+05    2.00     9200.0       (86)
R317. CH3+C2H6<=>C2H5+CH4               6.140E+06    1.74    10450.0       (86)
R318. CH2OH+O2<=>HO2+CH2O               1.800E+13    0.00      900.0       (86)
R319. CH3O+O2<=>HO2+CH2O                4.280E-13    7.60    -3530.0       (86)
R320. C2H+O2<=>HCO+CO                   5.000E+13    0.00     1500.0       (86)
R321. C2H+H2<=>H+C2H2                   4.070E+05    2.40      200.0       (86)
R322. C2H3+O2<=>HCO+CH2O                3.980E+12    0.00     -240.0       (86)
R323. C2H4(+M)<=>H2+C2H2(+M)            8.000E+12    0.44    88770.0       (86)
      Low pressure limit:  0.70000E+51 -0.93100E+01  0.99860E+05
      TROE centering:      0.73450E+00  0.18000E+03  0.10350E+04  0.54170E+04
         H2               Enhanced by    2.000E+00
         H2O              Enhanced by    6.000E+00
         CH4              Enhanced by    2.000E+00
         CO               Enhanced by    1.500E+00
         CO2              Enhanced by    2.000E+00
         C2H6             Enhanced by    3.000E+00
R324. C2H5+O2<=>HO2+C2H4                8.400E+11    0.00     3875.0       (86)
R325. 2HCCO<=>2CO+C2H2                  1.000E+13    0.00        0.0       (86)
R326. NNH+CH3<=>CH4+N2                  2.500E+13    0.00        0.0       (86)
R327. NNH+O2<=>HO2+N2                   5.000E+12    0.00        0.0       (86)
R328. NNH+O<=>OH+N2                     2.500E+13    0.00        0.0       (86)
R329. NCO+O2<=>NO+CO2                   2.000E+12    0.00    20000.0       (86)
R330. H2CN+N<=>N2+CH2                   6.000E+13    0.00      400.0       (86)
R331. CH2+N2<=>HCN+NH                   1.000E+13    0.00    74000.0       (86)
R332. CH2(S)+N2<=>NH+HCN                1.000E+11    0.00    65000.0       (86)
R333. C+NO<=>CO+N                       2.900E+13    0.00        0.0       (86)
R334. CH+NO<=>H+NCO                     2.000E+13    0.00        0.0       (86)
R335. CH+NO<=>N+HCO                     3.000E+13    0.00        0.0       (86)
```

```
R336. CH2+NO<=>H+HNCO                  3.100E+17   -1.38     1270.0       (86)
R337. CH2+NO<=>OH+HCN                  2.900E+14   -0.69      760.0       (86)
R338. CH2+NO<=>H+HCNO                  3.800E+13   -0.36      580.0       (86)
R339. CH2(S)+NO<=>H+HNCO               3.100E+17   -1.38     1270.0       (86)
R340. CH2(S)+NO<=>OH+HCN               2.900E+14   -0.69      760.0       (86)
R341. CH2(S)+NO<=>H+HCNO               3.800E+13   -0.36      580.0       (86)
R342. CH3+NO<=>HCN+H2O                 9.600E+13    0.00    28800.0       (86)
R343. CH3+NO<=>H2CN+OH                 1.000E+12    0.00    21750.0       (86)
R344. HCNO+H<=>H+HNCO                  2.100E+15   -0.69     2850.0       (86)
R345. HCNO+H<=>NH2+CO                  1.700E+14   -0.75     2890.0       (86)
R346. CH3+N<=>H2CN+H                   6.100E+14   -0.31      290.0       (86)
R347. CH3+N<=>HCN+H2                   3.700E+12    0.15      -90.0       (86)
R348. HCO+HNO=CH2O+NO                  6.000E+11    0.00     2000.0     Est.  (1)
R349. CH2O+NO2=HCO+HONO                8.350E-11    6.68     8310.0       (87)
R350. HCO+NO2=CO+HONO                  1.240E+23   -3.29     2355.0      (1,88)
R351. HCO+NO2=H+CO2+NO                 8.390E+15   -0.75     1930.0      (1,88)
R352. CHOCHO(+M)=HCO+HCO(+M)           2.940E+14    0.00    67900.0     Est.   bb
      Low pressure limit:  0.91900E+50 -0.94300E+01  0.74016E+05
         H2O               Enhanced by    1.200E+01
         N2                Enhanced by    1.500E+00
         NO                Enhanced by    1.500E+00
         CO2               Enhanced by    5.000E+00
         CH2O              Enhanced by    2.000E+00
         NO2               Enhanced by    5.000E+00
         CO                Enhanced by    5.000E+00
         CHOCHO            Enhanced by    5.000E+00
         H2                Enhanced by    1.500E+00
R353. CHOCHO+OH=H2O+CO+HCO             3.400E+09    1.18      447.0     Est.   cc
R354. CHOCHO+H=H2+CO+HCO               4.580E+10    1.05     3280.0     Est.   dd
R355. CHOCHO+O=OH+CO+HCO               4.130E+11    0.57     2762.0     Est.   ee
R356. CHOCHO+NO2=HONO+CO+HCO           7.940E+11    0.00    19800.0        ff
R357. CHOCHO+NO=HNO+HCO+CO             1.000E+13    0.00    41000.0     Est.   gg
R358. HCO+HCO=CH2O+CO                  3.000E+13    0.00        0.0       (89)
R359. HCO+HCO=H2+CO+CO                 5.200E+12    0.00        0.0        hh
R360. HCO+CHOCHO=CH2O+CO+HCO           1.000E+13    0.00    11000.0        Est.
R361. CH2CO(+M)=CH2+CO(+M)             3.000E+14    0.00    71000.0        ii
      Low pressure limit:  0.36000E+16  0.00000E+00  0.59300E+05
         H2O               Enhanced by    1.200E+01
         N2                Enhanced by    1.500E+00
         NO                Enhanced by    1.500E+00
         CO2               Enhanced by    5.000E+00
         CH2O              Enhanced by    2.000E+00
         NO2               Enhanced by    5.000E+00
         CO                Enhanced by    5.000E+00
         CHOCHO            Enhanced by    5.000E+00
         H2                Enhanced by    1.500E+00
R362. CH2CO+O=CH2O+CO                  7.630E+11    0.00     1351.0     Est.   jj
R363. CH2CO+O=HCO+H+CO                 7.630E+11    0.00     1351.0     Est.   jj
R364. CH2CO+O=HCO+HCO                  7.630E+11    0.00     1351.0     Est.   jj
R365. CH2CO+OH=CH2O+HCO                3.330E+12    0.00        0.0     Est.   jj
R366. CH2CO+OH=CH2OH+CO                3.330E+12    0.00        0.0     Est.   jj
R367. CH2CO+OH=CH3+CO2                 3.330E+12    0.00        0.0     Est.   jj
R368. CH2CO+H=CH3+CO                   1.800E+13    0.00     3380.0       (89)
```

Notes to Table B-1

a. The string "Est." followed by a reference means the expression was estimated in that work; with no reference, it means it was estimated in this work; with a footnote, the estimate is explained in the footnote.

b. Expression from Tsang and Herron (*1*), using the choice for low pressure appropriate to N_2 collider. Efficiencies from Baulch (*3*), taken from those for the reverse reaction, except the one for CO_2 is from Tsang and Herron.

c. Expression from Röhrig et al. (*4*), with low-pressure limit rekeyed to N_2, using an N_2/Ar relative efficiency ratio of 1.5. N_2/Ar, N_2O/Ar from Baulch (*3*), CO_2/N_2 from Tsang and Herron (*1*), and H_2O/Ar, O_2/Ar from Glaborg et al. (*5*).

d. High pressure limit expression from Tsang and Herron (*1*). Low-pressure limit expression from Glarborg et al. (*6*) (which was for M = N_2). H_2O/N_2 from Miller and Bowman (*7*) (possibly estimated therein but seems quite reasonable), and N_2O/N_2 estimated herein.

e. Expression from Tsang and Herron (*1*), using the choice for low pressure appropriate to N_2 collider. CO_2/N_2 from Tsang and Herron (*1*), H_2O/N_2 from Overend et al. (*8*), N_2O/N_2 estimated herein.

f. Expression from Tsang and Herron (*1*), using the choice for low pressure appropriate to N_2 collider. CO_2/N_2 from Tsang and Herron, and N_2O/N_2 and H_2O/N_2 estimated herein.

g. Expression from Tsang (*9*), using the choice for low pressure appropriate to N_2 collider. CO_2/N_2 from Tsang, and N_2O/N_2 and H_2O/N_2 estimated herein.

h. Expression from Tsang (*9*), keyed to Ar = 1.0. N_2/Ar, and CO_2/Ar from Tsang.

i. Expression from Tsang and Herron (*1*), keyed to N_2 = 1.0. Efficiencies as compiled in Hanson and Saliman (*10*) for reverse reaction.

j. See section 2.2.1 in main body of text.

k. Expression and efficiencies from Allen et al. (*14*), except efficiency of N_2O is estimated herein.

l. Results for R90 for 400 K <T <870 K are reported in Williams et al. (*24*); a k_i form that is the sum of two exponentials was given. Only the portion that defines k_i at high T is used herein; it should be reliable to somewhat above 600 K. There is a pressure dependence below 600 K that is not well understood, suggesting the possibility of as yet unidentified stabilization products, and for this reason, and because lower T does not matter for the

present application, the low T limb is not used. A further complication is that the NCO + N_2 channel could open at higher T. It is doubtful, though, that significant enough concentrations of both CN and N_2O might ever be simultaneously present for this reaction to affect the DZ mixtures.

m. The total disappearance rate for NCO + NO → products was obtained by fitting the results of refs *27–33*, the results of Mertens et al. (*30*) being first restricted to the range of their measurements, 2380–2660 K. The branching ratio between R101 and R102 was taken from the measurements of Cooper et al. (*34*) for 296–623 K, where it was found to be constant; we have assumed that to be the case for all T.

n. The total disappearance rate for NCO + NO_2 → products was obtained by fitting the results of refs *33*, *35*, *36*. The branching ratio between R104 and R105 was taken from the measurement of Park and Hershberger (*35*) at 298 K and assumed to be constant vs. T.

o. The complicated expression of Miller and Melius (*37*), which requires the differencing of two duplicate reaction rate coefficients, was precisely refitted to the simpler expression shown by Williams and Fleming (*38*).

p. The expression for the deceptively simple-looking R111 was obtained by Anderson as described in Anderson and Bozzelli (*40*). Briefly, relevant experimental results from the literature were critically selected, and reanalyses of some were performed. The results from refs *41–46* were included in the fit resulting in the present recommended expression. For Dean et al. (*42*), our reanalysis took into account a key reaction, R56 that was missing from the authors' original analysis; this yields a result whose slope has much improved agreement with the trend of all the data. For Marshall et al. (*44*), the expression is the sum of two exponential functions, dominated by low and high T portions. Only the high T portion was used, which is appropriate for 714–1230 K. For the flame study of Venizelos and Sausa (*46*), as mentioned in their later work (*46b*), the authors' final result was 1.1 times that of ref *46*; the data were expressed as one point at 2000 K, the approximate temperature where that study is most sensitive. The present fit is thus based on data in the range 714–2850 K. Extrapolation to somewhat higher T would probably be reasonable, but there would be some concern about usage at lower T, especially at high pressures, because of possible competition from N_2O + H + M → HNNO + M, which needs further study (discussion and estimates are given in Anderson and Bozzelli [*40*] and Dean and Bozzelli [*47*]). Also, at high T, the NNH + O product channel (–R112) is reached, but only a very small fraction of the reactants goes to those products so it can be ignored in the fitting procedure. The present expression has only been intended as a preliminary result; we hope at some time in the future to perform a more careful reanalysis of Dean et al. (*42*) and include some other relevant studies that had to be discarded but for which—much more complicated—reanalysis might be possible; this would result in some, likely modest, revision to our expression. However, despite its

preliminary nature, due to the corrections to analysis errors in earlier studies, we believe the present expression is more well founded than prior recommendations. The Marshall et al. (*44*) result has been used in most solid propellant combustion modeling. At high T (above ~2000 K), the present result is about a factor of 1.3 larger than a rather long extrapolation of the Marshall et al. (*44*) result suggests; the Marshall et al. (*44*) result is, in turn, larger than prior recommendations. Additionally, there is significant upward curvature in the present expression even for the T >714 K part of the Arrhenius plot, likely due to contributions from both addition – elimination and direct abstraction reactions, which cannot be differentiated in kinetics experiments; due to the shorter T range of the Marshall et al. (*44*) study, the curvature at high T was not obvious. Thus this revision could help in modeling of N_2O oxidized flames, which has typically resulted in predicted flame velocities lower than experiments (for the latter three points, see the discussion in Anderson and Bozzelli [*40*]).

q. Estimated by the Quantum-Rice-Ramsperger-Kassel (QRRK) method, see Anderson (*50*).

r. Unpublished QRRK estimate of J. W. Bozzelli and A. M. Dean (~1993).

s. Total for NH + NO_2 from Harrison et al. (*53*), branching ratio from Quandt and Hershberger (*54*), both at 298 K; assumed constant vs. T.

t. The expression was obtained by fitting selected expressions from refs *55–59*, covering the range 213 K $\leq$T $\leq$657 K.

u. High-pressure limit from (*63*) and low-pressure limit from Davidson et al. (*52*).

v. Estimate of D. L. Yang, T. Yu, and M. C. Lin in Meads et al. (*64*), as quoted therein. Several results that are briefly reviewed therein agree fairly well. Lin and coworkers' work apparently was never published but is representative. There is a moderately large scatter in results, indicative that error limits of perhaps a factor of 3 would pertain at combustion temperatures and perhaps more at lower temperatures. However, the reaction is not important for the present application.

w. The present expression results from a fit based on refs *69–71*, with results weighted for the respective error limits (Anderson and Meagher, unpublished, 1995). Note that experiments of Borisov et al. (*72*) also produced a result,and of Zuev and Starikovskii (*73*) an upper limit. We find that although the Borisov et al. expression is in fair agreement, measurements for the authors' conditions are quite insensitive to the subject reaction and therefore must be discarded. The upper limit from Zuev and Starikovskii is larger than, and thus agrees with, the current expression. The studies of Kaufman and Kelso (*69*) and Fishburne and Edse (*70*) were first reanalyzed to account for important reactions missed in those early works (R95, R114, and R115 for the former, R95 for the latter). The current expression is about a factor of 4 larger than the ab initio estimate of Mebel et al. (*39*) at T >1500 K, and the difference is even larger at lower T. However, results are within the combined error limits, at least for

high T, as the precision of the present recommendation is about a factor of 2 at low T and 3 at high T, while that of the calculation is probably a factor of ~2.5. Clearly, the error limits one might choose for a recommendation would have to be large, due to both the differences in, and the scarcity of, available studies. This reaction is therefore in need of further work. Fortunately, while the present sensitivity and pathway results indicate the reaction plays a slight role for nitrate ester DZs (see section 5.1), the results also show that although the indicated error limits in rate coefficient are large, an error of that magnitude would not produce a major error in the present predictions. But, the issue should be kept in mind for other applications.

x. The expression for k_{174} in Thaxton et al. (*68c*) is many orders above collisional at temperatures above ~1000 K, and thus is much too large to be believed. Lin deferred comment, so for the present, we have retained the expression from his earlier private communication (*68b*, an unpublished manuscript which was apparently later revised and appeared as reference *68c*). The expression is in need of further study, and that is being pursued in our laboratory, but it is highly unlikely the reaction is at all significant for DZ conditions.

y. Total of R178 and R179 from Tsang (*9*), branching ratio from Miller and Bowman (*77*), and ratio assumed constant vs. T.

z. The high- and low-pressure limits for R192, which represent collisionally induced dissociation of NNH, were estimated in Bozzelli and Dean (*48*); a simple Lindemann falloff form was assumed herein. That assumption deserves further study. Also, the collisional efficiencies were estimated herein and are subject to considerable error. However, the reaction is closely, partially equilibrated under most propellant combustion conditions, so results are not usually sensitive to the rate coefficient. There is a separate predissociation contribution that, of course, does not involve collisions and thus is not pressure dependent; this is represented by R193. The predissociation lifetime, whose inverse is that separate reaction's rate coefficient, was also briefly reviewed in Bozzelli and Dean (*48*); we use their recommendation but note this parameter has been the subject of considerable controversy.

aa. The expression was kindly estimated for our use via the QRRK method by Bozzelli (*84*) for N_2 collider. Results indicate that up to 30 atm the reaction is in the low-pressure limit at T above ~600 K. More recently, we discovered a very similar, updated expression, similarly derived, is now available from Dean and Bozzelli (*47*). Plots show the expressions are almost identical from 1000–3000 K, are slightly different (~25%) at 600 K, and differ by about a factor of 2 at 300 K (where falloff effects might make either expression incorrect anyway); the differences in expressions are certainly within precision of the calculations. Most combustion modeling is quite insensitive to the rate coefficient because the reaction typically partially equilibrates rapidly; see, e.g., the discussion for nitramine DZ cases in section 5.2 in the main body of text. Thus, the choice between the two expressions is immaterial.

bb. Unpublished QRRK estimate of Anderson (1998).

cc. Estimated to be like OH + CH_2O = H_2O + HCO. Recommendation for the latter reaction from Baulch et al. (*89*).

dd. Estimated to have a rate constant expression twice that of R229.

ee. Estimated to be like O + CH_2O = OH + HCO. Recommendation for the latter reaction from Baulch et al. (*89*).

ff. Reaction rate coefficient taken from Thomas (*90*). Note the products are uncertain and assumed as shown.

gg. Assumed to be like the recommendation of Tsang et al. (*1*) for CH_2O + NO = HNO + HCO; note that recommendation was based on an estimate also, so there is considerable uncertainty.

hh. Determined by the ratio of (H_2 + 2CO)/(CH_2O + CO) products recommended in Tsang and Hampson (*15*).

ii. Expression from recommendation of Warnatz (*91*). Efficiencies estimated herein.

jj. Total disappearance rates for CH_2CO + O, and for CH_2CO + OH were both obtained from Baulch et al. (*89*). At least three product channels are possible for each, and the divisions between them are unknown. They were assumed equal herein. Users should watch for sensitivity to these reactions and be aware there is great uncertainty regarding the products. These reactions are unimportant for the present application.

References

1. Tsang, W.; Herron, J. T. Chemical Kinetic Database for Propellant Combustion. I. Reactions Involving NO, NO_2, HNO, HNO_2, HCN, and N_2O. *J. Phys. Chem. Ref. Data* **1991**, *20*, 609–663.

2. Kee, R. J.; Rupley, F. M.; Miller, J. A. *Chemkin-II: A Fortran Chemical Kinetics Package for the Analysis of Gas-Phase Chemical Kinetics*; SAND 89-8009; Sandia National Laboratories: Albuquerque, NM, September 1989.

3. Baulch, D. L.; Drysdale, D. D.; Horne, D. G. *Evaluated Kinetic Data for High-Temperature Reactions. Vol. 2. Homogeneous Gas Phase Reactions of the H_2-H_2-O_2 System*. Butterworths: London, 1973.

4. Röhrig, M.; Petersen, E. L.; Davidson, D. F.; Hanson, R. K. The Pressure Dependence of the Thermal Decomposition of N_2O. *Int. J. Chem. Kinetics* **1996**, *28*, 599–608.

5. Glarborg, P.; Johnsson, J. E.; Dam-Johansen, K. Kinetics of Homogeneous Nitrous Oxide Decomposition. *Combust. Flame* **1994**, *99*, 523–532.

6. Glarborg, P.; Østberg, M.; Alzueta, M. U.; Dam-Johansen, K.; Miller, J. A. The Recombination of Hydrogen Atoms with Nitric Oxide at High Temperatures. *Proc. Combust. Inst.* **1998**, *27*, 219–226.

7. Miller J. A.; Bowman, C. T. Mechanism and Modeling of Nitrogen Chemistry in Combustion. *Prog. Energy Combust. Sci.* **1989**, *15*, 287–338.

8. Overend, R.; Paraskevopoulos, G.; Black, C. Rates of OH Radical Reactions. II. The Combination Reaction OH + NO + M. *J. Chem. Phys.* **1976**, *64*, 4149–4154.

9. Tsang, W. Chemical Kinetic Database for Propellant Combustion. II. Reactions Involving CN, NCO, and HNCO. *J. Phys. Chem. Ref. Data* **1992**, *21*, 753–791.

10. Hanson, R. K.; Salimian, S. Survey of Rate Constants in the N/H/O System. In *Combustion Chemistry*, Gardiner, W. C., Ed.; Springer-Verlag: New York, 1985; Chapter 6.

11. Mebel, A. M.; Lin, M. C.; Morakuma, K. Ab Initio MO and TST Calculations for the Rate Constant of the HNO + NO_2 → HONO + NO Reaction. *Int. J. Chem. Kinetics* **1998**, *30*, 729–736.

12. Mertens, J. D.; Chang, A. Y.; Hanson, R. K.; Bowman, C. T. A Shock-Tube Study of the Reactions of NH With NO, O_2, and O. *Int. J. Chem. Kinetics* **1991**, *23*, 173–196.

13. Mertens, J. D.; Chang, A. Y.; Hanson, R. K.; Bowman, C. T. Reaction Kinetics of NH in the Shock Tube Pyrolysis of HNCO. *Int. J. Chem. Kinetics* **1989**, *21*, 1049–1067.

14. Allen, M. T.; Yetter, R. A.; Dryer, F. L. High-Pressure Studies of Moist Carbon Monoxide/Nitrous Oxide Kinetics. *Combust. Flame* **1997**, *109*, 449–470.

15. Tsang, W.; Hampson, R. F. Chemical Kinetic Database for Combustion Chemistry. Part I. Methane and Related Compounds. *J. Phys. Chem. Ref. Data* **1986**, *15*, 1087–1279.

16. Michael, J. V.; Sutherland, J. W. Rate Constant for the Reaction of H With H_2O and OH With H_2 by the Flash Photolysis—Shock Tube Technique Over the Temperature Range 1246–2297 K. *J. Phys. Chem.* **1988**, *92*, 3853–3857.

17. Masten, D. A.; Hanson, R. K.; Bowman, C. T. Shock Tube Study of the Reaction H + O_2 → OH + O Using Laser Absorption. *J. Phys. Chem.* **1990**, *94*, 7119–7128.

18. Sutherland, J. W.; Michael, J. V.; Pirraglia, A. N.; Nesbitt, F. L.; Klemm, R. B. Rate Constant for the Reaction of O(^{3}P) With H_2 by the Flash Photolysis–Shock Tube and Flash Photolysis–Resonance Fluorescence Techniques; 504K ≤ T ≤ 2495 K. *Proc. Combust. Inst.* **1988**, *21*, 929–941.

19. Wooldridge, M. S.; Hanson, R. K.; Bowman, C. T. A Shock Tube Study of the OH + OH → H_2O + O Reaction. *Int. J. Chem. Kinetics* **1994**, *26*, 389–401.

20. Wooldridge, S. T.; Hanson, R. K.; Bowman, C. T. Simultaneous Laser Absorption Measurements of CN and OH in a Shock Tube Study of HCN + OH → products. *Int. J. Chem. Kinetics* **1995**, *27*, 1075–1087.

21. Sims, I. R.; Smith, I. W. M. Rate Constants for the Radical-Radical Reaction Between CN and O_2 at Temperatures Down to 99 K. *Chem. Phys. Lett.* **1988**, *151*, 481–484.

22. Wooldridge, S. T.; Mertens, J. D.; Hanson, R. K.; Bowman, C. T. A Shock Tube Study of the Reactions of CN and NCO With NO_2. *Proc. Combust. Inst.* **1994**, *25*, 983–991.

23. Wang, N. S.; Yang, D. L.; Lin, M. C.; Melius, C. F. Kinetics of CN Reactions With N_2O and CO_2. *Int. J. Chem. Kinetics* **1991**, *23*, 151–160.

24. Williams, B. A.; Pappas, P.; Nelson, H. H. Kinetics and Product Channels of the Reaction CN + N_2O. *J. Phys. Chem.* **1995**, *99*, 13471–13475.

25. Ko, T.; Fontijn, A. High-Temperature Photochemistry Kinetics Study of the Reaction H + NO_2 → OH + NO From 296 to 760 K. *J. Phys. Chem.* **1991**, *95*, 3984–3987.

26. Atkinson, R.; Baulch, D. L.; Cox, R. A.; Hampson, R. F., Jr.; Kerr, J. A.; Troe, J. Evaluated Kinetic and Photochemical Data for Atmospheric Chemistry: Supplement III. *J. Phys. Chem. Ref. Data* **1989**, *18*, 881–1097.

27. Perry, R. A. Kinetics of the Reactions of NCO Radicals With H_2 and NO Using Laser Photolysis–Laser Induced Fluorescence. *J. Chem. Phys.* **1985**, *82*, 5485–5488.

28. Hancock, G.; McKendrick, K. G. Vibrational Relaxation of NCO(X) by Rare Gases and Rate Constant Measurement of the NCO + NO Reaction. *Chem. Phys. Lett.* **1986**, *127*, 125–129.

29. Atakan, B.; Wolfrum, J. Kinetic Studies of the Reactions of NCO Radicals With NO and O_2 in the Temperature Range Between 294 and 1260 K. *Chem. Phys. Lett.* **1991**, *178*, 157–162.

30. Mertens, J. D.; Dean, A. J.; Hanson, R. K.; Bowman, C. T. A Shock Tube Study of Reactions of NCO With O and NO Using NCO Laser Absorption. *Proc. Combust. Inst.* **1992**, *24*, 701–710.

31. Jones, W. E.; Wang, L. CARS Investigation of the Kinetics of Reactions of NCO With NO. *Can. J. Appl. Spectros.* **1993**, *38*, 32–36.

32. Wategaonkar, S.; Setser, D. W. The F + HNCO Reaction System—A Flow Reactor Source for NCO ($X^2\Pi$) and NF ($X^3\Sigma^-$). *J. Phys. Chem.* **1993**, *97*, 10028–10034.

33. Juang, D. Y.; Lee, J. S.; Wang, N. S. Kinetics of the Reactions of NCO With NO and NO_2. *Int. J. Chem. Kinetics* **1995**, *27*, 1111–1120.

34. Cooper, W. F.; Park, J.; Hershberger, J. F. Product Channel Dynamics of the NCO + NO Reaction. *J. Phys. Chem.* **1993**, *97*, 3283–3290.

35. Park J.; Hershberger, J. F. A Diode Laser Study of the NCO + NO_2 Reaction. *J. Phys. Chem.* **1993**, *97*, 13647–13652.

36. Wooldridge, S. T.; Mertens, J. D.; Hanson, R. K.; Bowman, C. T. A Shock Tube Study of the Reactions of CN and NCO With NO_2. *Proc. Combust. Inst.* **1994**, *25*, 983–991.

37. Miller, J. A.; Melius, C. F. The Reactions of Imidogen With Nitric Oxide and Molecular Oxygen. *Proc. Combust. Inst.* **1992**, *24*, 719–726.

38. Williams, B. A.; Fleming, J. W. Comparison of Species Profiles Between O_2 and NO_2 Oxidizers in Premixed Methane Flames. *Combust. Flame* **1995**, *100*, 571–590.

39. Mebel, A. M.; Lin, M. C.; Morakuma, K.; Melius, C. F. Theoretical Study of Reactions of N_2O With NO and OH Radicals. *Int. J. Chem. Kinetics* **1996**, *28*, 693–703.

40. Anderson, W. R.; Bozzelli, J. W. Calculation of Pressure Dependent Rate Coefficients for Modeling Combustion of Solid Propellants. *Proceedings 39th JANNAF Combustion Subcommittee Meeting, JSC CD-25*, Colorado Springs, CO, December 2003; Paper CS-3A-7.

41. Albers, E. A.; Hoyermann, K.; Schacke, H. K.; Schmatjko, J.; Wagner, H. G.; Wolfrum, J. Absolute Rate Coefficients for the Reaction of H-Atoms With N_2O and Some Reactions of CN Radicals. *Proc. Combust. Inst.* **1975**, *15*, 765–773.

42 a. Dean, A. M.; Steiner, D. C.; Wange, E. E. A Shock Tube Study of the $H_2/O_2/CO/Ar$ and $H_2/N_2O/CO/Ar$ Systems: Measurements of the Rate Constant for $H + N_2O = N_2 + OH$. *Combust. Flame* **1978**, *32*, 73–83.

b. Dean, A. M.; Johnston, R. L.; Steiner, D. C. Shock-Tube Studies of Formaldehyde Oxidation. *Combust. Flame* **1980**, *37*, 41–62.

43. Hidaka, Y.; Takuma, H.; Suga, M. Shock-Tube Studies of N_2O Decomposition and N_2O-H_2 Reaction. *Bull. Chem. Soc.* (Japan) **1985**, *58*, 2911–2916.

44. a. Marshall, P.; Fontijn, A.; Melius, C. F. High-Temperature Photochemistry and BAC-MP4 Studies of the Reaction Between Ground-State H Atoms and N_2O. *J. Chem. Phys.* **1987**, *86*, 5540–5549.

b. Marshall, P.; Ko, T.; Fontijn, A. High-Temperature Photochemistry Kinetics Studies of the Reactions of $H(1^2S)$ and $D(1^2S)$ With N_2O. *J. Phys. Chem.* **1989**, *93*, 1922–1927.

45. a. Zuev, A. P.; Starikovskii, A. Y. Reactions in the Nitrous Oxide-Hydrogen-Argon System at High Temperatures. *Khim. Fiz.* **1991**, *10*, 347–360.

b. Starikovskii, A. Y. Kinetics and Mechanism of Reaction in N_2O-CO System at High Temperatures. *Khim. Fiz.* **1994**, *13*, 94–120.

46. a. Venizelos, D. T.; Sausa, R. C. Laser-Induced Fluorescence, Mass Spectrometric, and Modeling Studies of Neat and NH_3-Doped $H_2/N_2O/Ar$ Flames. *Combust. Flame* **1998**, *115*, 313–326.

b. Venizelos, D. T.; Sausa, R. C. Detailed Chemical Kinetics Studies of an $NH_3/N_2O/Ar$ Flame by Laser-Induced Fluorescence, Mass Spectrometry, and Modeling. *Proc. Combust. Inst.* **2000**, *28*, 2411–2418.

47. Dean, A. M.; Bozzelli, J. W. Combustion Chemistry of Nitrogen. In *Gas-Phase Combustion Chemistry*, Gardiner, W. C., Jr., Ed.; Springer-Verlag: New York, 2000; Chapter 2.

48. Bozzelli, J. W.; Dean, A. M. O + NNH: A Possible New Route for NO_x Formation in Flames. *Int. J. Chem. Kinetics* **1995**, *27*, 1097–1109.

49. Meagher, N. E.; Anderson, W. R. Kinetics of the $O(^3P) + N_2O$ Reaction. 2. Interpretation and Recommended Rate Coefficients. *J. Phys. Chem. A* **2000**, *104*, 6013–6031.

50. Anderson, W. R. The Chemical Mechanism of H_2/NO Combustion at Intermediate Temperatures and Its Relation to the Dark Zone of Propellants. *30th JANNAF Combustion Subcommittee Meeting,* CPIA Publication No. 606, 1993, Vol. II, p 205.

51. Zhang, S.; Truong, T. N. Direct Ab Initio Dynamics Studies of the $N + H_2 \leftrightarrow NH + H$ Reaction. *J. Chem. Phys.* **2000**, *113*, 6149–6153.

52. Davidson, D. F.; Kohse-Hoinghaus, K.; Chang, A. Y.; Hanson, R. K. A Pyrolysis Mechanism for Ammonia. *Int. J. Chem. Kinetics* **1990**, *22*, 513–535.

53. Harrison, J. A.; White, A. R.; Phillips, L. F. Kinetics of Reactions of NH With NO and NO_2. *Chem. Phys. Lett.* **1986**, *129*, 346–352.

54. Quandt, R. W.; Hershberger, J. F. Product Branching Ratios of the $NH(^3\Sigma^-) + NO$ and $NH(^3\Sigma^-) + NO_2$ Reactions. *J. Phys. Chem.* **1995**, *99*, 16939–16944.

55. Francis, P. D.; Jones, A. R. ESR Measurement of the Reaction Between H Atoms and N_2H_4. *J. Chem. Phys.* **1971**, *54*, 5085–5088.

56. Gehring, M.; Hoyermann, K.; Wagner, H. G.; Wolfrum, J. Die Reaktion von Atomarem Wasserstoff mit Hydrazin. *Ber. Bunsenges. Phys. Chem.* **1971**, *75*, 1287–1294.

57. Stief, L.; Payne, W. A. Absolute Rate Parameters for the Reaction of Atomic Hydrogen With Hydrazine. *J. Chem. Phys.* **1976**, *64*, 4892–4896.

58. Chobanyan, S. A.; Mkryan, T. G.; Sarkisyan, E. N. Kinetics of the Reaction of Hydrogen Atoms With Hydrazine. *Kinet. Catal.* **1985**, *26*, 857–859.

59. Vaghjani, G. L. Laser Photolysis Studies of Hydrazine Vapor: 193 and 222 nm H-Atom Primary Quantum Yields at 296 K, and the Kinetics of $H + N_2H_4$ Reaction Over the Temperature Range 222–657 K. *Int. J. Chem. Kinetics* **1995**, *27*, 777–790.

60. Miller, J. A.; Glarborg, P. Modeling the Thermal De-NO_x Process: Closing in on a Final Solution. *Int. J. Chem. Kinetics* **1999**, *31*, 757–765.

61. Ko, T.; Marshall, P.; Fontijn, A. Rate Coefficients for the $H + NH_3$ Reaction Over a Wide Temperature Range. *J. Phys. Chem.* **1990**, *94*, 1401–1404.

62. Sutherland, J. W.; Patterson, P. M.; Klemm, R. B. Flash-Photolysis Shock-Tube Kinetic Investigation of the Reaction of $O(^3P)$ Atoms With Ammonia. *J. Phys. Chem.* **1990**, *94*, 2471–2475.

63. Holzrichter, K.; Wagner, H. G. On the Thermal Decomposition of Ammonia Behind Shock Waves. *Proc. Combust. Inst.* **1981**, *18*, 769–775.

64. Meads, R. F.; Maclagan, R. G. A. R.; Phillips, L. F. Kinetics, Energetics, and Dynamics of the Reactions of CN With NH_3 and ND_3. *J. Phys. Chem.* **1993**, *97*, 3257–3265.

65. Soto, M. R.; Page, M.; McKee, M. L. Theoretical Study of the Reaction of OH With HNO. *Chem. Phys.* **1991**, *153*, 415–426.

66. Soto, M. R.; Page, M. Ab Initio Variational Transition-State-Theory Reaction Rate Calculations for the Gas-Phase Reaction H + HNO → H_2 + NO. *J. Chem. Phys.* **1992**, *97*, 7287–7296.

67. Lin, M. C.; He, Y. S.; Melius, C. F. Theoretical Interpretation of the Kinetics and Mechanisms of the HNO + HNO and HNO + 2NO Reactions With a Unified Model. *Int. J. Chem. Kinetics* **1992**, *24*, 489–516.

68. a. Lin, M. C.; He, Y.; Melius, C. F. Communication: Implications of the HCN → HNC Process to High-Temperature Nitrogen-Containing Fuel Chemistry. *Int. J. Chem. Kinetics* **1992**, *24*, 1103–1107.

b. Lin, M. C. Emory University, Altanta, GA. Private communication, ~1995.

c. Thaxton, A. G.; Lin, M. C.; Lin, C. Y.; Melius, C. F. Thermal Oxidation of HCN by NO_2 at High Temperatures. *Proceeding 21st Internationl Sympusium on Shock Waves*, Great Keppel Island, Australia, 20–25 July 1997; Vol. I, 245–250.

69. Kaufman, F.; Kelso, J. R. Reaction Between Nitric and Nitrous Oxide. *J. Chem. Phys.* **1955**, *23*, 602–603.

70. Fishburne, E. S.; Edse, R. Shock-Tube Study of Nitrous Oxide Decomposition. *J. Chem. Phys.* **1964**, *41*, 1297–1304.

71. Gvozdev, A. A.; Nesterenko, V. B.; Nichipor, G. V.; Trubnikov, V. P. Kinetics of Thermal Decomposition of Nitrous Oxide in a $2NO_2 = 2NO + O_2$ Mixture. *Vestsi Akad. Navuk BSSR, Ser. Fiz.–Energ. Navuk* **1979**, *3*, 73–77.

72. Borisov, A. A.; Skachkov, G. I.; Oguryaev, A. A. Ignition of N_2O + NO Mixtures at High Temperatures. *Kinetika I Kataliz (*English Translation) **1973**, *14* (2), 294–300.

73. Zuev, A. P.; Starikovskii, A. Y. Reactions Involving Nitrogen Oxides at High Temperatures. The Reaction of N_2O With O. *Khim. Fiz.* **1991**, *10*, 179–189.

74. Gvozdev, A. A.; Nesterenko, V. B.; Nichipor, G. V.; Trubnikov, V. P. Study of the Irreversible Thermal Decomposition of Dissociating Nitrogen Tetroxide. *Vestsi Akad. Navuk BSSR, Ser. Fiz.–Energ. Navuk* **1979**, *2*, 74–81.

75. Larson, C. W.; Stewart, P. H.; Golden, D. M. Pressure and Temperature Dependence of Reactions Proceeding via a Bound Complex. An Approach for Combustion and Atmospheric Chemistry Modelers. Application to HO + CO → [HOCO] → H + CO_2. *Int. J. Chem. Kinetics* **1988**, *20*, 27–40.

76. He, Y.; Lin, M. C.; Wu, C. H.; Melius, C. F. The Reaction of HNCO With NO_2 in Shock Waves. *Proc. Combust. Inst.* **1992**, *24*, 711–717.

77. Miller, J. A.; Bowman, C. T. Kinetic Modeling of the Reduction of Nitric Oxide in Combustion Products by Isocyanic Acid. *Int. J. Chem. Kinetics* **1991**, *23*, 289–313.

78. Miller, J. A.; Melius, C. F. A Theoretical Analysis of the Reaction Between Hydrogen Atoms and Isocyanic Acid. *Int. J. Chem. Kinetics* **1992**, *24*, 421–432.

79. He, Y.; Wu, C. H.; Lin, M. C.; Melius, C. F. The Reaction of CN With NO at High Temperatures in Shock Waves. *Proceedings 19th Internationl Sympusium on Shock Waves,* Marseille, France, July 1993, pp 89–94.

80. Wagal, S. S.; Carrington, T.; Filseth, S. V.; Sadowski, C. M. Absolute Rate Constants for the Reactions of $CH(X^2\Pi)$ With NO, N_2O, NO_2, and N_2 at Room Temperature. *Chem. Phys.* **1982**, *69*, 61–70.

81. Park, J.; Giles, N. D.; Moore, J.; Lin, M. C. A Comprehensive Kinetic Study of Thermal Reduction of NO_2 by H_2. *J. Phys. Chem. A* **1998**, *102*, 10099–10105.

82. Hsu, C. C.; Lin, M. C.; Mebel, A. M.; Melius, C. F. Ab Initio Study of the H + HONO Reaction: Direct Abstraction vs. Indirect Exchange Processes. *J. Phys. Chem. A* **1997**, *101*, 60–66.

83. Mebel, A. M.; Lin, M. C.; Melius, C. F. Rate Constant of the HONO + HONO → H_2O + NO + NO_2 Reaction From Ab Initio MO and TST Calculations. *J. Phys. Chem. A* **1998**, *102*, 1803–1807.

84. Bozzelli, J. W. New Jersey Institute of Technology, Newark, NJ. Private communication, 1995.

85. Diau, E. W.; Halbgewachs, M. J.; Smith, A. R.; Lin, M. C. Thermal Reduction of NO by H2—Kinetic Measurement and Computer Modeling of the HNO + NO Reaction. *Int. J. Chem. Kinetics* **1995**, *27*, 867–881.

86. Bowman, C. T.; Hanson, R. K.; Davidson, D. F.; Gardiner, W. C., Jr.; Lissianski, V.; Smith, G. P.; Golden, D. M.; Frenklach, M.; Goldenberg, M. GRI-Mech version 2.11 (see also http://www.me.berkeley.edu/gri_mech/).

87. Xu, Z. F.; Lin, M. C. Kinetics and Mechanism for the $CH_2O + NO_2$ Reaction: A Computational Study. *Int. J. Chem. Kinetics* **2003**, *35*, 184–190.

88. Lin, C. Y.; Wang, H. T.; Lin, M. C.; Melius, C. F. A Shock Tube Study of the $CH_2O + NO_2$ Reaction at High Temperatures. *Int. J. Chem. Kinetics* **1990**, *22*, 455–482.

89. Baulch, D. L.; Cobos, C. J.; Cox, R. A.; Esser, C.; Frank, P.; Just, Th.; Kerr, J. A.; Pilling, M. J.; Troe, J.; Walker, R. W.; Warnatz, J. Evaluated Kinetic Data for Combustion Modeling. *J. Phys. Chem. Ref. Data* **1992**, *21*, 411–734.

90. Thomas, J. H. Gas-Phase Reactions of Nitrogen Dioxide. Part 2. The Oxidation of Glyoxal. *J. Chem. Soc. Faraday Trans.* **1953**, *49*, 630–635.

91. Warnatz, J. Rate Coefficients in the C/H/O System. In *Combustion Chemistry*, Gardiner, W. C., Ed.; Springer: NY, 1984; Chapter 5.

List of Symbols, Abbreviations, and Acronyms

A_k	Arrhenius A-factor for reaction *k*
C	total creation rate of species
D	total destruction rate of species
DZ	dark zone
$\Delta H^{O}_{f,T}$	heat (enthalpy) of formation at temperature T
F	a computed solution variable (e.g., temperature or a species mole fraction)
F_m	maximum value of *F* on computational domain
k_i	rate constant of reaction i
K_i	equilibrium constant of reaction i
L_{DZ}	length of dark zone
M	average molecular weight
P	pressure
R	ideal gas constant
r_b	solid propellant burning rate
ρ_g	gas mixture density
ρ_s	solid mixture density
S_k	sensitivity to reaction k (logarithmically normalized)
SS_k	steady-state parameter for species k
T_{DZ}	dark zone temperature
τ_{DZ}	dark zone ignition delay time
v	convective flow velocity

NO. OF
COPIES ORGANIZATION

1 (PDF only) DEFENSE TECHNICAL INFORMATION CTR
DTIC OCA
8725 JOHN J KINGMAN RD
STE 0944
FORT BELVOIR VA 22060-6218

1 DIRECTOR
US ARMY RESEARCH LAB
IMNE ALC HRR
2800 POWDER MILL RD
ADELPHI MD 20783-1197

1 DIRECTOR
US ARMY RESEARCH LAB
RDRL CIM L
2800 POWDER MILL RD
ADELPHI MD 20783-1197

1 DIRECTOR
US ARMY RESEARCH LAB
RDRL CIM P
2800 POWDER MILL RD
ADELPHI MD 20783-1197

1 DIRECTOR
US ARMY RESEARCH LAB
RDRL D
2800 POWDER MILL RD
ADELPHI MD 20783-1197

ABERDEEN PROVING GROUND

1 DIR USARL
RDRL CIM G (BLDG 4600)

NO. OF COPIES	ORGANIZATION
1	US ARMY ARDEC RDAR MEM L M DONADIO BLDG 65S PICATINNY ARSENAL NJ 07806-5000
1	US ARMY RDECOM ARDEC RDAR MEE W D PARK BLDG 382 PICATINNY ARSENAL NJ 07806-5000
5	US ARMY ARDEC RDAR MEE W P HUI L LOPEZ K CHUNG J SHIN M KAUFFMAN BLDG 382 PICATINNY ARSENAL NJ 07806-5000
1	US ARMY ARDEC SFAE AMO CAS J RUTKOWSKI BLDG 171M PICATINNY ARSENAL NJ 07806-5000
1	US ARMY ARDEC AMSRD AAR AEE W J O'REILLY BLDG 382 PICATINNY ARSENAL NJ 07806-5000
1	REDECOM ARDEC AMSRD AAR AEM J J HIRLINGER BLDG 65N PICATINNY ARSENAL NJ 07806-5000
1	PM TMAS SFAE ASM TMA MS R KOWALSKI BLDG 171A PICATINNY ARSENAL NJ 07806-5000

NO. OF COPIES	ORGANIZATION
1	ST MARKS POWDER GENERAL DYNAMICS R PULVER 7121 COASTAL HWY CRAWFORDVILLE FL 32327
1	ST MARKS POWDER GENERAL DYNAMICS J DRUMMOND 7121 COASTAL HWY CRAWFORDVILLE FL 32327
1	ST MARKS POWDER GENERAL DYNAMICS J HOWARD 7121 COASTAL HWY CRAWFORDVILLE FL 32327
1	RADFORD ARMY AMMO PLANT W WERRELL PO BOX 1 RT 114 RADFORD VA 24143
2	ATK C AAKHUS M JANTSCHER MN07 LW54 5050 LINCOLN DR EDINA MN 55436
1	ATK LAKE CITY K ENLOW PO BOX 1000 INDEPENDENCE MO 64051-1000
1	US ARMY ARDEC AMSRD AR WEE S MOY BLDG 321 PICATINNY ARSENAL NJ 07806-5000
1	US ARMY RDECOM ARDEC RDAR MEE W T MANNING BLDG 382 PICATINNY ARSENAL NJ 07806-5000
1	US ARMY ARDEC AMSRD AR WEE A ENG BLDG 21 PICATINNY ARSENAL NJ 07806-5000

NO. OF COPIES ORGANIZATION

1 US ARMY ARDEC
RDECOM ARDEC
R SURAPANENI
BLDG 3022
PICATINNY ARSENAL NJ 07806-5000

2 ARMY RSRCH OFC
CHEMICAL SCI DIV
R ANTHENIEN
J PARKER
PO BOX 12211
RESEARCH TRIANGLE PARK NC
22709-2211

6 US ARMY AVN & MIS CMND
AMSRD AMR PS PT
J LILLY
N MATHIS
R MICHAELS
M MORRISON
G DRAKE
L PLEDGER
BLDG 7120
REDSTONE RD
REDSTONE ARSENAL AL 35898

1 DIRECTOR
AMRDEC
WEAPONS DEV & INT DIREC
RDMR WDN
J NEIDERT
7120 REDSTONE ARSENAL AL 35898

2 DIRECTOR
NVL SURF WARFARE CNTR
C MICHIENZI
H HAYDEN
4081 N JACKSON RD RM 18
INDIAN HEAD MD 20640-5116

1 COMMANDING OFFICER
NVL ORDNANCE SAFETY
& SECURITY ACTVTY
R SWANSON
INDIAN HEAD MD 20640-5151

1 DIRECTOR
NVL SURF WARFARE CNTR
A STERN
INDIAN HEAD MD 20640

NO. OF COPIES ORGANIZATION

1 COMMANDER
NVL AIR WARFARE CNTR
NAVAIR WEAPONS DIV
S BLASHILL
2400 E PILOT PLANT RD
MS 5300
CHINA LAKE CA 93555-6107

2 DIRECTOR
NVL AIR WARFARE CNTR
E WASHBURN
M GROSS
1900 N KNOX RD
BLDG 1371 MS 6204
CHINA LAKE CA 93555-6106

2 PURDUE UNIVERSITY
SCHOOL OF AERONTC & ASTRNTC
S HEISTER
T POURPOINT
701 W STADIUM RD
WEST LAFAYETTE IN 47907

1 PURDUE UNIV
S F SON
130 CHAFFEE HALL
500 ALLISON RD
WEST LAFAYETTE IN 47907-2088

1 PRINCETON UNIV
DEPT OF MECHL & ARSPC ENGRG
C LAW
D325 ENGRG QUADRANGLE
PRINCETON NJ 08450

1 PRINCETON UNIV
DEPT OF CHEMISTRY
H RABITZ
FRICK LAB
PRINCETON NJ 08544

2 STANFORD UNIV
DEPT OF MECHL ENGRG
D DAVIDSON
R HANSON
BLDG 520
STANFORD CA 94305

1 AERODYNE RSRCH INC
O OLUWOLE
45 MANNING RD
BILLERCA MA 01821

NO. OF COPIES ORGANIZATION

3 CALIFORNIA INST OF TECHLGY
MATLS & MOLECULAR SIMULATION CTR
S DASGUPTA
W GODDARD
S ZYBIN
MS 139-74 BECKMAN INST
PASADENA CA 91125

1 NORTH CAROLINA STATE UNIV
DEPT OF CHEM & BIOL ENGRG
P WESTMORELAND
911 PARTNERS WAY
RALEIGH NC 27695

4 PENNSYLVANIA STATE UNIV
DEPT OF MECHL & NUCLEAR ENGRG
K KUO
S THYNELL
R YETTER
T LITZINGER
UNIVERSITY PARK PA 16802

1 RENSSELAER POLYTECHNIC INST
DEPT CHEM ENGRG
A FONTIJN
TROY NY 12180-3590

1 UNIV NORTH TEXAS
DEPT OF CHEM
P MARSHALL
BOX 305070
DENTON TX 76203-5070

1 TEXAS TECH UNIV
DEPT MECH ENGRG
M PANTOYA
LUBBOCK TX 79409-1021

1 UNIV UTAH
DEPT CHEM
C WIGHT
SALT LAKE CITY UT 84112

1 UNIV ILLINOIS
DEPT CHEM
D DLOTT
A208 CHEMICAL LIFE SCIENCES LAB
BOX 01-6 CLSL MC-712
600 S MATTHEWS AVE
URBANA IL 61801

NO. OF COPIES ORGANIZATION

1 UNIV ALABAMA-BIRMINGHAM
DEPT CHEM
S VYAZOVKIN
BIRMINGHAM AL 35294

1 UNIV SOUTHERN CALIFORNIA
DEPT AEROSPACE AND MECH ENGRG
F EGOLFOPOULOS
VITERBI SCH OF ENGRG
3650 MCCLINTOCK AVE
LOS ANGELES CA 90089-1453

2 SANDIA NATIONAL LAB
COMBUSTION RSCH FACLTY
R BEHRENS
S MAHARREY
LIVERMORE CA 94551-0969

1 ATK ENERGETIC SYS DIV
S RITCHIE
RADFORD ARMY AMMUNITION PLANT
PO BOX 1
RADFORD VA 24143

1 ATK AEROSPACE SYSTEMS
P BRAITHWAITE
PO BOX 707 MS 244
BRIGHAM CITY UT 84302-0707

1 NEW JERSEY INST OF TECH
DEPT OF CHEM
J BOZZELLI
NEWARK NJ 07102

1 UNIV CALIFORNIA AT SAN DIEGO
F WILLIAMS
MAE 0411
LA JOLLA CA 92093

1 UNIV CALIFORNIA AT SAN DIEGO
DEPT MECH ARSPC ENGRG
K SESHADRI
9500 GILMAN DR
LA JOLLA CA 92093-0411

1 AUBURN UNIV
DEPT CHEM AND BIOCHEM
R BLUMENTHAL
AUBURN AL 36849

NO. OF COPIES ORGANIZATION

1 M BECKSTEAD
117R S LYNNWOOD DR
OREM UT 84097

1 GEORGIA INST TECH
SCH AEROSPACE ENGRG
V YANG
313 MONTGOMERY KNIGHT BLDG
270 FERST DR NW
ATLANTA GA 30332

1 CALIFORNIA INST TECH
MATERIALS AND MOLECULAR
SIMULATION CNTR
S DASGUPTA
MS 139-74
PASADENA CA 91125

5 N MEAGHER
40 W COURT ST
CORTLAND NY 13045

1 J VANDERHOFF
553 COMMERCE ST
HAVRE DE GRACE MD 21078

2 T PARR
D HANSON-PARR
934 E JAVIS AVE
RIDGECREST CA 93555

1 EMORY UNIV
DEPT OF CHEMISTRY
M C LIN
ATWOOD 227
ATLANTA GA 30322

1 CHEMICAL PROPULSION INFO
ANALYS CTR
E LIU
10630 LITTLE PATUXENT PARKWAY
STE 202
COLUMBIA MD 21044

ABERDEEN PROVING GROUND

34 DIR USARL
RDRL WMP G
N ELDREDGE
RDRL WML
B FORCH
J NEWILL
M ZOLTOSKI

NO. OF COPIES ORGANIZATION

RDRL WML B
J BRENNAN
S BUNTE
E BYRD
A COHEN
B HOMAN
W MATTSON
J MORRIS
B RICE
R SAUSA
M SCHROEDER
RDRL WML C
B ROOS
K MCNESBY
RDRL WML D
W ANDERSON (5 CPS)
A BRANT
R BEYER
L M CHANG
C CHEN
J COLBURN
P CONROY
A HORST
A KOTLAR
M MCQUAID
M NUSCA
J RITTER
J SCHMIDT
A WILLIAMS

NO. OF
COPIES ORGANIZATION

1 TECHNICAL UNIV DENMARK
DEPT OF CHEMICAL ENGRG
P GLARBORG
2800 LYNGBY
DENMARK

1 OFFICE NATIONAL D'ETUDES ET
DE RECHERCHES AEROSPATIALES
(ONERA)
G LENGELLE
CHATILLON
FRANCE

INTENTIONALLY LEFT BLANK.